Studies of Prebiotic Physical Models towards Understanding the Emergence of Biological Homochirality

A thesis submitted to

University College London (UCL)

For the degree of

Doctor of Philosophy

In the Faculty of

Mathematics and Physical Sciences

October 2019

Rebecca Emily Marchington

Chemistry Department

20 Gordon Street

London

WC1H 0AJ

Declaration

I, Rebecca Emily Marchington, confirm that the work presented in this thesis is my own. Where information has been derived from other sources, I confirm that this has been indicated in the thesis.

Abstract

The homochirality of biological molecules is critical to the structure of biological polymers which form the structures in living organisms that allow them to exist. It is central to the fundamental mechanisms of life such as molecular recognition and the helical structure of DNA; and what is most profound is the universality of it – everywhere we look in nature, amino acids exist in the L-enantiomer and carbohydrates exist as the D-enantiomer, and that homochirality is carried forward throughout the construction of living things on the macro level. The origin of this homochirality has perplexed generations of scientists since it was first discovered by Pasteur in the 19th century and is a fundamental problem within the study of the Origin of Life.

In recent years, prebiotic synthesis has leaped forward, identifying a number of not only plausible, but likely routes to the precursors of RNA, thought by some to be the first biological polymer on Earth and the root of simple living organisms. However, it has been demonstrated that for chiral RNA to polymerise, its constituent building blocks (nucleotides) must be enatio-pure, otherwise oligomerisation is inhibited. As yet, chemistry has lacked a robust explanation for how such homochirality would have arisen under prebiotic conditions when all thermodynamic rules should form both enantiomers in equal amounts. Here, we report prebiotically-plausible enantio-enrichment of nucleotide precursor molecules (aminooxazolines, oxazolidinone thiones and oxazolidinones) and related compounds, from near-racemic conditions using crystallographic approaches and applying them to new substrates. This work views the homochirality problem from a new angle and in so doing expands the crystallographic landscape of pre-biotic chemistry, opening the door to crystal engineering in Origin of Life studies.

Impact Statement

The results obtained in this work clearly demonstrate that enantiomeric amplification can be achieved from a small imbalance of enantiomers in solution to lead to homochirality in crystals of RNA precursors. With this knowledge we can begin to determine the ways in which all chiral prebiotic building blocks came to be homochiral.

Analysis of the crystals formed in these and future studies, we will be able to identify novel crystallographic synthons and trends that may be exploited for crystal engineering. By forming a more complete picture of how and why those compounds crystallise in the structures that they do we can design ways in which to control that process, and develop a crystal engineering stratagem that pertains directly to some of the most important class of compounds in the natural world – amino acids, carbohydrates, nucleotides - and their polymers – proteins, polysaccharides, and RNA/DNA. These compounds have a huge role to play in the development of therapeutics, genomics and diagnostics and their crystalline properties have an enormous impact on their biological activity. By investigating them thoroughly we can extend enantiomeric amplification and crystal engineering to improve synthesis and efficacy of drugs, design new biomaterials for exotic new applications and so on.

It is by improving our understanding of fundamental effects and forces in the natural world, and how they affect our lives and environment, that we gain access to new ideas, technologies, and entire new fields of study, in which a rich vein of human benefits lies waiting to be tapped. This is, and always has been, the noble pursuit of science, and hopefully this tiny piece of the much larger puzzle contributes in its own way to that end.

Acknowledgements

Firstly, I would like to thank my supervisors; Matthew Powner and Kreso Bucar, for giving me the opportunity to carry out research in such a fascinating area. I would like to thank all members of the Powner group, both past and present for many hours of discussion. My special thanks must go to Shaun, Christian, Merina and Joanna for endless coffee, crystals, and corrections.

Finally, I would like to thank my husband, family and friends, without whose support this would have been impossible.

Table of Contents

Table of Figures

Table of Schemes

Table of Tables

Abbreviations

A	adenine
Ac	acetyl
Ar	aryl
ATP	adenosine triphosphate
aq.	aqueous
t-Bu	*tert*-butyl
Bn	benzyl
Bz	benzoyl
°C	degrees Celsius
C	cytosine
c	concentration
ca.	*circa* (Latin: about)
calcd	calculated
cAMP	adenosine-3¢,5¢-cyclic phosphate
cat.	catalytic
CI	chemical ionisation
cm^{-1}	wavenumber
conc.	concentrated
COSY	correlated spectroscopy (NMR)
HPLC	High Performance Liquid Chromatography
DCM	dichloromethane
Dowex®	Dowex® ion exchange resin
ES	electrospray

Et	ethyl
Ether	diethyl ether
G	guanine
GC	gas chromatography
GMP	guanosine monophosphate
GTP	guanosine triphosphate
h	hour(s)
h*v*	electromagnetic irradiation (UV)
HMBC	heteronuclear multiple-bond correlation multiple-quantum correlation
HPLC	high pressure liquid chromatography 10
HR	high resolution
Hz	Hertz
inc.	including
IR	infrared
J	NMR coupling constant measured in Herts
LA	Lewis acid
lit.	literature (reference)
m	milli
M	molar
Me	methyl
MHz	megahertz
min(s)	minute(s)
mL	millilitre(s)
mmol	millimole(s)
m.p.	melting point
MS	mass spectrometry

µl	microlitre
µM	micromolar
m/z	mass / charge ratio
NADH	nicotinamide adenine dinucleotide
NMR	nuclear magnetic resonance
op.	open chain
PG	protecting group
Ph	phenyl
Pi	inorganic phosphate
PNA	peptide nucleic acid
PPi	inorganic pyrophosphate
ppm	parts per million
Pr	propyl
quant.	quantitative yield
R	unspecified group
rac-	racemic mixture
RNA	ribonucleic acid
rt	room temperature
sca-	scalemic mixture
sat.	saturated
T	thymine
$t_{1/2}$	half life
TBDMS	*tert*-butyldimethylsilyl
THF	tetrahydrofuran
UV	ultraviolet

Numbering and Nomenclature

Pentose sugars (Fisher projections in natural D-series)

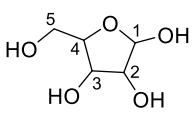

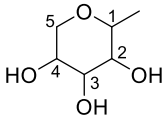

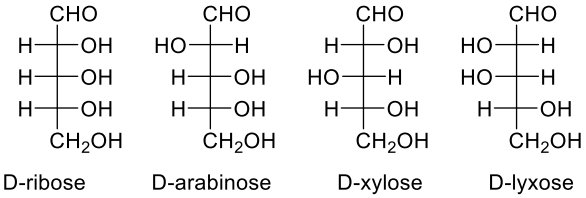

Pentose Oxazolines

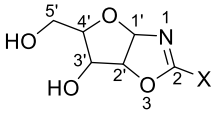

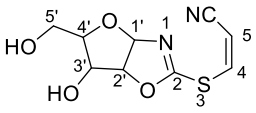

Aminals

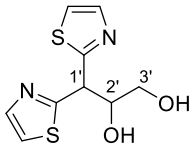

Anhydronucleosides

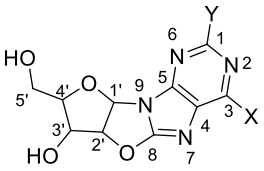

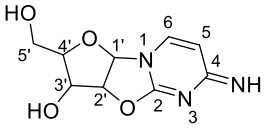

Nucleosides

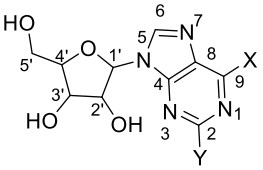

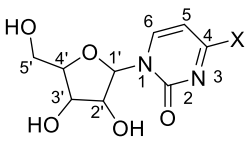

1 Introduction

1.1 The Origin of Life

How life started on Earth, or elsewhere in the universe for that matter, has been the subject of intense philosophical, theological, and more recently, scientific discourse for millennia. From religious texts, to modern day scientific journals, few topics have sparked such curiosity and imaginative theories.

In the modern era, it is a widely held belief that a primordial soup of chemical precursors to living systems formed as the result of the unique environments that arose on Earth when our solar system was in its infancy. Reconciling the vast chasm of both time and complexity between that chemical world, and the biological world we observe now in nature, is the pursuit of the study of the Origin of Life.

We can use a top-down approach to extrapolate theories about how the appearance of molecules like DNA evolved or emerged from simpler building blocks such as RNA; or, a bottom-up approach, to discover how it may have been possible to synthesise the smaller building blocks, such as nucleobases, from a range of chemical feedstocks, such as methane, formaldehyde, and carbon dioxide, etc. For a holistic view of the origin these two threads must be ultimately woven into a continuous model.

One of the most striking phenomena in nature is the homochirality we observe uniformly across biological systems. This *enantio*-specific bias must have been established very early on in Earth's history, certainly prior to life's universal common ancestor (LUCA), which is predated

by transcription and translation (DNA, RNA and proteins) that exploits and requires chirospecific iteration (such as Watson-Crick Templated replication). Homochirality is very hard to explain when one considers the chemical origins of the primordial soup. Many prebiotic precursors are ultimately achiral, so where and how did homochirality arise? How was symmetry broken? How did uniform homochirality become expressed across the entire biological system?

The chemical conditions that give rise to biological building blocks should do so in an entirely racemic manner in a system that has no inherent chirality (such as that we imagine to be present in the 'primordial soup' scenario). Therefore, in order for one enantiomer to become dominant in a mixture of enantiomers, the symmetry of the system must first be broken to give one hand an edge. Using amplification, increasing the difference in concentration between the two enantiomers, could be increased to 100% over time using ripening techniques which will be discussed later. Symmetry breaking is not unusual and is observed in a number of physical systems due to infinitesimally small fluctuations in a system that lead to a collapse into one state rather than another, for example in ferromagnetism.[1]

A key subfield within the study of the Origin of Life on Earth focuses on how this unexpected result came to be. However, very few studies to-date have thoroughly investigated the key intermediates in important synthetic routes on the path to living cells. For example, nucleotides and their precursors.

Origin of Life studies have generally focused on recapitulating the central dogma of molecular biology, as seen in Figure 1, that describes the flow of genetic information within all extant

biological systems. For a more intimate understanding of how living systems and biological processes arose, such as that shown in Figure 1, we must understand the chemistry of the early Earth when it is believed that the first such systems would have developed.

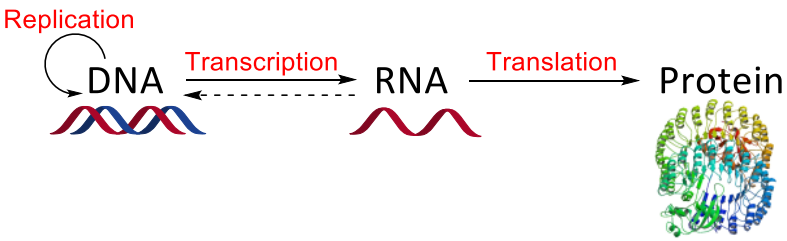

Figure 1:Central Dogma of Molecular Biology

The Earth is approximately 4.5 billion years old. For the first 700 million years it went through a series of large impacts by objects left over from the formation of the solar system in the period known as 'The Late Heavy Bombardment' (LHB).[2,3] Due to the enormous energy released by these impacts, the barrage would have evaporated any oceans and likely sterilised the planet. [4,59] This means that if any living systems had developed before the LHB, they are very unlikely to be the ancestors of the life we have on the Earth today.[5] Even if the formation of biomolecules such as amino acids, sugars, purines and pyrimidines occurred, UV irradiation would have destroyed such organic compounds quickly, unless they were isolated in rocks or a prebiotic ocean.[6] To account for the presence of organic compounds it has also been postulated that asteroids, comets or smaller meteorites or even interplanetary dust could have brought large quantities of reduced carbon to the planet.[7] Carbonaceous meteorites carry large quantities of organic compounds; and remarkably, some of those meteorites exhibit significant enantiomeric excess (*ee*) which favour the canonical L-amino acids. For example, in the Murchison meteorite, L-isovaline is observed in up to L_{ee}= 18.5%, in the Murray meteorite L-isovaline L_{ee}= 6%, and in the Orgueil meteorite L-isovaline L_{ee}= 15.2%.[8]

By investigating the spectra of interstellar gases, over 130 astronomical molecules have been identified to-date in outer space, and we can expect many more will be discovered as radio and infrared telescope technology improves.[9] The molecules identified in molecular clouds and envelopes expelled by evolved stars are collectively known as the prebiotic feedstock (Figure 2).[6] These feedstock molecules that are of guaranteed non-biological origin, are often used to inform prebiotic chemistry.

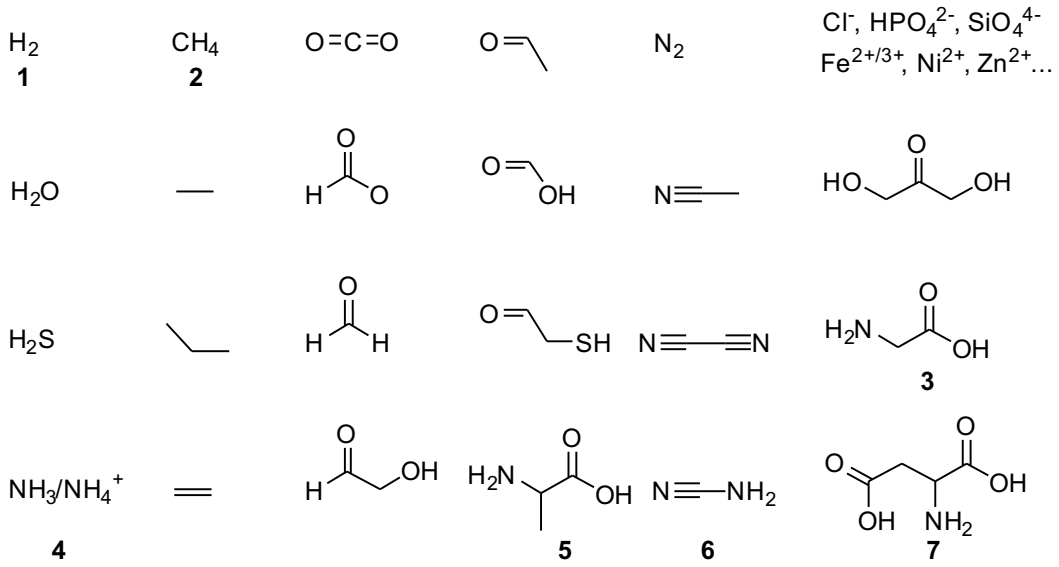

Figure 2: Prebiotic feedstock of molecules

Prebiotic chemistry is the study of reactions that could have occurred on the primitive Earth, and forms part of the pursuit to study the origin of life. It is not yet known with absolute certainty which molecules, or what conditions, were present on the primitive Earth, and it is still the topic of much debate; principally as a result of the scarcity of available rock records from such an early period.[10] Although some experiments have demonstrated that extreme conditions such as high temperature and pressure, such as that found near geothermal vents

in the deep ocean, or that generated during high energy impacts, could have played a role in the origins of life, there is a broad agreement on what is required for a reaction to be prebiotically plausible.[11–13] These are based on the conditions we observe within biological cells we see today:

a) Primary reagents should be derivable from the prebiotic feedstock molecules.
b) Reactions should ideally require no solvent other than water, and reactions should be carried out at moderate pH.
c) Solid-state reactions should not require excessive drying of reactants, which could not be achieved by evaporation of water.
d) Reactions should not require excessive temperature and pressures.

As one may expect there is an ongoing significant debate surrounding what prebiotic conditions actually are, however, to define the conditions too precisely could hinder the origin of life studies.

Seminal work by Urey and Miller in 1953 demonstrated a spark discharge experiment that aimed to understand which prebiotically relevant molecules could be formed in an environment mimicking that of the early Earth (as far as was understood at the time).[14] Miller and Urey synthesised amino acid glycine (**3**) from strongly reducing mixture of gases such as methane (**2**), ammonia (**3**), hydrogen (**1**) and water by spark discharge (simulating lightening in these early environments).[15] The reaction mixture was analysed by paper chromatography and showed that a handful of amino acids were present; glycine (**3**), α-alanine (**5**), and possibly aspartic acid (**7**) in small amounts.[14] It was proposed that the α-amino acids were formed by the reaction of aldehydes with HCN and ammonia, through the Strecker reaction (Figure 3).[16]

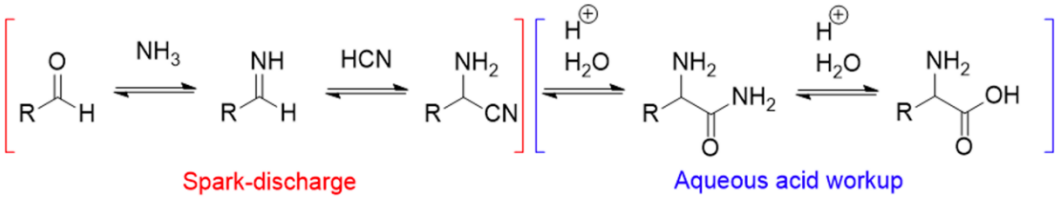

Figure 3 : Proposed Mechanism from the Miller-Urey Experiments

Miller and Urey, like many scientist at this time, believed that the atmosphere of the primitive Earth was strongly reducing.[15] However, it is now thought that the primitive Earth's atmosphere was more likely only weakly reducing or even a neutral atmosphere. It is commonly accepted the Earth's prebiotic atmosphere contained gases such as CO_2, N_2, CO, and H_2O, along with small amounts of reduced gases such as H_2, H_2S and CH_4.[17,18] Moreover, there is strong evidence that the early Earth's mantle had the same oxygen fugacity as the modern Earth and so was probably set when the Earth's core was formed.[19,20] Nonetheless, the strongly reducing atmosphere suggested by Miller and Urey's research cannot be entirely ruled out and further investigation in the field is required to fully understand the nature of the prebiotic atmosphere.[5]

Since this early publication, similar experiments have shown that a racemic mix (50:50 ratio between the L and D form) of 17 amino acids are formed under the same conditions.[21] After Miller's death in 2007, several boxes that contained vials of residues were found remaining from a volcanic discharge experiment, which simulates the lightning observed in a steam-rich volcanic eruption.[22] These residues were reanalysed and 22 amino acids were identified, several which had not previously been identified in Miller's initial experiment.

In 2002, Munnoz Caro *et al.* demonstrated the results of their experiments which investigated how interstellar ice can be a source for spontaneous amino acid generation in space.[23] They reported the detection of sixteen amino acids, many which of which have also been found on meteorite samples.

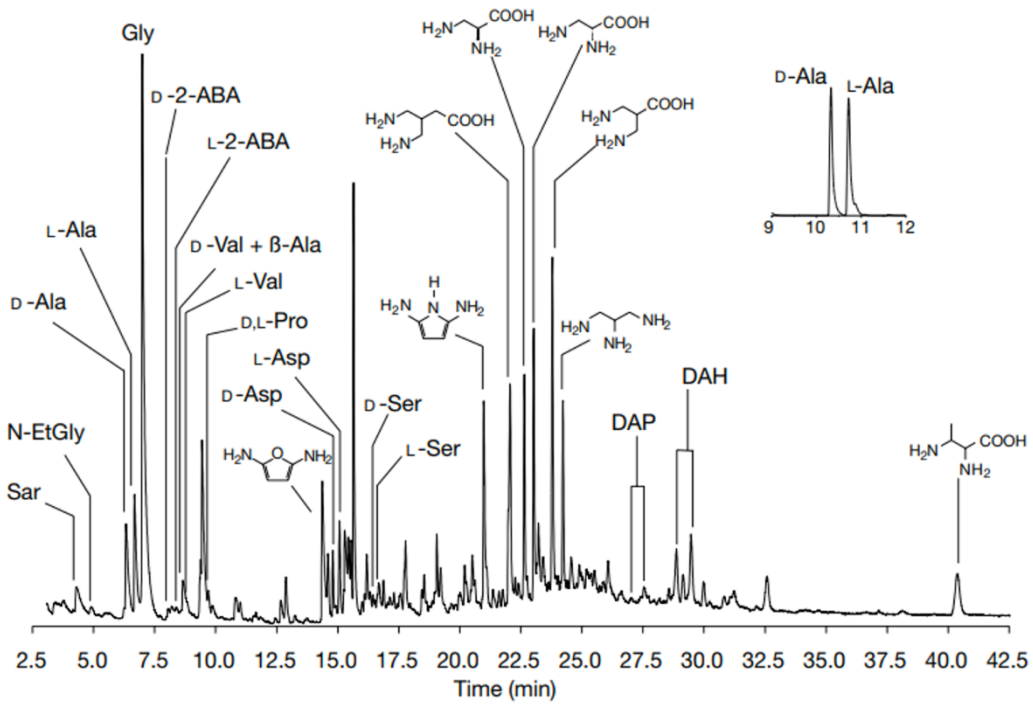

Figure 4: Munnoz Caro et al. reporting the gas chromatogram illustrating the many compounds generated under stimulated interstellar conditions.[23]

During the Earth's formation, temperatures were too high for any water to remain on the planet and so must have originated from where water could freeze: the snow line.[24] There is therefore growing acceptance that the water present on Earth today was delivered by asteroids that originated from further out in the solar system. Isotopic analysis supports this as the chemical fingerprint of oceanic water samples closely matches that of carbonaceous chondrites – meteorites which also contain a high amount of organic carbon material,

including amino acids, carboxylic acids, carbonyls, sulphonic/phosphonic acids, and saturated/aromatic hydrocarbons.[25]

So, it can be seen there are a number of viable explanations for how prebiotic building blocks might have been created either on the earth or brought to earth by asteroids. So, using these basic components, how could they have been assembled into the molecules that are essential to life?

1.2 The RNA World Theory

The RNA World theory originated from a question posed in the late 1960s: which came first - proteins or nucleic acids?[26] At the time, it was known that through the mutation and replication of nucleic acids, more complex biological systems could be created from simpler ones. So, the answer to this question seemed obvious: nucleic acids. This was rationalised using Watson-Crick base pairing and in particular the understanding that nucleic acids are responsible for transferring genetic information. Woese[27], Crick[28] and Orgel[8] all recognised that an autonomous RNA organism would only be plausible if RNA was able to have all of the different functionalities currently exhibited by proteins.

RNA is essential for life as it is responsible for some of the most fundamental cell processes. It participates in DNA replication as a primer, carries the genetic information to the ribosome to be translated in the form of mRNA, and tRNA molecules charge the correctly charged amino acid to the ribosome to enable genetic decoding. But the full catalytic potential of RNA was only revealed by the discovery of molecular structure of the ribosome.

Ribozymes are enzymes composed of RNA, rather than proteins. The structure of the ribosome was found to have an active site made solely of RNA.[29,30] While proteins form part of the ribosomes' structure, no amino acids are located in the active site and typically the closest is 18 Å from the peptidyl transfer centre site.[31] For their ground-breaking work on the ribosome and identifying the catalytic nature of ribozymes within living cells, Altman and Cech received the Nobel Prize in Chemistry in 1989.[32] The function of the ribosome (and mRNA/tRNAs within the ribosome) beautifully demonstrate RNA's role as both phenotype and genotype in biology, this makes RNA a very interesting target as the first prebiotic polymer and has been widely seen as a molecular fossil and as a "smoking gun" for key evidence for the RNA world.

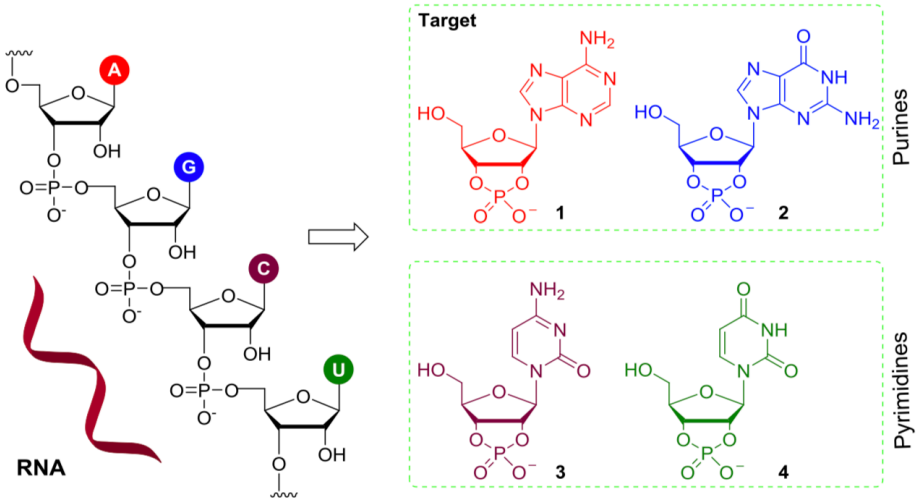

Figure 5: RNA strand highlighting the different bases; adenine (A), guanine (G), cytosine (C) and uracil (U).

RNA is in principle able to replicate without the need for protein catalysts through a process coordinated by Watson-Crick base pairing, mis-incorporation (or errors) in the replication process allow evolution to occur. [31,33] RNA exhibits remarkable functional versatility, because it contains four molecular-recognition units (bases, shown in Figure 5) that can complement their own copying as well as, at the polymeric level, three-dimensional structural versatility allowing it to fold into many different complex tertiary structures, some of which are similar

to proteins in their ability to bind substrates and catalyse a range of chemical transformations.[29] Further the presence of RNA monomers in essential enzyme co-factors such as ATP, FAD, acetyl-CoA and NADH/ NADPH that are required for the function of many (peptide) proteins in extant biology (Figure 6), is seen by many as another smoking gun for the RNA world.[34]

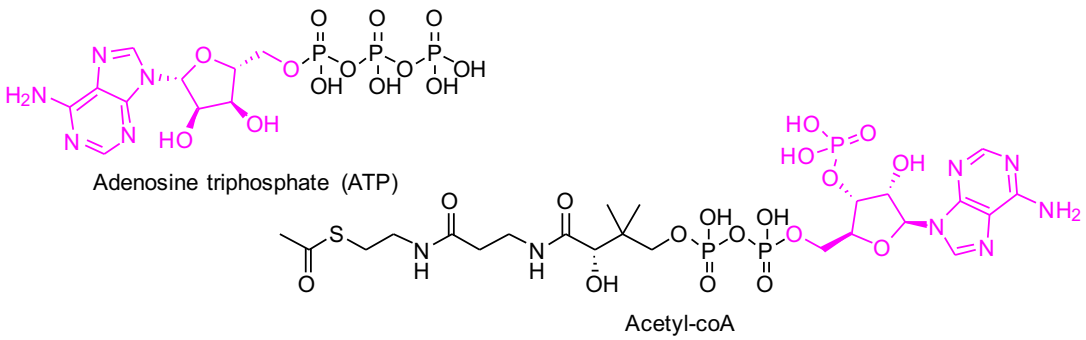

Figure 6: Examples of co-factors containing RNA. RNA structure represented in pink.

For an RNA world theory to be valid, we require a robust and prebiotically-plausible synthesis of RNA nucleotides and a mechanism for their subsequent oligomerisation to yield functional biopolymers.

1.3 Synthesising Activated Nucleotides

Traditional approaches to RNA using prebiotic feedstock have involved the attempted one-pot reaction of sugar and base, and subsequent phosphorylation (Figure 7).

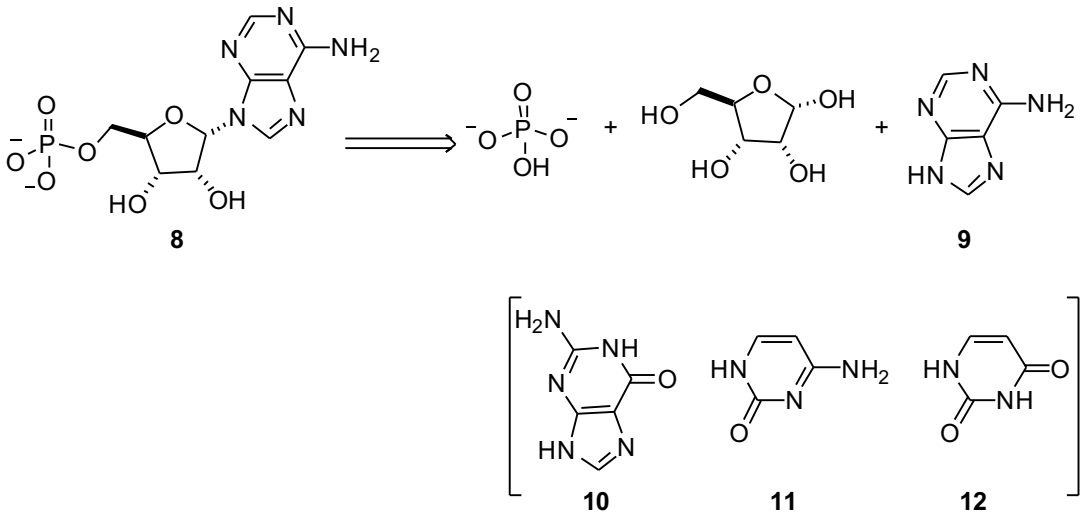

Figure 7: Traditional retrosynthetic analysis of RNA: inorganic phosphate, ribose (shown in furanose form) and nucleobase. (Shown as adenoside-5'-phosphate (8) as an example with adenine as the free nucleobase (9). The alternative nucleobases are guanine (10), cytosine (11) and uracil (12) shown in brackets.)

Traditional disconnection instincts suggest the above synthetic route so strongly, that it was widely accepted as dogmatic. However, the significant kinetic and thermodynamic obstacles imposed by this route make the chemistry essentially non-viable.[35]

In pursuit of the presumed route issues have included low yields in the synthesis of the nucleobases and poor selectivity for ribose in the preparation of the sugars, which is also unstable and cannot be purified by prebiotically-sound means.[36–42] What's more, in trying to attach pre-formed pyrimidine, kinetic and thermodynamic barriers pose insurmountable obstacles, and it is not possible to control regio- or stereo- selectivity of purine attachment, which also proceeds with poor yield.[42]

For more than sixty years the problem of prebiotic ribosylation of nucleobases to form ribonucleotides was a major issue for origin of life studies. But, in 2009, using a new systems

chemistry approach, Powner and co-workers demonstrated a prebiotically plausible synthesis of activated ribonucleotides.[43]

This elegant synthesis centres around the use of the simple prebiotic molecules cyanamide (**6**), glycolaldehyde (**13**) and glyceraldehyde (**14**) under prebiotic conditions (Scheme 1).[43] Firstly, cyanamide (**6**) and glycolaldehyde (**13**) react in water (1 M, pH 7 phosphate buffer) to form 2-aminooxazole (**15**), which can then nucleophilically react with glyceraldehyde (**14**) to form the pentose aminooxazolines (**AO**) in 95% yield, again in aqueous phosphate at pH 7.[43] The major pentose aminooxazolines products formed are *arabino*-aminooxazoline (**AAO**) (33%) and *ribo*-aminooxazoline (**RAO**) (44%), both with complete furanosyl selectivity.

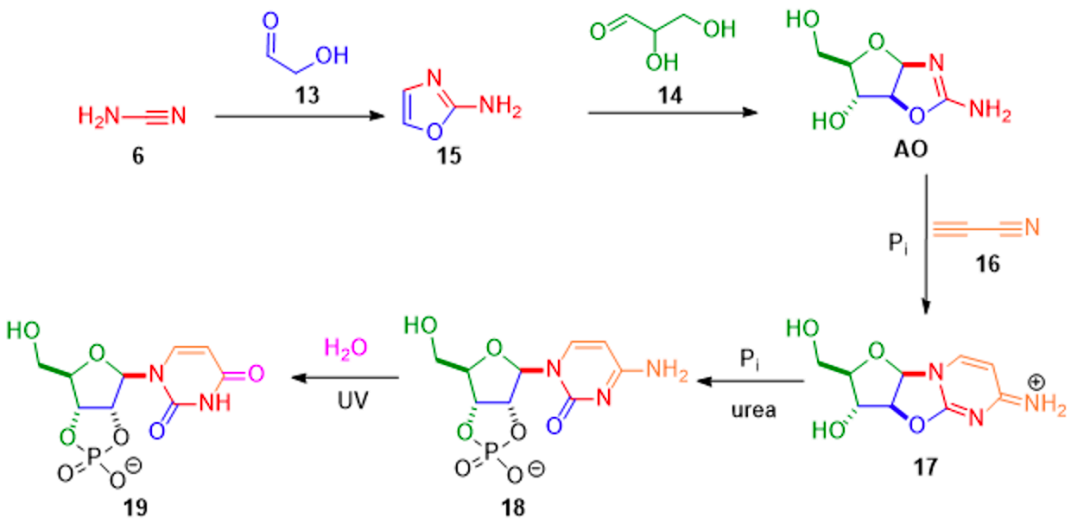

Scheme 1: Activated Nucleotide Synthesis by Powner et al [43] – colour coded to highlight the contribution of each reagent

The pentose aminooxazoline (**AO**) reacts with cyanoacetylene (**16**) (in buffered aqueous phosphate, pH 7) affords the anhydronucleoside (**17**) cleanly. If this is carried out in unbuffered aqueous solution at pH 7 it results in the hydrolysis of the anhydronucleoside. The

anhydronucleoside then undergoes a regioselective phosphorylation of the secondary alcohol on C3 and subsequent nucleophilic inversion of C2 to give a 2′,3′-cyclophosphate upon heating with phosphate and urea. It has been speculated that the electron delocalisation of the lone pair (*n*) of O5′′ and the antibonding orbital (π^*) of C2 makes O3′′ comparatively more nucleophilic, and therefore more available for phosphorylation.[44] Under UV irradiation, cytidine (**18**) is converted to uridine (**19**) which are both necessary for RNA. The irradiation is also particularly convenient as it removes the other pyrimidine side products.[43]

The inorganic phosphate plays four key roles in the synthesis shown above: 1. By acting as an acid base catalyst in the reaction between cyanamide (**6**) and glycolaldehyde (**13**); 2. It leads to higher chemoselectivity for the reaction of the aminooxazolines (**AO**) and cyanoacetylene (**16**); 3. It acts as a buffer allowing the pH to be maintained and to inhibit the hydrolysis of anhydro*arabino*nucleoside (**17**); and, finally, 4. It is essential in the final phosphorylation step to form the required cyclic phosphates (**19**).[43,45]

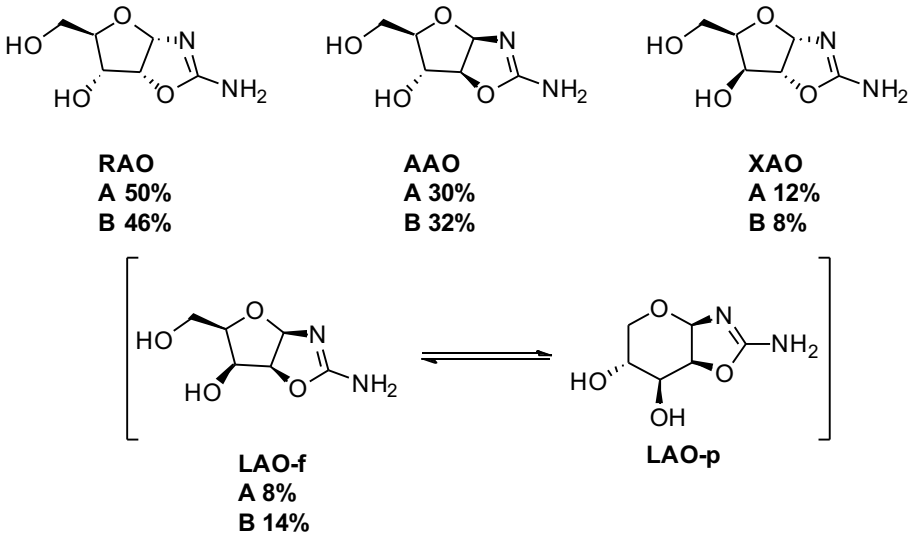

Figure 8: Aminooxazolines formed from Powner et al.'s synthesis.[43] Shown as a proportion of conformer formed as % of total (**16**) in A - 1 M P_i or B - H_2O

The critical step in the synthesis of RNA, is the formation of the aminooxazolines (**AO**) which are synthesised through prebiotically available small molecules; and additionally by-passes the need for the free sugar (Figure 8).

Ribo-aminooxazoline (**RAO**) ($t_{1/2}$ > 1 week) has been shown to be 70 times more stable than *ribo*se ($t_{1/2}$ < 3 hours) under comparable aqueous conditions (pH 10, 55 °C), which has led to it being highlighted as a stable candidate compound that was harnessed during the pathway to biological structures.[46,47] This is important when compared to the retrosynthetic pathway which utilises ribose as a key synthon (Figure 7).

The differing solubility of pentose aminooxazolines (**AO**) was first observed by Joyce, when he noted that **RAO** spontaneously crystallises selectively from a mixture of pentose aminooxazolines (**AO**).[47] So it follows that purification can be achieved using serial crystallisations that can mimic dry and wet cycles (similar to the Earth's day/night cycle), and separate the two products, leaving **AAO** in solution and **RAO** crystals. This enriches the desired **AAO** in the solution, which can then react with cyanoacetylene (**16**) as discussed.

It has also been noted that scalemic (mixtures of enantiomers at a ratio other than 1:1 or 1:0) glyceraldehyde (**14**) (>60% enantiomeric excess) with 2-aminooxazole (**15**) can lead to enantioenrichment and spontaneous crystallisation of pure homochiral **RAO**, which has implications for the origins of homochirality on the early Earth, that will be discussed later.[35] It is also possible to use phosphate in the interconversion of **RAO** to **AAO** via a general acid-base catalysed C2''-epimerisation (Figure 9).

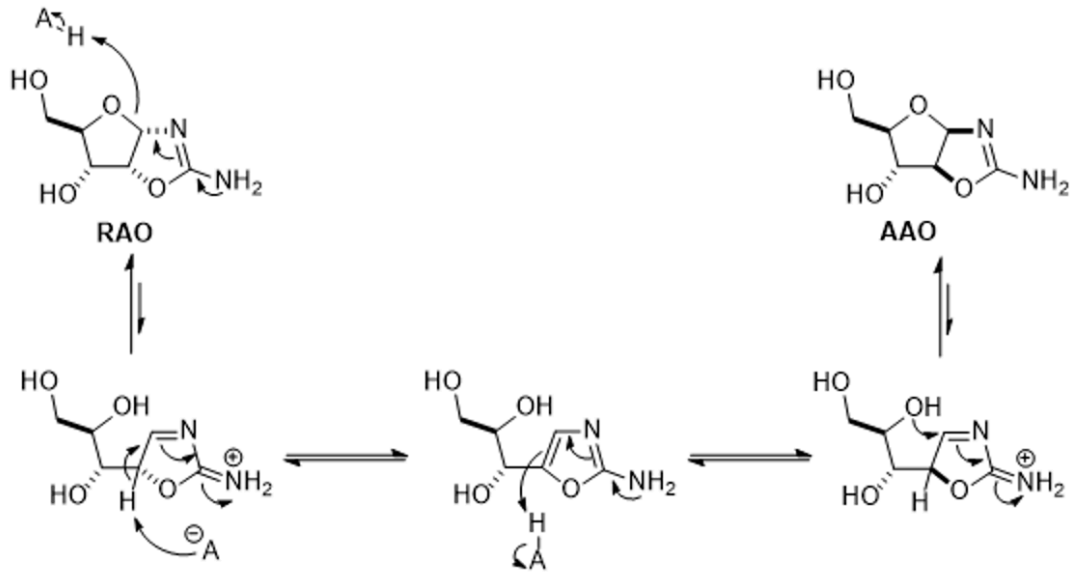

Figure 9: Suggested mechanism for interconversion between RAO and AAO via phosphate. H-A, general acid; A-, general base.

The crystallisation of **RAO**, leaves behind **XAO**, and **LAO**, which are the minor products in the mixture of aminooxazolines produced.[43] As **XAO** and **LAO** are only assessable *via* C3' epimerisation from **RAO**, the interconversion of **RAO** and **AAO** can therefore be used to successfully remove **XAO** and **LAO** aminooxazolines.

1.3.1 Current Limitations of Prebiotic RNA Synthesis

Whilst this synthesis is a significant improvement on previous methods, there are still several limitations to consider. For example, it is necessary to use sequential addition of the components to control the chemistry and avoid undesirable side-reactions.[31,48–50] The synthesis of aminooxazolines *en route* to the pyrimidines requires glycolaldehyde (**13**) to react with cyanamide (**6**) to form 2-aminooxazole (**15**). However, for example, if glyceraldehyde (**14**) is also present it can/would react with cyanamide (**6**) to form 2-amino-5-hydroxymethyloxazole (**20**), which would inevitably lead to a mixture of products (Scheme 2).[51]

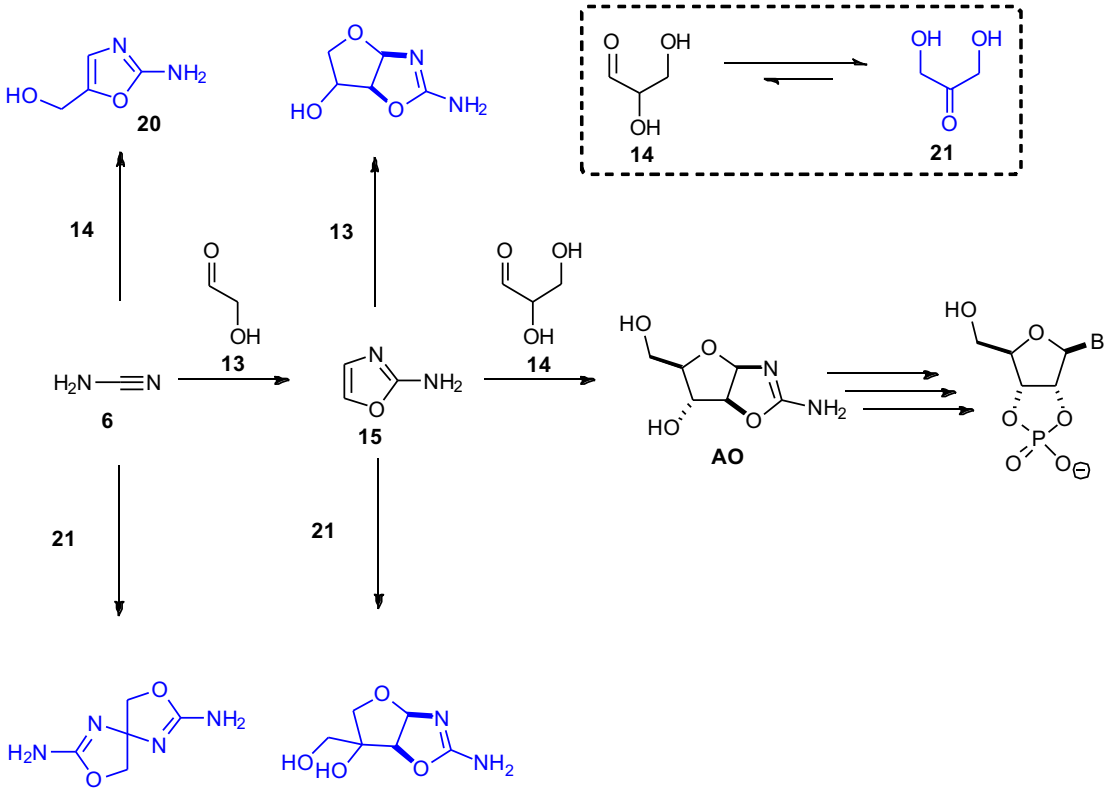

Scheme 2: The synthesis of pyrimidines requires controlled addition of the components (black). However, failing these steps other products form (blue). Furthermore, glyceraldehyde (**14**) is highly susceptible to an equilibrium with dihydroxyacetone (**21**). Adapted from Islam *et al*.[52]

A further issue arises from the aldose-ketose equilibrium of the glyceraldehyde (**14**) used in step 2, and with its more thermodynamically-favourable form, dihydroxyacetone (DHA, **21**). This occurs when glyceraldehyde (**14**) undergoes prolonged aqueous incubation and the rate is enhanced by general acid-base catalysts, such as phosphate. DHA (**21**) can then cause further losses to the desired pathway, by reacting with cyanamide (**6**) or 2-aminooxazole (**15**) to deliver more undesired aminooxazolines in the system. (Scheme 2).

It has been shown that 2-aminooxazole (**15**) is particularly volatile and undergoes sublimation when warmed, which could be useful to extract it from the mixture. It is then feasible that it could be precipitated as rain into a new pool containing glyceraldehyde (**14**).[53–55] Unfortunately, all currently-postulated prebiotic syntheses of glyceraldehyde (**14**) create a mixture of it and glycolaldehyde (**13**) and other aldose & ketose sugars.[55] To add to that, the presence of phosphate in a pool of glyceraldehyde (**14**) would lead to the formation of DHA (**21**) as discussed, demonstrating that there is more work to be done to develop this hypothesis for prebiotic nucleotide synthesis.

The developing work into the prebiotic pathway via ribose is still ongoing. In 2016, Carell's group demonstrated their synthesis of adenine and guanine bases from formamidopyrimidines (FaPy) which are generated under prebiotic conditions with good yields and regioselectivity.[56] Carell *et al.* extended their work to show how wet dry cycles may enable the continuous synthesis of canonical and non-canonical nucleosides in parallel. Carell also claims that these can be converted to the phosphorylated nucleotides using recently-reported methodologies, though they have not yet been able to incorporate this step into their own continuous synthesis.[57,58]

More recently, Becker has published a method that grants one-pot access to pyrimidine nucleosides starting from small molecules, driven by wet-dry cycles. Moreover, as it is compatible with the synthesis of purines, it opens the door to accessing all Watson-Crick bases in a single concurrent system.[59]

As with all things, there is more than one way to skin the synthetic cat, and the work presented here focuses on the Powner *et al.* route, in particular the interesting crystalline properties of

the aminooxazolines (**AO**) as a precursor to RNA and the ways in which this route, and potentially crystallisation, can be leveraged to amplify the enantiomeric excess to the levels we observe in nature.

1.3.2 Crystallisation-Driven Synthesis of Nucleotide Precursors

The prebiotic ribonucleotide synthesis developed by Powner *et al.* requires the selective reaction of glycolaldehyde (**13**) with cyanamide (**6**).[43] There is a constitutional relationship between β-mercaptoacetaldehyde (BMA) (**22**) and glycolaldehyde (**13**) (with a single chalcogen substitution), and this relationship seen in the proteinogenic amino acids, cysteine and serine (which are formal product of Strecker reaction with **22** and **13**, respectively) .[60,61] As **13** is important for prebiotic (Strecker) synthesis of proteinogenic amino acids and prebiotic synthesis of canonical nucleotides, it was hypothesised that BMA (**22**) could have equal importance in both amino acid and nucleotide abiogenesis. The influence of **22** on prebiotic nucleotide chemistry would therefore be worth further investigation.[26] It has been shown that **22** reacts with cyanamide (**6**) in water, at neutral pH, to form 2-aminothiazole (**23**) in a similar fashion, though kinetically much faster, than how glycolaldehyde (**13**) reacts with cyanamide (**6**) to form 2-aminooxazole (**15**) (Scheme 3).[60]

Interestingly, selective formation of 2-aminothiazole (**23**) from BMA (**22**) and cyanamide (**6**) was subsequently demonstrated even when in stoichiometric competition with 25 other aldehydes, ketones and sugars.[62]

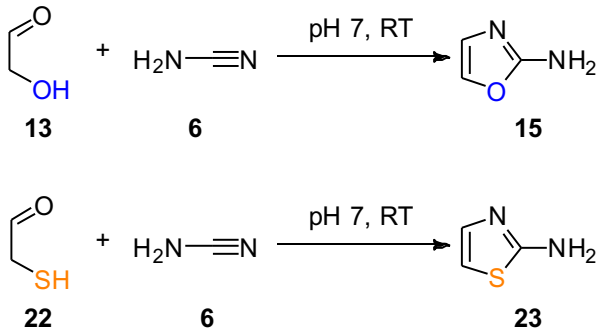

Scheme 3: Glycolaldehyde (**13**) and cyanamide (**6**) to form 2-aminooxazole (**15**). BMA (**22**) and cyanamide (**6**) to form 2-aminothiazole (**23**)

Islam *et al.* went on to demonstrate a robust synthesis of pyrimidine *ribo*nucleotides by utilising 2-aminothiazole (**23**) *via* the selective formation of aminal (**24** & **25**) from glycolaldehyde (**13**) and glyceraldehyde (**14**) even in the presence of a complex mixture of aldose and ketose sugars (

Scheme 4: Time resolved separation of hydroxy-aldehydes 13 and 21 from a complex sugar mixture by 25 aminal formation crystallisation as in Islam et al.[63]:

).[63]

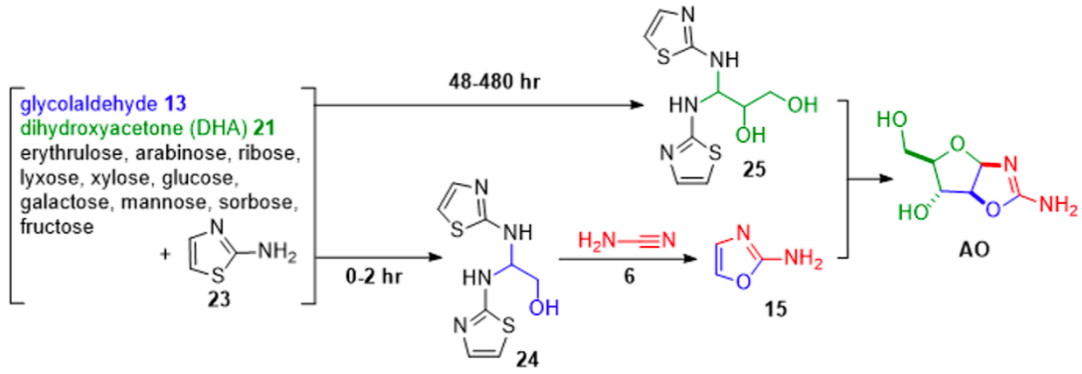

Scheme 4: Time resolved separation of hydroxy-aldehydes 13 and 21 from a complex sugar mixture by 25 aminal formation crystallisation as in Islam et al.[63]:

Here, aminal formation occurs in a time resolved manner which grants access to **AO**. Addition of 2-aminothiazole (**23**) to a solution of a mixture of sugars, (in which all glyceraldehyde (**14**) is converted to the more thermodynamically stable ketose-form, DHA (**21**)) leads to rapid crystallisation (0-2 hours) of the aminal (**24**). In the prebiotic world, this could separate (**24**) from the remaining solution given appropriate geological or environmental conditions.

Additional cyanamide (**6**) can then be added, resulting in (**24**) breaking up to form 2-aminooxazole (**15**) and 2-aminothiazole (**23**) quantitatively. Given more time, the initial solution will yield a second aminal (**25**) through reaction of 2-aminothiazole (**23**) and the minor aldose isomer (**14**) in the equilibrating mixture of DHA (**21**). This again leads to another separation element that removes the mixture of sugars from the crystals.

Finally, the combination of glyceraldehyde aminal (**25**) with the separately generated (**15**) results in the high yielding formation of (**AO**). This occurs even in the presence of the residual 2-aminothiazole (**23**) which has been found to be unreactive towards nucleophilic carbon bond formation with hydroxyaldehydes.[60,63]

This addition enables a route forward to overcome the side products (Scheme 3) that could result from the Powner *et al.* synthesis.[43] Importantly, this synthetic contribution also provides a mechanism for the prebiotic selection of natural α-amino acids over the unnatural α,α-di-substituted equivalents (Scheme 5). This leverages the selective crystallisation of the aminal that is accessed *via* 2-aminothiazole with aldehydes but not accessible from ketones. Aminal-

induced crystallisation provides a chemical selectivity for Strecker aldehydes of the natural amino acids from a complex mixture.

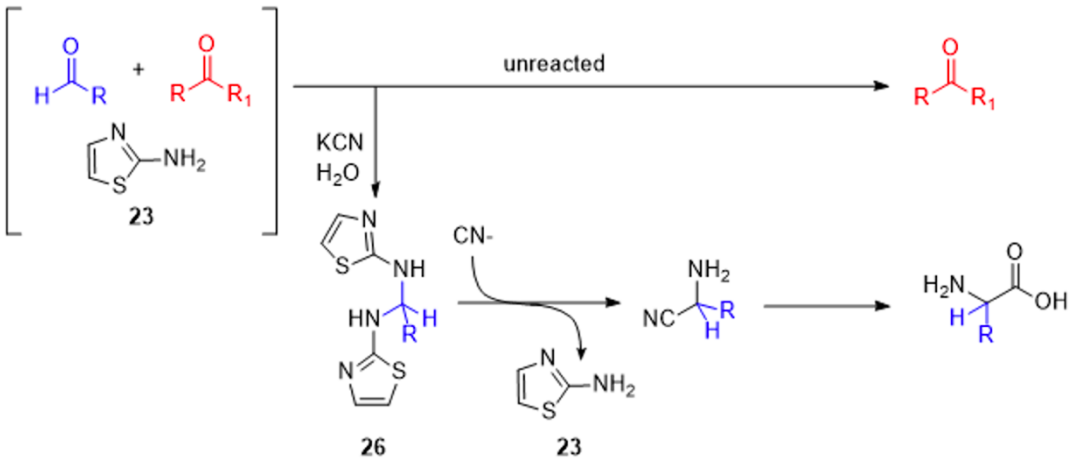

Scheme 5: Aminal-induced crystallisation of Strecker aldehydes (blue) from a mixture of aldehydes and ketones (red). The Strecker aldehyde aminal (**26**) can then react with cyanide to form the aminonitriles and then the proteinogenic amino acids.

1.3.3 Synthesis of Purine Nucleotide Derivatives via Sulfur

So far, one of the remaining targets of Origin of Life studies is a prebiotic route to the purine nucleotides. In 2017 Stairs *et al.* demonstrated a novel prebiotic synthesis of the purine nucleotides, which is prebiotically viable and builds upon the Powner *et al.* synthesis discussed previously (Scheme 6).[64]

Starting with glycolaldehyde (**13**) and thiocyanic acid (**27**) (prebiotically produced from hydrogen cyanide and sulfur)[65] affords 2-thiooxazole (**28**) in high yield (85%). Prebiotic purification of 2-thiooxazole can be achieved by crystallisation directly from water and could be moved and accumulated on the early Earth and transported by sublimation.[66,67] Addition of glyceraldehyde (**14**) then yields the pentose oxazolidinone thiones (**OT**). Again the *ribo*-

oxazolidinone thione (**ROT**) and *arabino*-oxazolidinone thione (**AOT**) are the major stereomers present.[64] The pentose oxazolidinone thiones (**OT**) are also produced in the furanose form, with the exception of *lyxo*se-oxazolidinone thione (**LOT**) which forms a 2:1 mixture of pyranose: furanose. The **OT** undergo activation by reaction with cyanoacetylene (**16**) at the exocyclic sulfur-atom to quantitatively furnish the S-cyanovinyl derivative (**CVOT**).[64] Interestingly, there is then a point of divergence from the pyrimidine and the purine synthesis whereby adding ammonia to the thione **CVOT** leads directly to the aminooxazolines (**AO**) in good yield (45%).

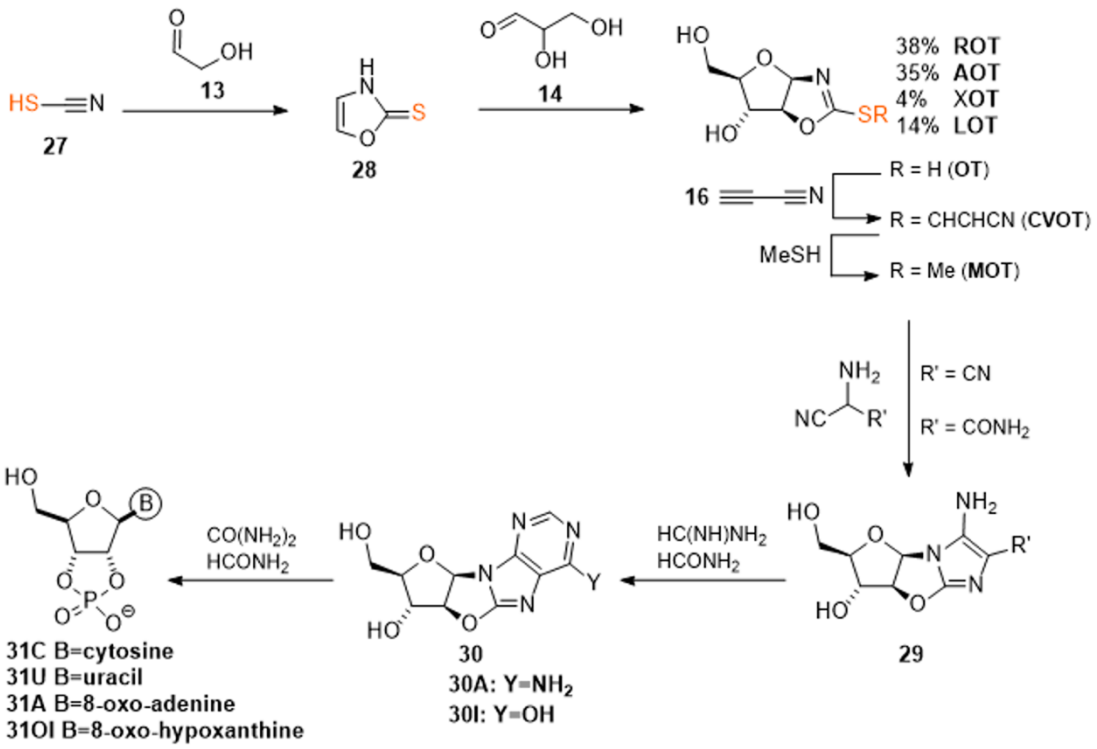

Scheme 6: Prebiotic synthesis of purine nucleotides. Adapted from Stairs et al.

OT can also undergo sequential addition of cyanoacetylene (**16**) and methanethiol to furnish the methyl oxazolidinone thione (**MOT**) in up to 50% yield,[64] which is observed to be more

stable than the S-cyanovinyl thione (**CVOT**).[64] Addition of HCN trimer (R'=CN) to the methyl thione **MOT** followed by cyclisation led to the anhydronucleoside **29**. This can then undergo formylation and urea-mediated phosphorylation to afford 8-oxo-purine nucleotides (**31**). Whilst this neat synthesis does not answer the question of homochirality, it does provide impressive and prebiotically sound routes to access nucleotides.

Roberts *et al.* later described a divergent synthetic route to access Watson-Crick base-pairing *arabino*-furanosyl nucleosides (ANA).[68] The authors demonstrated that sulphur regio-selectively adds into the C8 carbon atom of purines by incubating the substrate with H_2S in water to afford 8-mercaptopurines.[68] Irradiation in water then reduces the purines to afford the arabino-furanosyl nucleosides (ANA) in excellent yield. The methodology was extended to the complete set of canonical nucleosides: A, C, G and U. Given ANA's remarkable qualities as a genetic polymer – namely its participation in RNA phophodiester cleavage; its ability to form helices and stem-looped structures that mimic DNA and RNA respectively; its ability to form Watson-Crick base-paired duplexes and be reverse/transcribed from/to DNA; and it's superior resistance to hydrolysis compared to RNA –make it an excellent candidate for the first such polymer.[69]

Once again, we see inventive routes to prepare genetic polymers from chiral building blocks reported in the literature. Yet still the issue of how homochirality arose in the first instance remains unanswered. It is of course possible that organisms developed based on one handedness whilst others developed based on the other. Due to evolution one of these was selected for different reasons and we ended up with a Last Universal Common Ancestor (LUCA) that was based on single enantiomers. The viability of this options is not known. However, it is also possible that homochirality arose before biology developed.

1.4 Biological Homochirality

Chirality is a property of asymmetry that most commonly results in structures having 'non-superimposable mirror images, as shown in Figure 10. Chirality was first defined by Kelvin in 1893 at a conference of the Oxford University Junior Scientific Club (Kelvin 1904). Homochirality, is when a system contains one of these mirror images, and can be observed throughout the microscopic and also macroscopic worlds – from the stereochemistry of amino acids, through the structure of tissues and organs, to the directionality of cows chewing the cud.[70]

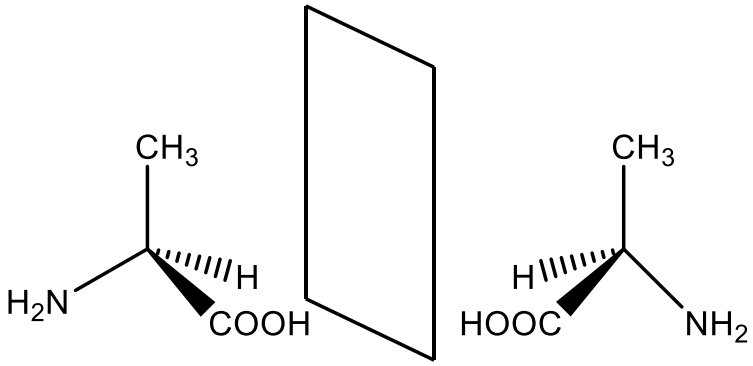

Figure 10: Mirror image enantiomers of the amino acid alanine

The crucial organic molecules associated with life are chiral, they can possess non-superimposable left- (L) or right- (D) handed 3D mirror image structures and are usually optically active (able to rotate the plane of polarised light). In nature, (bar rare exceptions) the amino acid monomers which make up proteins are L, and sugars, like the ribose and 2-deoxyribose monomers found in RNA and DNA, respectively, all exist in the D-configuration.[71] Homochirality of these important monomers is a prerequisite to form the 3D structures of a peptide, or for the catalytic function of enzymes and is essential to establishing the double helix which is present in DNA.

Moreover, homochirality is also essential for the polymerisation of activated mononucleotides which are severely inhibited in racemic conditions (cross chiral inhibition).[72] In the RNA world, non-enzymatic replication is central to the natural progress of selection from random mixtures of oligonucleotides towards something more ordered and complex, so homochirality is therefore also central to the origin of life.[73]

In building up the RNA world, the abiotic synthesis of nucleotides first requires the synthesis of the ribose moiety, and it has been noted that in the reaction with cyanamide it forms the stable bicyclic aminooxazolines that readily crystallise out from complex mixtures.[43] One can therefore envisage that by exploiting this behaviour, if it were possible to break the symmetry of the system to induce an enantiomeric excess, and then amplify that excess crystals, one would gain access to homochiral nucleotides, and therefore homochiral RNA.[74]

1.5 Chirality and Crystallisation

Symmetry breaking describes the process of developing an imbalance between L and D enantiomers in a racemic or prochiral system. This imbalance is typically described as an enantiomeric excess *(ee)* $=\frac{c(D)-c(L)}{c(D)+c(L)}$ where c(D) and c(L) are concentrations of right and left handed molecules, respectively.[75]

The first experimental example of chemical chirality came following Pasteur's famous experiment involving tartaric acid; observing two compounds, the first was obtained from tartar deposited in the containers of fermenting grape juice during wine making.[76] This

material is D-tartaric acid, and it was known at the time that it can rotate the trajectory of a plane of polarised light to the right hand side. The second compound was known to have the same chemical and physical properties, however without optical rotation, and was also found to have the same elemental composition.

Pasteur noted that, while visually inspecting crystals of ammonium sodium tartrate under a microscope, that there were two subtly different types of crystal in the sample, each type was a mirror image of the other. He then proceeded to separate out these crystals into separate batches, re-dissolved them and found that each did possess optical rotation, but in opposite directions. Pasteur correctly noted at this time that chirality was able to occur through a tetrahedral or helical arrangement of atoms. Interestingly, he later noted in his memoir that changing the base from ammonium to calcium resulted in "changes in the composition of the products".[77]

This second compound was, of course, racemic tartaric acid. In 1848 Pasteur found that the sodium ammonium salt of racemic tartaric acid crystallised as a mixture (conglomerates) of non-superimposable mirror images crystals. Fortuitously, he was working with a conglomerate compound, only 5-10% of all currently known organic compounds crystallise as conglomerate crystals.[78] For example, only 2 of the 20 proteinogenic amino acids (threonine and arginine) crystallise as conglomerate crystals.

When a racemate is crystallised, there are three ways in which they may do so: [78]

1. **Conglomerate** – when an enantiomer has a preference to bind with other molecules of the same rather than the opposite enantiomer, a mixture of enantiomerically pure

crystals will form. Approximately only ten percent of known racemic chiral compounds will form conglomerates – Louis Pasteur was very fortunate to have observed the crystallisation of tartaric acid which is one of those compounds.[78]

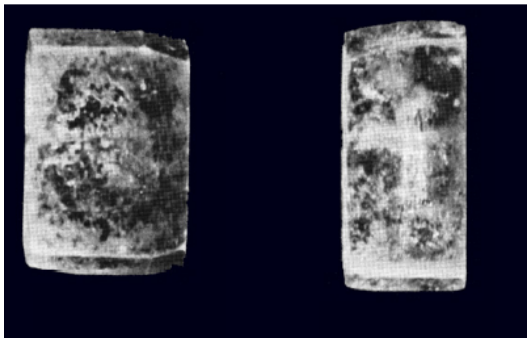

Figure 11: The two enantiomers of ammonium sodium tartrate acid form visibly different conglomerate crystals which Pasteur observed and picked in 1832.[79]

2. **Racemic (true racemate)** – When enantiomers have a higher affinity for molecules of the opposite enantiomer than the same, then they will form racemic crystals in which both enantiomers are present in equal amounts, arranged uniformly throughout the crystal.
3. **Solid solution (also pseudo-racemic)** – When there is a very close affinity between the same and opposite enantiomers, crystals are formed that have a disordered arrangement of molecules throughout.

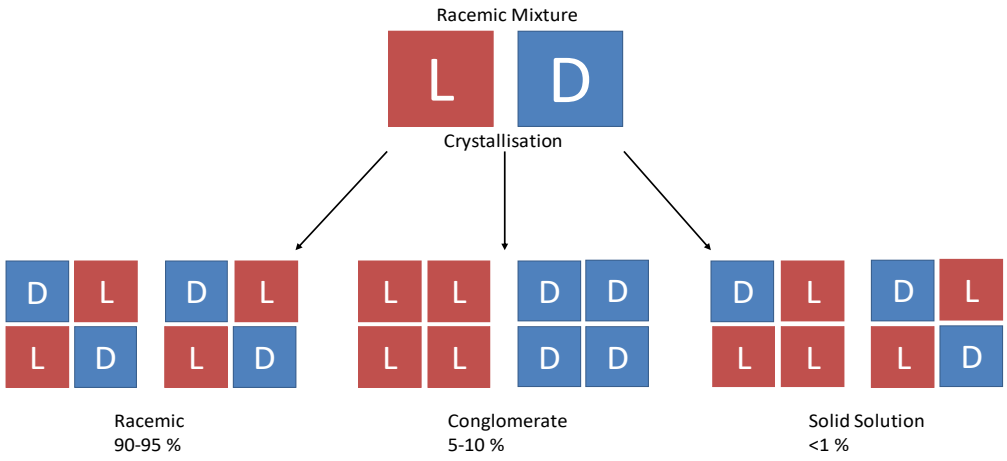

Figure 12: Types of packing of chiral molecules

Whereas 90-95% of compounds form racemic crystals, and approximately 1% of compounds form a solid solution (a random arrangement of each enantiomer within the unit cell) (Figure 12).[80] The way that molecules are arranged in three dimensional space is described by Space Groups.

1.6 Space Groups

When a compound crystallises, the molecules can pack into 230 different space groups, where 65 of them are classified as enantiomorphous, whereby enantiopure molecules will always crystallise into one of these groups. Racemates will crystallise into achiral crystals where the two separate enantiomers will pack into the same crystal where they are associated *via* a glide plane or a centre of inversion. Of the possible 65 chiral space groups, for enantiomers crystallising as conglomerates, the most frequently observed space groups are $P2_12_12_1$ (58 %) and $P2_1$ (30%).[81]

1.7 Prebiotic Building Blocks

Meteorites, specifically carbonaceous chondrites, are some of the earliest solid materials and provide an unique chemical and physical record for the formation of the solar system.[82] The organic content within those meteorites was first characterised in the 1960s.[83] These studies have been found to contain a wide range of hydrocarbons, carboxylic acids, hydroxy acids, amino acids and others. [84] Most amino acids in meteorites exist racemically, however some have shown to vary *ee* within different meteorites. The *ee* value changes significantly for different amino acids and also for the same amino acid in different meteorite samples, even

within the same chondrite.[82] In a section of the Murchison meteorite an *ee* value of 30% was found for L-alanine,[85] however 60% has been found for D-*allo*-isoleucine.[86]

There have been many experiments exploring how molecular single handedness may have emerged that support the earlier theoretical models. These include chemical models such as the Soai autocatalytic reaction, and physical models which will be discussed in this thesis. There is obviously no way of precisely elucidating what happened on the early Earth that led to the life we have present today. What we are able to do, however, is examine experimental and theoretical work that has aimed to explore questions such as: what could serve as the template for a bias of one enantiomer over the other that, given naturally, would have likely been racemic? And how would that bias be maintained and propagated to enable us to observe the single chirality that is present today?

An important first consideration is that, since many organic reactions require the presence of a catalyst, how might the initial prebiotic building blocks have been formed? This is essential to explore when determining what might be deemed to be 'prebiotically reasonable' for everything which follows. Surely in an environment that lacks advanced biological catalysts such as enzymes, then the very first synthesis reactions must have been autocatalytic.

1.8 Autocatalysis

An autocatalytic reaction is one in which the product acts as the catalyst for its own formation (Scheme 7a).[87] Autocatalysis is characterised by the presence of an exponential product/time curve, and additionally by a positive correlation between initial product concentration and reaction rate. This occurs due to the rate of reaction is proportional to the concentration of

the product. Autocatalytic efficiency is often limited, and full exponential growth is not seen. Inefficient systems will be anticipated to show linear growth.

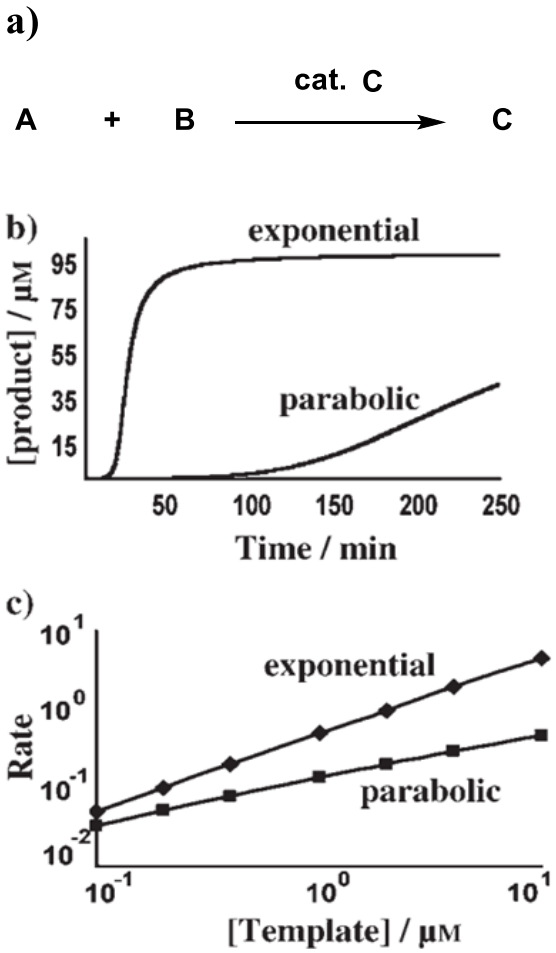

Scheme 7: a) General autocatalytic reaction. A and B react to form C, with C additionally catalysing the formation of more molecules of C. b) Autocatalytic kinetic profiles of parabolic and exponential growth. c) Autocatalytic kinetic log-log plot showing the rate of reaction is proportional to different concentrations. Taken from [88]

1.8.1 The Formose Reaction

A well-known, and prebiotically relevant autocatalytic reaction is the formose reaction, which was discovered in 1861 by Butlerow (Scheme 8).[89] Here, a non-enzymatic chain-condensation reaction of formaldehyde (**32**) takes place at high pH to form a complex mixture of sugars.

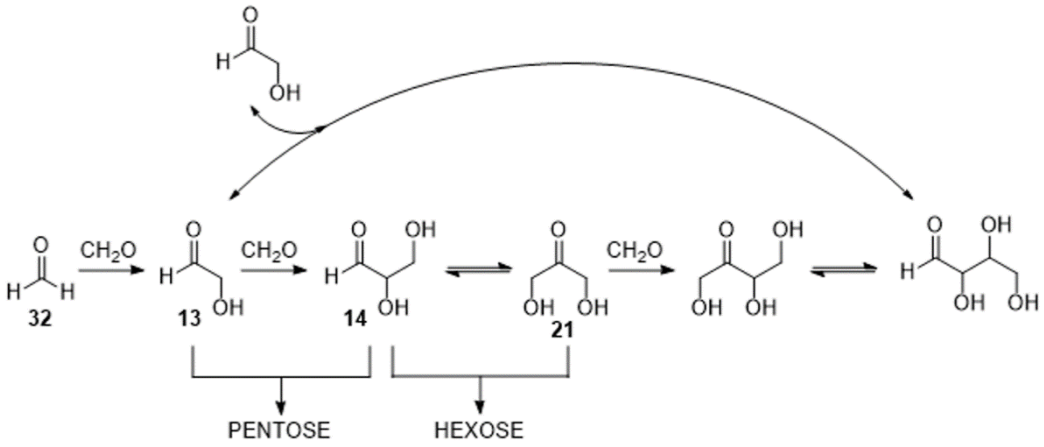

Scheme 8: Initial stages of the Formose reaction. Adapted from Luisi. [90]

This reaction is often quoted as a favoured source of prebiotically available sugars and has been studied at great length under multiple different conditions, catalysts and additives. [39,91–93] It has, however failed to give significant amounts of *ribo*se (key for RNA). This is due to the essential issue that it is an uncontrolled aldol condensation reaction. The first condensation involves reacting two molecules of formaldehyde (**32**) together via an umpolung mechanism which is slow. Once glycolaldehyde (**13**) is present this can react with more formaldehyde to create the three-carbon unit, glyceraldehyde (**14**). These can then come together to create the pentose sugars. However, various isomerisations and retro-aldol cleavage events can take place which can further complicate the mixture, eventually leading to "browning" whereby an intractable polymeric mixture is obtained.[39]

Despite the lack of selectivity, the formose reaction provides a way of building up complexity from simple organic molecules in a prebiotically favourable manner. It has been suggested that through a system involving borate minerals, that stabilisation can be achieved to result in the pentoses and pentuloses.[48] Other prebiotically relevant methods have also been

investigated as a means of improving the selectivity such as the presence of silicates [94] or carrying out the reaction in vesicles.[95]

Breslow has noted that the formose reaction starts by the autocatalytic conversion of formaldehyde to glycolaldehyde (**13**). [96] The diagnosis for the autocatalytic role was confirmed by two key observations; the reaction has a long initiation period where no or little reaction occurs which is then followed by rapid conversion; secondly the lag period can be eliminated by addition of an initiator including the products of the reaction such as glycolaldehyde (**13**). [87] The conversion of formaldehyde to glycolaldehyde (**13**) is thought to proceed *via* a formyl anion, however this has been challenged by Socha *et al.* who demonstrated that small impurities (carbohydrates) naturally present in formaldehyde (**32**) cause the autocatalysis, whereas freshly distilled **32** does not react in a similar fashion.[93] It has been demonstrated, however, that in the presence of minerals (montmorillonite) the freshly distilled **32** could undergo the reaction.[97] Whilst this is still debated it is generally accepted the reaction is initiated by the formyl anion.[90]

Breslow focussed on how an enantiomeric excess could occur in the formose reaction, as without some form of homochiral template, these reactions form racemic products.[98] They successfully demonstrated how L-amino acids can catalyse the formation of D-glyceraldehyde (**D**-**13**) within the formose reaction.[98] Out of the proteinogenic amino acids, only proline gave rise to the unnatural L-glyceraldehyde (**L**-**13**). This was later confirmed by Blackmond in an unrelated study into asymmetric catalysis by amino acids on α-amination of aldehydes.[99] Proline was once again found to produce to the opposite result in the presence of organic bases. But if carried out in the presence of $Bu_4N^+OAc^-$ it resulted in the natural D-

glyceraldehyde (**D-13**) (Scheme 9). It was therefore suggested the alkalinity of the environment plays an important role in the stereochemical outcome.[100]

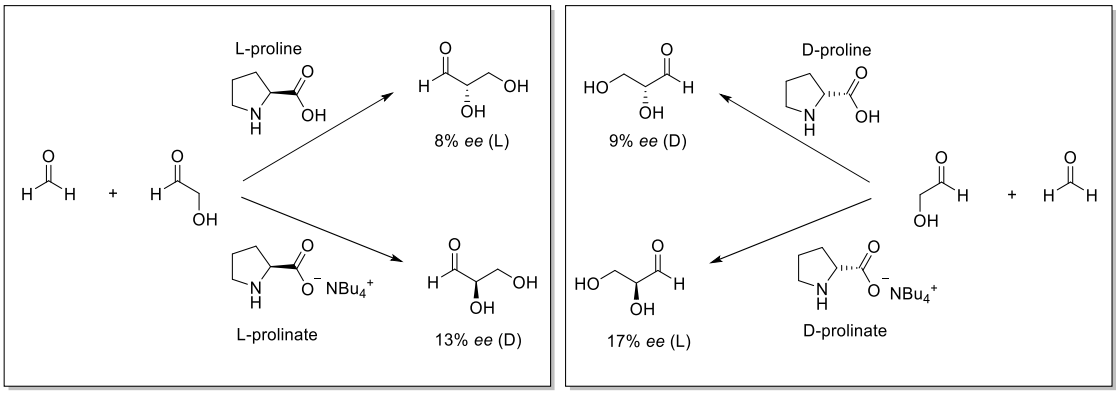

Scheme 9: Gaining enantiomeric excess of glyceraldehyde through the formose reaction in the presence of proline and prolinate catalysts.

1.8.2 The Frank Model

Autocatalysis has been theorised as having a role in the origin of biological homochirality. Sixty-five years ago, Frank developed a theoretical model for the evolution of homochirality using an asymmetric autocatalytic reaction mechanism.[101] Schematically, this is shown in Figure 13.[102] In this mechanism, a chiral product acts as the chiral catalyst needed for its production, and simultaneously acts to minimise the synthesis of the opposite enantiomer. This results in the development of an enantiopure molecule from a near-racemic mixture. This process is also advantageous as there is no separation required for the catalyst and product. In the final sentence of this noteworthy paper, it was stated: "A laboratory demonstration may not be impossible." [102]

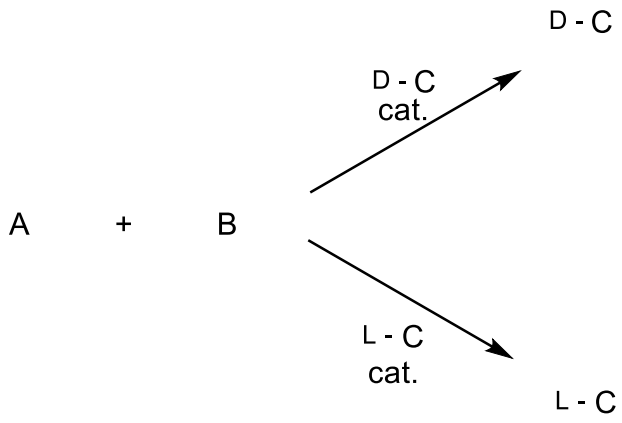

Figure 13: Franks proposed asymmetric autocatalytic reaction. A and B are achiral and D-C and L-C are chiral products and act as chiral catalysts[103]

Franks model predicts that an enantiomer of the same handedness can self-replicate, and opposite enantiomers show mutual antagonism; they "deactivate" each other, and so cannot continue to replicate. Therefore, if an initial imbalance of enantiomers is present, this can lead to amplification over time. It is also assumed that at every "cycle" a pair will be selected for mutual antagonism, which will lead them to become deactivated. Moreover, each remaining enantiomer will also self-replicate leading to the amplification. However, the smaller the initial imbalance, the greater number of substrates are lost in the deactivation process before significant enrichment is achieved. But, if the substrate pool is large enough, and the process keeps occurring, the selectivity of the autocatalytic production of one enantiomer will eventually prevail.

Franks model is best represented diagrammatically (Figure 14), in a scenario where a small group of D and L enantiomers exist in an unlimited pool of substrate molecules. At the top left of Figure 14 an initial imbalance of L:D of 3:2 or 20% *ee*. Within this system, one L:D pair is selected for mutual antagonism, while the remaining molecules (2L:1D) will self-replicate. This

results in 4L:2D, which translates to an *ee* value of 33%. Repetition of the self-replication and mutual antagonism process leads to 50% *ee*, and 67% *ee* over two cycles.[75] This simple model provides an insight into how self-replication and inhibition are a possible means to homochirality, however it does not provide any mechanical understanding of how this would occur.

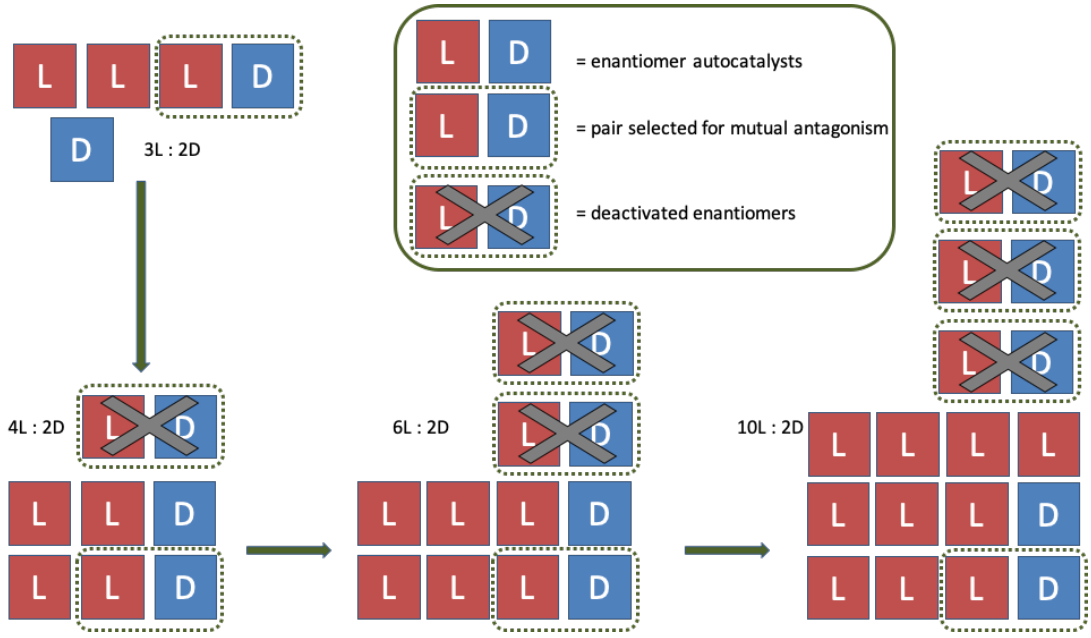

Figure 14: Illustration of the Frank model for the evolution of homochirality using autocatalytic replication and mutual antagonism (redrawn).48 Asymmetric amplification is achieved; 20% ee, 33% ee, 50% ee, 67% ee.

1.8.3 The Soai Reaction

In 1990 Soai and co-workers demonstrated an asymmetric autocatalytic reaction that gave the first experimental proof-of-concept that enantiomeric amplification could be achieved from a small imbalance of enantiomers using autocatalysis.[104] Soai described the autocatalytic alkylation of pyrimidyl aldehydes with dialkyzincs (Scheme 10). The reaction of the aldehyde (**33**) with $Zn(iPr)_2$ (**34**) led to high enantiomeric excess in the product (**35**) and low *ee* of the

catalyst. The rate of reaction is increased through addition of catalytic amounts of the product.[105]

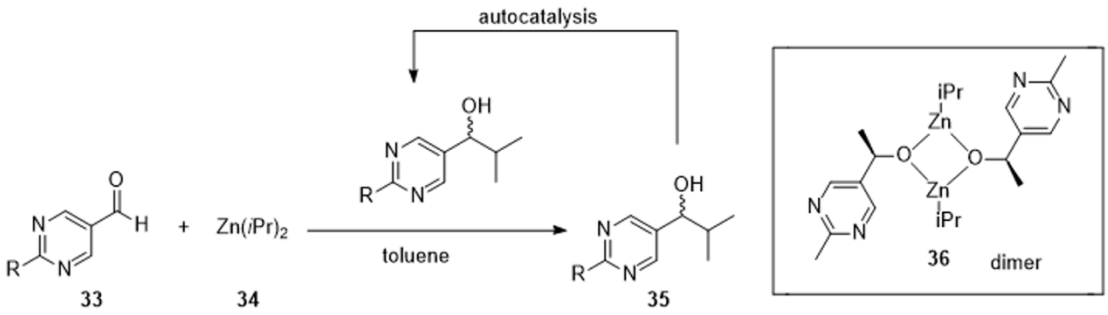

Scheme 10: The Soai autocatalytic reaction

Initially studies involved changing the alkylating agent and including a wider scope of substrates such as chiral diols,[106] ferrocene derivatives, [107] and nicotinamides.[108] The most effective substrates were shown to be 2-alkynyl-5-pyrimidly alcohols when alkylated using diisopropyl zinc.

Beyond these investigations, the reaction was shown to be easily manipulated by subtle sources of chirality. As it only requires a small initial imbalance that stems from a very small *ee* catalyst, and will lead to high product *ee* values.[109] A particularly notable example of this is achieved from chiral molecules based upon 5-pyrimidyl alkanols (**37**) that act as an initial catalyst with *ee* of 0.00001 % to a final product (**39**) *ee* of >99.5% over three rounds (Scheme 11).[109]

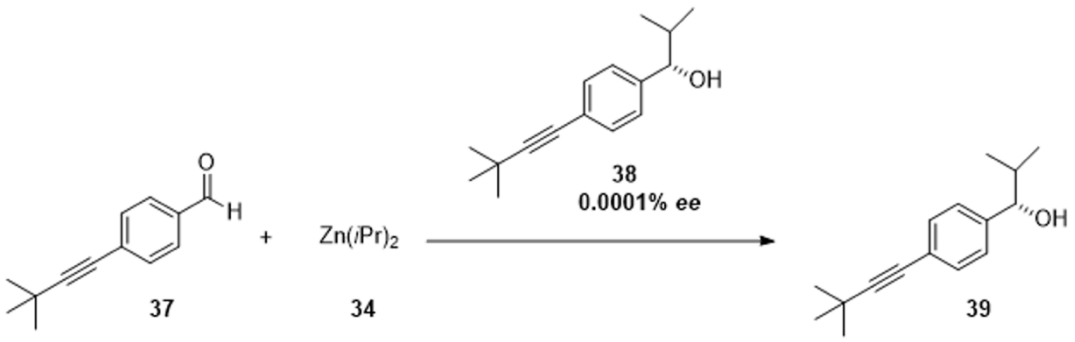

Scheme 11: Notable example of the Soai reaction achieving amplification from a very small initial ee value (0.0001%)

Amplification can also be achieved through different chiral initiators such as circularly polarised light, or even chiral solids such as quartz.[110,111] It has also been demonstrated that the small energy difference between ^{13}C and ^{12}C can be amplified to result in enantiomeric amplification over repeated autocatalytic cycles.[112] This can also be achieved through substituting other isotopically chiral molecules (oxygen and hydrogen) which leads to directed chirality over many autocatalytic cycles.[113,114]

Blackmond, Brown and co-workers conducted the first mechanistic studies on the Soai reaction using NMR, computational work, and in-situ kinetic studies.[105,115–118] The Soai reaction follows the Frank model as the product is compelled to dimerise, which forms equal amounts of hetero- and homo- chiral dimers (**36**) (Scheme 10).[119] The homochiral derivatives are active catalysts, which can participate in the autocatalytic cycle, whereas the heterochiral species are inactive. This enables mutual antagonism to occur. Amplification of *ee* can only be achieved if there is a way to reduce the activity of the undesired enantiomer, which the Soai reaction achieves.[120] Blackmond further mathematically demonstrates how the inhibition within the Frank model is key to gain the amplification.[121]

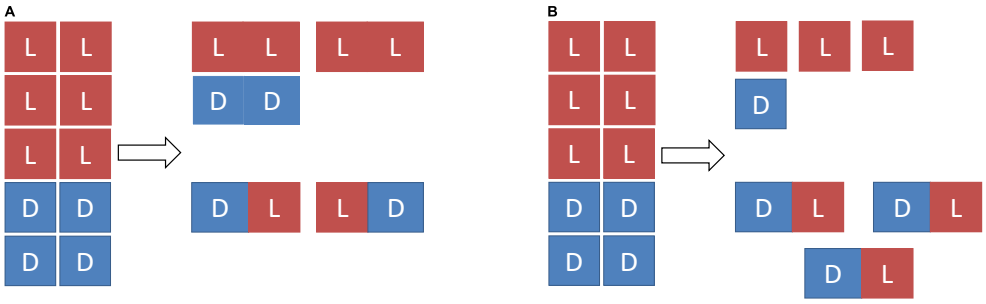

Figure 15: A - amplification of active dimers whereby the homochiral dimers have higher reactivity than racemic dimers. B - monomers act as catalysts where the racemic dimers are able to act as a non-reactive reservoir.

More recently, the importance of the initially suggested higher-order oligomer structures for the asymmetric amplification and spontaneous symmetry breaking to occur in the Soai reaction has been revealed and confirmed by using single crystal X-ray diffraction analysis.[122,123] Earlier NMR studies suggested an equilibrium between homochiral and racemic square dimers, which has been further confirmed by more detailed kinetics studies whereby the reaction shows the dimers are able to act as an active catalyst rather than acting as a non-reactive reservoir (Figure 15). This was crystallised as both the racemic and the enantiopure compound. A tetrameric structure forms whereby two zinc alkoxides form a square dimer that are bridged by a pyrimidine ring that is coordinated to the alkoxide Zn atom to form the 12 membered macrocycle (Figure 16).[124]

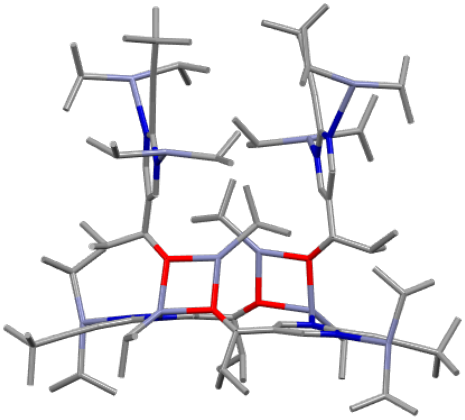

Figure 16: Single X-ray crystal structure found by Matsumo et al.[125]

It was later argued by Singleton and Vo that the initial symmetry-breaking of the Soai reaction was not a true example of asymmetric synthesis.[126] Trace amounts of chiral impurities present in the Soai reaction resulted from toluene and benzene which was due to solvent choice.[126,127] This result is important to the theory behind biological homochirality, since these traces of optical impurities from the solvent led to a single chiral state. Initial optical activity could have arisen from a range sources - such as circularly polarised light, meteorites, or random chance - it follows then that biological homochirality could be no more than statistical inevitability rather than a biological invention, or the product of something bigger.[86,128,129]

The Soai reaction has been of particular interest over many years, a particularly insightful mini-review analysing further studies into the Soai reaction through influence of the reaction parameters such as; chiral induction methods or even no chiral source, the amount of catalyst, the solvent and finally the reaction temperature are described by Gehring *et. al*. [130] This reaction has been shown to have a limited substrate tolerance and a narrow scope of reaction conditions, which prohibits its application to different, prebiotically relevant mechanisms.

1.8.4 Mannich and Aldol Reactions

The Mannich reaction has been speculated as a route to gain access to asymmetric autocatalytic reactions that is prebiotically plausible, unlike the Soai reaction.[87] A simple asymmetric autocatalytic Mannich reaction was used to demonstrate how an external catalyst could be used to affect the absolute configuration of the product (Scheme 12). [131,132] It was found that the product *ee* and catalyst *ee* were directly proportional, meaning the enantioselectivity of the reaction is comparable to what is obtained when an external catalyst such as proline is used.[131] A template directed mechanism has been put forward as one of the possible mechanisms due to the chiral product preferentially catalysing the formation of new product molecules but this has been highly debated.[132–135]

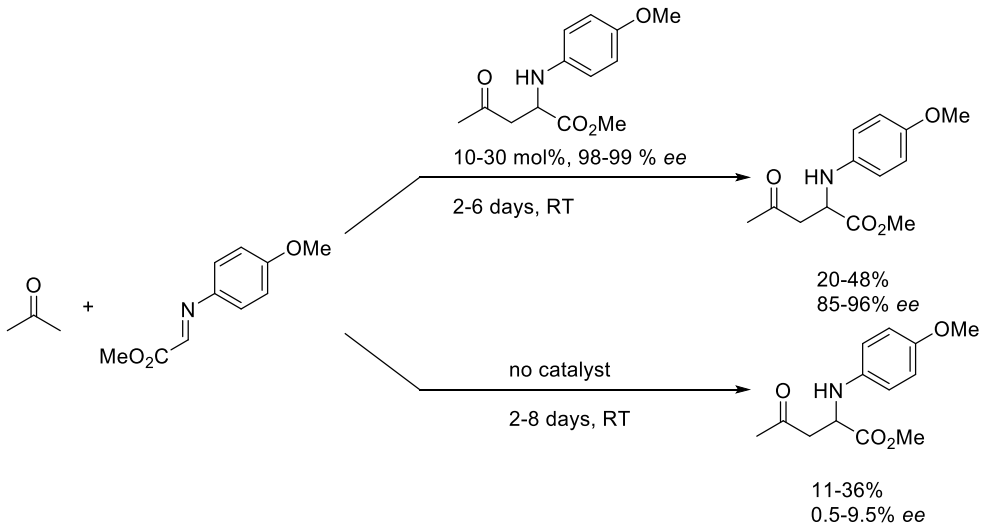

Scheme 12: Tsogoeva asymmetric autocatalytic Mannich reaction. Redrawn from ref.[132]

Whilst the Soai reaction serves as an elegant mechanism for the emergence of homochirality, the reaction uses dialkyl zinc chemistry that requires an inert atmosphere and is not able to take place in aqueous solvents. This obviously limits the prebiotic relevance; however the Mannich reaction can address this, particularly by proceeding in the presence of water as

demonstrated by Amedjkouh and Brandberg (Scheme 13).[136] The reaction showed good diastereo- and enantiosectivity showing modest *ee*'s (47%).

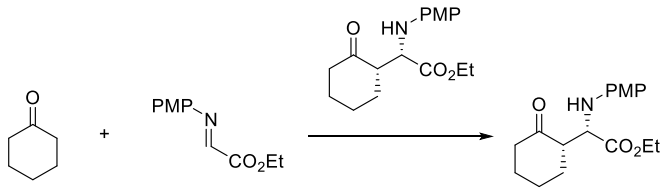

Scheme 13: Amedjkouh and Brandberg Mannich reaction

1.8.5 Asymmetric Autocatalysis Initiators

There is strong evidence of strong circularly polarized light (CPL) in the infrared region of the star formation area of the Orion nebula.[137] It has been demonstrated that CPL can be left (L-) or right (R-) handed which has been used to induce *ee* in different chiral compounds.[138–140] However it has often been found that the *ee* induced is too small to lead to enantioenrichment in compounds relevant to the origin of life. For example; the use of CPL on racemic leucine only induces an *ee* of 2%.[141]

Recently, an example has been reported whereby an organic compound is significantly enantioenriched through asymmetric photodegradation followed by asymmetric autocatalysis. What's more, it takes place by employing the inherent chirality of CPL leading to high final *ee*'s (Scheme 14).[124]

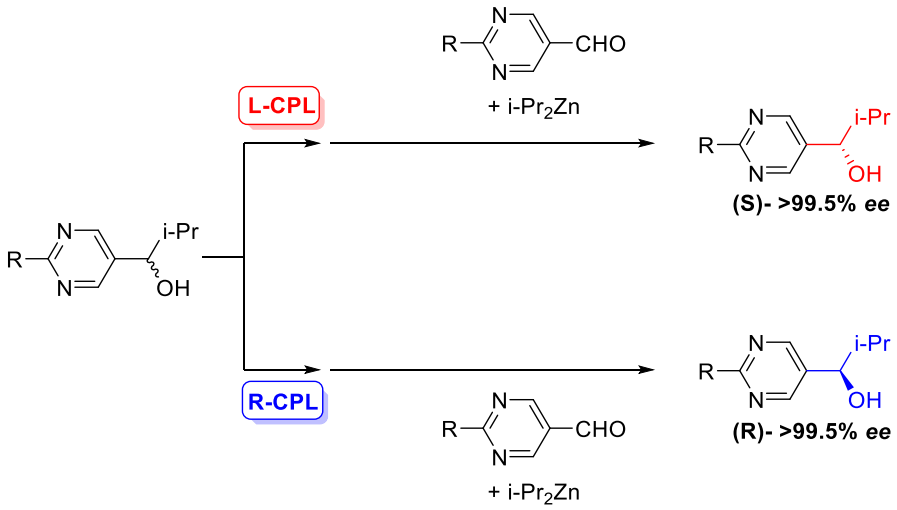

Scheme 14: Asymmetric autocatalysis initiated by irradiation with CPL. Redrawn from[124]

Asymmetric autocatalysis resulting in high enantiomeric purity has also been demonstrated using enantioenriched proteinogenic amino acids as the inducing agent.[142,143] Alanine has been used to induce the production of the alkanol in high *ee* values (92%) even when the *ee* of the initiator was as low as 1% or even 0.1% (Scheme 15).[143] Amino acids have been detected in meteorites, often with enantiomeric enrichment, therefore if a method to gain enantiomeric amplification could be found, these amino acids could provide an understanding towards the origin of homochirality.[144–146]

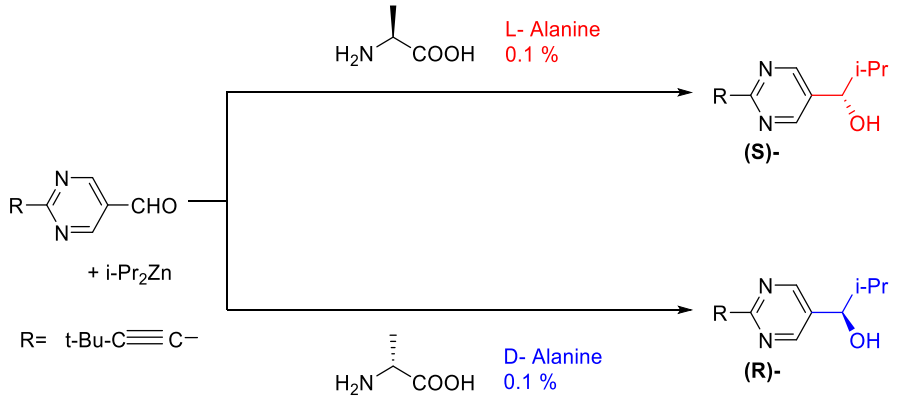

Scheme 15: Alanine induced asymmetric autocatalysis to lead to high ee values (94%).

Chiral isotopomers arising from carbon isotope substitution can be an initiator for asymmetric autocatalysis. Various prebiotically relevant amino acids have been focused on in the literature, including the simplest achiral α-amino acid, glycine which has been detected in the coma of a comet.[147,148] Additionally α-methylalanine, L-enriched methyl subsitituted amino acids were detected in meteorites as deuterium enriched forms.[144,149] As shown in Scheme 16 chiral meteoritic amino acids have been used as an approach towards the extra-terrestrial origin of homochirality.[113,114,144,150–152] More recently, Blackmond *et al*. have investigated the Soai mechanism and the role of chiral initiators that are enantiomeric only due to an isotope.[153,154] These studies found that when any given chiral directing force is large enough to overcome the stochastic noise, the Soai reaction is able to enter its autocatalytic nature to lead to enantiomeric excess.[154]

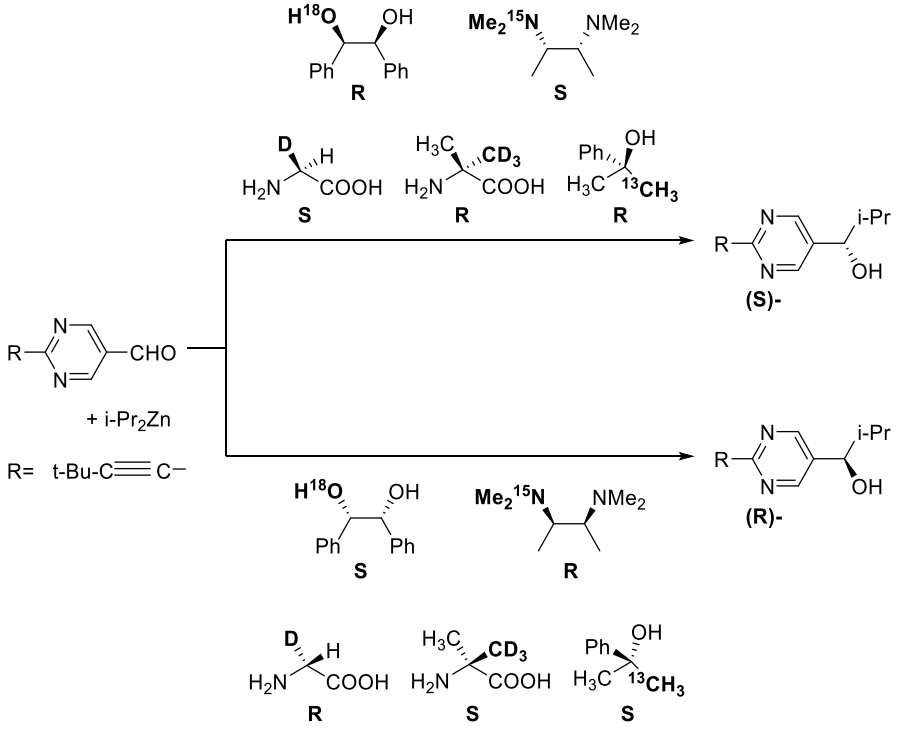

Scheme 16: Asymmetric autocatalysis initiated by chiral isotopomers of hydrogen (H/D), carbon ($^{12}C/^{13}C$), nitrogen ($^{14}N/^{15}N$) and oxygen ($^{16}O/^{18}O$) substitution. Redrawn.[124]

Nucleobases are theorised to have been synthesised on the early Earth from hydrogen cyanide and cyanoacetylene.[155,156] One of those nucleobases adenine, has been successfully isolated from meteorites and there are routes to gain access to such compounds. As such, they have been investigated based on their crystal chirality.[157–159] Cytosine crystallises from methanol forming chiral conglomerate crystals with space group $P2_12_12_1$ later confirmed by circular dichroism (CD) spectra.[160] These chiral crystals of cytosine spontaneously form from achiral cytosine affording enantioenriched crystals when stirring takes place during crystallisation.[161] Furthermore it has been shown that under vacuum and thermal conditions cytosine monohydrate crystals form enantiomerically pure anhydrous cytosine polycrystalline powder.[162,163] It has been demonstrated that through using this method to gain access to the enantioenriched crystals, that achiral cytosine is able to act as a chiral initiator for asymmetric autocatalysis with amplification of chirality to lead to a near enantiopure compound.[162]

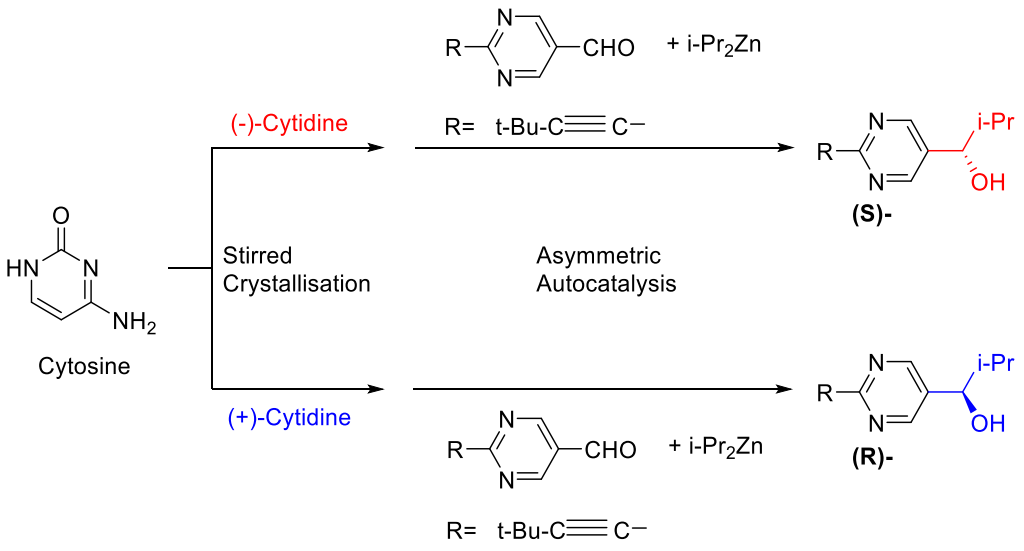

Scheme 17: Stirred crystallisation of cytidine leading to formation of enantiomorphs of cytidine crystal, followed by highly enantioselective asymmetric autocatalysis.

A similar phenomenon has also been observed when crystallisation of adenine in nitric acid leads to adeninium dinitrate (adenine.2HNO_3) in pure enantiomeric space group of $P2_12_12_1$.[164]

Early on, Pasteur hypothesised that the Earthly magnetic field may have induced the emergence of early chiral biopolymers, which led him to perform many (unsuccessful) reactions under the influence of a strong magnetic field.[165] Barron noted that the symmetry requirements for an enantioselective result induced by magnetic fields *per se* is not allowed.[166] Kelvin stated that "the magnetic rotation alone has neither left handed nor right handed quality" and de Gennes demonstrated that even in an electric field and a magnetic field, there is no observation of induced asymmetry, as hypothesised by Curie.[167–169] However, there has been some progress in the form of the magnetochiral anisotropy effect, which is seen through a specific spin interaction and not by a magnetic field *per se*.[170,171] This concept is founded on the observation that charge polarisation in chiral molecules is also accompanied by spin polarisation. This is promoted further by the polarised spin of a chiral molecule which is able to interact enantiospecifically with ferromagnets that have their spin aligned perpendicular to their surface.[172,173] Again, it is not the magnetic field that induces this interaction, but the interaction between electrons in the substrate and those in the molecule *via* the electron spin exchange reaction. Enantiospecific crystallisation of three amino acids have been induced by ferromagnetic substances.[174] The amino acids chosen were three amino acids known to crystallise as conglomerates: asparagine (Asn); glutamic acid hydrochloride (Glu.HCl); and threonine (Thr).[174,175] Control experiments ruled out the possibility of statistical fluctuations etc. Various ferromagnetic substances were used such as gold on Ni-coated silicon to create a ferromagnetic layer, as shown in Figure 17 (Left). A proposed mechanism for how enantioselective crystallisation is induced by ferromagnets is shown on the right-hand side in Figure 17. When a chiral molecule is in proximity to the ferromagnetic surface, charge polarisation occurs, accompanied by spin polarisation. The attractive interaction is strongest when the spin of the ferromagnetic substance is antiparallel to the spin within the chiral

molecule. This therefore allows the chiral molecule to have greater residence time at the magnetic site and therefore a probability of crystallisation.

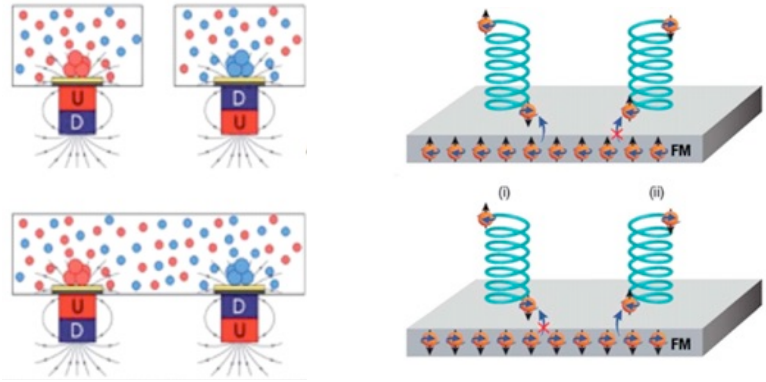

Figure 17: Blue (South), Red (North). Left: (Top) A magnet positioned with North up or down is positioned underneath a ferromagnetic substance.). (Bottom) The magnets are placed in a racemic mixture of the chiral molecules. Right: Proposed mechanism for enantiospecific crystallisation.[174]

1.9 Eutectic Model

An alternative to Franks model is to consider the phase behaviour of chiral molecules, in particular crystal–solution eutectic systems. The eutectic composition of a compound is determined through partially dissolving a compound in water, where the Gibbs phase rule states that the solution composition at the equilibrium is fixed at the eutectic point. The equilibrium that is established between crystal and solution provides a basis for a system similar to selective partitioning between solids and gases using sublimation.

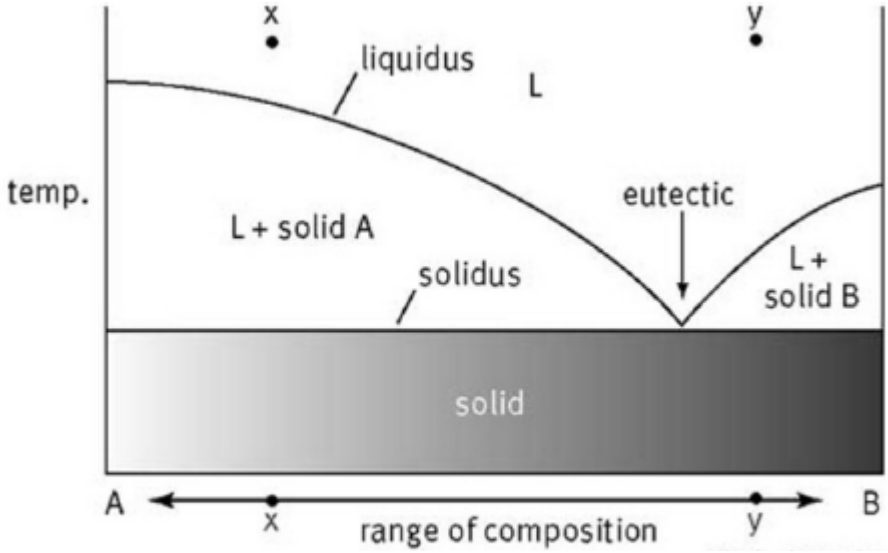

Figure 18: A phase diagram for two compounds exhibiting in a eutectic system.[176]

As discussed in Section 1.5, chiral molecules that preferentially crystallise as single enantiomer crystals are called conglomerates. These form when homochiral intermolecular interactions are stronger than heterochiral interactions, i.e. L-L or D-D has stronger crystal lattice energy than L-D. Whether a crystal forms as a racemic crystal or a conglomerate is a property of the substrate at a given pressure and temperature.[100] One interesting physical property of conglomerates is that they exhibit significantly higher solubility compared to a racemic crystal containing both enantiomers.[177] This is referred to as Meyerhoffer's double solubility rule that was first established over a century ago.[178] When either a conglomerate or racemic crystal forms, at equilibrium, the composition of the solution phase at a certain temperature and pressure is called its eutectic point.[68] This point obeys the Gibbs phase rule, and may have an *ee* value between 0-100%.[179] For conglomerates with equal numbers of D and L present in the solution, the ee^{eut} is 0, and for a racemic crystal it will result in a non-zero ee^{eut}.[75]

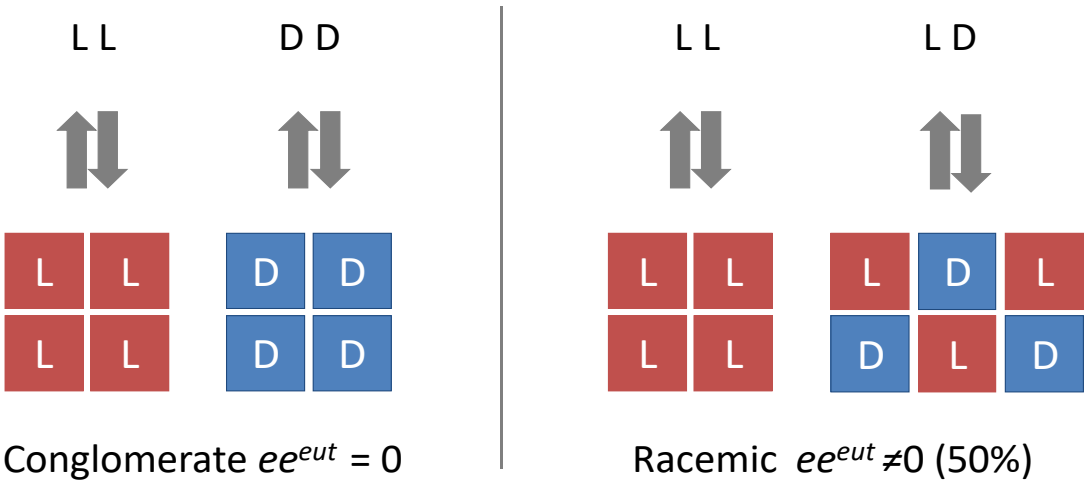

Figure 19: Coloured boxes represent solid state crystals, letters represent solution state molecules. Left: conglomerate. Right: racemic crystal system with an excess of L present.

This is explained by using Meyerhoffers double solubility rule.[180] Conglomerate crystals, whether that be a L crystal or a D crystal have the same solubility, so at equilibrium the solution phase will contain equal numbers of L and D.[180] This remains to be true even when there are unequal numbers of L and D crystals present (**Error! Reference source not found.**).[75] For a racemic compound, where there are different numbers of L and D crystals, 1:1 L:D crystals will form favourably, until all the minor enantiomer is used up. The remaining excess homochiral crystals of the major enantiomer will form. The racemic crystal will then give equal numbers of each enantiomer to the solution phase, as will the homochiral crystal.[75] This is only achieved per the solubility of each crystal. This leads to an overall enrichment in solution of the major enantiomer.

This method has been demonstrated as a useful model for explaining the origin of biological homochirality as it allows us to gain solution-phase enantioenrichment of amino acids.[181] Employing a solution containing different amounts of enantiopure L and D molecules, an equilibrium shown in **Error! Reference source not found.** arises. The minor enantiomer is then

only present in the solution-phase to the degree that it can dissolve from the L:D crystal. It follows that if the solubility of the L:D crystal is adjusted so that it is lower than the homochiral crystal, then the minor enantiomer will become "trapped" in the solid phase, while the solution phase results in a higher *ee* from the homochiral crystal dissolving.[75] Therefore tuning the eutectic point would lead to enantioenrichment in the solution phase. The prebiotic importance of these results is remarkable due to further studies suggesting that cycles of rain and evaporation could lead to pools where the solid-solution phase equilibrium can be produced.[182]

In 1969 Morowitz noted that enantioenrichment in solution is controlled by the thermodynamics of chiral compounds that form relatively insoluble L:D crystals.[183] This theory has been extended by researchers such as Blackmond and Breslow who have reported high eutectic *ee* values for amino acids and biologically relevant nucleosides.[181,184,185]

Blackmond noted that a few of the proteinogenic amino acids form fairly insoluble L:D crystals which implies that the solutions have high eutectic *ee* values.[181] It was observed that under solid-solution equilibrium, serine exhibited a >99% ee^{eut} meaning that from a nearly racemic sample, an almost fully enantiopure solution can be observed.[181] Whilst this provides a basis to gain access to enantiopure solutions, this relies on the compounds high ee^{eut}, which is not always possible, for example valine has a relatively low ee^{eut} of 47%.[181] However, there has been exciting new work within the area which reports that *via* hydrogen bonding, a selection of small, achiral molecules can be added to the solid state in order to "tune" the ee^{eut} of amino acids, even when they have a low ee^{eut}.[186] When these newly–incorporated co-solvate molecules are added, the solubility of the L:D crystal is reduced relative to the enantiopure crystal. This leads to solution enantioenrichment (**Error! Reference source not found.**).

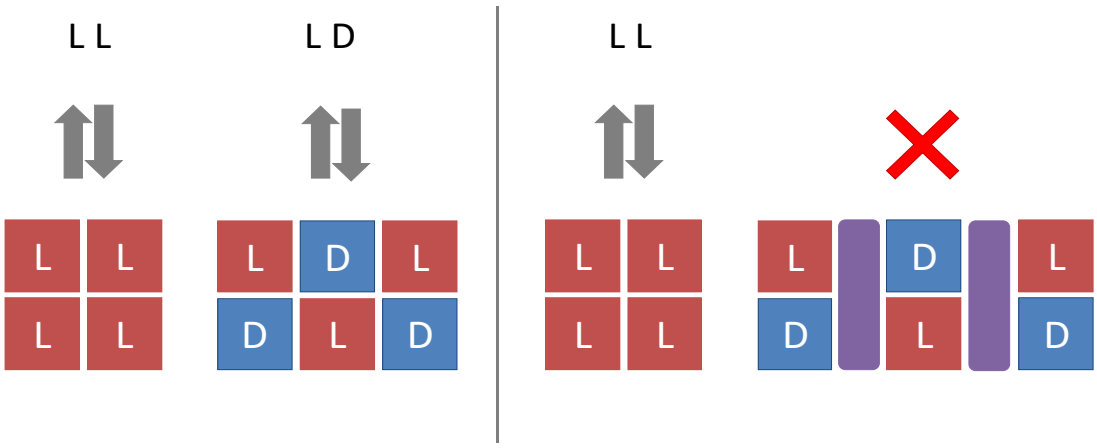

Figure 20:Left- equilibrium that arises when slight initial imbalance. Right: Tuning the eutectic ee by adding a co-solvate molecule (purple) that reduces the solubility of the L:D crystal.

Blackmond has shown that the eutectic composition of chiral amino acids can be tuned using achiral dicarboxylic acids which co-crystallise leading to solution enrichment of up to 98% *ee.*[186] Here co-crystallization occurs when two or more different molecules aggregate to form a single homogeneous crystal lattice *via* non-covalent bonds.[187]

The dicarboxylic acids that were screened are of prebiotic relevance such as; oxalic acid, malonic acid, succinic acid, fumaric acid and maleic acid etc. It was mentioned that urea, thiourea or any of the heterocyclic bases did not have any effect on the amino acid ee^{eut}.[186] One of the biggest enhancements occurs with valine (natural ee^{eut}=47%) and fumaric acid where it rises to 99% *ee*.[186] The cocrystal is formed using hydrogen bonding between valine and fumaric acid (2:1 ratio). It was further demonstrated that through an incorporation of a molecule of $CHCl_3$ into the proline crystal lattice, the ee^{eut} rises from 47% to 88%.[181] These solutions outline themselves as viable candidates to act as the asymmetric catalysts or building blocks for homochiral complex systems, forming the basis of biochemistry.

1.9.1 Comparing the Eutectic Model and Asymmetric Autocatalysis

Asymmetric autocatalysis described by the Frank model differs from the eutectic model in several ways.[188] Firstly, whilst the "mutual antagonism" phase of the Frank model could be comparable to formation of less soluble heterochiral crystals as described by the eutectic model, this is not the case. This is because the eutectic model does not provide a way to increase the major enantiomer as seen in asymmetric autocatalysis. In the eutectic model, the maximum amount of amplification is controlled by that specific molecules eutectic value, which is key property of that substance. For example, amino acids such as isoleucine, proline and alanine show maximum solution *ee* values of 50-60%.[181] This is seen in a select number of amino acids.[181] That is different compared to asymmetric autocatalysis for which, over many cycles, the *ee* can increase exponentially.[101]

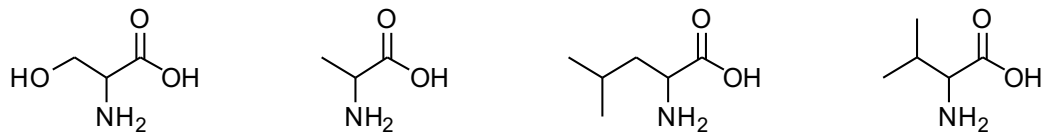

Ser ee^{eut}>99% **Ala** ee^{eut}=60% **Leu** ee^{eut}=87% **Val** ee^{eut}=46%

Figure 21: A few amino acid eutectic ee values shown by their structure and three letter code.

1.10 Conglomerate Formation from Achiral Molecules Leading to Enantioenrichment in the Solid Phase

1.10.1 Eve Crystal Enantioenrichment

It has been known for over a century that some achiral compounds crystallise as conglomerates. Further, achiral compounds can crystallise in polar (chiral) space groups. In such structures the compound remains achiral but exhibits crystal structures that lack a centre

of symmetry or a mirror plane. In the late 19th century, Kipping and Pope reported the crystallisation of $NaClO_3$.[189] They found that it crystallises as separate chiral solids, which form rectangular prisms with the cubic chiral space group $P2_13$.[190] This work was then repeated by Kondepudi who counted 525 crystals to show that there was the expected 50:50 distribution.[191] Kondepudi then showed that a supersaturated solution could be stirred vigorously to lead to one enantiomer being formed (Figure 22).[191] When the solution is not stirred, the first crystal formed has an equal chance of being either hand. However, upon stirring, the first crystal formed "Eve" (primary nucleation) is smashed by the stirring blade into smaller crystals of the same enantiomer. This increases the surface area where the same enantiomer can nucleate on the Eve crystal before another is formed (secondary nucleation).[190] Eve crystals of the opposite enantiomer are not able to form as there is a decrease in solution concentration as more L crystals add to the L "Eve" crystal.[190] Over time, this leads to a single chiral solid state (99% *ee*) which requires no pre-existing chiral imbalance.[119]

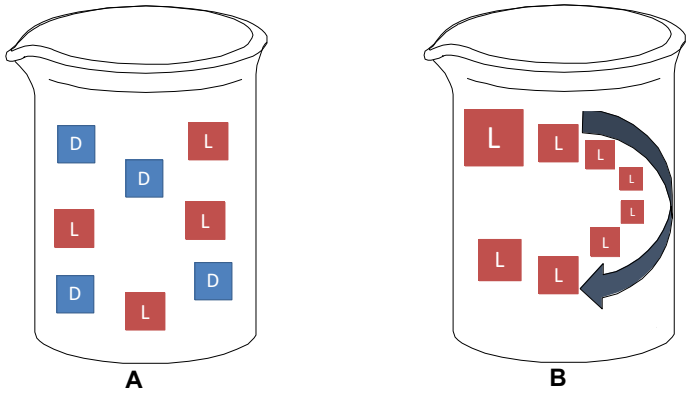

Figure 22: A- Kondepudi experiment with no stirring, equal quantities of D and L crystal are produced. B- With rapid stirring, crystals form from fragments of the Eve crystal leading to enrichment of one enantiomer (redrawn)32

1.10.2 Viedma Ripening

The $NaClO_3$ system has been the focus of another remarkable finding by Viedma, eponymously referred to as Viedma Ripening.[192] It is important to remember that $NaClO_3$ crystallises as two chiral crystals (conglomerates), however in solution $NaClO_3$ is achiral as it exists as ions or clusters that lack chirality.[192] Viedma stirred saturated solutions of equal numbers of L and D crystals of $NaClO_3$ in the presence of glass beads, which led to the system forming one single enantiomeric solid (Figure 23).[192]

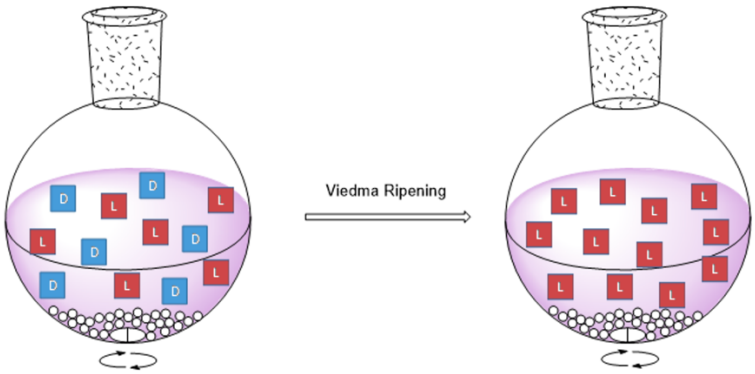

Figure 23: Viedma Ripening

Without stirring, the system is at equilibrium and no new crystals would nucleate. However, when the glass beads are added, this provides energy to the system due to the greater agitation of the crystals as they are stirred. Viedma postulated that the increased attrition of the crystals exaggerated both the dissolution and crystallisation which naturally occurs in any dynamic solid-solution system.[193] The Gibbs–Thomson rule states that larger crystals grow more readily than smaller ones, and that larger crystals do not dissolve as easily as small ones.[194] Smaller crystals are able to dissolve faster than the larger ones due to the surface-volume ratio being relatively high, and therefore the surface energy is also high. Stirring with glass beads creates a greater number of smaller crystals which can dissolve more easily, leading to a slight supersaturation in the solution. This supersaturation is not enough to lead

to new crystals being formed through primary nucleation, however the solid-solution equilibrium responds by increasing the rate of production of solution-phase $NaClO_3$ attaching to existing crystals.[193] This eventually leads to an overall increase of one enantiomer as shown in Figure 23. This method is reliable because a single enantiomer is created without an initial *ee*, which suggests that the random fluctuations in the crystal composition are enough to lead to a break in symmetry.[195]

It has been remarked that whilst the process is very straightforward to perform at the bench, the underlying mechanism is much more complicated.[191] Many computational models have been used to elucidate what is occurring in the flask, which have been distilled into four key processes by Kondepudi et al.[191]

1. Racemisation in solution – For it to be possible for solid enantiomers to interconvert in solution they must continually racemise in solution. It is unlikely that clusters of a single enantiomer will encounter other clusters of the same enantiomer and will therefore re-dissolve more readily. Therefore, the solution is enriched with the enantiomer that has not crystallised out of solution, and then racemises to redress the balance, and the crystals receive a supply of their own enantiomer, allowing them to grow. This continually removes material from solution.
2. Ostwald Ripening – Larger crystals grow at the expense of the growth rate of smaller crystals which will eventually re-dissolve. This allows the crystals to reach a thermodynamically stable volume to surface area ratio. The Gibbs energy of the system is decreasing for the larger crystals and eventually complete deracemisation occurs as a result of Viedma ripening so that only large crystals of a single enantiomer remain.

3. Crystal clusters are incorporated into larger crystals of the same enantiomer – Small crystals are broken up and can then incorporate into larger crystals.
4. Attrition – the larger crystals are also ground to create smaller fragmented crystals that helps to maintain the Ostwald ripening process and thus decreases the time take for de-racemisation to occur.

Viedma carried out many reactions without glass beads and used stirrer bars instead. He found that experiments containing a "smooth" stirrer bar contained a racemic mixture of conglomerate crystals, whereas when the stirrer bar had a ridge around the centre (pivot ring) it led to only one enantiomer of the salt.[196] It is thought this is due to the pivot ring forcing a small space between the rest of the bar and the bottom of the flask, where the stirring is then able to crush crystals caught in that space leading to an increased deracemisation process.

The applications of crystal engineering have been expanded upon greatly since it's discovery resulting in its application to pharmaceutical purification, synthesis of homochiral MOFs, and elevated it as the 'probable' origin of homochirality in the origin of life.[195,197–200]

1.10.3 Chiral Amnesia

Chiral amnesia can be explained using the $NaClO_3$ model. Once a molecule of $NaClO_3$ dissolves from its crystal form, it no longer has chirality and has no "memory" of what previous chirality it had in the crystal form.[178] It follows, then, that the solution-phase $NaClO_3$ has no preference to form one hand or the other of the crystal.

Ostwald ripening is when a first-order phase transformation results in a 2-phase mixture in which the second phase is dispersed within the matrix of the first. This system has a large surface area and therefore seeks to reduce the growing size scale of the second phase, consequently decreasing the total interfacial area between the two phases.[201]

Therefore the solution-phase $NaClO_3$ does prefer to add to larger crystals over smaller ones (Ostwald ripening), which means if there are more large crystals of one enantiomer, this leads to an increased amount of crystalline solid of that enantiomer.[75,178,202] This is referred to as 'Chiral Amnesia'. This suggests that the system is never far from equilibrium conditions, and uses dissolution and re-accretion to restore the balance.[75]

1.10.4 Chiral Amnesia and Conglomerates

In systems that rapidly racemise in solution to form crystalline conglomerates, it is sometimes possible to observe Total Spontaneous Resolution – whereby a racemic or achiral solution rapidly crystallises into crystals of a single enantiomer. These systems are thought to be analogous to the achiral system of $NaClO_3$ (Figure 24). In 1941, Having described the three requirements that are needed for a racemic mixture to undergo total spontaneous resolution listed below:[203,204]

a) The compound must form separate (conglomerate) R and S crystals.
b) The compound can rapidly racemise in solution.
c) The rate of crystal growth is high, and the rate of nucleation is low.

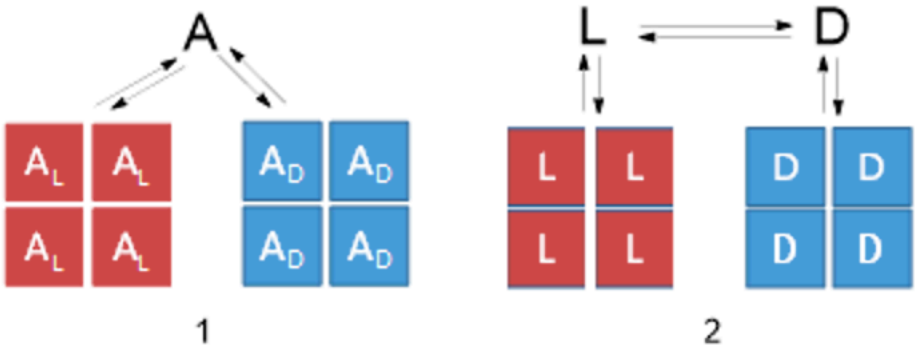

Figure 24: Solution - solid equilibria for molecules that form conglomerates from 1) achiral molecules - for example NaClO3, 2) chiral molecules that form conglomerates (boxes represent crystalline form and the black lettering represents solution-phase material).

This hypothesis was shown to be true where a near-racemic mixture of biologically-relevant, enantiomorphic crystals formed single solid phase chiral crystals using Viedma ripening.[205] In Noorduin's example (Scheme 18) the imine (25) shown forms conglomerate crystals from a rapidly racemising solution in the presence of base. Scalemic mixtures[1] of the imine (25) were stirred at room temperature in the presence of glass beads which led to a rise in ee over time to eventually produce a solid of single chirality.[205]

It was also shown that without glass beads, over time, the solid phase *ee* remained the same. Using seeds of chiral additives with a racemic mixture could lead to the single enantiomeric state. Phenyl-glycine was added to a racemic system and stirred in the presence of glass beads.[205] Even at concentrations as low as 0.1 mol%, this led to enough of a chiral bias to gain a single chirality in the solid phase. Use of (S)-phenylglycine as an additive led to an enantioenrichment of the R imine (R-25-solid), and addition of (R)-phenyl-glycine lead to

[1] A mixture of enantiomers at a ratio other than 1:1

formation of S crystals (S-25-solid). When phenylglycine was added at higher concentrations, the resolution time was decreased.[205]

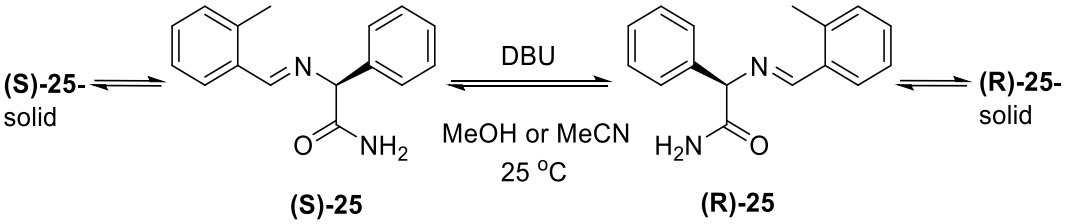

Scheme 18:Using Viedma Ripening on biologically relevant chiral molecules that form conglomerate crystals

It has been demonstrated that Viedma ripening is industrially viable, as Noorduin showed that the reaction can be scaled up to volumes of up to 320 mL.[206] Moreover, Viedma ripening has been successfully studied using a number of pharmaceutically-relevant molecules, including a Clopidogrel intermediate and Naproxen, which both underwent complete deracemisation using this process.[207,208]

Through further investigations using modelling studies it has been established that there are three main factors that are important in the Viedma ripening process. Firstly, racemisation in solution is required in order to convert all of one enantiomer to the other in the solid phase, unless it is for an achiral molecule that crystallises as a racemic conglomerate. Secondly, Wilhelm Ostwald in 1896 noted that a thermodynamically stable state will be reached through continued dissolution and growth of crystals, where the surface area to volume ration of the solid system is diminished.[195] This leads towards a tendency for larger crystals to grow at the cost of smaller ones. This means that during Viedma ripening process, when one enantiomer creates a sufficiently large crystal, it leads to deracemisation where the final solid state

corresponds to the crystal which was originally larger.[195] Finally, attrition is required to continue to provide small crystals to the system, which means that the Ostwald ripening effect is enriched, leading to shorter deracemisation times.

Solution-phase racemisation offers a method to use Viedma ripening to gain homochirality. This has been shown to be viable for an amino acid derivative, for a Mannich reaction and for the proteinogenic amino acid aspartic acid.[205,209,210] Aspartic acid has been found to convert from one homochirality to another even without the glass beads, particularly through input of thermal rather than mechanical energy (Scheme 19).[209] This suggests that whilst grinding allows Ostwald ripening to push the system away from equilibrium , thermal energy is also able to do this through crystal growth.[75]

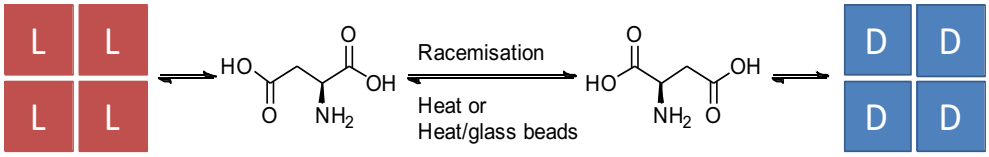

Scheme 19: Aspartic acid crystals changing from one homochiral crystal to another via solution phase racemisation driven by thermal or mechanical energy.

1.11 Physical Mechanisms for Building Blocks and Polymers

One of the challenges for prebiotic chemists is to identify plausible means of purifying key intermediates away from unwanted side products without using the modern methods we are accustomed to and in situations that are feasible on the primordial Earth. If not purified or separated, they can often cause problems in later reactions or hinder the yield. One means of investigating how purification could take place on the early Earth is to try to identify physical properties of these molecules (e.g. their solubility or crystallinity) and use geochemical scenarios (such as wet/dry cycles or high pressure) to allow the reaction to take place.

The discovery of ribozymes and the isolation of many functional RNAs that catalyse a variety of chemical transformations *in vitro* have led to wide acceptance of the RNA world hypothesis.[27,211,212] As such, a number of studies focus on demonstrating a prebiotically-plausible synthesis of nucleotides and oligonucleotides. The synthesis of *ribo*se deriving from the formose reaction, and a pathway towards purine and pyrimidine nucleobases has been demonstrated.[89,213,214] Biopolymers, including RNA, have been shown to have a remarkable tendency to self-select for chirality. As discussed earlier, Joyce *et. al* identified the phenomenon of enantiomeric cross inhibition in the formation of (D)-guanosine. In an enantio-pure solution of (D)-guanosine-5'phospho-2-methylimidazole monomer the reaction proceeds orders of magnitude faster than when there is presence of activated (L)- monomer in the reaction mixture. In some case they observed that polymer formation was inhibited completely.[215] What's more, chiroselective transfer of an aminoacyl group templated by RNA has been demonstrated to be able to control the stereochemistry of the resultant RNA strand.[216]

However, this is not without limitations such as the notoriously complex mixture of products that are formed in the formose reaction, and the instability of ribose under the common reaction conditions (half-life of 73 min at pH 7 and 100˚C, or 44 years at pH 7 and 0 ˚C).[41] As discussed, the combination of the sugar, nucleobase and phosphate is very ineffective for purines and not successful for pyrimidines.[42] However, success came from Powner *et al.* synthesis which demonstrated a novel, prebiotically plausible route to access the pyrimidine ribonucleotides starting from simple building blocks, glycolaldehyde (**13**) and cyanamide (**6**).[43]

This pathway provides good yields for each step, however there are three interesting physical methods used for the purification of the compounds. The first comes from the initial high yielding (90%) formation of 2-aminooxazole (**15**), that has a notable volatility. It has been suggested that through sublimation and condensation, possibly during diurnal rhythms where the temperature rises and cools could 2-aminooxazole (**15**) have been purified.[217]

The second comes from the formation of the aminooxazolines (**AO**) by condensation of 2-aminooxazole (**15**) and glyceraldehyde (**14**). At this stage, four diastereomeric products are formed (*ribo*-, *arabino*-, *xylo*-, *lyxo*-) resulting from the two new chiral centres that are created. The major stereomers present are *ribo*- and *arabino*-aminooxazoline (**RAO**, **AAO**). The desired **AAO** compound can be purified by spontaneous crystallisation of **RAO** by product which leaves the **AAO** in solution.

The last purification is during the final step using UV irradiation which purifies the cytidine nucleotide by selective hydrolysis of the major by-products, as well as the α-anomer.[43] Additionally, the UV offers a secondary route to another nucleotide by partial conversion of cytidine to uridine.

To successfully form RNA, the final step involves forming oligomers from the available *ribo*nucleotide monomers. This is difficult as nucleotides contain hydroxyl groups of similar nucleophilicity, meaning inter-monomer bonding is very challenging, specifically between the 2′- and 3′′-hydroxyl moieties. In the Sutherland method, these 2′′-3′′ cyclic nucleotides are able to condense into RNA chains under particularly strong dehydrating conditions, however with poor regiospecificity that results in a combination of 3′′-5′′ and 2′′-5′′ linkages with a chain

length of up to 6.[218] Therefore, investigations have taken place into activating the nucleotides in a hope of a more efficient and selective polymerisation.

To achieve oligomerisation, activation of the monomer units is required to overcome the entropy lost making long oligomers. Additionally, oligomerisation needs to be preferential over hydrolysis, and the longer chains need to be preferentially formed compared to many short chains. Orgel suggested a range of activating groups for non-enzymatic templated nucleotide polymerisation resulting in 2-methylimidazole which successfully forms long chains (up to 14 monomers) of oligo-guanosine templated by oligo-cytidine.[219] Inorganic catalysts such as montmorillonite clay have been used to improve efficiency of polymerisation of 5''-monophosphate nucleotides activated with leaving groups such as imidazole, adenine and 1-methyladenine.[220] Particularly with 1-methyladenine as the activating group, the yields for 3''-5'' linkages have been greater than 80%. [221]

The importance of phase transitions for purification in Sutherland's method has led to researchers to wonder whether these transitions could be important for purification of early-Earth polymers also. The purity of the oligomers and the lengths available would have been limited by the specificity of the chemistry and the purity of the monomer pool. It has been known since the late 1940s that duplex DNA can form liquid crystal (LC) phases when hydrated, which actually had an important role in the interpretation of DNA by allowing the alignment of the chains so that the x-ray structure factor of a single chain was not complicated by interchain correlations.[222,223] Liquid crystals are characterised by the assembly of mainly anisometric building blocks that form soft condensed matter.[224]

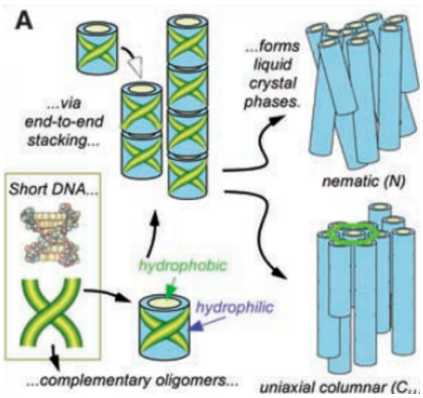

Figure 25: Liquid crystals, from Nakata et al.[225] =

Liquid crystals are, as the name suggests, a state of matter thermodynamically in between a solid and a liquid. The order seen in a solid, in this case a crystal, is both positional and orientational whereby the molecules occupy specific sites in the lattice, where as in liquids, the molecules diffuse randomly throughout the container, with the molecular axis constantly changing.[226] The liquid crystal phases can diffuse like a liquid, but also possess a degree of orientational order, and sometimes positional order which can be defined by an order parameter, most commonly achieved by finding the average of the second Legendre polynomial.[226]

Liquid crystals have been used in the context of origins of life to show that oligomers (5 to 20 bases) of short double stranded DNA (dsDNA) can phase-separate from a solution of single stranded DNA (ssDNA) oligomers by forming LC aggregates.[225,227] This aggregation is a result of short dsDNA segments' ends being hydrophobic due to the exposed terminal nucleobases, which means they can coaxially stack into longer DNA duplexes. Nevertheless, this observed coaxial stacking is not the solitary reason for LC construction; purified dsDNA will only spontaneously aggregate at higher concentrations.[225] The phase separation observed between ssDNA and dsDNA can be attributed to a combination of depletion-type entropic

forces, which can be accredited to flexibility mismatch, and the energy gained when stacking the paired terminals of dsDNA.[227] In other words, the flexible ssDNA mixed with the rigid dsDNA promotes aggregation as the ssDNA in solution maximises the entropy by minimising the volume occupied by the dsDNA through LC formation. This phenomenon has been well investigated in solutions of concentrated polymers that spontaneously undergo colloid aggregation to enable phase separation to take place.[228]

This method provides a reasonable scenario whereby oligomers that form the double stranded helices could be separated away from oligomers that do not, possibly due to possessing incorrect linkages and therefore unable to hybridise resulting in them remaining in the solution phase Figure 26.[217] This process while demonstrated with DNA should apply to similarly rigid polymers such as double strand RNA, which could be induced by other flexible molecules such as polypeptides.

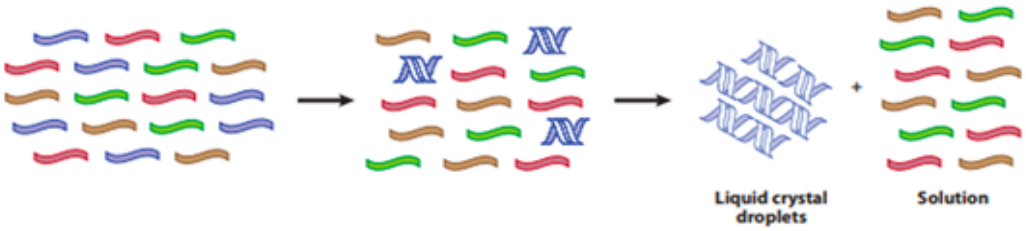

Figure 26: How liquid crystal formation can lead to nucleic acid oligomer purification. From left to right: A pool of single strand DNA whereby some strands (blue) can form duplexes, and the others (green, brown and red) cannot due to modified bases, incorrect linkages or racemic nucleotides. The blue duplex strands can hybridise to form short double stranded helices where by at high concentrations, the short double stranded nucleic acids can phase separate into liquid crystal droplets.[217]

Nematic LCs are the simplest liquid crystal phase, in this phase the molecules are generally low-molecular weight, rod-like or disc-like organic compounds that can be visualised to detect

and measure chirality as through a chiral, non-racemic dopant, the cholesteric (N*) phase can be formed.[229] The cholesteric (chiral nematic) phase is the fundamentally the same as a nematic phase, however it has an additional helical change in orientation of the director (Figure 27).[230] Nematic LCs display characteristic defect texture changes when doped with chiral additives. Recently it has been demonstrated that liquid crystals formed by DNA, dyes and other flat ionic molecules in water have shown amplification of chirality.[224] Here, adenosine monophosphate (a nucleotide and a building block used for NAD^+, $NADP^+$ and FAD) was attached to luminescent gold nanoclusters which induce chiral nematic LCs that could be visually measured.

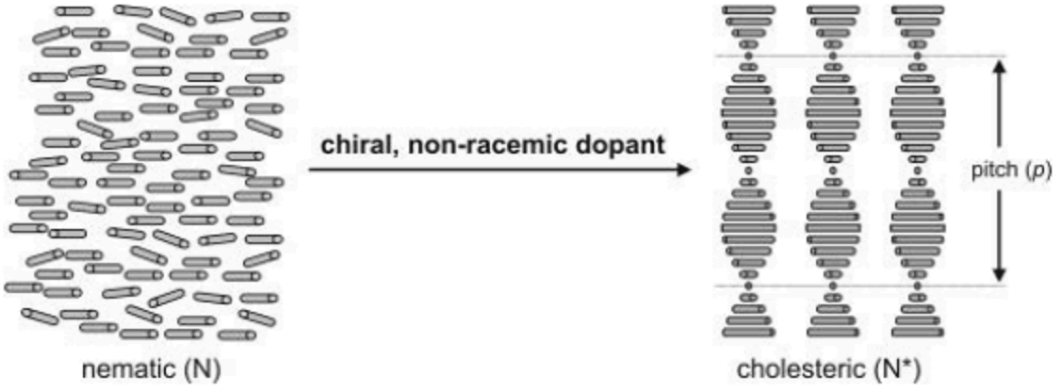

Figure 27: Nematic to cholesteric (chiral nematic) phase

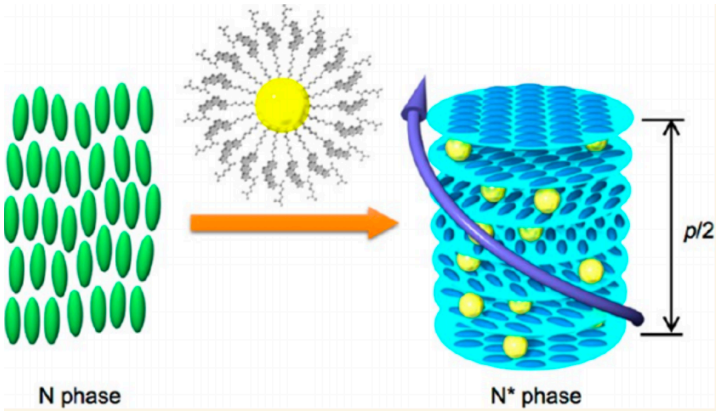

Figure 28: Nematic (N phase) to cholesteric (N phase) through a chiral, non-racemic dopant (in this case chiral ligand capped NPs)*

1.11.1 The Concentration Problem

How such spontaneous self-assembly would occur and how the energy resulting from an increase in local order would have been sourced is a key question. The most obvious, and simple method would be to have local high concentrations of the building blocks required, hence lowering the entropic cost of self-assembly. This is often necessary for many prebiotic self-assembly processes such as template directed polymerisation or membrane formation where due to weak interactions, higher concentrations are required. Additionally, even for reaction steps where precipitation is required, saturated monomer concentrations are needed. As water is the main solvent used for prebiotic chemistry and is itself a competing nucleophile, so again, high concentrations are necessary to favour product formation over hydrolysis.

A method by which solutions may become more concentrated that is often cited, is how pools of liquid can be evaporated.[231] This could be feasible if environments such as ponds or tidal pools were created with pockets of high substrate concentration, in which prebiotic chemistry could occur. Whilst this method is frequently referenced, it is important to note that due to differences between experimental equipment such as shape of vessels, absorption on the surface etc, it is hard to produce environments in line with what could have been present on the early Earth.[231] This can lead to poor reproducibility between experiments; however this should not affect the prebiotic practicality of evaporation.

Freezing is also readily used in the prebiotic context to provide concentration as through the formation of ice crystals, the eutectic solution left behind between the ice crystals leads to a higher concentration of solutes. This has been demonstrated prebiotically whereby dilute solutions of activated nucleotides are frozen which led to polymerisation being greatly

enhanced which has been said to suggest that ice deposits on the early Earth could have enabled short and medium size sequences of RNA to be formed that could provide a microenvironment suitable for the formation of biopolymers or their precursors.[228,232,233]

Thermal gradients have been noted as particularly abundant dissipative systems on the early Earth. This led Braun and co-workers to investigate these natural temperature gradients as a means to accumulate single nucleotides leading from a dilute solution to molar concentrations.[234] Oceanic alkaline vents have shown an unusual porous rock structure which contains a network of narrow channels with a close proximity to both hot vent water, and cold ocean water, meaning a significant gradient of temperature is able to occur.[235] This temperature gradient allows the vertical convective flow to occur whereby hot fluid rises and cold fluid sinks, and also the thermal diffusion of molecules horizontally across the temperature gradient (Figure 29). This coupling of physical processes has been noted previously in the Clusius-Dickel separation, which is an industrial process from 1953.[236]

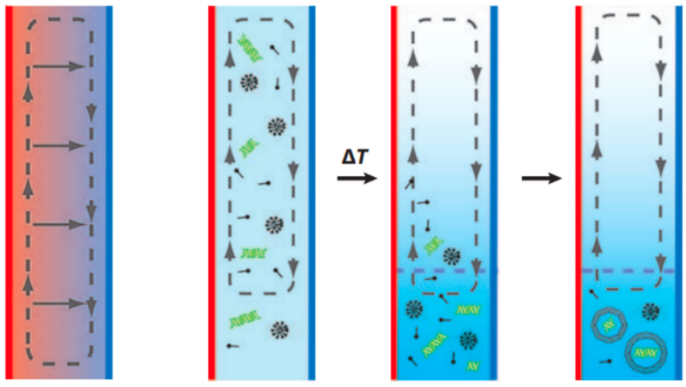

Figure 29: Hydrothermal vent setting schematic showing the basic principle of the hydrothermal vent, and how a dilute prebiotic soup could lead to high concentrations of nucleic acids. Copied from Szostak.[217]

Whilst Braun suggested that nucleotides and nucleic acid oligomers were able to reach large accumulations (>10^{10}-fold enrichment) this was only achieved through numerical simulations.[234] This was then later demonstrated experimentally using dilute solutions of nucleotides, oligonucleotides and fatty acids resulting in high concentrations pockets leading to the self-assembly of large vesicles containing DNA.[237] This was achieved by mimicking the unique rock structure found in vent formation by using square borosilicate microcapillaries and holding the capillary clamped between a heat source and a heat sink to mimic the temperature gradient. By doing this it was shown that >1000-fold enrichment was observed in response to the mimicked environment. This is of particular importance not only due to the ability to concentrate molecules on the prebiotic Earth, but also in the way that the molecules are concentrated. The accumulation is specific, meaning that at a certain temperature gradient, the concentration effect observed depends on the coupling between the channel diameter of the capillary and the thermal diffusivity of the solute.[217] This results in specific molecules being concentrated, so for example, where freezing and evaporation concentrate all solutes and therefore generate brine-like solutions, thermal diffusion columns only concentrate specific molecules. Furthermore, the local concentration is kept high at all times due to the constant input of thermal energy *via* heating of the channel wall.

Most recently, small gas-filled bubbles that were trapped in and reacted with the surface of volcanic rocks could have led to the formation of the first cycles of molecular evolution.[12] When these bubbles are exposed to a temperature gradient it results in the bubble exhibiting different temperatures on the surface. This results in that on the warmer side of the bubble, higher concentrations are able to accumulate.

It is important to note that these hydrothermal systems are more suitable in an environment that enables thermal diffusion to take place effectively, this is not in marine environments because they feature high salt concentrations which constrain thermal diffusion. Sea water additionally contains high levels of divalent salts which inhibit membrane assembly from fatty acids. Therefore, the hydrothermal vent scenario favours a freshwater hydrothermal system, which is an obvious constraint.

2 Relevance & Aims

At some point in the history of the Earth's development, the environmental conditions were able to combine available basic organic building blocks into the first biopolymers capable of self-replication. Those building blocks may have originated from oceanic vents, lightning strikes, or delivered by carbonaceous meteorites. It has been shown by the work described in the introduction that there are plausible synthetic chemical explanations for the ways in which it is possible to build up these polymers, in-keeping with the RNA World hypothesis. However, how and why the homochirality that we observe across nature came to be remains unexplained. Plausible explanations come from the theories that crystallisation could be attributed to those such as Viedma and Ostwald ripening to induce significant chiral amplification.

Stairs *et al.* divergent synthesis of purine and pyrimidine nucleotides provides a key route to the building blocks of RNA. The intermediate *arabino*-aminooxazoline (**AAO**) and *arabino*-oxazolidinone thione (**AOT**) have been identified. With that in mind, how might crystallisation techniques, and more specifically chiral amplification of the precursors to RNA be used to grant us access to homochiral biopolymers.

This work will build upon the oxazoline synthesis to investigate the amplification that has been previously demonstrated by ribo-aminooxazoline (**RAO**) to investigate the crystalline properties of **AAO** and **AOT** (as well as any relevant intermediates) to ultimately grant access to enantiopure purine and pyrimidine nucleotides, and therefore homochiral RNA under pre-biotic conditions. Thus, this bridges the gap from the racemic pool of the primordial Earth to the homochiral natural world that we see today.

3 Crystallisation Properties of Pentose Oxazoline Derivatives – Introduction

The aim of the project was to investigate crystal structures of prebiotically important compounds, en route to the canonical nucleotides, and thereby elucidate the plausible causes for the enantioenrichment of those compounds under prebiotic conditions. More specifically, crystallisation was used to achieve this enantioenrichment, and so crystallographic methods, namely single crystal X-ray diffraction (SXRD) and powder X-ray diffraction (PXRD), were used to analyse the samples and confirm the results.

Remarkable progress has been made toward elucidating a prebiotic synthesis of the canonical nucleotides in recent years.[43,64] In 2017 a divergent prebiotic synthesis of both pyrimidine and purine ribonucleotides was developed that highlighted *arabino*-aminooxazoline (**AAO**) and *arabino*-oxazolidinone thione (**AOT**) as key intermediates has been identified (Scheme 20).[64] *Ribo*-aminooxazoline (**RAO**) has previously been shown to amplify *ee's* upon crystallisation, and this enrichment has been proposed to be important to the origin of biological homochirality.[238] If a way was found to produce and suitably crystallise **AAO** and **AOT** they may also lead to enantiomerical enrichment *en route* to nucleotides. However, the crystallisation properties of **AAO** and **AOT** are unknown, moreover, it is not understood which molecular and crystal properties of **RAO** lead to its formation of conglomerate crystals and further study of these crystallisation are warranted.

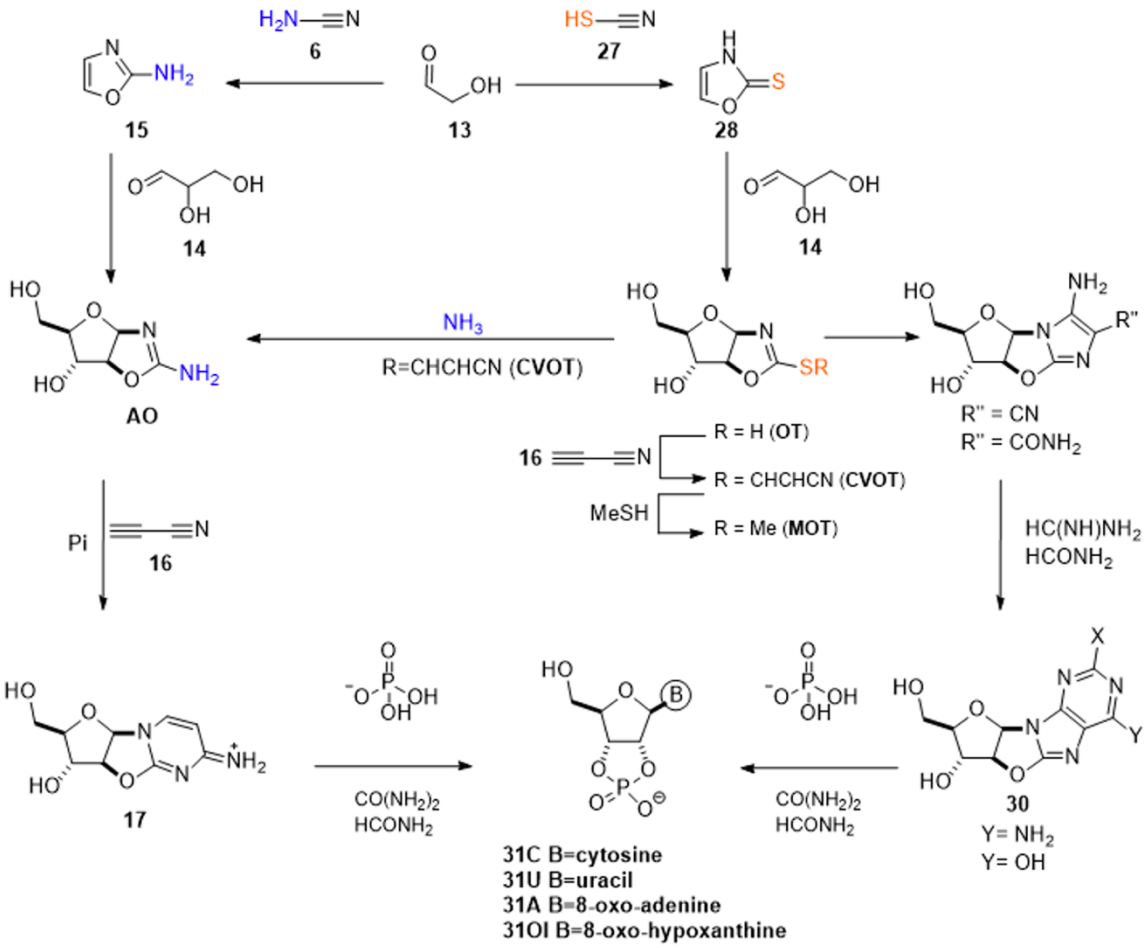

Scheme 20: Divergent prebiotic synthesis of pyrimidine and purine ribonucleotides, B refers to the base. Redrawn from Stairs et al.[64]

It is instructive to review the types of crystallisation behaviour commonly found. Crystals may be formed as; a racemic solid that contain a 1:1 ratio of D:L molecules, or as a conglomerate in which each crystal (domain) is comprised of molecules of a single enantiomer and the crystals themselves are mirror images (Figure 30). Racemic compounds are more prevalent on planet earth than conglomerate in a ratio of 10:1.[239]

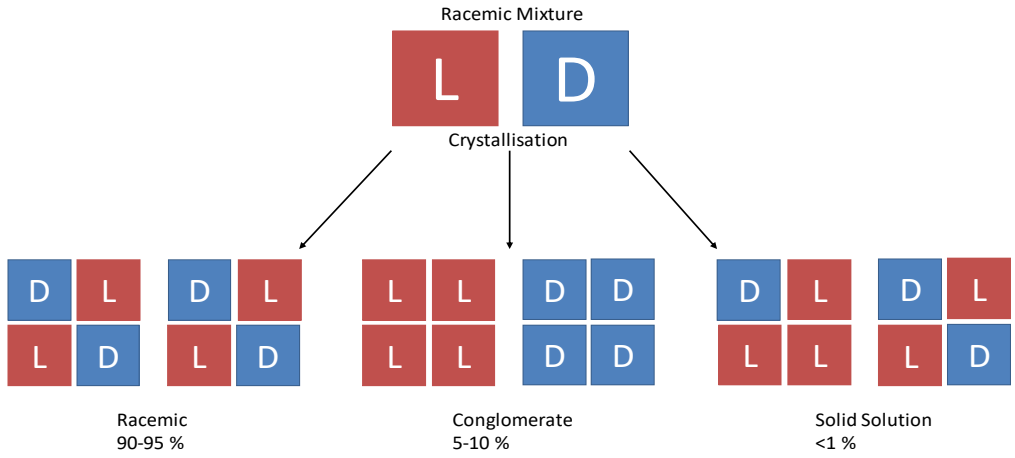

Figure 30: Crystal Packing for enantiomeric molecules

3.1 Pentose Aminooxazolines (AO)

Powner *et al.* have previously identified that the pentose aminooxazolines (**AO**) are key prebiotic intermediates for pyrimidine ribonucleotide synthesis.[43] This synthesis is initiated by the iterative reaction of the prebiotically-available C_2 and C_3 sugars glycolaldehyde (**13**) and glyceraldehyde (**14**), with cyanamide (**6**) (Scheme 21). Initially glycolaldehyde (**13**) reacts with cyanamide (**6**) at pH 7 in the presence of inorganic phosphate, affording the heterocyclic molecule, 2-aminooxazole (**15**) in high yield (90%). This can then go on to react with the C_3 sugar, glyceraldehyde (**14**), to furnish a diastereomeric mixture of aminooxazolines (**AO**) in near-quantitative yield (95%).[43]

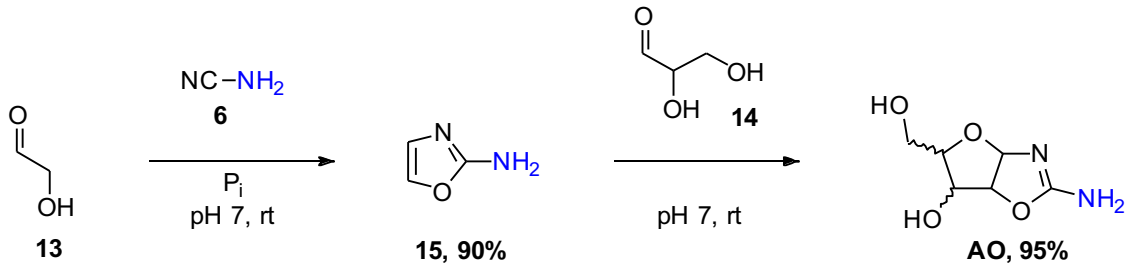

Scheme 21: Prebiotic synthesis of aminooxazolines from prebiotically available small molecules.

This route is an effective way to by-pass the traditional glycosidation reaction while selectively forming the furanosyl nucleoside precursors.[42,240] When this reaction takes place, five stereoisomers of pentose aminooxazolines are formed; *ribo*-aminooxazoline (**RAO**, 44%), *arabino*-aminooxazoline (**AAO**, 33%), *xylo*-aminooxazoline (**XAO**, 13%) and *lyxo*-aminooxazoline (**LAO**) (**LAO-*p*** (7%) : **LAO-*f*** (1%)). **RAO**, **AAO** and **XAO** all favour the furanosyl form in water, however **LAO** will preferentially sit in the pyranosyl form 5:1 (***LAO-p***: ***LAO-f***) shown in Figure 31.[42,240] This unusual *lyxose*-behaviour has been attributed to the **LAO** series interconverting *via* an open chain intermediate likely due to steric crowding on the β-face in the furanosyl form.[240] Initially there is a kinetic preference for the furanosyl-form, *via* 5-exo-trig > 6-exo-trig cyclisation, but this initial preference is then converted across to thermodynamic pyranosyl preference.

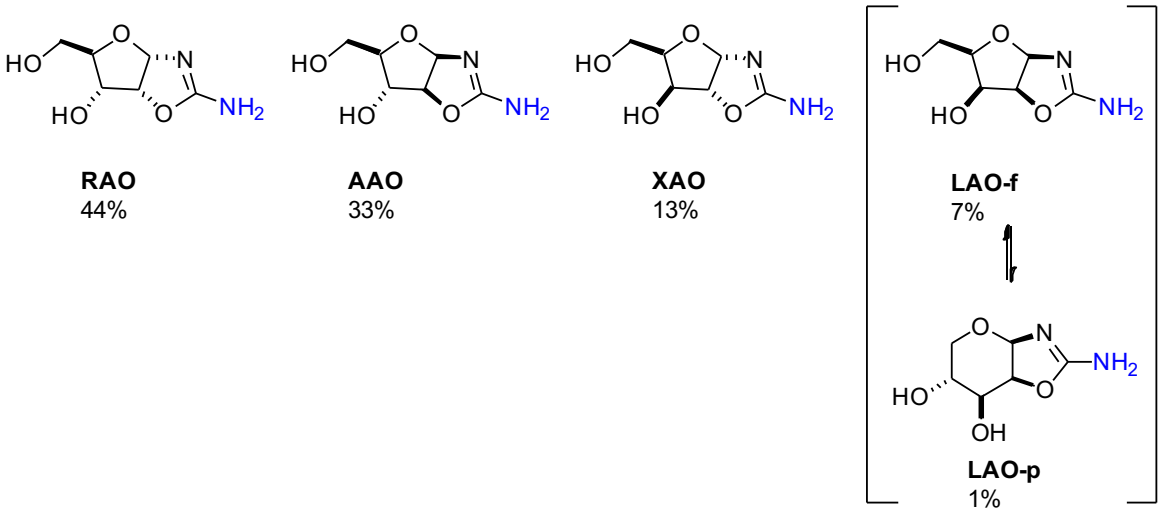

*Figure 31: Stereomers formed from the reaction of glyceraldehyde **14** and 2-aminooxazole **15**: **RAO**, **AAO**, **XAO**, **LAO-f** and **LAO-p** in the relative constitutions.*

The reaction proceeds with high **RAO** and **AAO** diastereoselectivity which is particularly interesting as both **RAO** and **AAO** are only one stereochemical inversion step away from the β-ribo stereochemistry of RNA as seen in Figure 32.

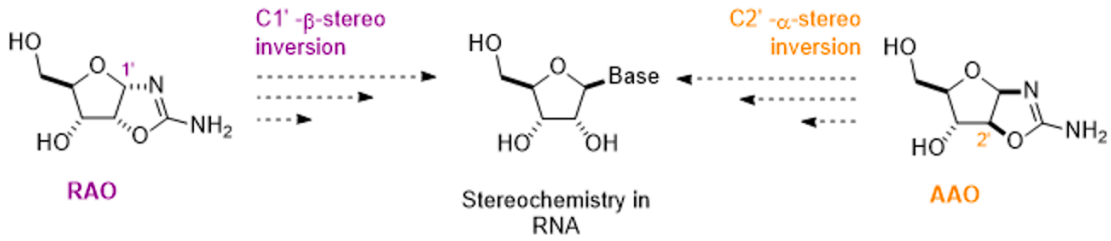

*Figure 32: Comparison of stereochemistry of **RAO** and **AAO** with the required natural β-ribo stereochemistry of RNA.*

With respect to chirality this oxazoline-mediated nucleotide synthesis is of particular interest due to the different solubilities observed, in particular **RAO** which ultimately leads to the purification of **RAO** away from the crude mixture *via* spontaneous crystallisation. Interconversion of **RAO** to **AAO** via general acid-base catalysed C2' epimerisation in phosphate buffer solution results in purification and *ee*-amplification of both **AAO** and **RAO** but **XAO** and **LAO** remain in the crude supernatant mixture and cannot be re-accessed (due to requiring C3' epimerisation) from **RAO** crystals. This would then lead to the **RAO** forming an equilibrium e.g. **RAO** (solid) <-> **RAO** (aq) and **RAO** (aq) <-> **AAO** (aq). This goes some way to resolving the complication of different pentose diastereomers that are present in the initial mixture.

Whilst this synthesis is a great step forwards, without access to the highly enantioenriched sugars, the nucleotides formed would not lead to informational polymers that carry the genetic code due to chiral cross inhibition as discussed earlier.[241] Therefore, a way to access enantiopure forms of the sugars/nucleotides is of high importance for their reasonable function replicating polymers.

The reaction of scalemic ribose (*sca-**ribo***-**40**) (60% enantiomeric excess) with cyanamide **6** can lead to the crystallisation of pure homochiral **RAO**.[238] This crystalline behaviour was observed when scalemic ribose (*sca-**ribo***-**40**) (0.5 M) and cyanamide (**6**, 1.0 M) were heated at 60 °C, pH 9, for 5 h and then incubated overnight at −4 °C. The crystals that were obtained were analysed by optical rotation.

3.1.1 Synthesis of Aminooxazolines

To further investigate these remarkable properties of oxazolines and extend our understanding of this stereo-amplification method, we set out to thoroughly investigate the crystallisation properties of the oxazolines (not just **RAO**). Investigation of **AAO**, and **XAO**, alongside **RAO** (Figure 31), would give a holistic view of these properties to establish a rationale for why **RAO** exhibits this intriguing and useful behaviour and understand with other isomers (if any) exhibit the same properties.[238] We then applied that knowledge to the preparation of oxazolidinone thiones (**OT**) and oxazolidinones (**OX**) to expand this understanding further to other relevant and important prebiotic molecules.

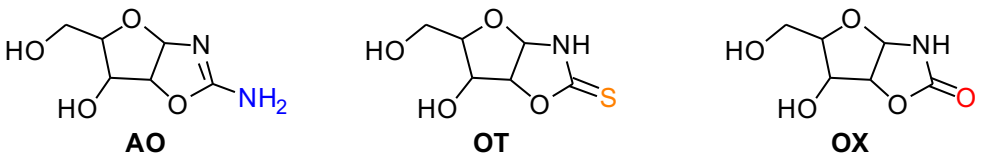

Figure 33: Chosen prebiotic intermediates to be investigated

The aminooxazolines (**AO**), oxazolidinone thiones (**OT**) and oxazolidinones (**OX**) were chosen for the investigations as the compounds are structurally equivalent allowing us to broaden our understanding of the properties of these crystals and to investigate if these properties

were general. It is possible that we would thus discover interesting and important effects, yet unknown, which will become significant in future origin of life studies.

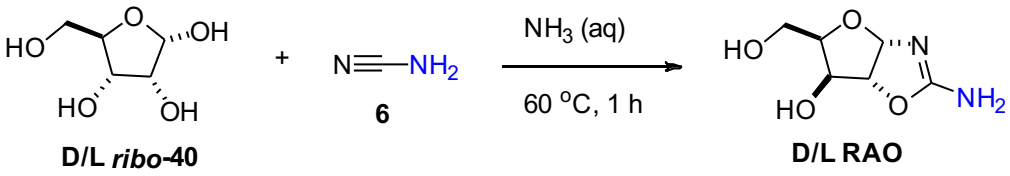

Scheme 22: Enantioenrichment crystallisation experiment performed by Anastasi et al.

As a starting point, the reported **RAO** enantioenrichment experiment was repeated as reported in the literature (Scheme 22).[238] Solutions of D-, L- and scalemic (sca-) ribose (**ribo-40**) (0.5 M) with a range of different *ee* values (Figure 34) were reacted with cyanamide (**6**, 1 M) at pH 9, 60 °C and heated for 5 h and then at −4 °C for 24 h. The crystals formed were then separated, washed with ice cold water and dissolved in phosphate buffer (0.25 M) at pH 4.5. The resultant solutions were analysed by polarimetry. The results confirmed those presented in the literature, where *ribo*-aminooxazoline (**RAO**) shows enantioenrichment from a starting solution of 60% *ee*.[238]

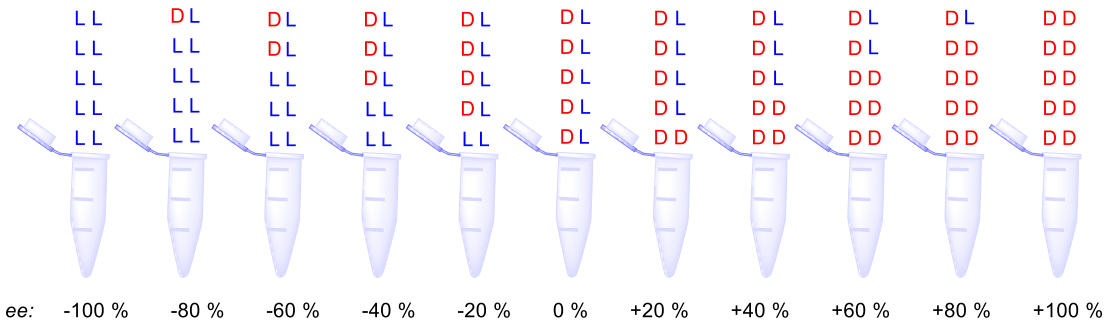

Figure 34: How the enantiomeric scalemic solutions were set up, where L = L enantiomer, D= D enantiomer and the resultant ee that is created.

It was also observed that heating the small reaction vessels in an oil bath or mantle was insufficient to achieve the expected results. However, performing the reactions in closed Eppendorf tubes allowed us to be much more consistent in heating the reaction and therefore achieving conversion to **RAO**.

Both enantiomers of the required aminooxazoline were synthesised in bulk and stock solutions were prepared of each of the enantiomers. This was then used to prepare the crystallisation mixtures according to volumes, which could be significantly more accurately measured than by weight. With the use of Eppendorf tubes, consistent heating, and stock solutions, reproducibility exceeded that reported in the literature and therefore represented a material optimisation of the protocol.

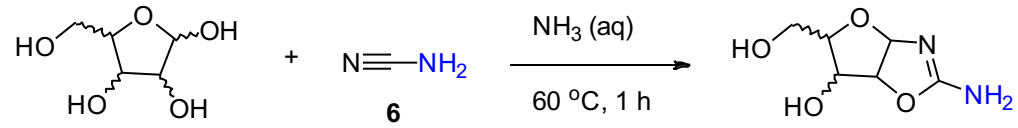

D/L ribose (D/L ribo-40)
D/L arabinose (D/L arabino-40)
D/L xylose (D/L xylo-40)

D/L RAO
D/L AAO
D/L XAO

Scheme 23: The synthetic route used to access the aminooxazolines in large quantities as described by Sutherland et al.[43]

In order to investigate the scalemic mixtures, approximately one gram of starting material was needed per crystallisation screen. Therefore, batches of the aminooxazolines were prepared according to a literature method (described by Sutherland *et al.*).[35] The pentose sugar (**40**) was dissolved in aqueous ammonia solution, cyanamide (**6**) was added and heated to 60 °C for 1 h and then cooled to room temperature (Scheme 23). Methanol was added to promote crystallisation, and the solution was cooled overnight at −4 °C, the resulting crystals were

collected by filtration and washed with ice cold (0 °C) methanol and dried under vacuum. They were then characterised to ensure the substrate purity (>90% by quantitative NMR assessed using a standard).

Lyxose analogues were not synthesised during this study. This was predominantly due to the tendency for lyxose (***lyxo*-40**) to tautomerise easily from the furanosyl to the pyranosyl configuration. As a result, crystallization and enantiomeric isolation did not occur during the protocol and thus lyxose crystals were not available for crystal studies.

3.1.2 Enantioenrichment of Aminooxazolines (AO)

3.1.2.1 Enantioenrichment of ribo-aminooxazoline (RAO)

Starting with a scalemic mixture of **RAO** in a solution of water (0.25 M, 1 mL) the solution is heated in a closed Eppendorf to 60 °C for 4 h in order to dissolve all the solid. The mixture was allowed to cool to r.t. and placed in the refrigerator (4 °C) for 24 h to allow sufficient opportunity for the formation of crystals. The crystals were then isolated by centrifugation, washed sparingly with ice-cold water (0 °C) and dried. The optical rotation was measured by dissolving the crystals in water and using a polarimeter. Each scalemic mixture was investigated in triplicate, and the experiment was run for mixtures of −100 % (L) to +100 % (D) in 20 % *ee* intervals. The recorded measurements were then plotted with standard deviations shown for the associated errors. The results are shown below. This process was then repeated for **AAO** and **XAO** and replicated across a range of reaction concentrations (0.1 M to 1 M) and in different solvents (water, ethanol, methanol.

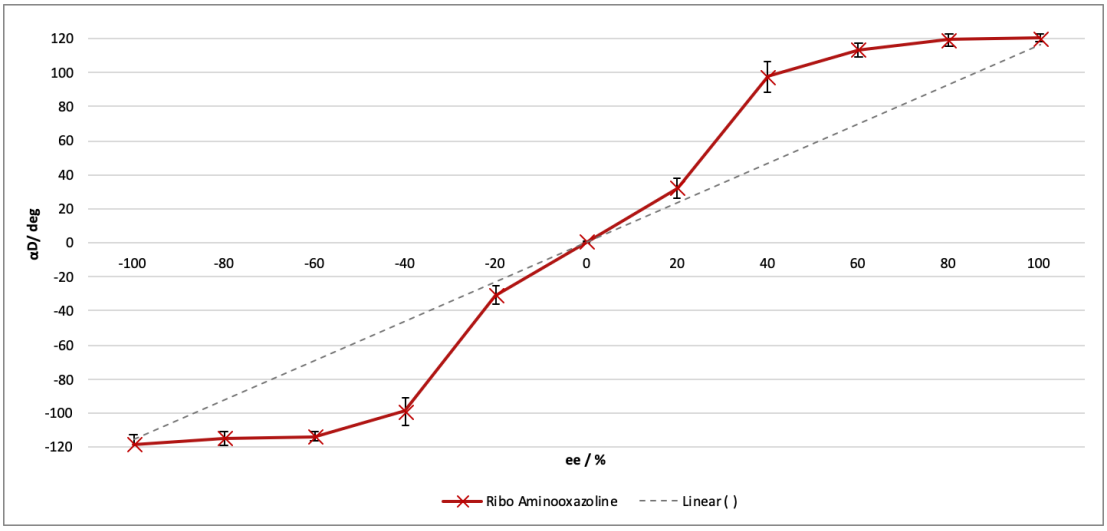

*Figure 35: Enantio-amplification of **RAO** (0.25 M, H_2O). The results were triplicated, and the average plotted along with the expected* ee *value. The dotted line shows the optical rotation if the crystals possessed the same* ee *value as the starting solution.*

In Figure 35 (left to right) it can be seen that from −100% ee through −80% ee there is a visible and substantial enantioenrichment of the crystal *ee*'s compared to the initial solution *ee* values (red line vs dotted black line). Moving to -60% the amplification is increased, with the optical rotation remaining broadly flat, indicating the ee is very close to that observed at -80%. Looking across to -40%, the optical rotation becomes slightly lower, but remains close to the ee value of the crystal observed between -100% and -60%. This result is an improvement on that reported in the literature by Sutherland, as they only observed 60% *ee* enrichment, whereas here we observed close to homochiral enrichment from 40% *ee*.[238] Approaching 0% the optical rotation line inverts in line with the expected trend and again at +40% there is significant amplification of *ee* in the crystals formed. The trend is, as expected, a mirror of the negative *ee's* and at 60% - 100% *ee* we see the same plateau in the line, indicating maximum enrichment in the product. Moreover, if we compare the observed optical rotation versus the expected value (the red line values vs. the dotted line values) we find that the largest amplification factor occurs around (+/−) 40%, where the amplification factor is 2.5× the expected value.

Expanding on Sutherland's results, using the optimised synthetic method that was described previously (see page 109) we were able to access the **AAO** and **XAO** aminooxazolines. It is worthy of note that crystallisations were attempted at various concentrations, with varying results, which are discussed below.

3.1.2.2 Enantioenrichment of arabino-aminooxazoline (AAO)

The synthesis of **AAO** proceeded with good yield (62 %) and high purity (90%). The scalemic mixtures were prepared and the crystallisation screen was carried out, in triplicate, an average calculated and plotted (Figure 36). For scalemic mixtures of 1 M of L- and D- **AAO**, once again an *ee* amplification curve is observed. At −100% *ee* through to −60% *ee*, the optical rotation curve remains broadly flat, and at −40%, there is a slight decrease in the observed *ee*, the curve again inverts through the origin and is mirrored in the negative *ee's*. The largest *ee* amplification once again observed at +/−40% initial (as with **RAO**).

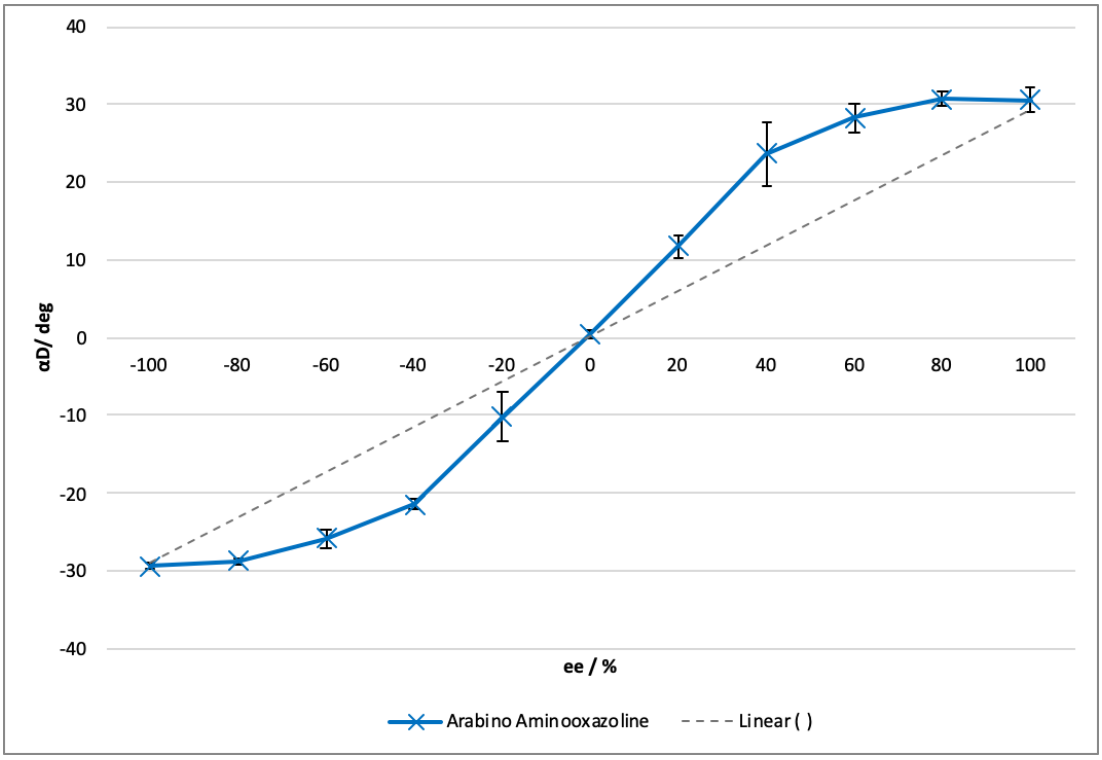

*Figure 36: Enantio-amplification of **AAO** (1.0 M, H_2O). The results were triplicated, and the average plotted along with the expected ee value. The dotted line shows the optical rotation if the crystals possessed the same* ee *value as the starting solution.*

3.1.2.3 Enantioenrichment of xylo-aminooxazoline (XAO)

The scalemic mixtures of D- and L- **XAO** (1 M) were crystallised from water and the optical rotations produced from the resultant crystals and plotted as shown below (Figure 37). In this case although the crystals demonstrate a degree of enantiomeric amplification, the trend more closely aligns with the 'expected' value up until the 60% *ee* mixture, indicating the crystals are forming at the same *ee* as the solution. However, from this point (60% *ee*) onwards, significant amplification occurs to nearly homochiral crystals. This indicates that **XAO** only undergoes enantiomeric amplification at higher *ee*'s that **AAO** and **RAO**. **XAO** gives maximal amplification of optical rotation at +/− 60%, this also aligns with the point at which enantiopure crystals are observed.

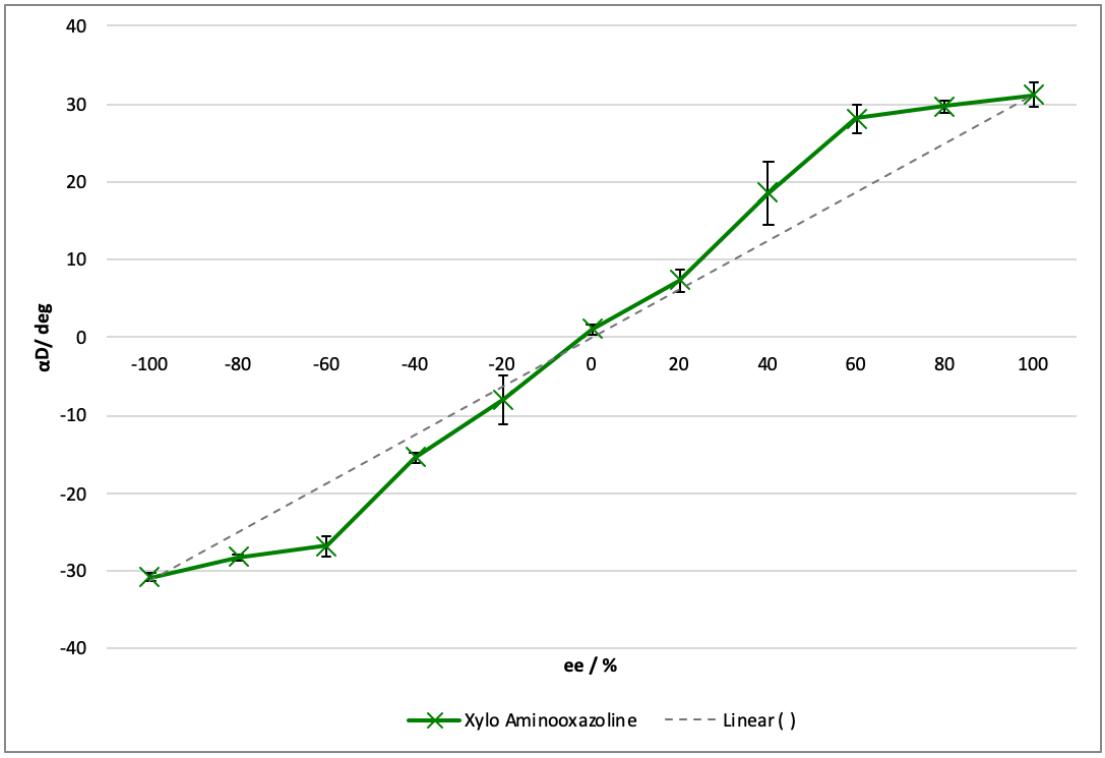

*Figure 37: Enantio-amplification of **XAO** (1.0 M, H_2O). The results were triplicated, and the average plotted along with the expected ee value. The dotted line shows the optical rotation if the crystals possessed the same* ee *value as the starting solution.*

3.1.3 Crystal Structure of Aminooxazolines (AO)

We predicted that the crystal packing and H-bonding motifs in the solid state could dictate the crystal characteristic of the aminooxazoline in the solid state, therefore crystal structures of all the aminooxazolines were obtained in order to achieve the maximum amount of data that could possibly be useful in order to identify characteristics (such as, hydrogen-bond patterns) which may influence conglomerate crystal formation, as all the aminooxazolines were shown to produce conglomerate crystals under the conditions mentioned above.

Analysis of the crystals obtained at the 0% *ee* (racemic mixture) by optical rotation was used to show that there is in fact no optical rotation present in the bulk material. This is important as at 0% *ee* the crystal should have no optical rotation as it should be a mixture of both L- and

D- molecules. The crystals obtained at 0% *ee* were then analysed by single crystal x-ray diffraction and several crystals were selected to be analysed. Analysis of multiple crystals obtained from the crystallisation from the 0% *ee* solution by single crystal x-ray diffraction revealed that **RAO**, **AAO**, and **XAO** were all formed as conglomerate (single-handed crystals), not racemic crystals.

3.1.3.1 Crystal structure of ribo-aminooxazoline (RAO)

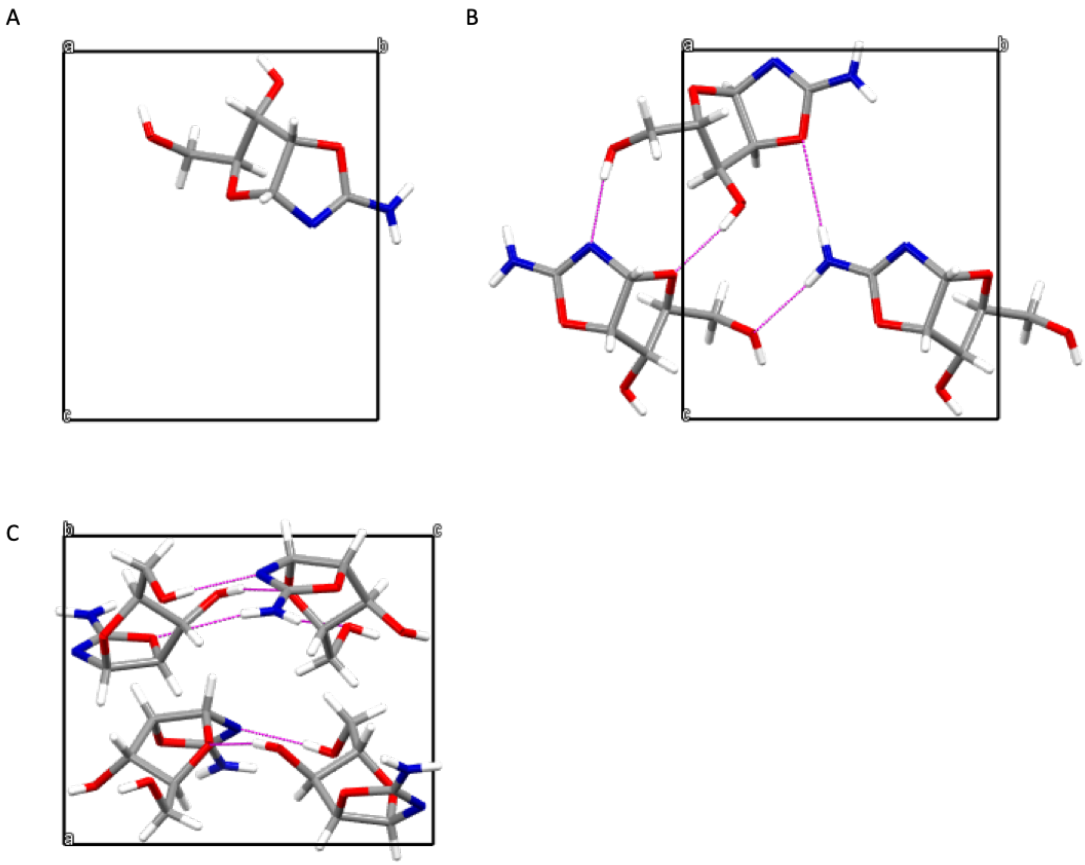

*Figure 38: D-**RAO** in A) the asymmetric unit. B) key interactions C) packing.*

Ribo-aminooxazoline (**RAO**) was highlighted as demonstrating conglomerate-forming behaviour at 0% *ee*. Therefore, the crystals at 0% *ee* were analysed by SXRD, which confirmed conglomerate crystals. Figure 38 shows D- and L- **RAO** crystallises in the orthorhombic $P2_12_12_1$

non-centrosymmetric space group with one molecule in the asymmetric unit. The molecules self-assemble to form a 10-atom hydrogen bonding ring motif characterized by the formation of hydrogen bonds (C3'-**O**H and C5'-O**H**) between both the hydroxyl groups of the sugar moiety along with the oxygen in the sugar ring (**O**1) and the nitrogen atom of the oxazoline ring. Finally, the hydrogen atom of the amino group (N2-**H**) interacts with the oxygen atom of the C5'-**O**H, while the other hydrogen atom (N2-**H**) interacts with the C3'-**O**H atom. The molecule forms planes in the bc plane and stacking perpendicular to the a-axis.

3.1.3.2 Crystal structure of arabino-aminooxazoline (AAO)

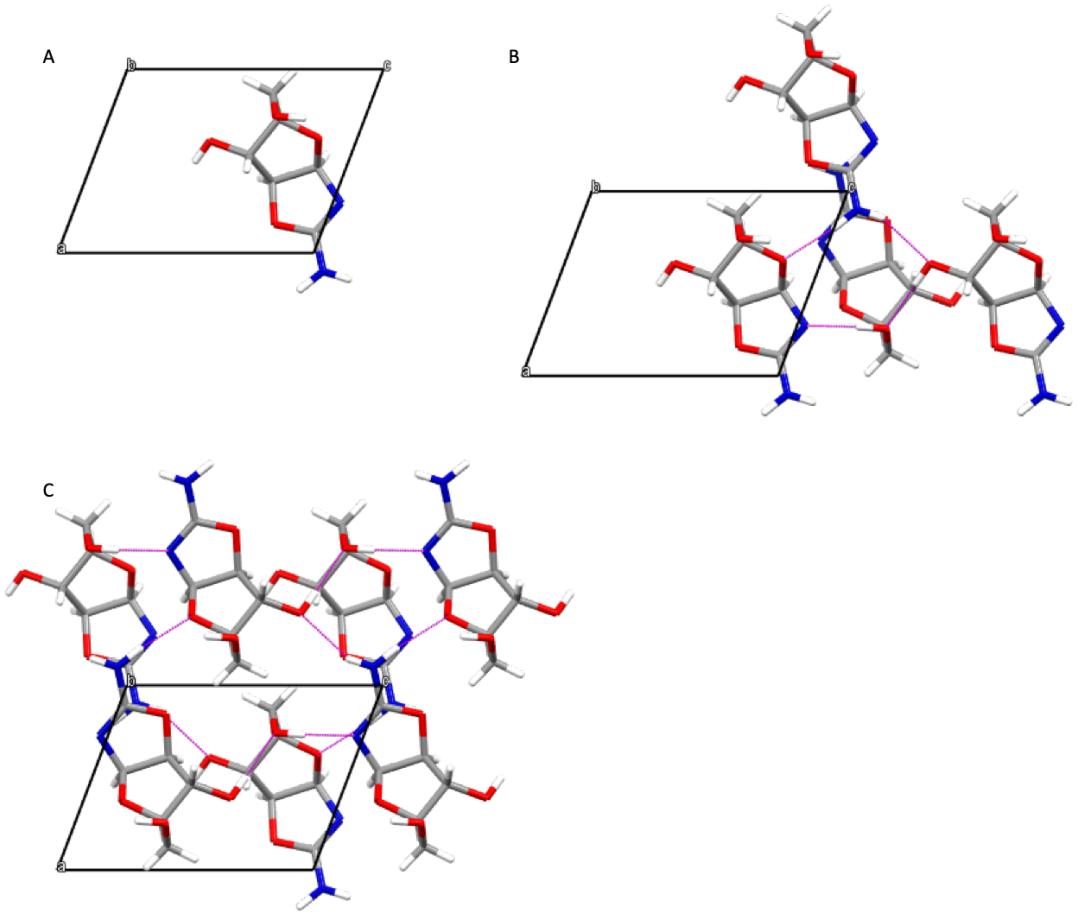

*Figure 39: D-**AAO** in A) the asymmetric unit. B) key interactions C) packing.*

AAO crystals obtained at 0% *ee* were analysed by SXRD, which confirmed conglomerate crystals (Figure 39). D- and L- **AAO** crystallises in the monoclinic $P2_1$ non-centrosymmetric space group with one molecule in the asymmetric unit. The molecules assemble into of a 10-membered ring formed by four different **AAO** molecules; the oxygen atom of the sugar ring (**O**1), the nitrogen atom (**N**1) of the oxazoline ring and two hydroxyl groups (C3'-O**H**, C5'-O**H**) of two different other molecules and finally the hydrogen atoms of the amino group (N2-**H**) which is repeated along the bc-axis creating a three-dimensional network.

3.1.3.3 Crystal structure of xylo-aminooxazoline (XAO)

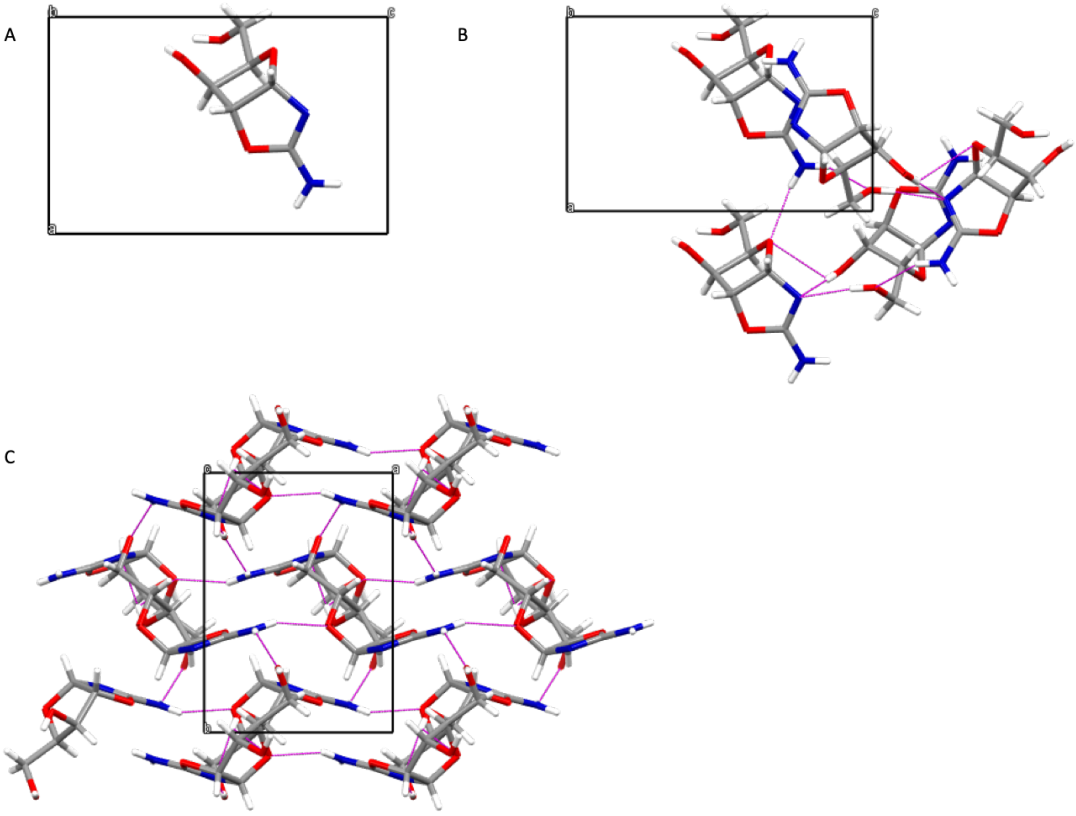

*Figure 40: D-**XAO** in A) the asymmetric unit. B) key interactions C) packing.*

XAO crystals obtained from 0% *ee* **XAO** solution were analysed by SXRD, which confirmed the presence of conglomerate crystals. D- and L- **XAO** crystallise in the orthorhombic $P2_12_12_1$ non-

centrosymmetric space group with one molecule in the asymmetric unit (Figure 40). **XAO** packs as a 14-membered hydrogen bonding motif that bridges five different **XAO** molecules. Specifically, this ring forms between **O**1···N2-**H**···C5'-**OH**···**N**1···N2-**H**···C5'-**OH**···**N**1 which results in a three-dimensional network.

3.2 Pentose Oxazolidinone Thiones (OT)

3.2.1 Synthesis of and Enantioenrichment of Oxazolidinone Thiones (OT)

Sulfur is important (essential) element for life, for example: two of the proteinogenic amino acids (methionine and cysteine) contain sulfur; it is essential in cysteine and the *zinc finger* protein motif; and is crucial to a number of important catalytic motifs such as the catalytic triad in cysteine proteases.[242,243] Sulfur is also present in essential cofactors, such as coenzyme A, which are instrumental in the citric acid cycle, ketogenesis and non-ribosomal peptide synthesis for the key process of metabolism.[244] This deep-seated requirement for sulfur chemistry in biological molecules, suggests that is it essential to investigate sulfurs role in origin of life research. Indeed, the leading process through which simple C2 and C3 sugars, glycolaldehyde (**13**) and glyceraldehyde (**14**), are produced utilise hydrogen sulfur as the stoichiometry reductant in a photochemical reductive homologation of hydrogen cyanide.[54] The by-product of this reaction is thiocyanic acid, which can also be generated quantitatively by the reaction of hydrogen cyanide and sulfur (S8). Therefore, the role of thiocyanic acid in nucleotide synthesis must be considered in detail. The synthesis of oxazolidinone thiones (**OT**) (from glycolaldehyde (**13**), glyceraldehyde (**14**), and thiocyanic acid (**27**) has been shown to be a point of divergence between purine and pyrimidine nucleotides, and access to these structures permit a viable, divergent route to prebiotic synthesis of ribonucleotides.[64]

With this in mind the *ribo*-, *arabino*- and *xylo*-oxazolidinone thiones (**ROT, AOT** and **XOT**) were prepared in order to investigate their respective crystallisation properties.[64] Each pentose sugar (ribose (***ribo*-40**), arabinose (***arabino*-40**) and xylose (***xylo*-40**) was treated with potassium thiocyanate (**41**) and concentrated hydrochloric acid at 60 °C for 24 h (Scheme 24). The resulting mixture was concentrated and purified by column chromatography ($CHCl_3$/ MeOH). The column purified produce was then re-crystallised initially using ethanol and then finally recrystallised from water. Whilst this synthetic strategy was successful for all three thiones, the scale up was not deemed suitable. Chromatography on this scale (>10 g) was not thought to be prudent, and the recrystallisation proved to be very low yielding (15%). Therefore, the oxazolidinone thiones were resynthesized and purified by Soxhlet extraction using refluxing ethanol, followed by recrystallisation in water. Soxhlet extraction and water crystallisation provided good yields (>60%) for all three thiones and were readily scalable avoiding the need for chromatography.

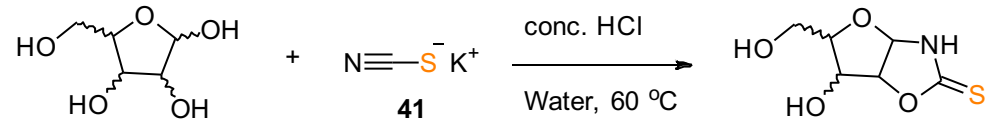

D/L ribose (D/L *ribo*-40)
D/L arabinose (D/L *arabino*-40)
D/L xylose (D/L *xylo*-40

D/L ROT
D/L AOT
D/L XOT

*Scheme 24: Synthesis of oxazolidinone thione (**OT**)*

3.2.2 Enantioenrichment of Oxazolidinone Thiones (OT)

The aminooxazoline scalemic enantioenrichment crystallisation screen was undertaken, for all three of the stereoisomers prepared (**ROT**, **AOT** and **XOT**), again with the enantioenrichment measured by optical rotations for the crystals formed from various *ee* mixtures.

3.2.2.1 Enantioenrichment of ribo-oxazolidinone thione (ROT)

Crystallisation of **ROT** (1.5 M), from aqueous solution was observed to yield a very impressive enantiomeric amplification (Figure 41). From a scalemic solution of +/− 40% *ee* **ROT**, the crystals formed exhibit optical rotations matching those of the optically pure compounds, and the curve was observed to quickly plateaus to yield enantiopure crystals. Such that although **ROT** was more soluble than **RAO**, it had an increased propensity for enantiomeric enrichment (albeit at a higher concentration, discussed in 3.8.1.2).

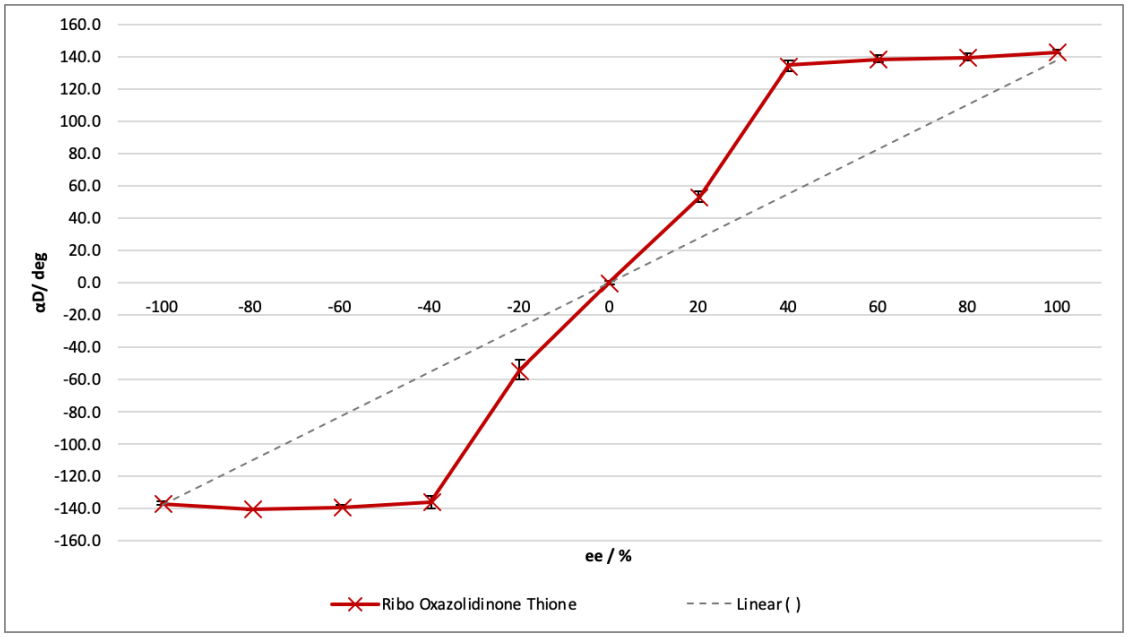

*Figure 41: Enantio-amplification of **ROT** (1.5 M, H_2O). The results were triplicated, and the average plotted along with the expected ee value. The dotted line shows the optical rotation if the crystals possessed the same* ee *value as the starting solution.*

*1.1.1.1 Enantioenrichment of arabino-oxazolidinone thione (**AOT**)*

AOT was observed to be even more soluble that **ROT**, however **AOT** (3 M) had an equally striking *ee* profile, though admittedly exhibiting the opposite trend. With **AOT**, it was observed to preferentially crystallise as the racemate, suppressing the solid phase *ee* and the optical rotation was 0 as far as +/− 60% *ee* (Figure 42). Interestingly as **AOT** forms racemic crystals,

the enantiomeric amplification occurs in the solution rather than within the crystal. The observed optical rotation in the supernatant solution was measured and found to be enriched by the same degree as the crystals were depleted in *ee* (Figure 43).

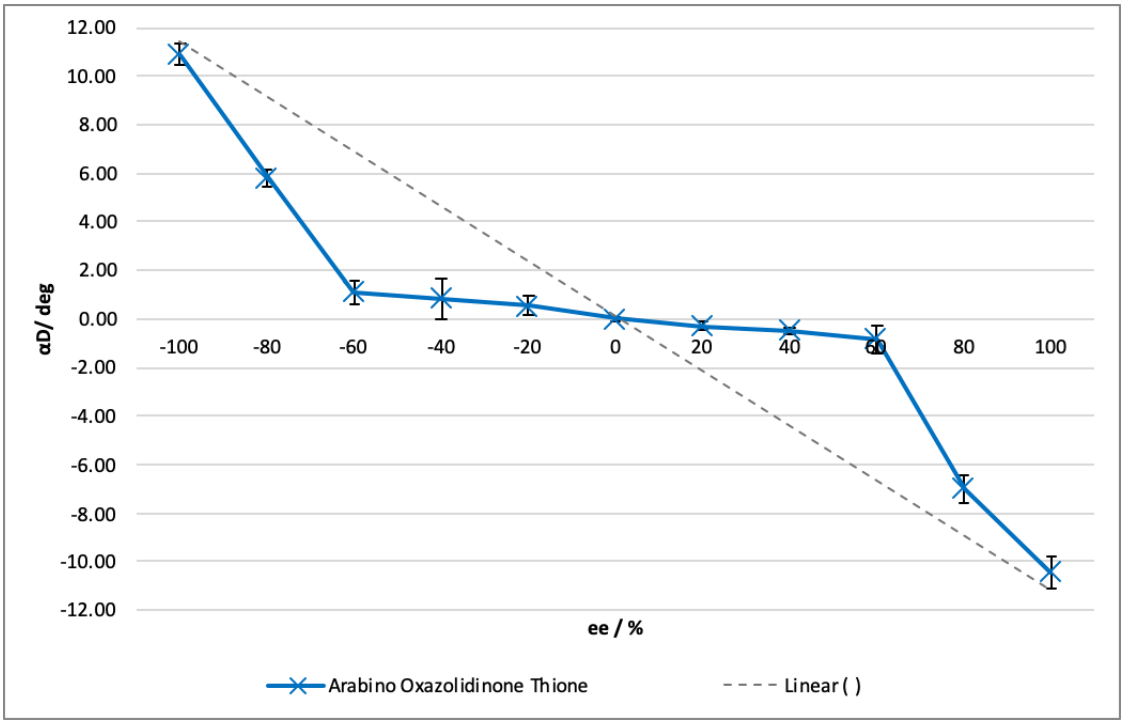

*Figure 42: Enantio-amplification of **AOT** (3 M, H_2O). The results were triplicated, and the average plotted. The dotted line shows the optical rotation if the crystals possessed the same* ee *value as the starting solution.*

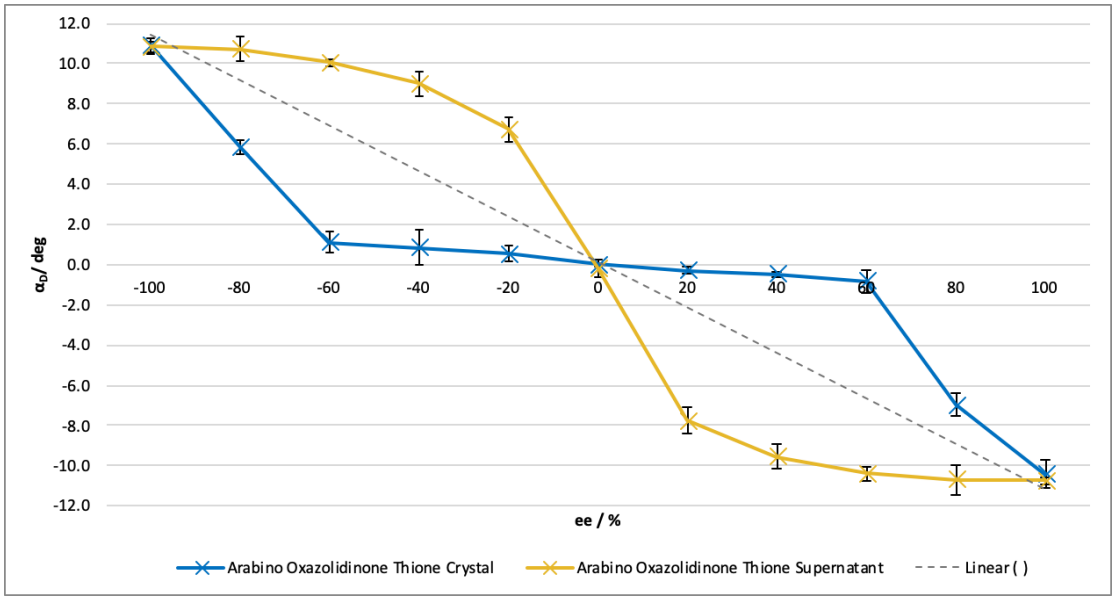

*Figure 43: Enantio-amplification of **AOT** crystals (blue) and supernatant (yellow) (3 M, H_2O). The results were triplicated, and the average plotted along with the expected ee value. The dotted line shows the optical rotation if the crystals possessed the same* ee *value as the starting solution.*

This surprising result was repeated to ensure reproducibility, and this observation was triplicated confirming this. The implication of the amplification occurring in the supernatant liquid is that we can imagine by removing the undesired racemic crystals, enriching the *ee* of the solute. Carrying the solution phase forward would furnish enriched nucleotide.

3.2.2.2 Enantioenrichment of xylo-oxazolidinone thione (XOT)

Next, *xylo*-oxazolidinone thione (**XOT**) was investigated in the same procedure as previously described. **XOT** shows analogous crystallisation to **AOT**, with a strong degree of solution phase *ee* amplification seen at the initial *ee*'s >20% (Figure 44). Across most of the initial *ee*-range (−60 to +60 % *ee*) optical rotation was not observed in the crystalline material, indicating racemic crystals had been formed, and when the solution *ee* was measured this demonstrated significant enantioenriched in all scalemic solutions.

However, for the most part (−60 to +60 % *ee*), the crystals optical rotation was demonstrated to be 0, indicating racemic crystals. Therefore, the solution *ee* was measured and shown to be enantioenriched as shown in Figure 44.

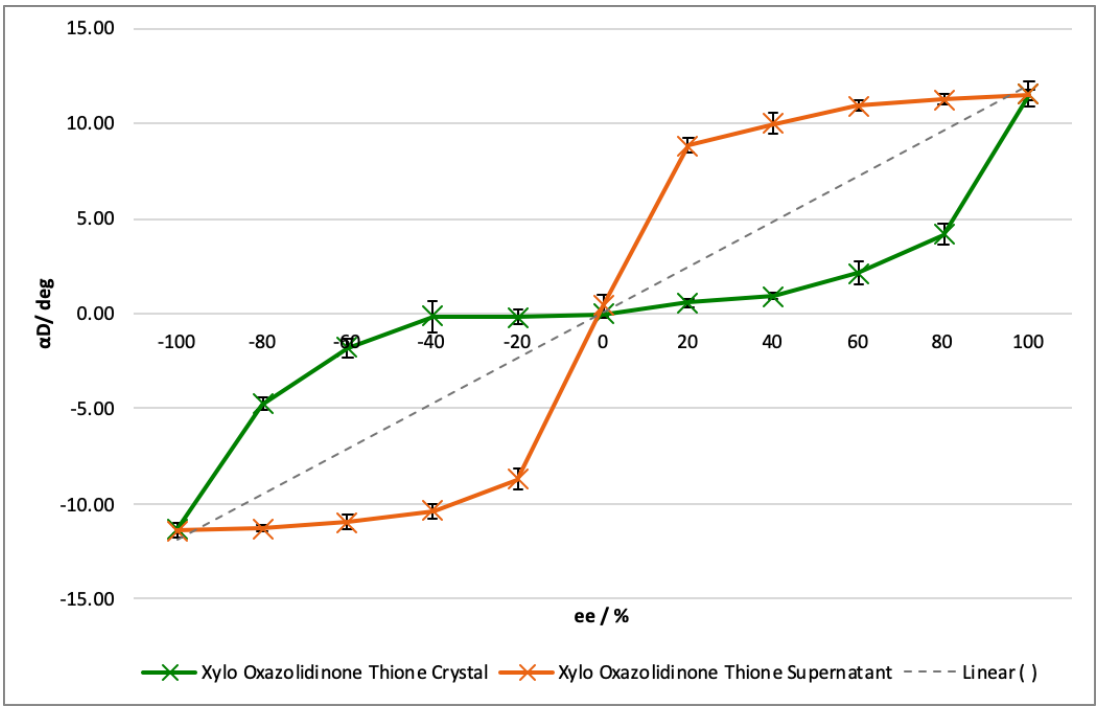

*Figure 44: Enantio-amplification of **XOT** crystals (green) and **XOT** supernatant (orange) (3 M, H_2O). The results were triplicated, and the average plotted along with the expected ee value. The dotted line shows the optical rotation if the crystals possessed the same* ee *value as the starting solution.*

3.2.3 Crystal Structures of Oxazolidinone Thiones (OT)

Once again, all the crystal structures of the oxazolidinone thiones (**OT**) were investigated as important prebiotic molecules that have not been looked at in a crystallographic point of view and could be used to indicate important behaviour that could be fundamental to understanding the origin of homochirality. The process was carried out using the same methodology as for the aminooxazolines (**AO**), whereby the optical polarimetry was measured first, then the SXRD data was collected. It was hoped that by investigating the solid phase

structure, it might reveal why a switch (from conglomerate to racemic) crystallisation was observed between the aminooxazolines (**AO**) and the oxazolidinone thiones (**OT**).

3.2.3.1 Crystal structure of ribo-oxazolidinone thione (ROT)

ROT was identified as possessing conglomerate behaviour as large enantioenrichment was observed by polarimetry. Therefore, the 0% *ee* crystals were analysed. Multiple single crystals were selected, and all were proven by single x-ray diffraction to be homochiral crystals, confirming conglomerate crystal formation from the solution of **ROT**.

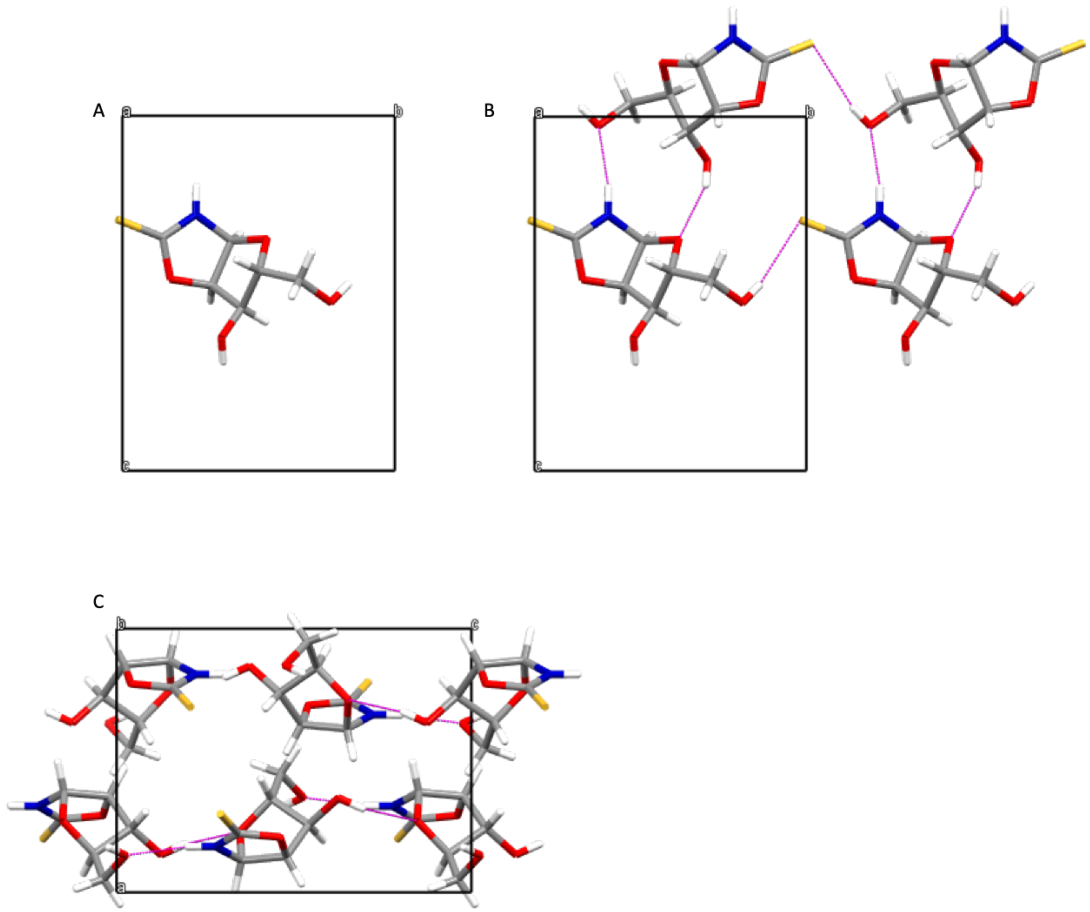

*Figure 45: D-**ROT** in A) the asymmetric unit. B) key interactions C) packing.*

L- and D- **ROT** crystallises in the orthorhombic $P2_12_12_1$ non-centrosymmetric space group with one molecule in the asymmetric unit (Figure 45). Two molecules come together through hydrogen bonds involving the sugar hydroxyl groups (C3'-O**H** and C5'-**O**H), the oxygen in the sugar ring (**O**1) and the nitrogen (N1-**H**) resulting in a 10 membered ring motif which forms ribbons along the c-axis. These ribbons are interlinked by interactions between **S**1 and C5'-O**H** in the bc plane, leading to the formation of planes that are stacked perpendicular the b-axis.

3.2.3.2 Crystal structure of arabino-oxazolidinone thione (AOT)

Arabino oxazolidinone thione (**AOT**) presented unusual behaviour during the enantioenrichment crystallisation screen. **AOT** was shown to preferentially form racemic crystals from −60% to +60% *ee* which was particularly interesting. The crystals were analysed to try to elucidate what structural feature(s) lead these crystals to preferentially form racemic crystals rather conglomerate crystals. The homochiral crystals were readily accessed by crystallisation from the homochiral solution allowing the two crystal forms to be directly compared.

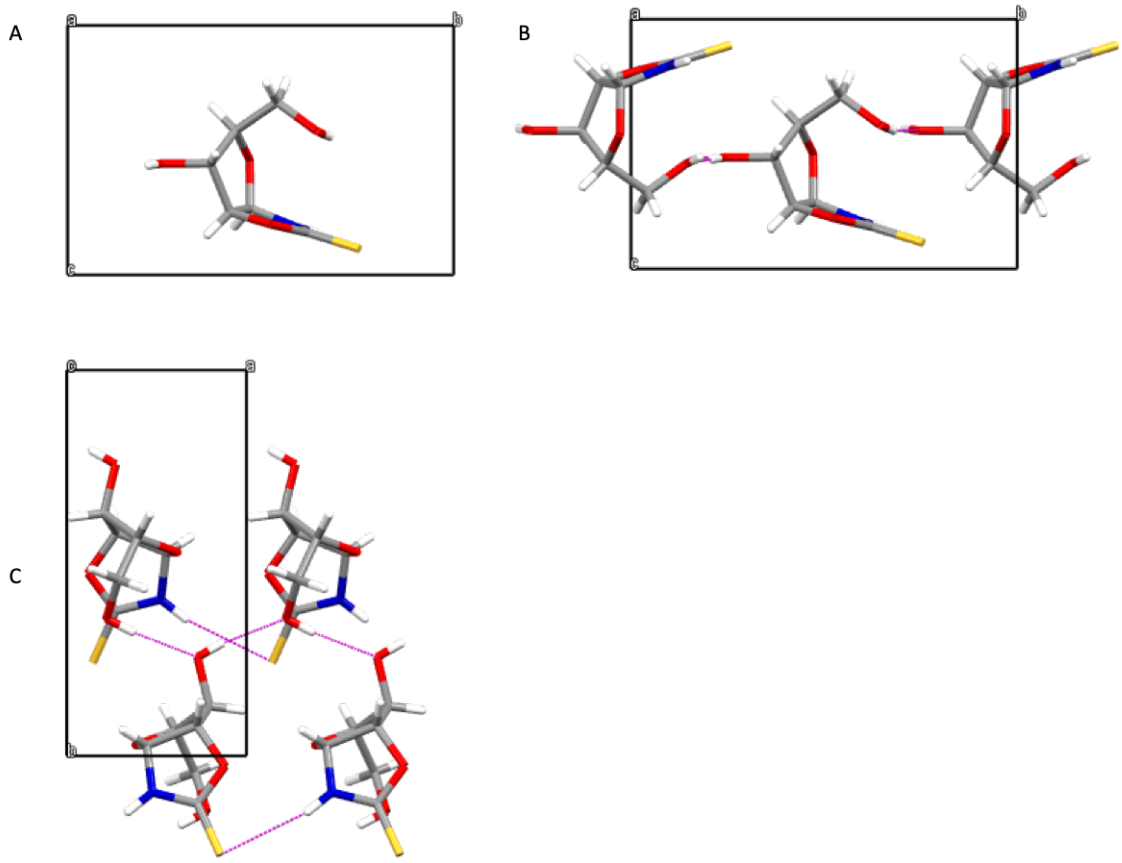

*Figure 46: D-**AOT** in A) the asymmetric unit. B) key interactions C) packing.*

For the homochiral L- and D- **AOT** it is observed that it crystallises in the monoclinic $P2_1$ non-centrosymmetric space group with one molecule in the asymmetric unit (Figure 46). The C5'-OH also has interactions with two different molecules C3'-OH via C5'O**H** and C3'**O**H and C5'**O**H ·· ·C3'O**H**. The structure also exhibits **S**1 ··· N1-**H** interactions, which both ultimately lead to the formation of unidirectional planes of molecules in the ac plane.

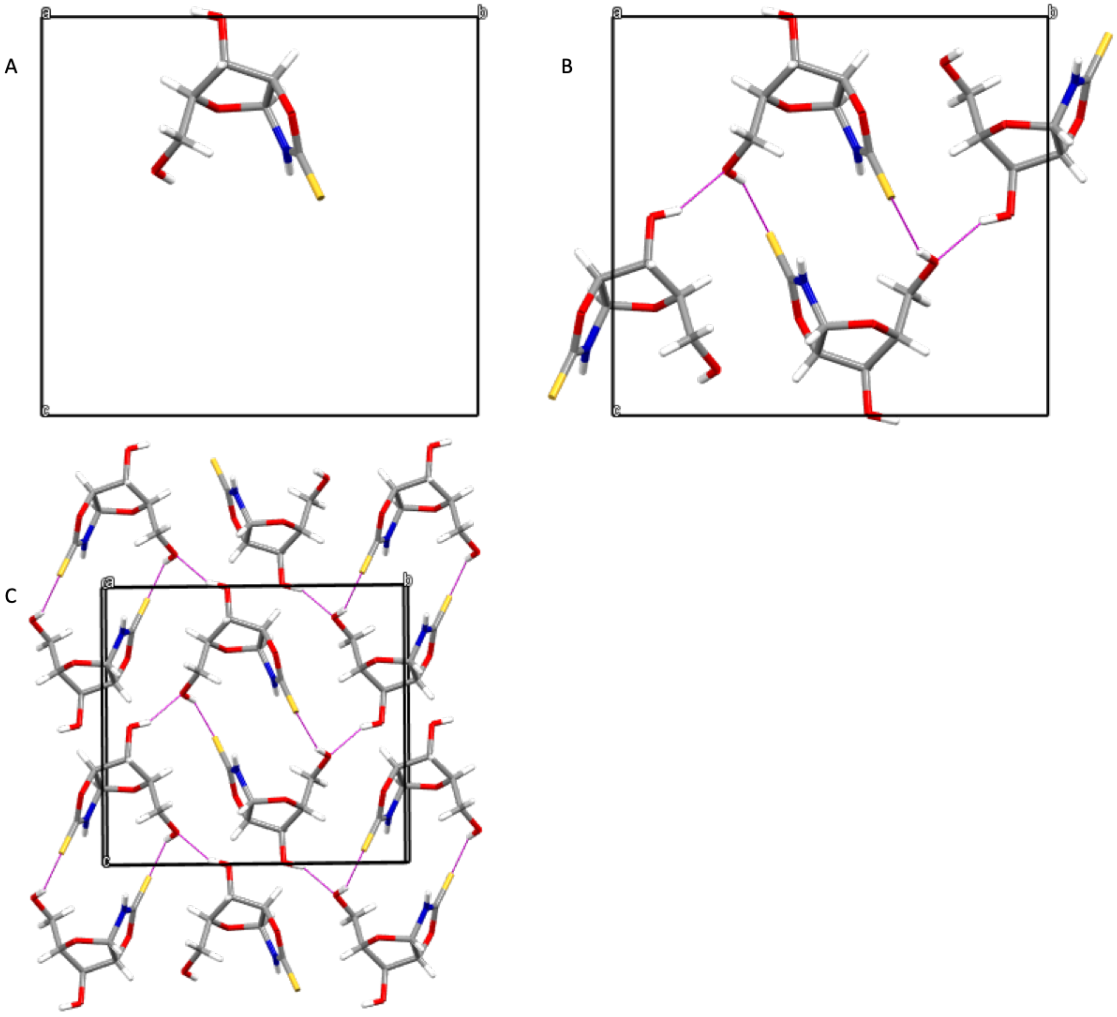

*Figure 47: Rac-**AOT** in A) the asymmetric unit. B) key interactions C) packing.*

Next the crystals obtained at 0% *ee* were analysed by SXRD. Here, racemic D- and L- **AOT** crystallises in the racemic, monoclinic $P2_1/c$ centrosymmetric space group with two molecules in the asymmetric unit, which are both enantiomers that assemble through interactions between **S**1 and C5'-O**H** (Figure 47). Additionally, the C5'**O**H atom interacts with the C3'-O**H** atom which links the ribbons of enantiomers.

3.2.3.3 Crystal structure of xylo-oxazolidinone thione (XOT)

Xylo oxazolidinone thione (**XOT**) exhibited similar behaviour to **AOT** during the scalemic enantioenrichment experiments, whereby racemic crystals were preferentially obtained. As before, the homochiral crystals were obtained for both enantiomers so the full data set could be investigated.

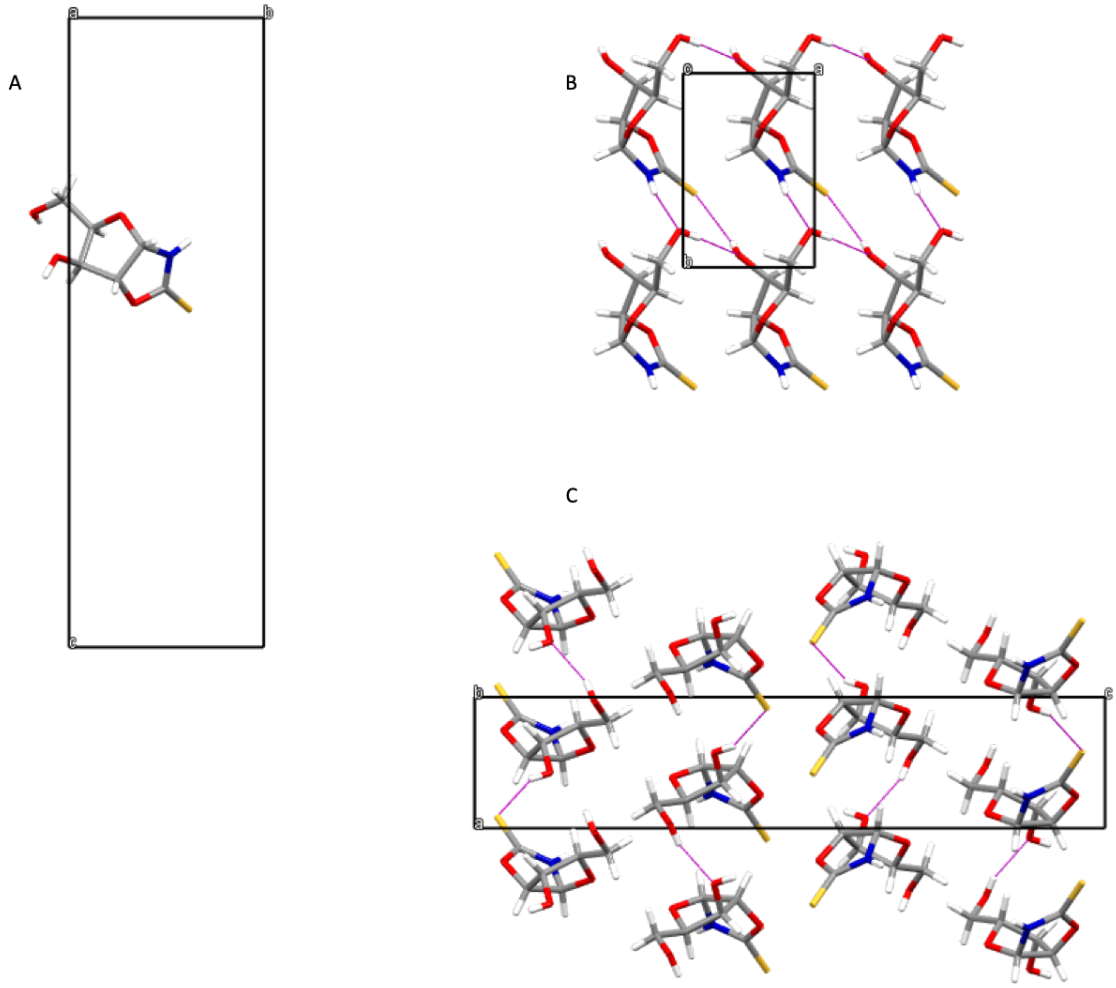

*Figure 48: D-**XOT** in A) the asymmetric unit. B) key interactions C) packing.*

Homochiral D and L **XOT** crystallises in the orthorhombic $P2_12_12_1$ non-centrosymmetric space group with one molecule in the asymmetric unit (Figure 48). There are interactions between N1-**H** and C5'-**O**H which form ribbons along the ab axis. The C5'-O**H** has further interactions

with C3'-**O**H which creates planes perpendicular the b axis. Furthermore, **S1** interacts initially with two other sulfur atoms (**S1**).

Racemic **XOT** crystallises in the orthorhombic $P2_12_12_1$ non-centrosymmetric space group with two molecules in the asymmetric unit (Figure 49). The formation of **S**1···C3'-O**H** interactions link the two enantiomers together along the *c* axis. Furthermore, enantiomers are also interacting through N1-**H**···C5'-**O**H forming dimer-like structures on the *bc* plane. The C5'-O**H** also forms interactions with another opposite enantiomers C5'-**O**H which creates stacking along the a*c* axis.

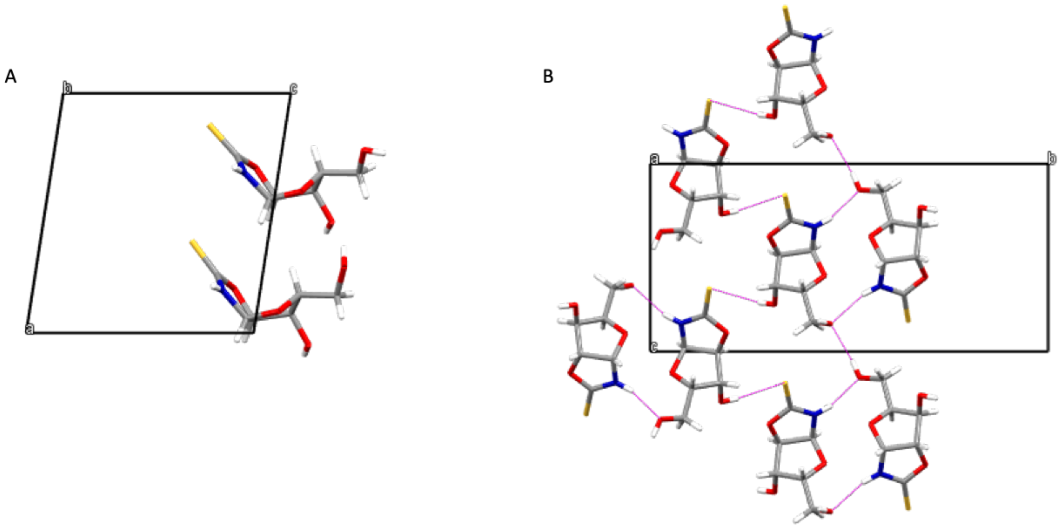

*Figure 49: Rac-**XOT** in A) the asymmetric unit. B) key interactions*

.

3.3 Pentose Oxazolidinones (OX)

Pentose oxazolidinones (**OX**) provided another interesting target compound for several reasons. Firstly, they are structurally similar to the two previous compounds that have been investigated; the C2 carbon is substituted with an oxygen in place of a nitrogen or sulfur. It

was thought that this structural relationship would yield further insight in the crystallisation behaviour of oxazolidinone structures.

Secondly, the oxazolidinones (**OX**) are often seen as a by-product in many prebiotic reactions. One of these observed routes is towards the purine nucleosides, where the cyanovinyl oxazolidinone thione (**CVOT**) in water can hydrolyse to the oxazolidinone (**OX**) and dicyanovinylsulfide (**41**), which has been previously confirmed by single crystal X-ray diffraction studies (Scheme 25).[64]

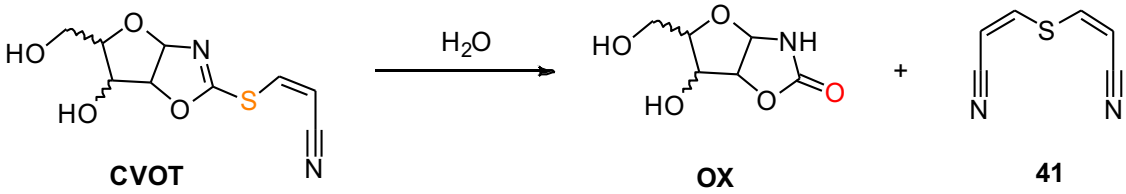

*Scheme 25: The degradation of S-cyanovinylated oxazolidinone thione (**CVOT**) in water to lead to the oxazolidinone (**OX**) and dicyanovinylsulfide (**41**).*

Furthermore, photoisomerisation studies of α-cytidine (α-*ribo*-**42**) have shown that *ribo*-oxazolidinone (**ROX**) is formed, in particularly low yield (4%), and that the competing cyclisation to the oxazolidinone **ROX**/ **AOX** and loss of the nucleobases has been identified as the source of nucleoside loss (Scheme 26).[35,45]

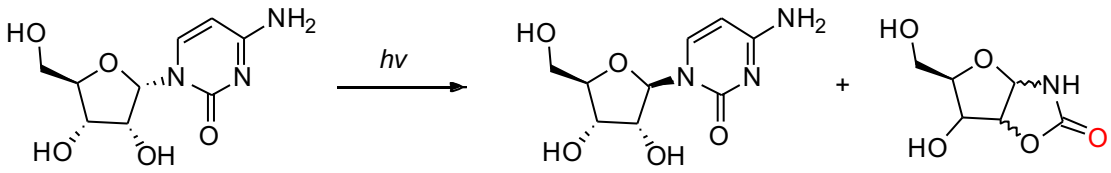

α-ribo-42 **β–ribo-42** **ROX/ AOX**

*Scheme 26: Orgel's one pot cytidine synthesis, with the final step using photoanomerisation leading to nucleoside loss and resulting in the production of oxazolidinone **OX**.*

3.3.1 Synthesis of Oxazolidinones

The synthesis of the pentose oxazolidinones (**OX**) were carried out according to the literature-reported method.[64] The pentose sugar (**40**, 20.0 mmol) was stirred with ammonium chloride and potassium cyanate (**42**) heated in water at 60 °C for 8 h (Scheme 27). This solution was then allowed to cool to room temperature, lyophilised to produce a yellow oil. The oil was then purified by silica gel flash column chromatography (FCC). Finally, the residue was recrystallised from ethanol and water in modest yields (21 – 45%) but resulted in just over a gram of the desired product which was inadequate for the requirement of this study.

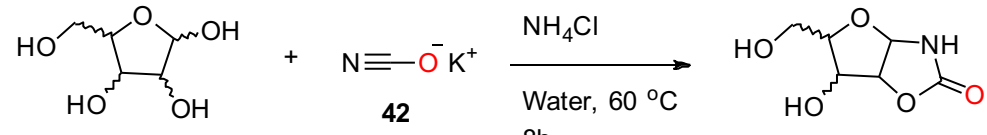

D/L ribose (D/L ribo-40)
D/L arabinose (D/L arabino-40)
D/L xylose (D/L xylo-40)

D/L ROX
D/L AOX
D/L XOX

Scheme 27: Synthesis of the oxazolidinones

This procedure was scaled up and although the material was achieved, the crystallisation was not straightforward. Solid material obtained using the described method of ethanol and water

was not crystalline. Different solvent systems were tried (Table 1), however no successful crystallisations was observed, only sticky powders were isolated. After a series of attempted re-crystallisations, a very small quantity of crystals was eventually obtained from water: ethanol (10:1), but the yield was very low (<1%). It was therefore considered an impurity may be hindering the crystallisation that was undetectable.

Table 1: Attempted crystallisations for the oxazolidinones

Attempted Crystallisations		
Water (100%)	Water: Methanol (1:99)	Water: Ethanol (1:10)
Methanol (100%)	Water: Methanol (1:10)	Water: Ethanol (1: 99)
Ethanol (100%)	Water: Methanol (100:1)	Water: Ethanol (10:1)
Ethyl Acetate (100%)	Water: Methanol (10:1)	Water: Ethanol (5:1)
Diethyl Ether (100%)	Water: Methanol (5:1)	Water: Ethanol (2:1)
Petrol Ether (100%)	Water: Methanol (2:1)	Water: Ethanol (1:1)
Chloroform (100%)	Water: Methanol (1:1)	Ethanol: Methanol (100:1)
DCM (100%)	Ethyl Acetate: Methanol (10:1)	Ethanol: Methanol (10:1)
Acetonitrile (100%)	Ethyl Acetate: Methanol (5:1)	Ethanol: Methanol (5:1)

The powder was reanalysed by NMR and TLC, whilst the NMR showed a small impurity of 5%, through various testing of TLC conditions, it was shown the material contained an impurity that was identified by a small spot on TLC (EtOAc/ MeOH 95:5, product spot R_f 0.35, impurity R_f 0.38). This was thought to be a side-product that is unable to cyclise due to an unfavourable conformational relationship of the alcohol nucleophile and -N=C=O electrophile prior to cyclisation. Due to the reactive nature of the intermediate species involved in the mechanism it was not possible to isolate this species for analysis.

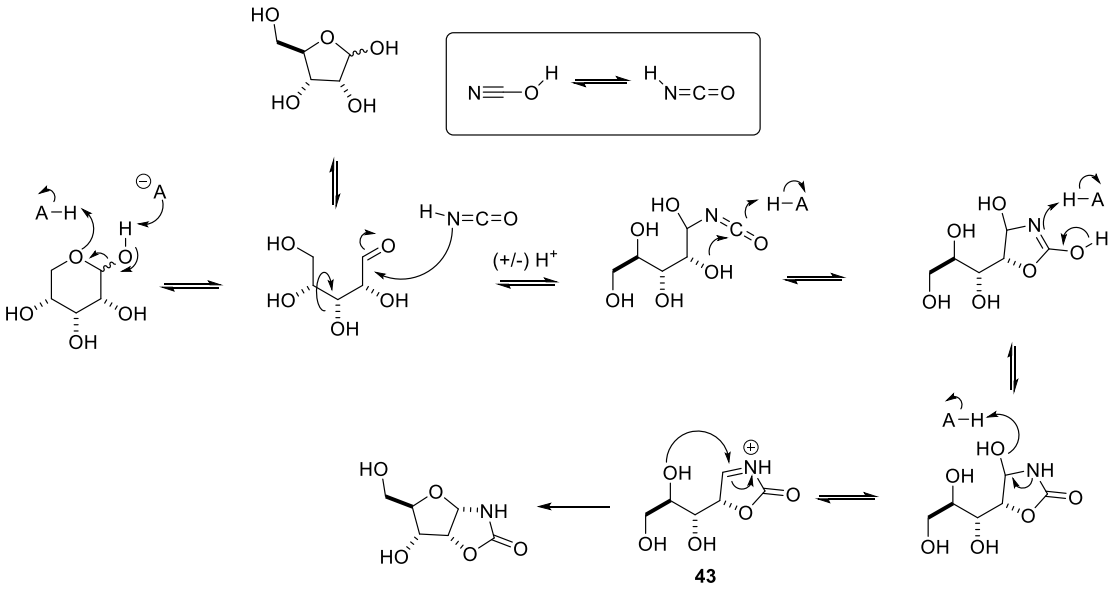

Figure 50: Proposed mechanism to form the intermediate

As discussed previously, the scalemic crystallisations require a large amount of material to be produced for one experiment, and for optimisation more is needed. Therefore, to acquire the necessary quantity of oxazolidinone for the enantioenrichment crystallisation screens, the synthesis required significant scaled up optimisation.

The scale up and optimisation proved to be particularly challenging. The reaction was scaled up, consequentially starting from 80 mmol of pentose sugar (12 g). Initially the reaction was carried out with 3 equivalents of potassium cyanate and ammonium chloride, heated in water at 60 °C. The reaction was monitored, and 8 h was found to be the most optimum time for all the oxazolidinones with regular monitoring by TLC. When the reaction was deemed to be complete, the reaction was lyophilised several times, to remove the large quantity of water. This was then consequently dissolved in a small amount of methanol (10 mL) and purified by gravity fed column chromatography. FCC proved to be inadequate to achieve the purification

of any of the oxazolidinones (**OX**) due to the side-product having a very similar R_f value even at different solvent systems and the speed at which those columns were run were deemed unsuitable. Early attempts of gravity fed column chromatography failed using smaller columns, and less solvent. Which ultimately meant the column had to be run with extreme precision following extensive optimisation. Eventual conditions were arrived at using in 2L EtOAc, 4L EtOAc: MeOH (99:1), 2L EtOAc: MeOH (95:5), in a 10 cm diameter column and run under gravity over the course of 10 h.

3.3.2 Enantioenrichment of Oxazolidinones (OX)

3.3.2.1 Enantioenrichment of ribo-oxazolidinone (ROX)

The scalemic enantioenrichment crystallisation experiments were performed for all three of the stereomers prepared (**ROX**, **AOX** and **XOX**), and the optical rotations were measured for the crystals formed from the scalemic solutions.

Ribo-oxazolidinone (**ROX**) was the first to be analysed. Crystallisation of **ROX** from water required high concentrations (> 3 M). At 3 M concentration it was noted that crystals appeared in the range of −40 to +40 % *ee* within 3 days, however the remaining mixtures took up to 2 weeks to fully crystallise. This was indicative of a preference of **ROX** to crystallise as racemic crystals. This was confirmed by dissolving the resulting crystals measuring the optical rotation of those and additionally the supernatant (Figure 51).

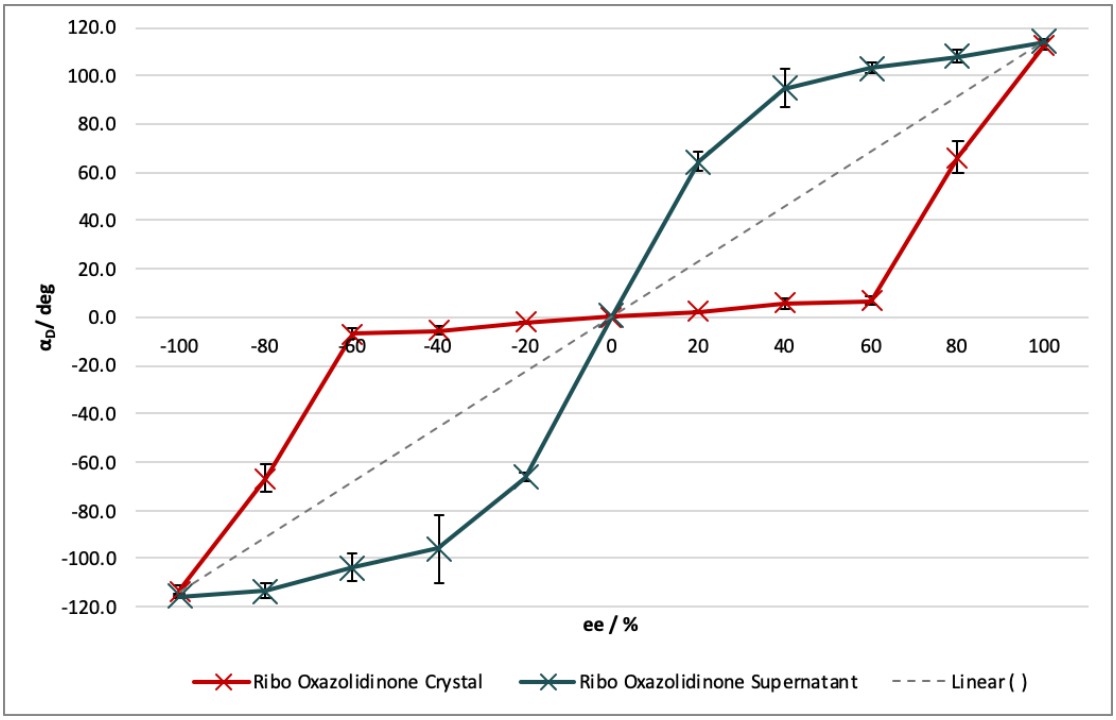

*Figure 51: Enantio-amplification of **ROX** crystals (red) and supernatant (blue) (3 M, H_2O). The results were triplicated, and the average plotted along with the expected ee value. The dotted line shows the optical rotation if the crystals possessed the same* ee *value as the starting solution.*

Scalemic **ROX** solutions were observed to only crystallise racemic crystals at *ee* less than 60%. This therefore indicates that enantioenrichment is occurring in the solution, therefore the supernatant's optical rotation was measured and confirmed the expected findings.

3.3.2.2 Enantioenrichment of arabino-oxazolidinone (AOX)

Arabino oxazolidinone (**AOX**), even at high concentrations proved to be particularly difficult to crystallise. Crystallisations were attempted at 3 M in H_2O and no crystals were formed, 4 M was subsequently tried and again failed. This was increase to 5 M however the initial material wouldn't dissolve. Both 3 M and 4 M concentrations were allowed to evaporate at rt over 2 weeks, however this led to the formation of an oil. It was therefore decided to try different solvents to try to initiate crystallisation. Different ratios and concentrations were tried in order to optimise the crystallisation at all scalemic mixtures. The most effective result was achieved

at 5 M **AOX**, in H_2O/ ethanol (1:1). Here, crystallisation took place over two weeks whereby the crystals around −20% to +20% *ee* took the longest to crystallise (2 weeks). Measurement of the optical rotations showed the largest enantioenrichment occurring from 60% *ee* suggesting homochiral crystals are being formed preferentially from the scalemic mixtures (Figure 52).

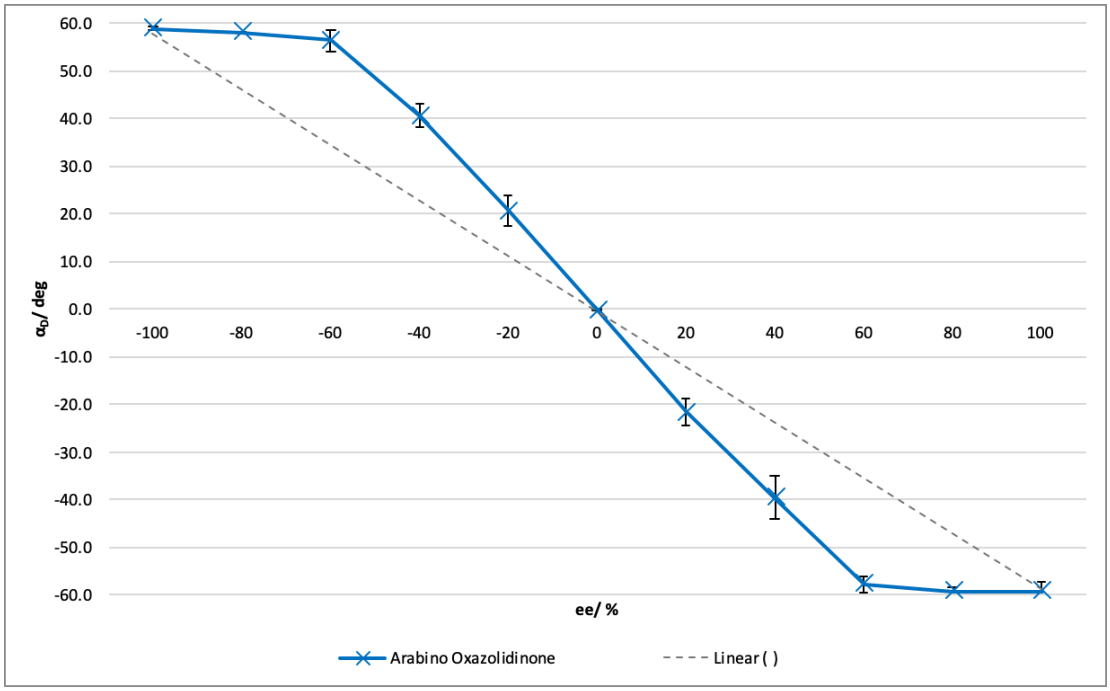

*Figure 52: Enantio-amplification of **AOX** crystals (blue) (3 M, H_2O/ethanol (1:1). The results were triplicated, and the average plotted along with the expected ee value. The dotted line shows the optical rotation if the crystals possessed the same* ee *value as the starting solution.*

3.3.2.3 Enantioenrichment of xylo-oxazolidinone (XOX)

Xylo-oxazolidinone (**XOX**) crystallisation was observed to be similar to that of the **AOX**, crystallisation did not take place in water, even at high molarities, and then the initial dissolving of the compound became the problem. Therefore, crystallisation was attempted at 5 M with 1:1 H_2O: Ethanol. This was partially successful at −20 to +20 % *ee* therefore a higher concentration of 6 M was tried with 1:1 H_2O: Ethanol at which the crystallisation was

successful, with the crystals between −40 to +40 % *ee* taking place before the remaining *ee's* suggesting the formation of racemic crystals. The optical rotation was measured and confirmed this observation. As before, the supernatant was also measured to anticipate the possible enantioenrichment in solution which is shown in Figure 53.

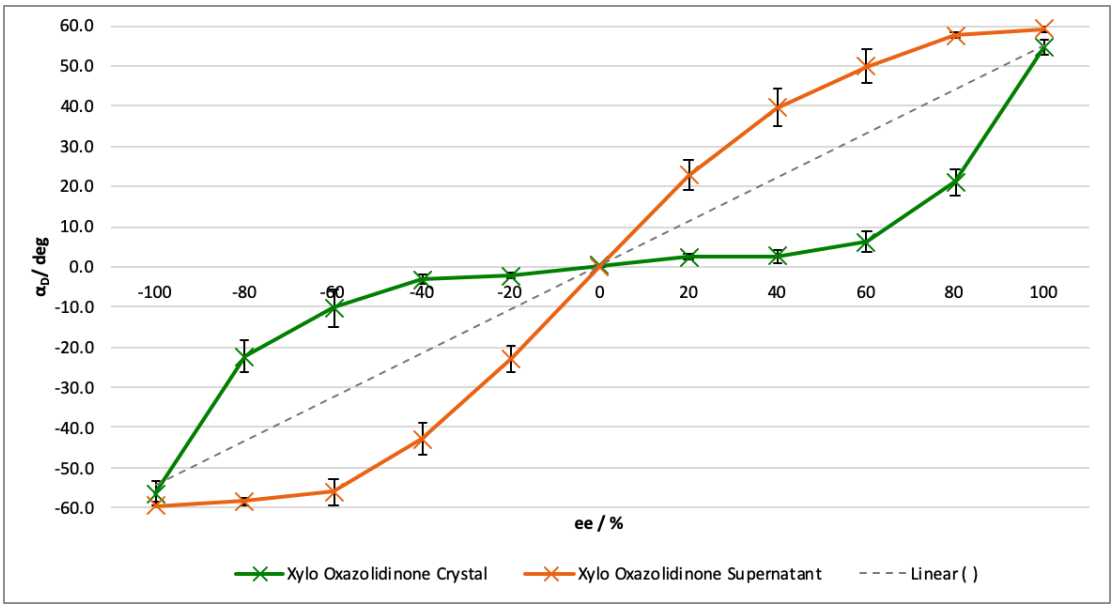

*Figure 53: Enantio-amplification of **XOX** crystals (green), supernatant (orange) (6 M, H_2O/ethanol (1:1). The results were triplicated, and the average plotted along with the expected ee value. The dotted line shows the optical rotation if the crystals possessed the same* ee *value as the starting solution.*

3.3.3 Crystal Structures of Oxazolidinones

3.3.3.1 Crystal structure of ribo-oxazolidinone (ROX)

For the homochiral L- and D- ribo oxazolidinone (**ROX**), it is observed that it crystallises in the monoclinic $P2_1$ non-centrosymmetric space group with one molecule in the asymmetric unit (Figure 54). **ROX** interacts through **O3** and N1-**H** to another molecule through the C3'-O**H**, and C5'-**O**H respectively along the bc plane. These ribbons are then connected to other ribbons along the same axis causing stacking on the b axis through C5'-O**H** to **O3**.

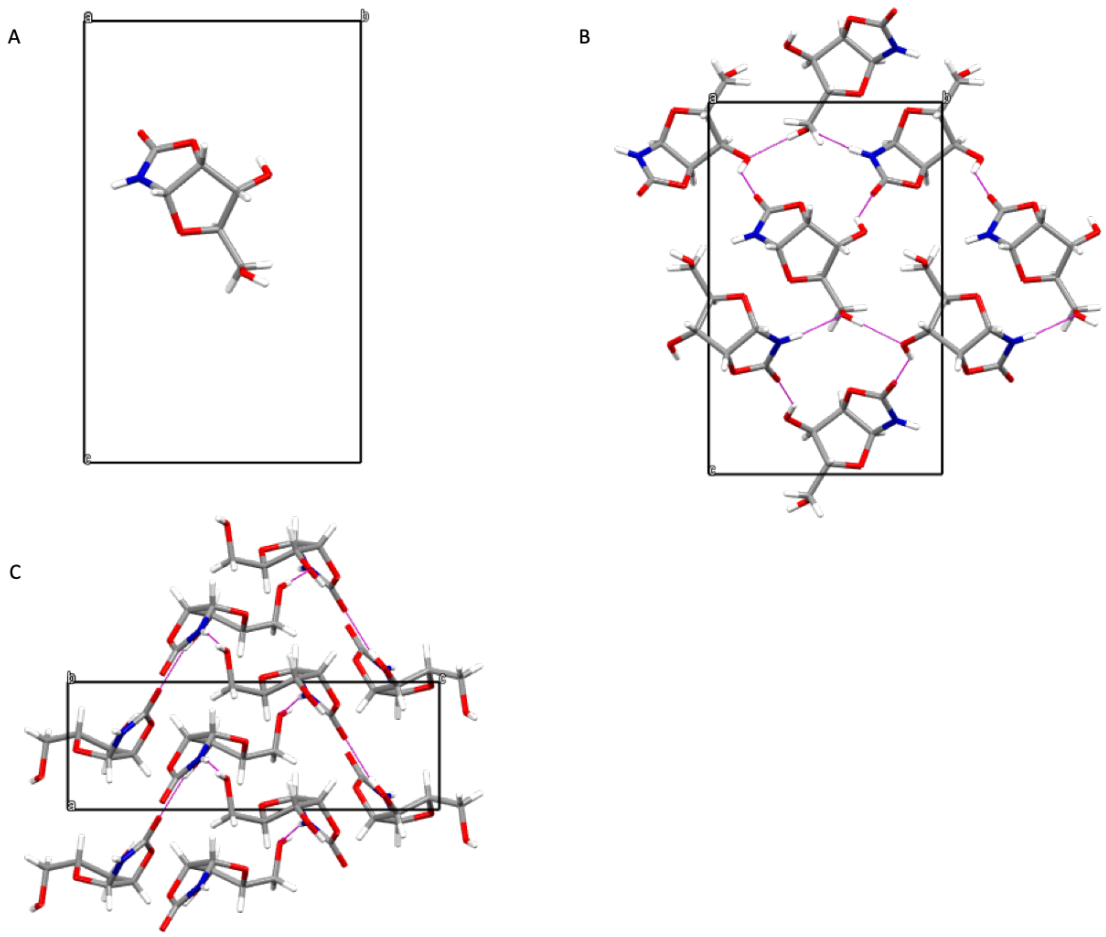

Figure 54: D-ribo-oxazolidinone in A) the asymmetric unit. B) key interactions C) packing.

ROX was found to crystallise at 0% *ee* as a racemic crystal, containing both enantiomers within the crystal lattice. Racemic **ROX** crystallises in the monoclinic $P2_1/c$ non-centrosymmetric space group with one molecule in the asymmetric unit (Figure 55). Strands of single enantiomers are connected directly to one other molecule via the N1-**H** ··· C5'-**O**H and **O3** ··· C3'-O**H**. These strands form in the *ab* plane and every other strand is the opposite hand of enantiomer.

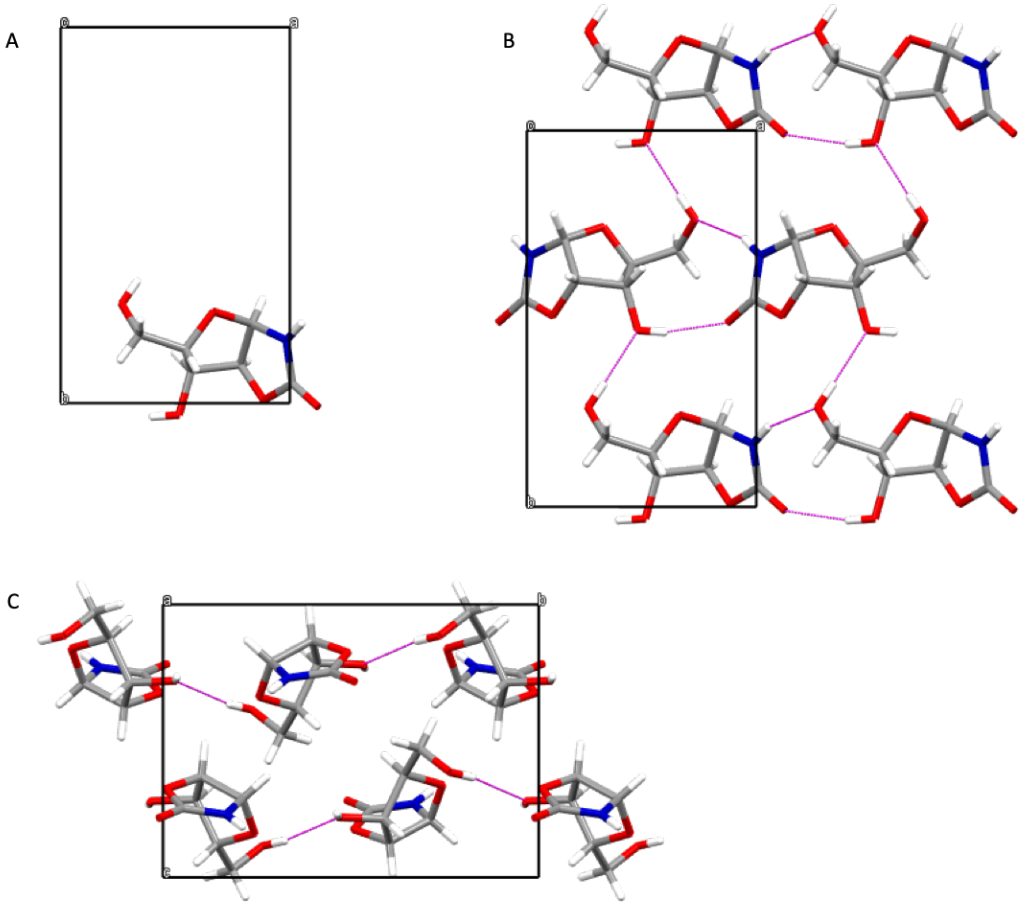

Figure 55: Rac-ribo-oxazolidinone in A) the asymmetric unit. B) key interactions C) packing.

3.3.3.2 Crystal structure of arabino-oxazolidinone (AOX)

AOX demonstrated conglomerate forming behaviour based upon the scalemic enantioenrichment experiments. Therefore, the crystals were collected and analysed. The crystals formed at the 0% *ee* were too small to be able to generate a successful SXRD structure, therefore PXRD was used to verify these findings (Figure 57). The homochiral crystal structures were also collected to try to pin point the structural basis for these interactions.

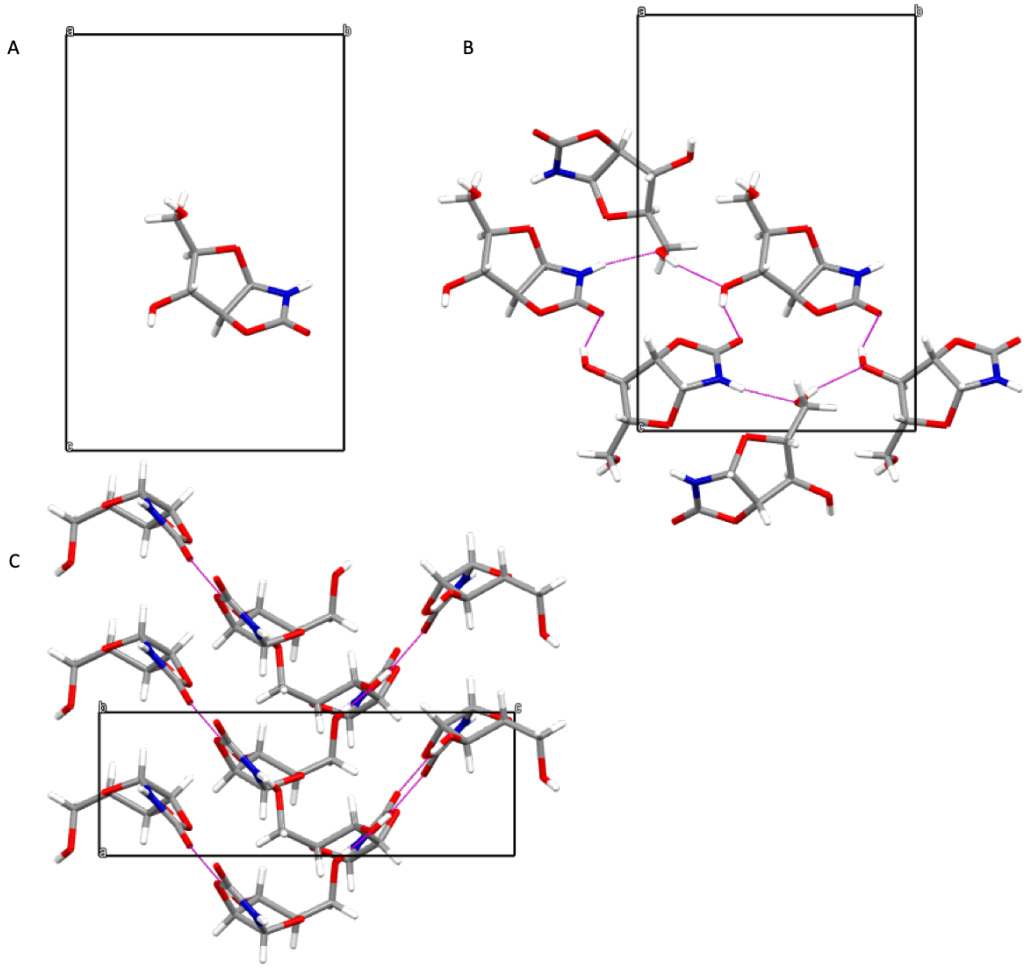

Figure 56: D-arabino-oxazolidinone in A) the asymmetric unit. B) key interactions C) packing.

Homochiral D & L **AOX** crystallises in the orthorhombic $P2_12_12_1$ non-centrosymmetric space group with one molecule in the asymmetric unit (Figure 56). There are interactions between N1-**H** and C5'**O**H, and C5'-O**H** further interacts with C3'-**O**H. The C3'-OH interacts with O3 which links back to another C3'OH which makes a 12 membered ring motif building along the bc plane.

The crystals obtained at 0% *ee* were analysed by PXRD along with the homochiral crystals that shows succinctly that **AOX** forms conglomerate crystals at 0% *ee* (Figure 57).

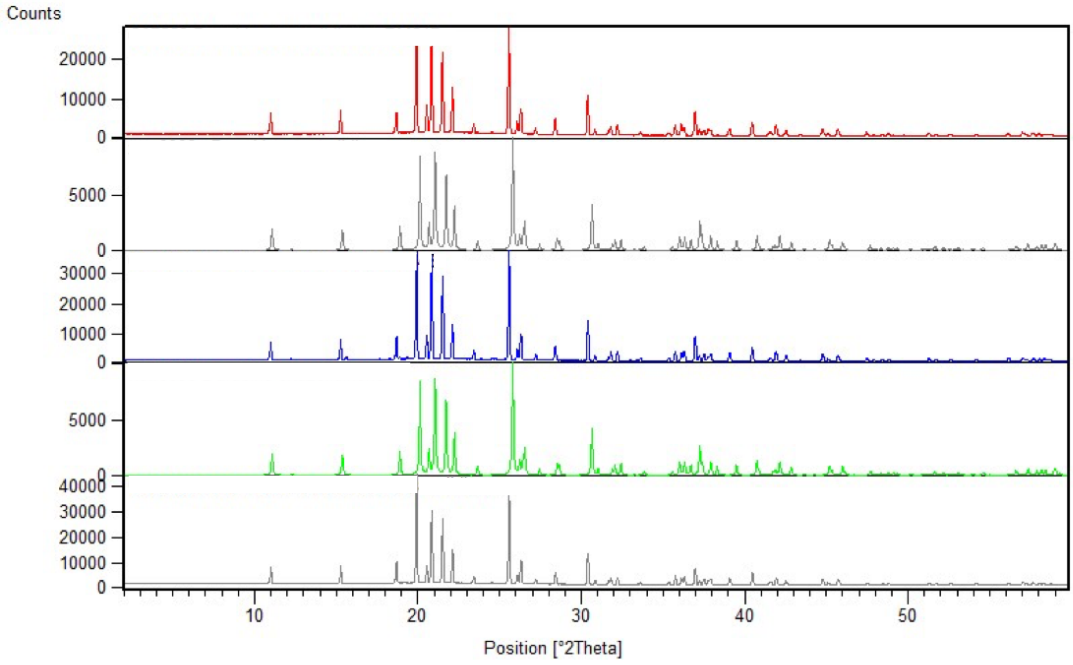

Figure 57: PXRD of D arabino oxazolidinone, L arabino oxazolidinone and racemic (0ee) arabino oxazolidinone

3.3.3.3 Crystal structure of xylo-oxazolidinone (XOX)

Homochiral L and D **XOX** crystallises in the monoclinic $P2_1/c$ non-centrosymmetric space group with one molecule in the asymmetric unit (Figure 58). Interactions takes place between four different molecules via N1-**H** ···C5′-**OH** ···C3′-**O**H ···**O3** ···C3′-O**H** ···**O3** along the a*b* plane to produce a three-dimensional structure.

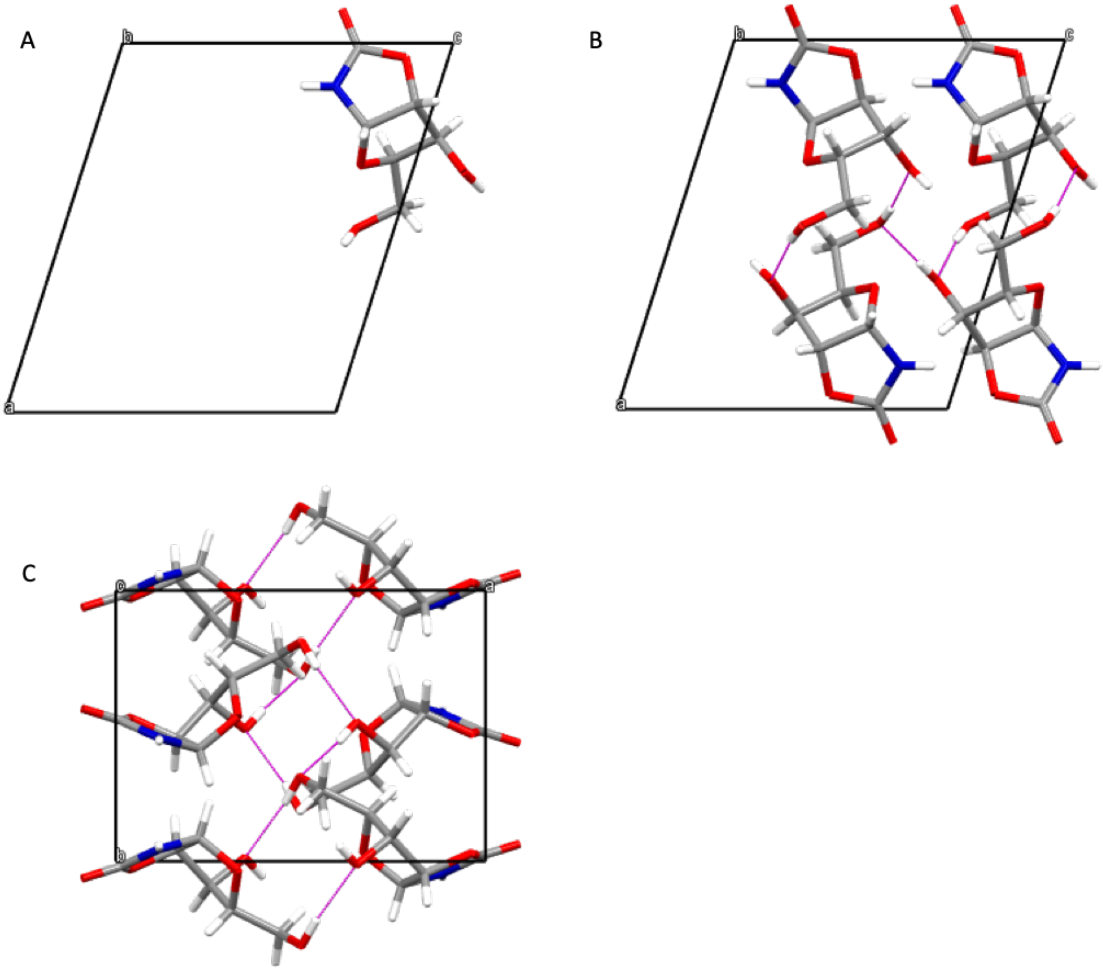

Figure 58: D-xylo-oxazolidinone in A) the asymmetric unit. B) key interactions C) packing.

In the racemic crystals obtained at 0% *ee.* The opposite enantiomers interact with each other via N1-**H** ···**O3** interactions. The enantiomers interact with the same enantiomer through interactions of the C5'-O**H** and C3'-**O**H and additionally the C3'**O**H and C5'O**H** forming a 12 membered ring motif.

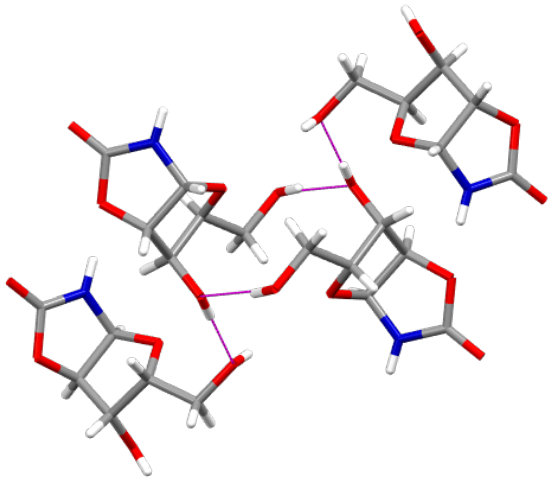

Figure 59: Racemic xylo oxazolidinone crystals obtained at 0% ee

3.4 Cyanovinyl-oxazolidinone Thiones

3.4.1 Synthesis of cyanovinyl-oxazolidinone thiones (CVOT)

Cyanovinyl oxazolidinone thione (**CVOT)** have been shown by Stairs *et al.* to be important precursor *en route* to the purine and pyrimidine nucleotides (Scheme 28). Oxazolidinone thiones (**OT**) can be activated with cyanoacetylene (**16**) to quantitively produce the cyanovinyl thione (**CVOT**).

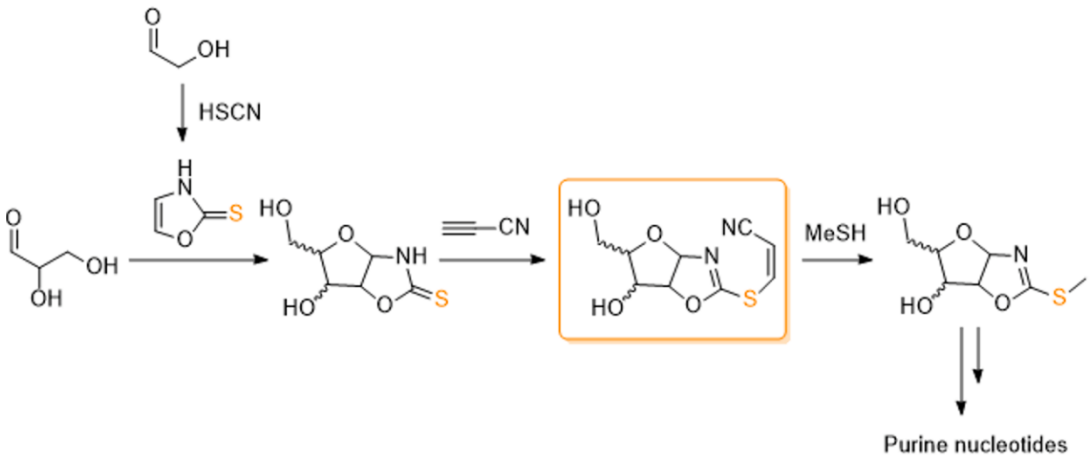

*Scheme 28: Prebiotic synthesis of cyanovinyl oxazolidinone thione (**CVOT**)*

Cyanoacetylene (**16**) plays a vital role in the synthesis of pyrimidines, making it an excellent choice for activation of **OT** for purine nucleotide synthesis. The synthesis is best achieved actually using the prebiotically plausible method whereby the oxazolidinone thione (**OT**, 3.46 mmol) is reacted with cyanoacetylene (**16**, 9.8 mmol) at room temperature for 1 h followed by lyophilisation to yield the cyanovinyl oxazolidinone thione (**CVOT**) which can be used without further purification. To achieve this, cyanoacetylene (**16**) first had to be synthesised (Scheme 29). This was completed by cooling liquid ammonia (150 mL) to −78 °C, with slow addition of methyl propiolate (**45**, 20 mL) and stirring for 1 h. The excess ammonia was then co-evaporated with anhydrous chloroform to result in solids which were crystallised in hot DCM to yield propiolamide in good yield (70%). Propiolamide (**46**) was then ground together with oven dried sand and P_2O_5 (30.0 g) and then heated to 130 °C at 100 torr over 1 h. Over that time, HCCCN was distilled from the sand mixture and collected as a solid at −78 °C in a cold trap. Due to the volatility of HCCCN these solids were weighed and immediately dissolved in water to form the aqueous solution of cyanoacetylene (**16**, 0.98 M).

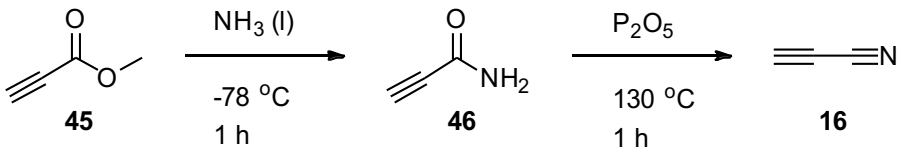

*Scheme 29: Synthesis of cyanoacetylene (**16**) starting from methyl propiolate (**45**) and liquid ammonia forming propiolamide (**46**) which can then be heated with P_2O_5 to give **16**.*

3.4.2 Enantioenrichment of cyanovinyl-oxazolidinone thiones (CVOT)

Due to the high concentration of cyanoacetylene (**16**) required for the reaction with oxazolidinone thiones, the essential synthetic effort needed to synthesise the oxazolidinone

thiones (**OT**), the crystallisation was optimised before achieving the enantioenrichment. Whilst, the full range of scalemic enantioenrichment crystallisation screen was not carried out, −100 %, 0 and +100 % *ee* mixtures were investigated at different concentrations (0.25 M – 5 M) to try to explore the crystals obtained at those vital points.

3.4.3 Crystal Structure of cyanovinyl-oxazolidinone thiones

3.4.3.1 Crystal structure of ribo-cyanovinyl-oxazolidinone thione (RCVOT)

Homochiral *ribo*-cyanovinyl-oxazolidinone thione (**RCVOT**) was observed to crystallise in the monoclinic $P2_1$ non-centrosymmetric space group with one molecule in the asymmetric unit. Each molecule interacts with 4 distinct molecules using both of the free hydroxyl groups (C5'**O**H and C3'-O**H**). The C5'-**OH** interacts with two C3'**OH** molecules using both the oxygen and hydrogen available. Where the C3'**OH** interacts further with the C5'-**OH** of two other molecules as shown in Figure 60. This creates a 10 membered ring motif which the cyano-vinyl motif is excluded from the core interactions. The hydroxyl interactions lead to ribbons packing along the *ac* plane resulting with a 3-D structure being built up in the *bc* plane.

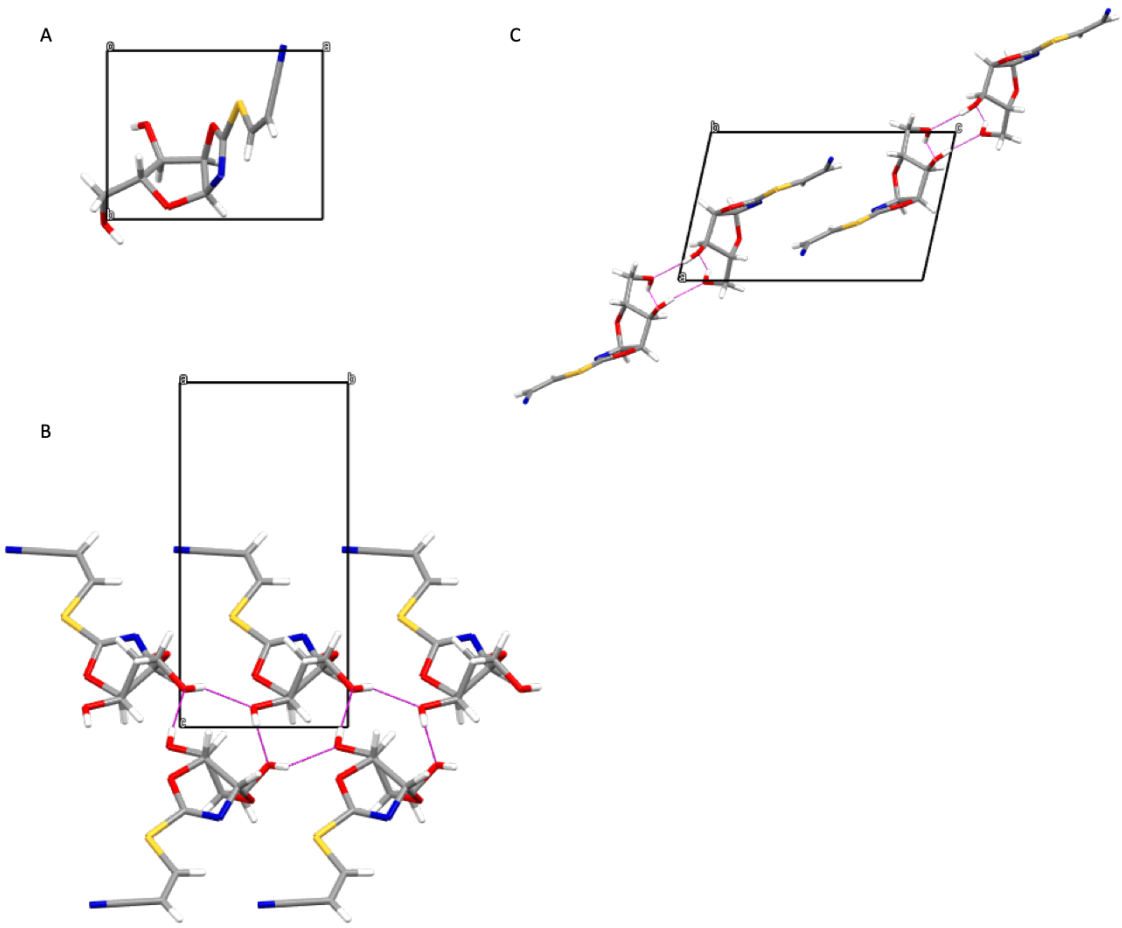

Figure 60: D-ribo-cyanovinyl oxazolidinone thione in A) the asymmetric unit. B) key interactions C) packing.

The ribo cyano-vinyl oxazolidinone thione (**RCVOT**) was not found to crystallise at the 0% *ee* point, despite the large range of solvents that were screened, the 0% *ee* solution was only observed to yield an amorphous solid.

*Table 2: Attempted crystallisations for ribo cyano-vinyl oxazolidinone thione (**RCVOT**)*

Attempted Crystallisations		
Water (100%)	Water: Methanol (1:99)	Water: Ethanol (1:10)
Methanol (100%)	Water: Methanol (1:10)	Water: Ethanol (1: 99)
Ethanol (100%)	Water: Methanol (100:1)	Water: Ethanol (10:1)
Ethyl Acetate (100%)	Water: Methanol (10:1)	Water: Ethanol (5:1)
Diethyl Ether (100%)	Water: Methanol (5:1)	Water: Ethanol (2:1)
Petrol Ether (100%)	Water: Methanol (2:1)	Water: Ethanol (1:1)
Chloroform (100%)	Water: Methanol (1:1)	Ethanol: Methanol (100:1)
DCM (100%)	Ethyl Acetate: Methanol (10:1)	Ethanol: Methanol (10:1)
Acetonitrile (100%)	Ethyl Acetate: Methanol (5:1)	Ethanol: Methanol (5:1)

3.4.3.2 Crystal structure of arabino cyanovinyl-oxazolidinone thione (ACVOT)

Limited arabino cyano-vinyl oxazolidinone thione (**ACVOT**), was obtained through the synthetic route, therefore it was important to use this material judiciously. Therefore, PXRD was used to evaluate how the crystals were formed that were isolated from the 0% *ee* **ACVOT** solution. PXRD was obtained for both D and L homochiral **ACVOT** and also for the crystals obtained at 0% *ee*. Comparison of these PXRD spectra showed that the crystals obtained from 0% *ee* solution were racemic crystals as they did not match the homochiral D or L **ACVOT** as characteristic peaks are missing (Figure 61).

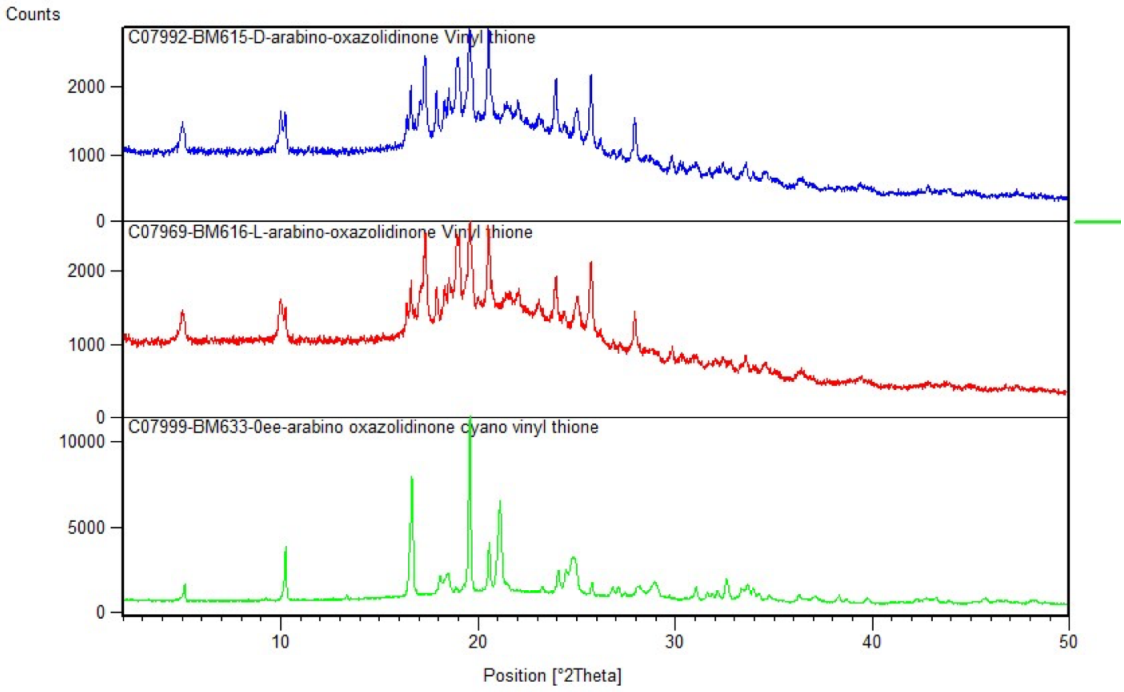

Figure 61: Top to bottom. PXRD of D arabino cyano-vinyl oxazolidinone thione, L arabino cyano-vinyl oxazolidinone thione and racemic arabino cyano-vinyl oxazolidinone thione.

3.5 Methyl-oxazolidinone Thiones

Methyl oxazolidinone thiones (**MOT**) have been shown by Stairs *et al.* to be important precursors in the synthesis of purine nucleotides. The cyanovinyl thione (**CVOT**) reacts with methane thiol to form **MOT** which can go on to form the purine nucleotides.[64]

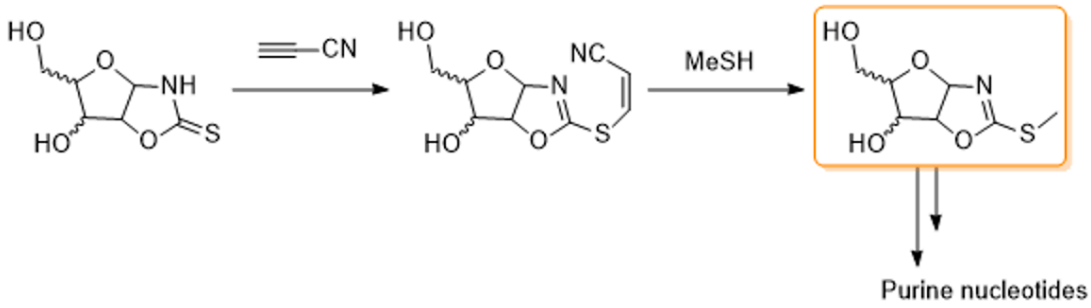

Scheme 30: Prebiotic synthesis of methyl oxazolidinone thione en route to purine nucleotides

Recalling the oxazolidinone thione results (Section 3.2), *ribo*-oxazolidinone thione (**ROT**) was shown to be forming conglomerate crystals preferentially, and full enantioenrichment took place from −40 % to +40 % *ee*. This led to the thought that from a crystal point of view, could we understand the interactions that take place in **ROT** that means it forms conglomerate crystals, that may potentially be blocked by the methyl group of another important prebiotic compound, methyl-oxazolidinone thione (**MOT**)?

3.5.1 Synthesis of Methyl-oxazolidinone Thiones (MOT)

Stairs *et al.* have previously demonstrated a robust, non-prebiotic, method to methylate the oxazolidinone thiones (**OT**) with iodomethane under basic conditions. Initially, this meant large quantities of the previously mentioned **OT** to be synthesised using the scaled-up synthesis. Once that material was purified using a column, the reaction was carried out under basic conditions with methyl iodide. Purification of this compound was accomplished by a column ($CHCl_3$/ MeOH 10:90).

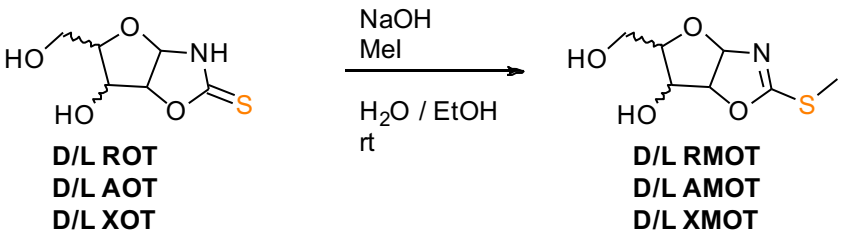

Scheme 31: Non-prebiotic synthesis of methylated oxazolidinone thiones.

Once the compound was isolated and characterised, crystallisation was performed. Crystallisation was achieved using a small amount of petroleum ether (40-60%), followed by additional ethyl acetate until cloudy, followed by more petroleum ether (40-60%) until crystallisation occurred.

3.5.2 Enantioenrichment of Methyl-oxazolidinone Thiones (MOT)

3.5.2.1 Enantioenrichment of ribo-methyl-oxazolidinone thione (RMOT)

The concentration dependence of *ribo*-methyl-oxazolidinone thione (**RMOT**) solubility was investigated and 3 M **RMOT** was found to be the highest concentration where the compound would dissolve at every scalemic mixture. However, after 6 weeks, no crystals had been observed. Therefore, multiple solvent systems were tried in order to achieve crystals at every scalemic point. Many prebiotically-relevant solvents (water, ethanol, methanol) were tried at a range of ratios, though they were not effective (Table 3). At 1:5 (H_2O/ MeOH) crystallisation was successful where the other systems had failed. The lid was removed from the crystallisation tube for 2 weeks to allow the solvent to evaporate. This led to crystals being formed at all concentrations.

*Table 3: Attempted crystallisations for **RMOT***

Attempted Crystallisations	
Water (100%)	Water: methanol (1:10)
Methanol (100%)	Water: methanol (1:5)
Ethanol (100%)	Water: methanol (1:2)
Ethyl Acetate (100%)	Water: methanol (1:1)
Diethyl Ether (100%)	Water: ethanol (1:10)
Petrol Ether (100%)	Water: ethanol (1:2)
Chloroform (100%)	Water: ethanol (1:1)
Acetonitrile (100%)	Water: ethanol (2:1)
Acetone (100%)	Water: ethanol (10:1)

The results show that **RMOT** preferentially forms racemic crystals from −60 % to +60 % *ee*. This was confirmed by analysing the solution *ee* also, to show that enantioenrichment occurs in the solution (Figure 62).

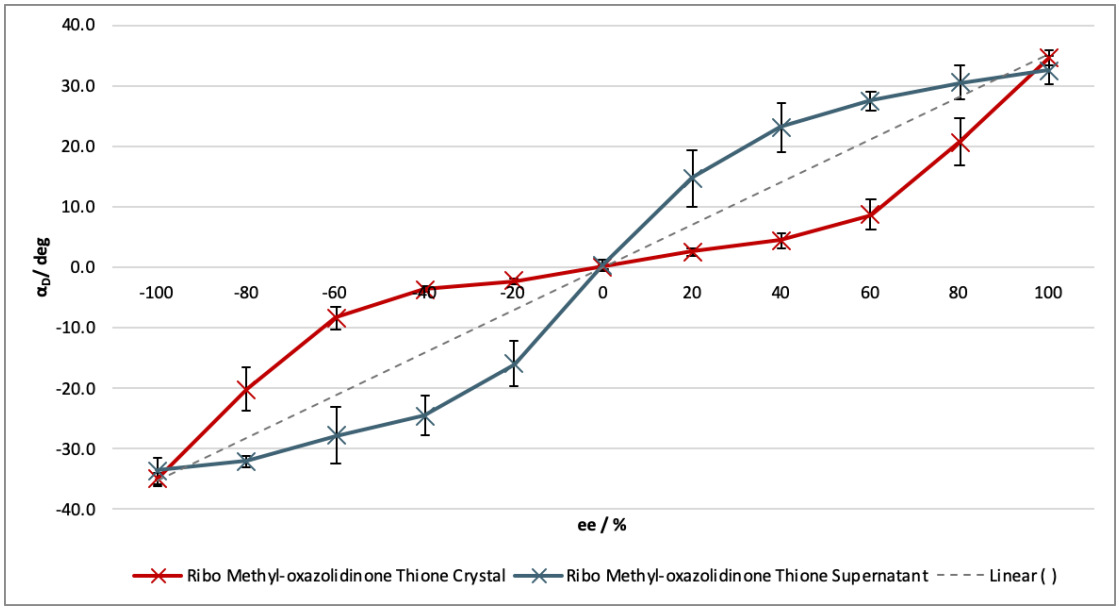

*Figure 62: Ribo methyl oxazolidinone thione crystals (**RMOT**) (red), the supernatant (blue) (3 M, 1:5 H_2O/ MeOH). The results were triplicated, and the average plotted along with the expected ee value. The dotted line shows the optical rotation if the crystals possessed the same* ee *value as the starting solution.*

3.5.2.2 Enantioenrichment of arabino and xylo methyl-oxazolidinone thione (AMOT, XMOT)

Arabino- and *xylo*- methyl-oxazolidinone thiones (**AMOT**, **XMOT**) were synthesised as described in good yield. Again, multiple different solvents and solvent ratios were tried for crystallisation. These crystallisations were left for 4 weeks at room temperature, and then allowed to stand in the fridge for a further 4 weeks. Finally, the lid of the Eppendorf was removed until the solvent had evaporated. However, crystallisation was not observed. The material returned as a sticky oil therefore material had to be remade as purifying the oil back to the solid proved unsuccessful.

*Table 4: Attempted crystallisations for arabino- and xylo- methyl-oxazolidinone thione (**AMOT, XMOT**).*

Attempted Crystallisations			
Water (100%)	Water: Ethanol (1:99)	Water: Ethanol (1:99)	Ethyl Acetate: Methanol (99:1)
Methanol (100%)	Water: Ethanol (1:10)	Water: Ethanol (1:10)	Ethyl Acetate: Methanol (10:1)
Ethanol (100%)	Water: Ethanol (1:5)	Water: Ethanol (1:5)	Ethyl Acetate: Methanol (5:1)
Ethyl Acetate (100%)	Water: Ethanol (1:2)	Water: Ethanol (1:2)	Ethyl Acetate: Methanol (2:1)
Diethyl Ether (100%)	Water: Ethanol (1:1)	Water: Ethanol (1:1)	Ethyl Acetate: Methanol (1:1)
Petrol Ether (100%)	Water: Ethanol (99:1)	Water: Ethanol (99:1)	Chloroform: Methanol (99:1)
Chloroform (100%)	Water: Ethanol (10:1)	Water: Ethanol (10:1)	Chloroform: Methanol (5:1)
Acetonitrile (100%)	Water: Ethanol (5:1)	Water: Ethanol (5:1)	Chloroform: Methanol (2:1)
Acetone (100%)	Water: Ethanol (2:1)	Water: Ethanol (2:1)	Chloroform: Methanol (1:1)

3.5.3 Crystal Structure of Methyl-oxazolidinone Thiones (MOT)

3.5.3.1 Crystal structure of ribo-methyl-oxazolidinone thione (RMOT)

Whilst the crystallisation of **AMOT** and **XMOT** were unsuccessful, it was considered useful to understand the structural features of the **RMOT**, which may be prove important to understanding the behaviour that leads to conglomerate vs racemic crystal formation. **RMOT** was detected to preferentially form racemic crystals during the scalemic enantioenrichment experiments. Therefore, the homochiral crystal structures were obtained along with the racemic crystal structures.

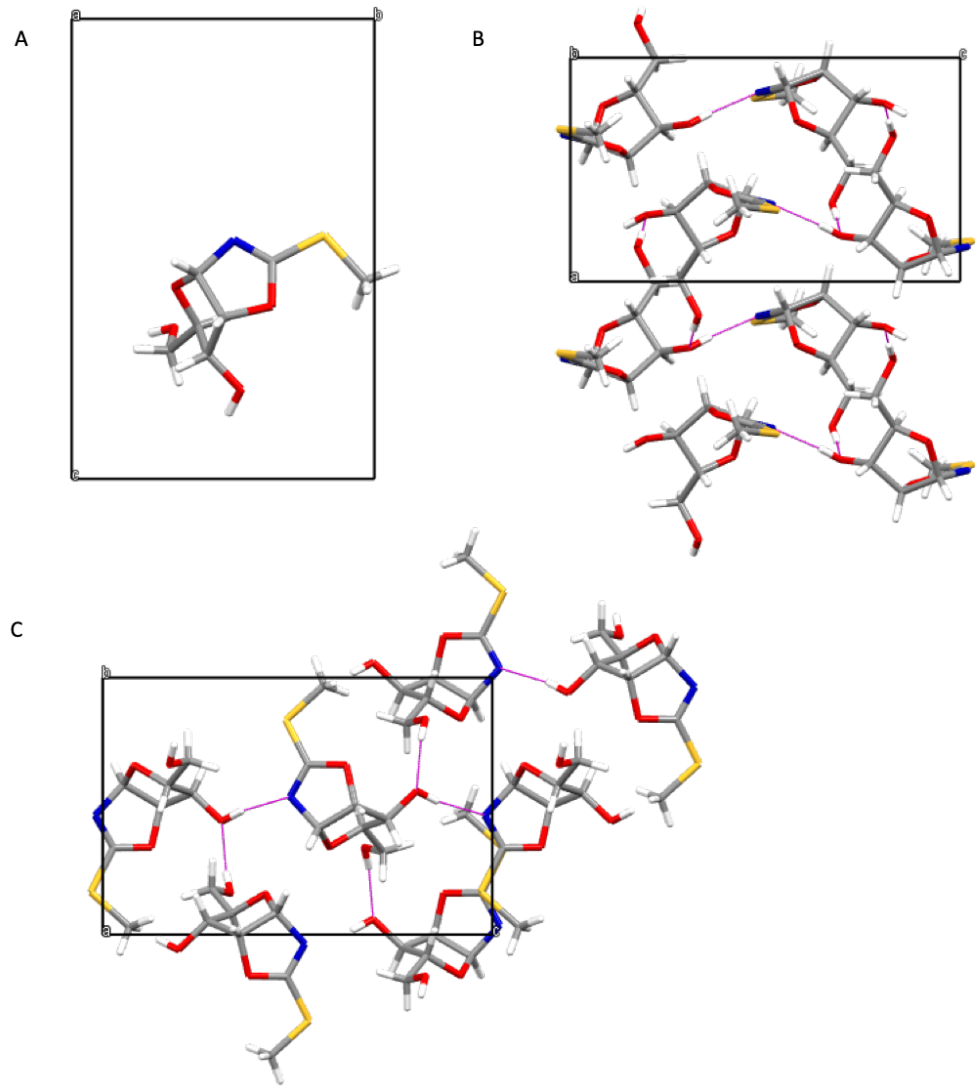

Figure 63: D-ribo-methyl oxazolidinone thione in A) the asymmetric unit. B) key interactions C) packing.

Homochiral D and L **RMOT** crystallises in the orthorhombic $P2_12_12_1$ non-centrosymmetric space group with one molecule in the asymmetric unit (Figure 63). The S1 atom is not involved in any hydrogen bonding in the three-dimensional network. There are interactions between **N**1 and C3′-O**H** which results in ribbons in the *bc* plane. The C3′-**O**H interacts further with C5′-O**H** which builds into the network.

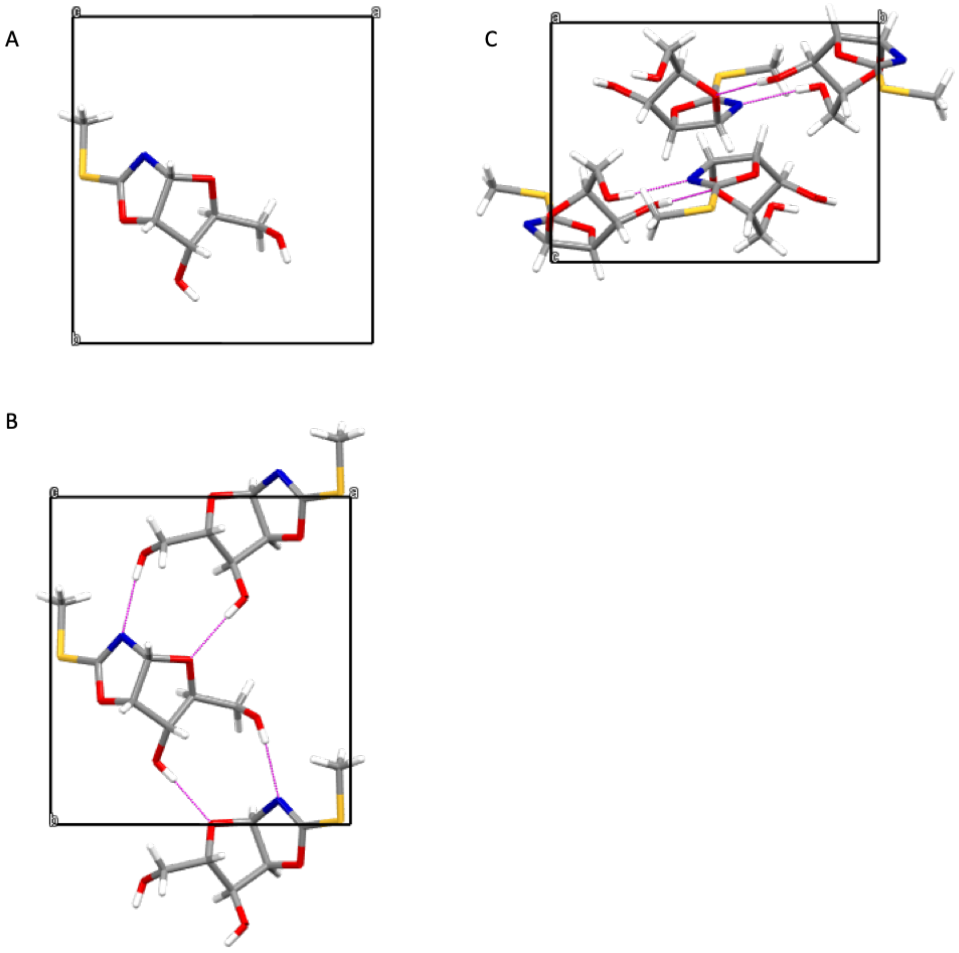

*Figure 64: Rac-**RMOT** in A) the asymmetric unit. B) key interactions C) packing.*

Racemic D and L **RMOT** crystallises in the monoclinic $P2_1/c$ non-centrosymmetric space group with one molecule in the asymmetric unit (Figure 64). Each enantiomer hydrogen bonds directly with two other molecules of the same hand. **N1** and **O1** interact with the C5'-O**H**, and C3'-O**H** respectively of another molecule. Furthermore, this is repeated within that molecule from the C5'-O**H**, and C3'-O**H** to the **N1** and **O1** of another molecule forming ribbons along the b axis. There is then a strand of the opposite enantiomer that surrounds that one strand above and below.

3.6 N-cyanoethyl Oxazolidinone Thiones (CEOT)

3.6.1 Synthesis of N-cyanoethyl oxazolidinone thione (CEOT)

The next compound to be investigated was N-cyanoethyl oxazolidinone thione (**CEOT**) which had previously been observed within the group upon the reaction of the oxazolidinone thione (**OT**) with acrylonitrile (**47**), which is a prebiotically plausible electrophile, and is also obviously structurally similar to cyanoacetylene (**16**) (Scheme 32).[9]

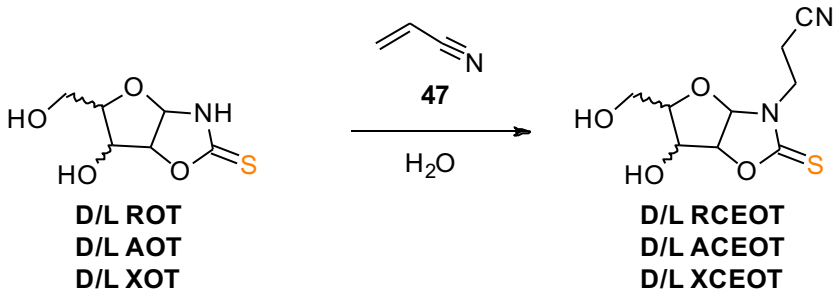

D/L ROT
D/L AOT
D/L XOT

D/L RCEOT
D/L ACEOT
D/L XCEOT

*Scheme 32: Synthesis of N-cyanoethyl adduct (**CEOT**) via acrylonitrile (**47**) in water.*

Oxazolidinone thione (**OT**) was reacted with acrylonitrile (**47**), at pH 9 for 10 h. The solution was then lyophilised and the lyophilisate purified by FCC (EtOAc/ MeOH 9:1) to yield the desired N-cyanoethyl oxazolidinone thione (**CEOT**) in good yield (93-97%).

The mechanism proposed is an addition and elimination reaction (Scheme 33A). This mechanism then yields the thermodynamically more stable N-cyanoethyl adduct (**CEOT**) rather than the alternative S-cyanoethyl adduct (Scheme 33B) that would be expected, in which the kinetic S-cyanovinyl adduct is observed due to the higher energy required for the vinyl anion formation than deprotonation at the sp^3 center adjacent to the electron withdrawing cyano-group.

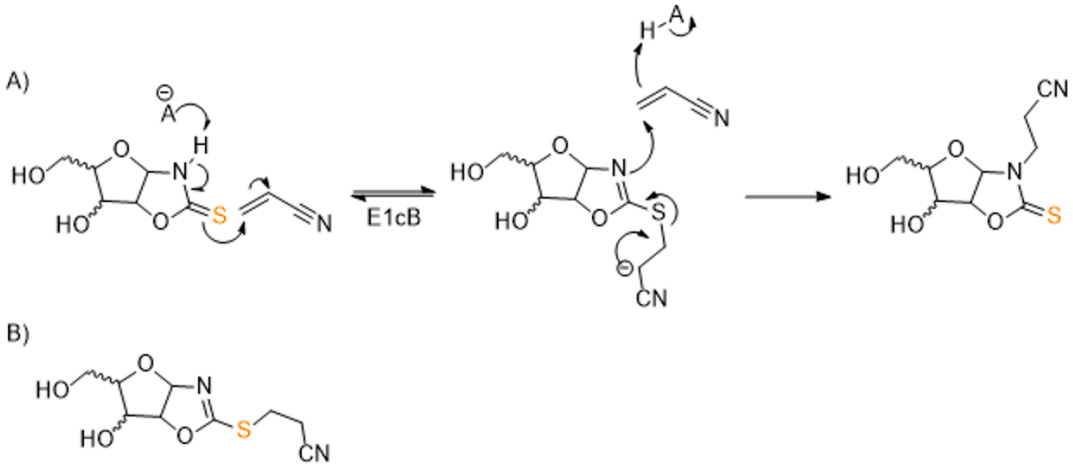

Scheme 33: A) Proposed mechanism for the N1 cyanoethylation of the oxazolidinone thione in aqueous solution. B) Expected S-cyanoethyl adduct.

3.6.2 Enantioenrichment of N-cyanoethyl oxazolidinone thione

With the (**CEOT**) in hand, −100, 0 and +100% solution *ee*'s were investigated in crystallisation experiments. Many different crystallisations were tried, but water was found to not to be suitable as a crystallisation solvent at any concentration (0.2 M to 3 M), therefore other solvents were examined. Suitable crystallisation was observed from a 1 M solution of **CEOT** in 1:10 MeOH/ EtOH. These crystallisations were then evaporated (in an open vessel) and until crystals began to form (after approximately 1 week). The crystals isolated were then analysed by optical polarimetry and single crystal X-ray structures were collected.[2]

[2] Unfortunately, *xylo*-N-cyanoethyl oxazolidinone thione (**XCEOT**) did not form any usable crystals at all points and due to limited starting material, this was not investigated further.

3.6.3 Crystal Structures of N-cyanoethyl oxazolidinone thione (CEOT)

3.6.3.1 Crystal structure of ribo N-cyanoethyl oxazolidinone thione (RCEOT)

Homochiral D and L ribo N-cyanoethyl oxazolidinone thione (**RCEOT**) crystallises in the monoclinic $P2_1$ non-centrosymmetric space group with one molecule in the asymmetric unit (Figure 65). The **S1** sulfur atom interacts with C3'-O**H**, which further can interact with C5'-O**H**.

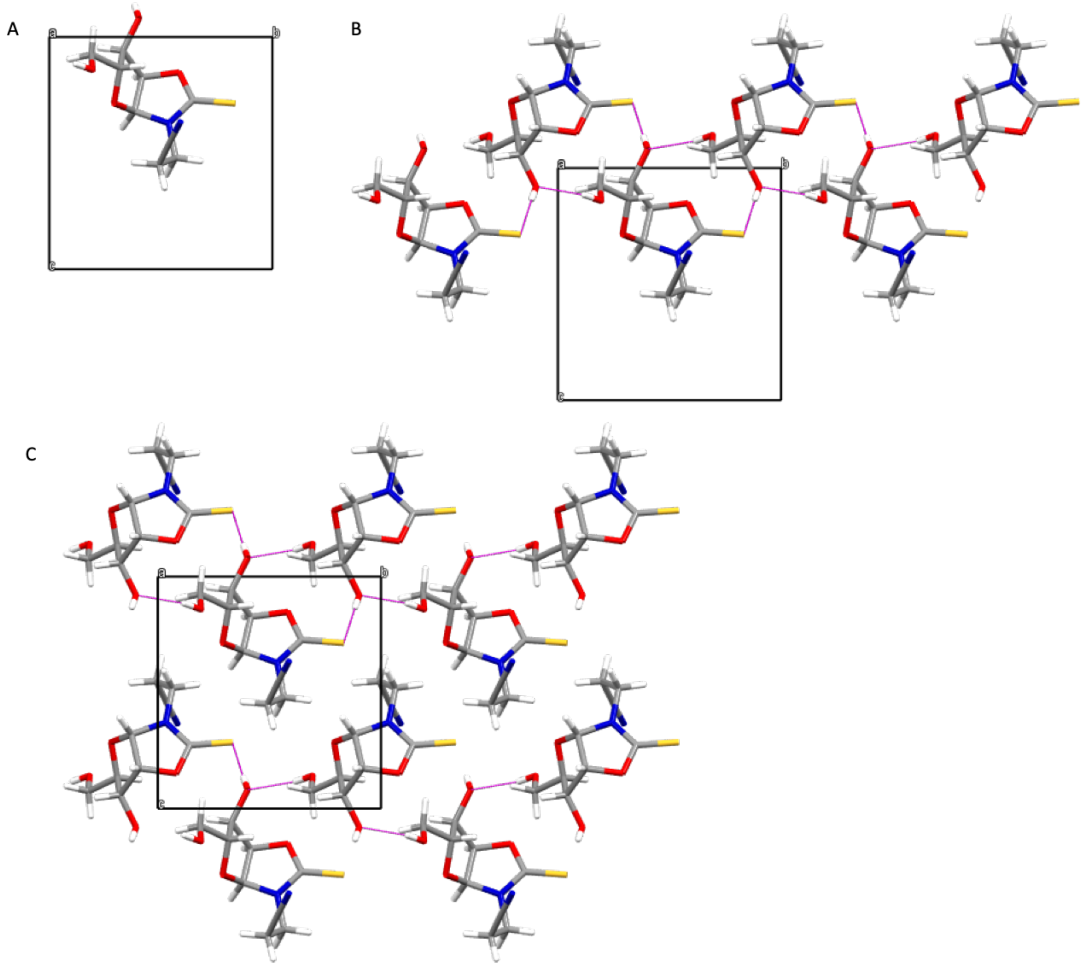

Figure 65: D-ribo-cyanoethyl oxazolidinone thione in A) the asymmetric unit. B) key interactions C) packing.

At 0% *ee* the crystals obtained were proven to be racemic that crystallises as space group P_{BCA} with one molecule in the asymmetric unit (Figure 66). A 15 membered ring is formed through the interactions of C5'-**O**H ···C3'-O**H** ···**S1** ···C5'-O**H** ···C3'O**H** which forms ribbons in the *bc* plane.

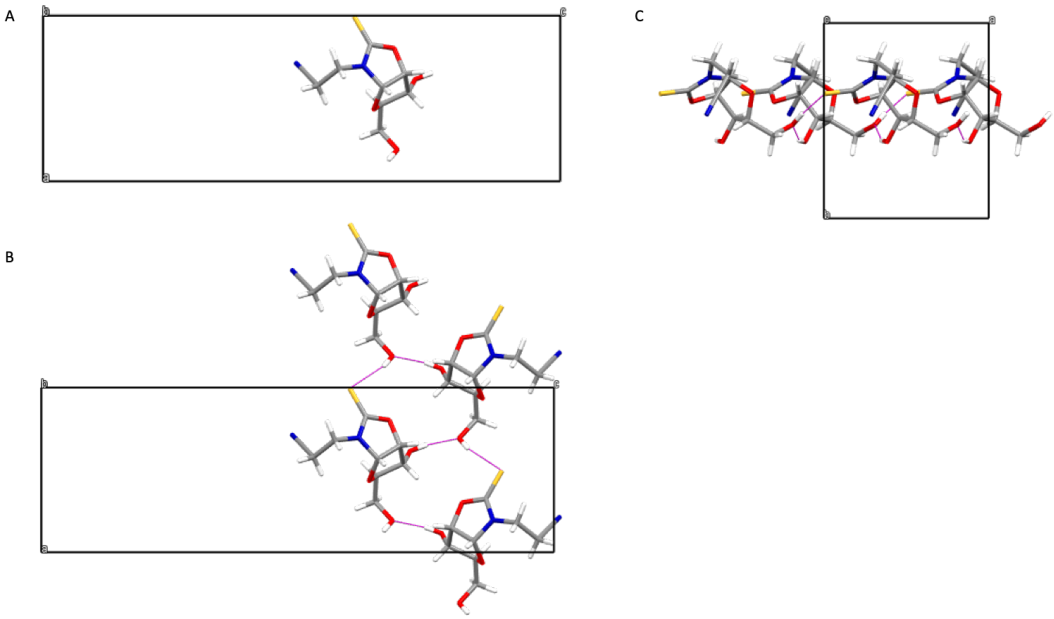

Figure 66: Rac-ribo-cyanoethyl oxazolidinone thione in A) the asymmetric unit. B) key interactions C) packing.

3.6.3.2 Crystal structure of arabino N-cyanoethyl oxazolidinone thione (ACEOT)

Homochiral D and L arabino N-cyanoethyl oxazolidinone thione (**ACEOT**) crystallises in the orthorhombic $P2_12_12_1$ non-centrosymmetric space group with one molecule in the asymmetric unit. The C5'-**O**H interacts with another molecules C3'-O**H** forming strands along the *bc* plane. The C5'-O**H** further interacts with **S1** in order to form planes along the *ab* plane as shown Figure 67.

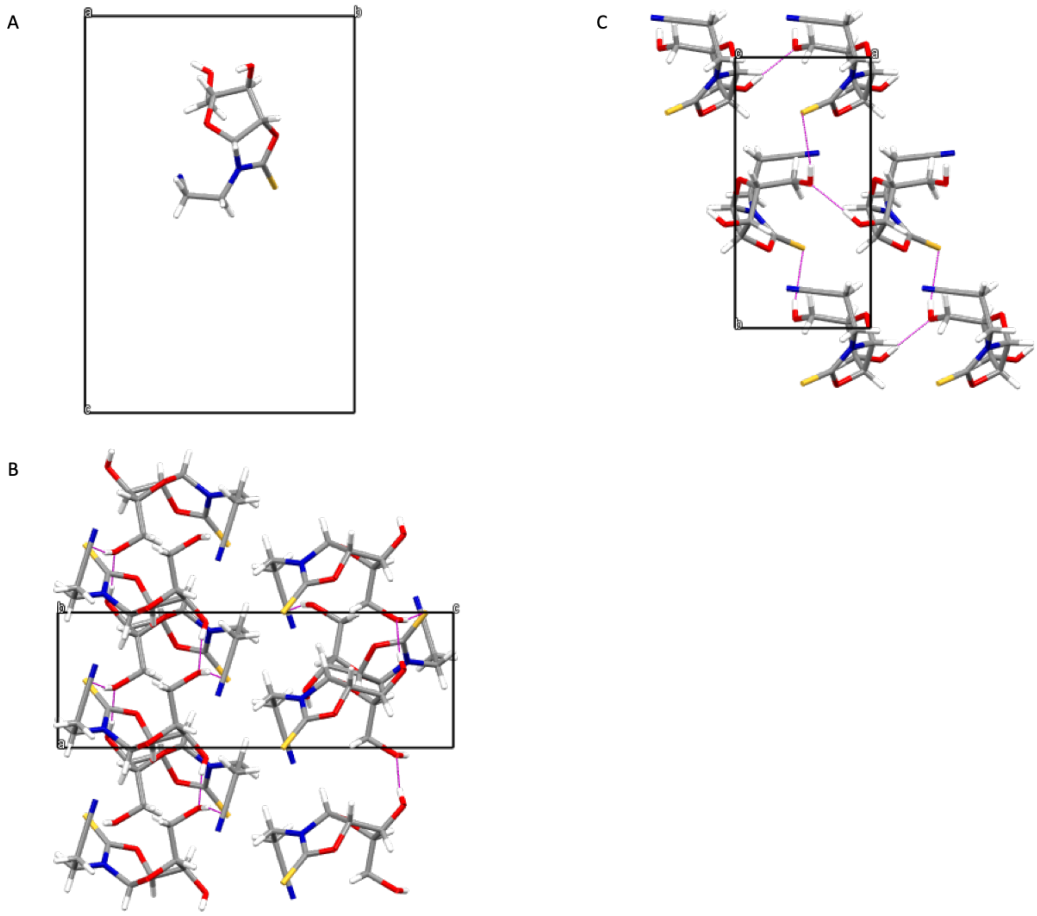

*Figure 67: D-**ACEOT** in A) the asymmetric unit. B) key interactions C) packing.*

The solid obtained from 0% *ee solution* were analysed by PXRD. The PXRD shows that the crystals obtained do not match those of the homochiral PXRD and therefore likely to be racemic crystals (Figure 68).

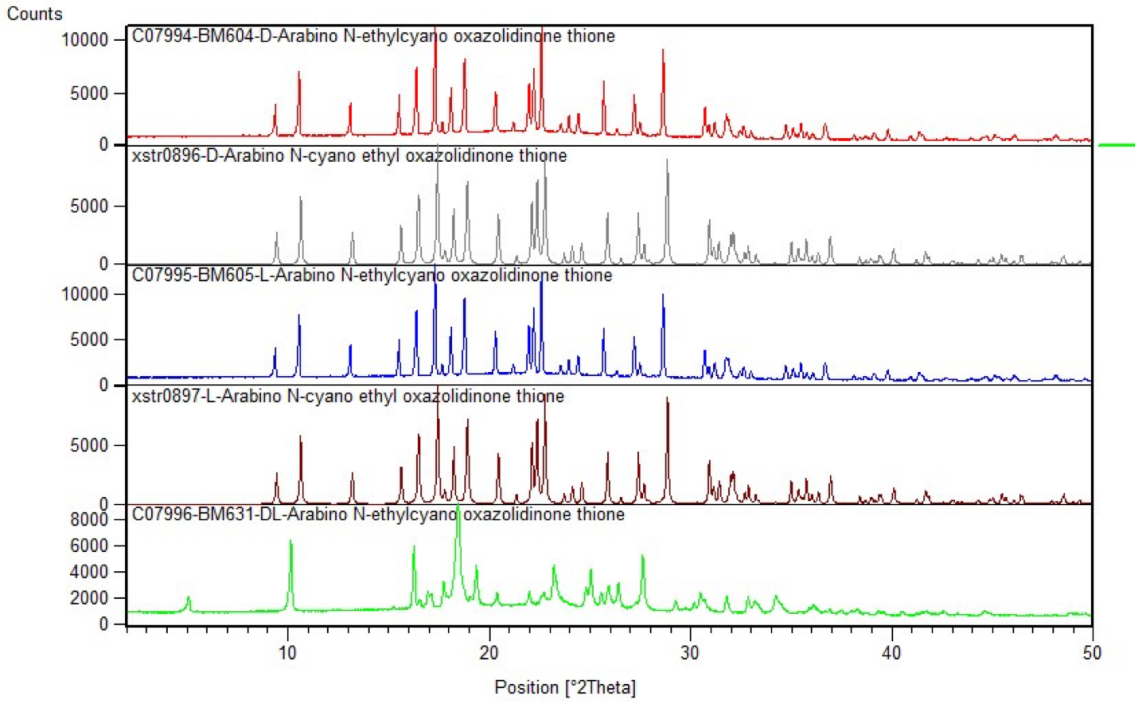

Figure 68: PXRD Arabino N-cyanoethyl oxazolidinone thione. Red and grey: ***D-ACEOT****, blue and brown:* ***L-ACEOT****, green: crystals obtained from 0% ee solution of* ***ACEOT****.*

3.7 Ribonucleotides

En route to the prebiotic synthesis of nucleotide there are many possible points at which *ee* enrichment could occur. Crystallisation of intermediates has been shown to effect *ee* enrichment, therefore seems reasonable that the nucleosides, which are sparingly soluble (before phosphorylation) in water may also affect *ee* enrichment. Therefore, it deemed to also be instructive to investigate the crystal properties of the nucleosides.

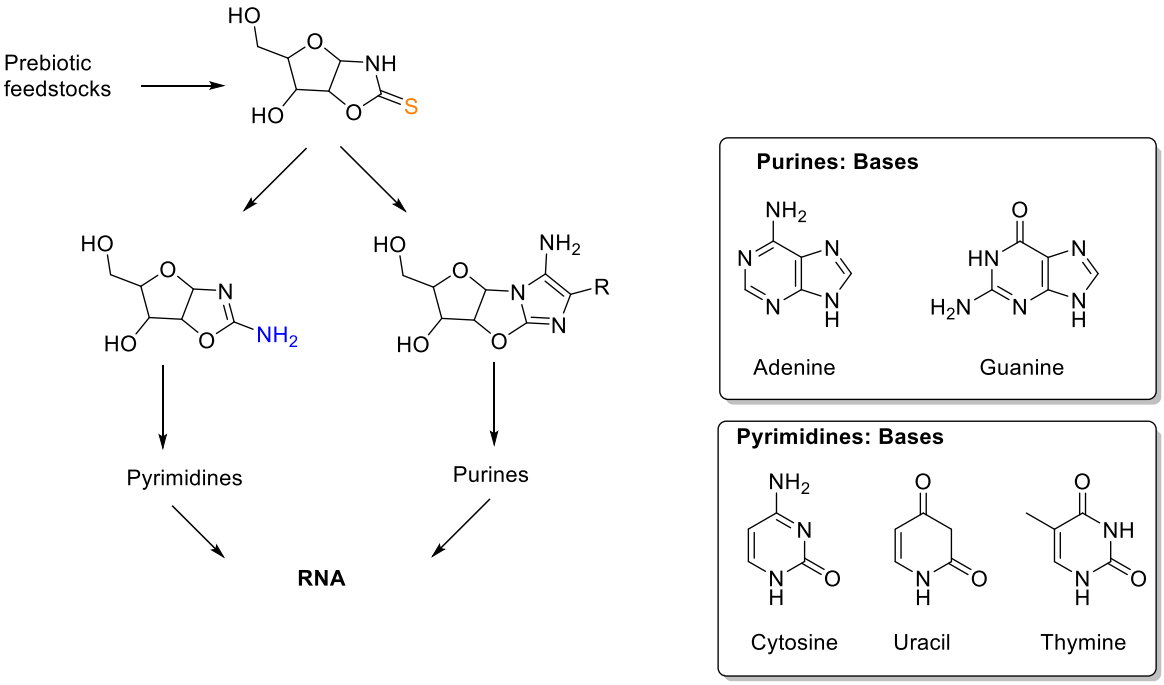

Figure 69: Prebiotic ribonucleotide synthesis by Stairs et al.[64]

One purine ribonucleoside (adenosine), and one pyrimidine ribonucleoside (cytosine) were chosen to be initially investigated (Figure 69).

3.7.1 α-Cytidine

The ribonucleoside α-cytidine (**α-ribo-42**) was synthesised from the aminooxazolines (**AO**). These aminooxazolines (**AO**) were reacted with cyanoacetylene (**16**) at pH 6.5 at room temperature over 24 h. This was then lyophilised followed by an ion exchange chromatography (gravity fed proton Dowex column over 1 day) which yielded pure *ribo*-2,2'-anhydrocytidine (**17**) in good yield (80%). With the anhydrocytidine (**17**) in hand, the final step was alkaline hydrolysis (Dowex (OH^-)) in water for 4 h followed by filtration and lyophilisation. This procedure was completed to yield both L- and D- α-cytidine (**α-ribo-42**) starting from the respective L- and D- **RAO**.

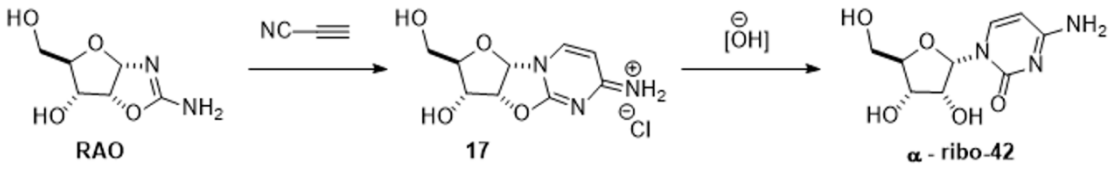

*Scheme 34: Synthesis towards α- cytidine (**α-ribo-42**) from **RAO**.*

Crystallisations were carried out in multiple solvent scenarios and solutions (Table 5). The most successful crystallisation occurred at water/ ethanol (1:100) where small crystals formed after 2 weeks when the lid had been removed for the entire time to allow the solvent to evaporate.

Attempted Crystallisations		
Water (100%)	Water: Methanol (10:1)	Water: Ethanol (10:1)
Methanol (100%)	Water: Methanol (1:100)	Water: Ethanol (1:100)
Ethanol (100%)	Water: Methanol (1:10)	Water: Ethanol (1:10)
Ethyl Acetate (100%)	Water: Methanol (1:5)	Water: Ethanol (1:5)
	Water: Methanol (1:2)	Water: Ethanol (1:2)
	Water: Methanol (1:1)	Water: Ethanol (1:1)

Table 5: Crystallisation scenarios attempted for the crystallisation of α- cytidine.

The racemic α -cytidine (**α-ribo-42**) was observed to crystallise in the $P2_1$ non-centrosymmetric space group with 2 molecules in the asymmetric unit. Interactions are observed between the two molecules from the C2'-O**H** ···**N3** and vice versa. Interactions between a further two molecules occur between the C5'-O**H** ···**O2** and vice versa.

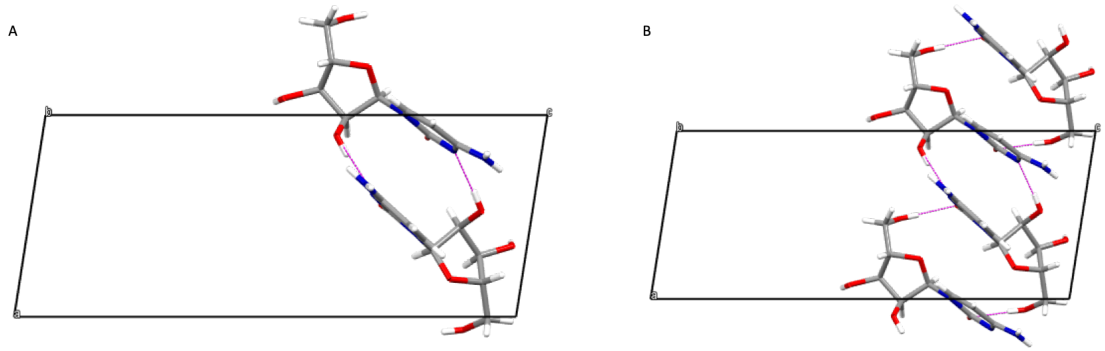

Figure 70: α- cytidine A) the asymmetric unit. B) key interactions.

3.7.2 β-Cytidine (β-ribo-42)

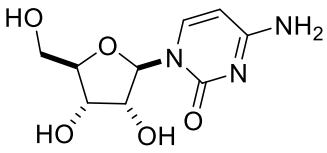

β - Cytidine

Although β-cytidine (**β-ribo-42**) was readily commercially available, the L enantiomer was prohibitively expensive and limited amounts were to be used in order to try to minimise costs. Therefore, the L, D and 0% *ee* were crystallised. Multiple crystallisations were tried (Table 6). The most successful was carried out at 1:10 H_2O/ EtOH which resulted in small crystals that were able to be analysed by SXRD.

Attempted Crystallisations		
Water (100%)	Water: Methanol (10:1)	Water: Ethanol (10:1)
Methanol (100%)	Water: Methanol (1:100)	Water: Ethanol (1:100)
Ethanol (100%)	Water: Methanol (1:10)	Water: Ethanol (1:10)
Ethyl Acetate (100%)	Water: Methanol (1:5)	Water: Ethanol (1:5)
	Water: Methanol (1:2)	Water: Ethanol (1:2)
	Water: Methanol (1:1)	Water: Ethanol (1:1)

*Table 6: Attempted solutions tried for the crystallisation of β-cytidine (**β-ribo-42**)*

The homochiral β-cytidine (**β-ribo-42**) crystallises in the orthorhombic $P2_12_12_1$ non-centrosymmetric space group with one molecule in the asymmetric unit. **O2** and C3′-**O**H form a 9-atom hydrogen bonded motif between two molecules through the N-$\mathbf{H_2}$ formed in the ab plane There is a further 10 membered ring formed through **N3** ···C3′-O**H** ···C5′-O**H** ···**O2** which all builds up into a 3D structure.

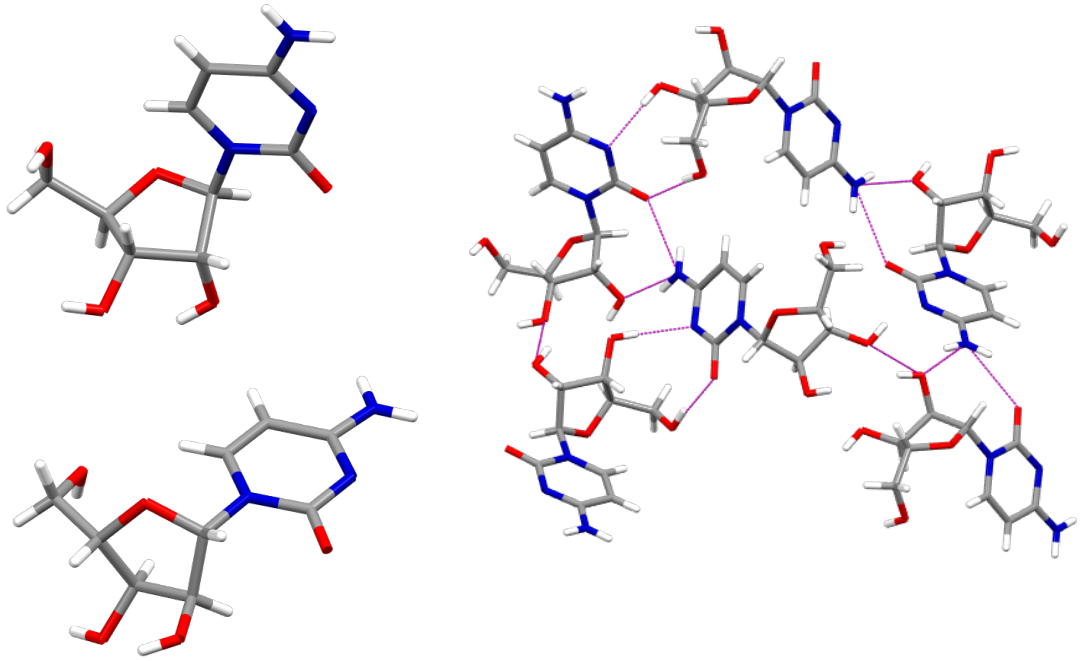

*Figure 71: D β-cytidine (**β-ribo-42**), L β-cytidine (**β-ribo-42**), and the bonding involved in D- β-cytidine (**β-ribo-42**).*

Racemic β-cytidine (**β-ribo-42**) crystallises in the monoclinic *P2₁/c* non-centrosymmetric space group with one molecule in the asymmetric unit. The same hand enantiomers interact through C5′-O**H** ···**O2** and **N3** ···C3′-O**H** forming a 10 membered ring motif that forms along the ac axis. Enantiomers of opposite hands interact through another 10 membered ring through C2′-O**H** ···C3′-**O**H and vice versa C3′-O**H** ···C2′-**O**H. There are further interactions between the same enantiomer through the N**H**$_2$···C2′-**O**H which that same molecule interacts through the C5′-**O**H ···N**H**$_2$ to form a dimer like structure.

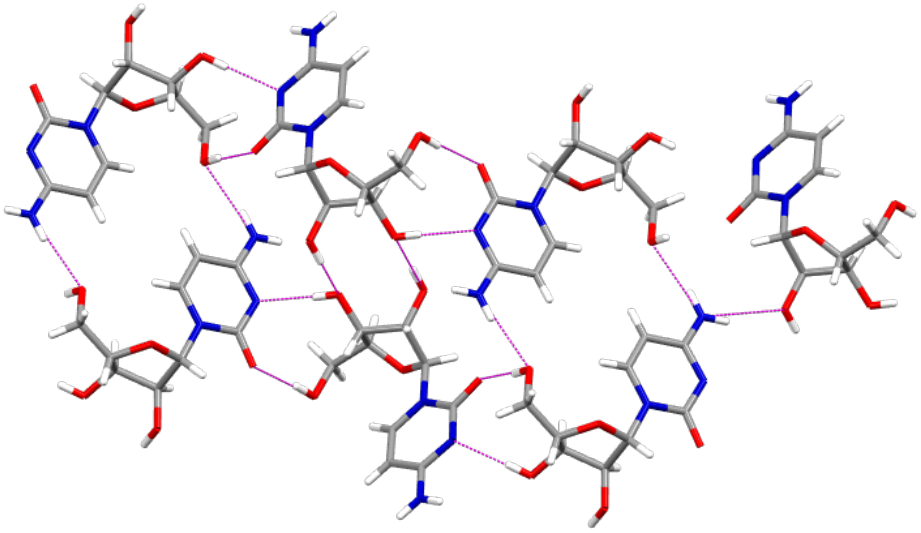

*Figure 72: Racemic β-cytidine (**β-ribo-42**)*

3.8 Enantioenrichment Comparison

3.8.1.1 Enantioenrichment of the Aminooxazolines

Within the aminooxazoline series, all three conformers form conglomerate crystals, which is unique amongst the pentose oxazolines studied in this work (Figure 73).

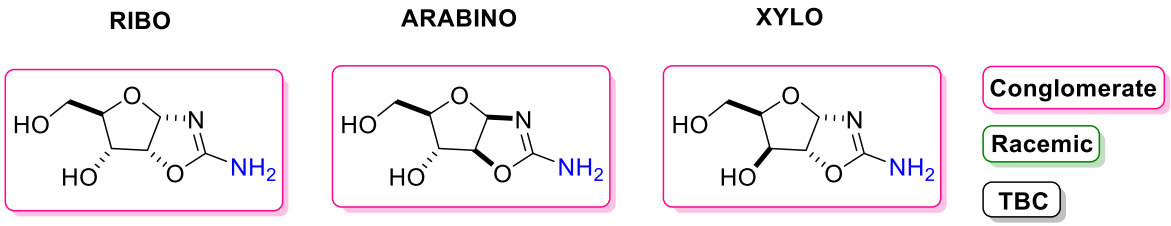

Figure 73: Summary of the crystals formed at 0% ee *for the aminooxazolines in water.* ***RAO*** *(0.25 M),* ***AAO*** *(1 M),* ***XAO*** *(1 M).*

The scalemic reactions all initially started out with trying to scope out the concentration at which the crystallisation could take place. **RAO** was particularly straightforward due to the relatively short length of time taken to optimise the scalemic experiments. The concentration at which the reaction proceeded best at was clear: 0.25 M in water. **RAO** has comparatively low solubility, so the maximum amount that can be dissolved in water is 0.5 M. However, at this concentration a significant amount of heating is required which results in rapid precipitation of amorphous solid rather than crystals. The reaction was attempted in ethanol, and an ethanol-water mixture (1:1) from high concentration (1 M) down to 0.1 where it would neither dissolve nor form crystals. The solubility of **AAO** and **XAO** is better (1 M) than that of **RAO**. This higher concentration is required because it is crucial to ensure that crystals are formed across the range of scalemic *ee* mixtures.

Compound	**Observed**	**Molarity in water / M**			
		0.25	0.5	0.75	1
Ribo Aminooxazoline (**RAO**)	Conglomerate	✔	-	-	-
Arabino Aminooxazoline (**AAO**)	Conglomerate	✗	✗	✗	✔
Xylo Aminooxazoline (**XAO**)	Conglomerate	✗	✗	✗	✔

Table 7: Concentration that the aminooxazolines crystallise out of water at over 2 weeks. Where green tick refers to crystals at all scalemic mixtures, red tick refers to mixed or no results at those concentrations and a line is when the compound would not dissolve.

In order to compare the enantiomeric amplification between the three, the results were normalised by taking the observed α_D as a percentage of the maximum rotation for that conformer. This is then represented as a bar chart (Figure 74) which allows us to visualise how the amplification changes based on conformer.

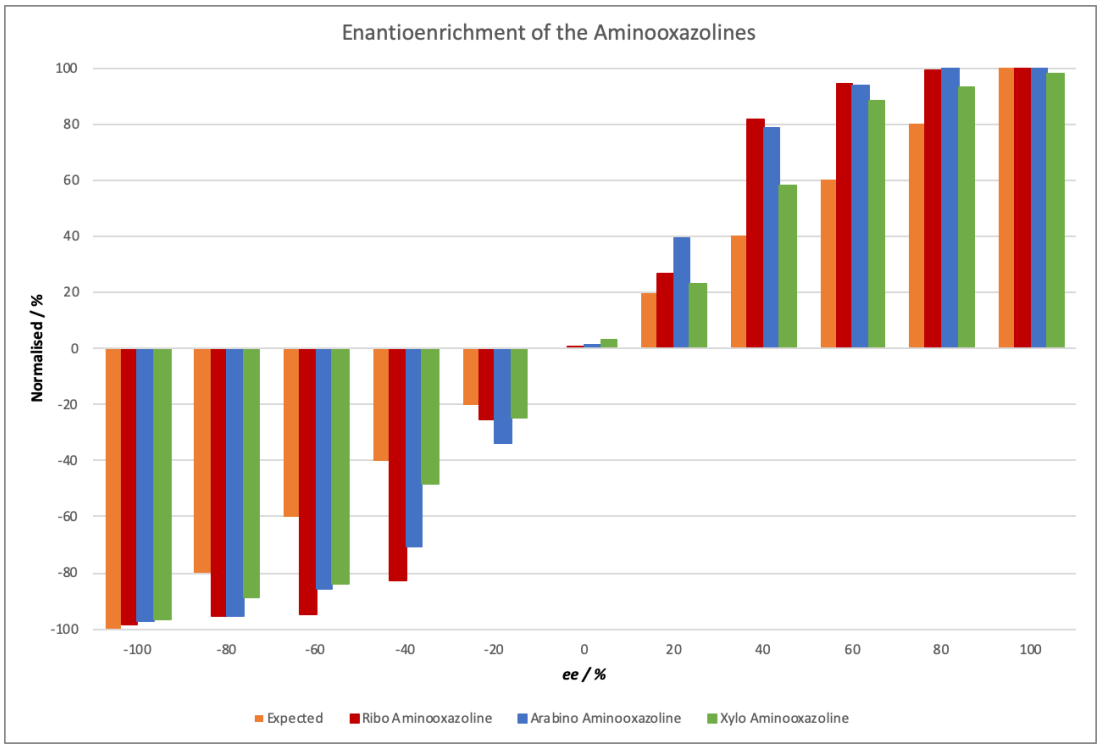

Figure 74: Enantiomeric amplification normalised for the aminooxazolines. Crystallisation took place in water, ***RAO*** *(0.25 M),* ***AAO*** *(1 M),* ***XAO*** *(1 M).*

It is clear from Figure 74 that **RAO** demonstrates the most striking amplification over the range of experiments. **AAO** demonstrates similar amplification, although interestingly, at +/−20% it is noticeably more enriched. **XAO** demonstrates the most modest amplification.

3.8.1.2 *Enantioenrichment of the Oxazolidinone Thiones (OT)*

The oxazolidinone thiones formed conglomerate crystals for the **ROT**, however for the **AOT** and **XOT** compounds, racemic crystals were observed to form.

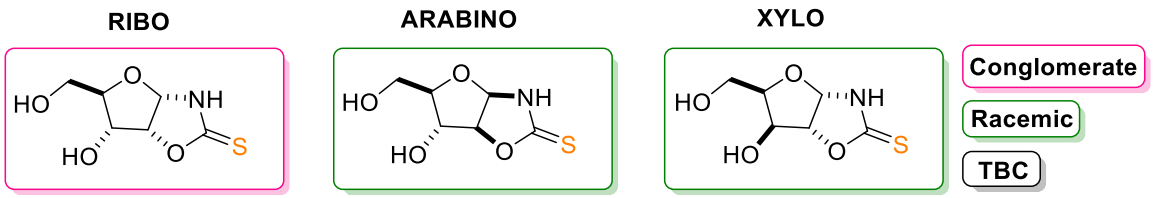

Figure 75: Summary of the crystals formed at 0% ee for the oxazolidinone thiones in water. ***ROT*** *(1.5 M),* ***AOT*** *(3 M),* ***XOT*** *(3 M).*

As with the aminooxazolines (**AO**), the reaction had to be scoped for what concentration the scalemic crystallisation takes place at. Fortunately, this was initially achieved by a Masters student (Cheng Cen), who quickly realised this was best achieved at 1.5 M for **ROT** and at 3 M for **AOT** and **XOT**. This was later investigated at the other molarities in order to rule out lower concentrations. At high concentrations however, the compound would often struggle to dissolve.

Compound	**Observed**	**Molarity in water / M**				
		0.5	1	1.5	3	5
Ribo Oxazolidinone Thione (**ROT**)	Conglomerate	✗	✗	✓	-	-
Arabino Oxazolidinone Thione (**AOT**)	Racemic	✗	✗	✗	✓	✓
Xylo Oxazolidinone Thione (**XOT**)	Racemic	✗	✗	✗	✓	✓

Table 8: Concentration that the oxazolidinone thiones (OT) crystallise out of water at over 2 weeks. Where green tick refers to crystals at all scalemic mixtures, red tick refers to mixed or no results at those concentrations and a line is when the compound would not dissolve.

This preference is demonstrated in the inversion of the curve (Figure 76) where the enrichment has been confirmed to actually occur in the solution rather than the crystal. When the results were normalised as discussed previously, the resulting bar chart shows this stark inversion as expected, with **XOT** showing the strongest preference to form racemic crystals and arabino a close second. **ROT** goes against the trend however, showing a very strong preference for conglomerate formation, which will later be compared against the other conglomerates.

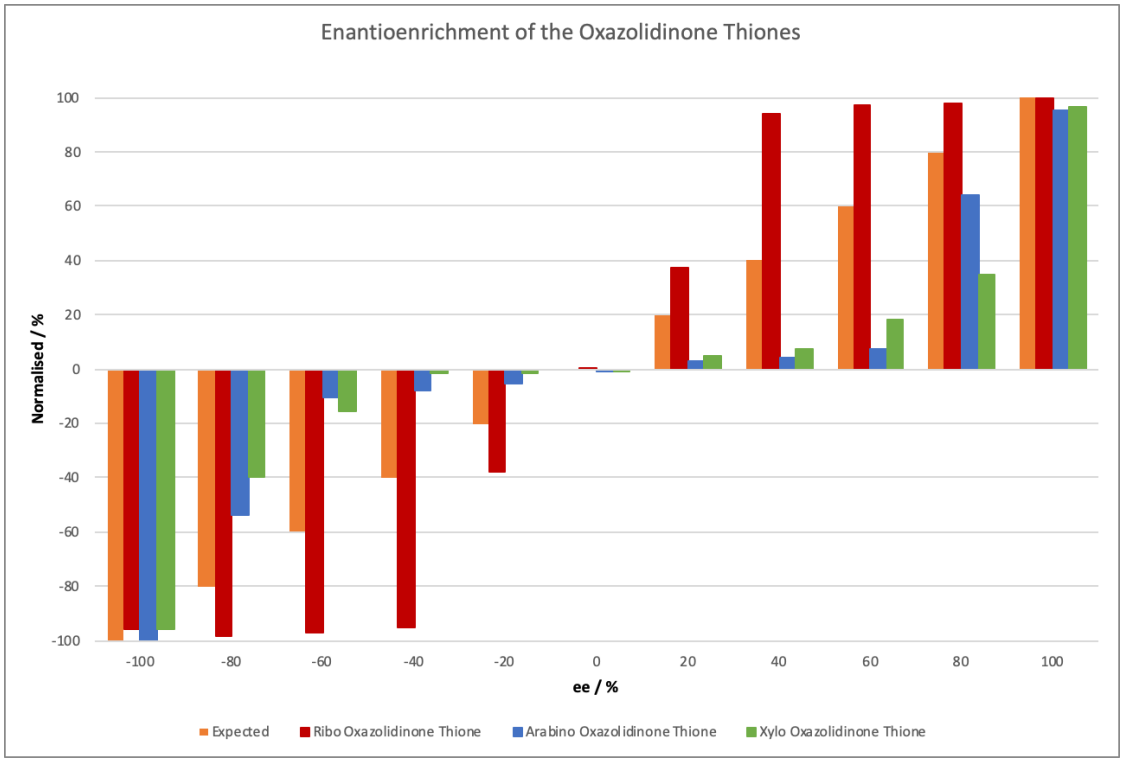

Figure 76: Normalised enantioenrichment of oxazolidinone thiones in water. ***ROT*** *(1.5 M),* ***AOT*** *(3 M),* ***XOT*** *(3 M).*

3.8.1.3 Enantioenrichment of the Oxazolidinones (OX)

Looking across the oxazolidinone series, **AOX** is the only conformer which forms conglomerate crystals, where **ROX** and **XOX** forms racemic crystals.

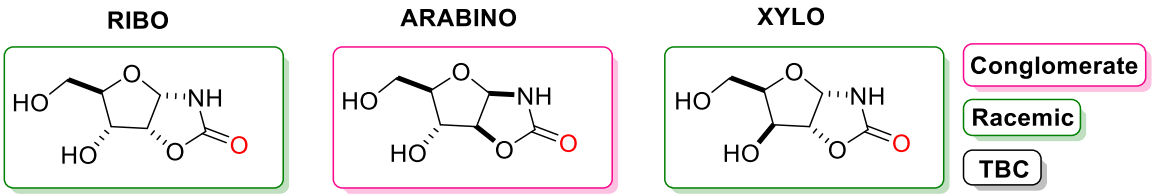

Figure 77: Summary of the crystals formed at 0% ee for the oxazolidinone. ***ROX*** *(1.5 M) in H_2O,* ***AOX*** *(3 M) and* ***XOX*** *(3 M) in ethanol/ H_2O (1:1).*

Following the particularly difficult large synthesis of the oxazolidinones, the crystallisation proved equally difficult to achieve. **ROX** was achieved in water at 1.5 M, however the **AOX** and **XOX** variants was not as simple. Eventually, through trying many different systems such as: H_2O (100%), ethanol (100%), methanol (100%), H_2O: methanol (1:1), and finally the winning combination of H_2O: methanol (1:1).

Compound	Observed	Molarity in water / M				
		0.5	1	1.5	3	5
Ribo Oxazolidinone (**ROX**)	Racemic	✗	✗	✓	-	-
Arabino Oxazolidinone (**AOX**)	Conglomerate	✗	✗	✗	✓	-
Xylo Oxazolidinone (**XOX**)	Racemic	✗	✗	✗	✓	-

Table 9: Concentration that the oxazolidinones crystallise out of water at over 2 weeks. Where green tick refers to crystals at all scalemic mixtures, red tick refers to mixed or no results at those concentrations and a line is when the compound would not dissolve.

As with the oxazolidinone thiones (**OT**), the curves shown in Figure 78 reflect the respective tendency, and again enrichment for the racemic forms takes place in the solution as racemic crystals are precipitated. The results were normalised to allow comparison as with the first two series of compounds, and we see the flatter line carried through for **ROX** and additionally

the **XOX** indicating racemic crystallisation. For the **AOX** conformer, we see only a modest amplification above the expected value (orange), however still interesting.

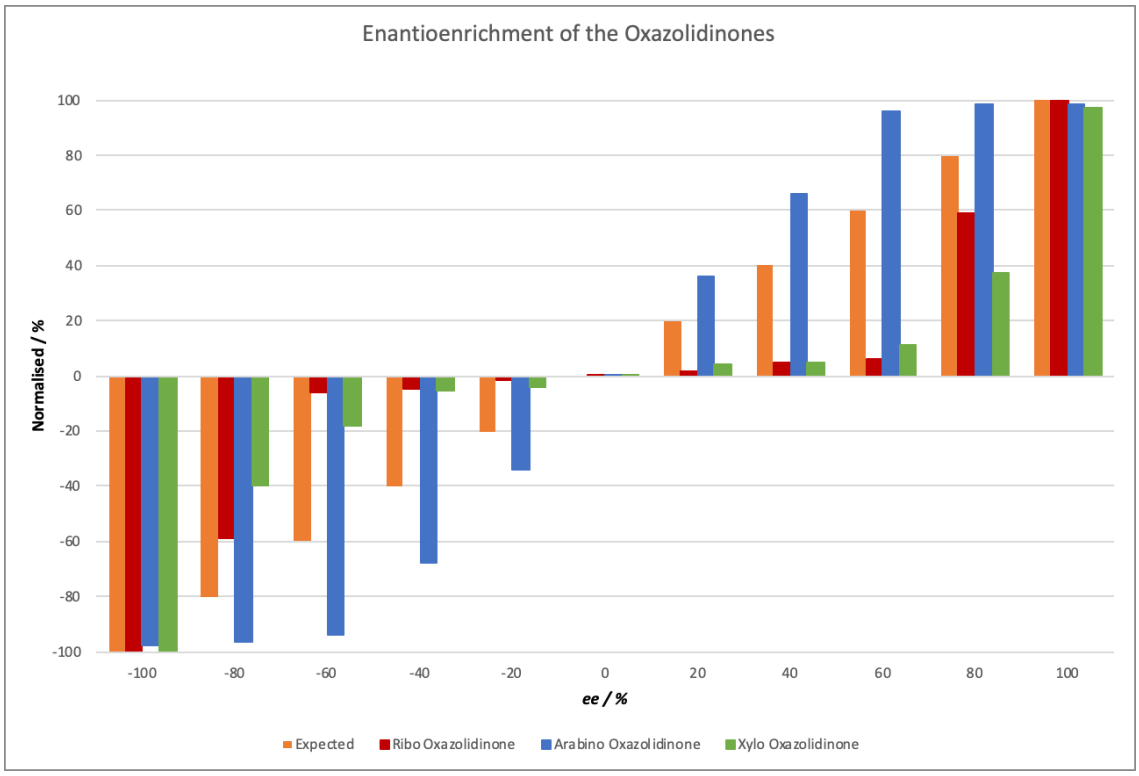

*Figure 78: Normalised enantioenrichment of the oxazolidinones Table showing the change in optical rotation of the crystals of **ROX** (1.50 M, H_2O), **AOX** (3.00 M, H_2O/ethanol (1:1)) and **XOX** (3.00 M, H_2O/ethanol (1:1))*

3.8.1.4 Enantioenrichment of the Conglomerates

In order to compare inter-series results, see Figure 79 which compiles the normalised values. Whilst this seems busy, it provides important clarified results. Initially, it is striking how enantiomerically amplified the **ROT** is, even down to an *ee* value of 40%. This is then shortly followed by the **RAO** which also shows impressive enantiomeric amplification.

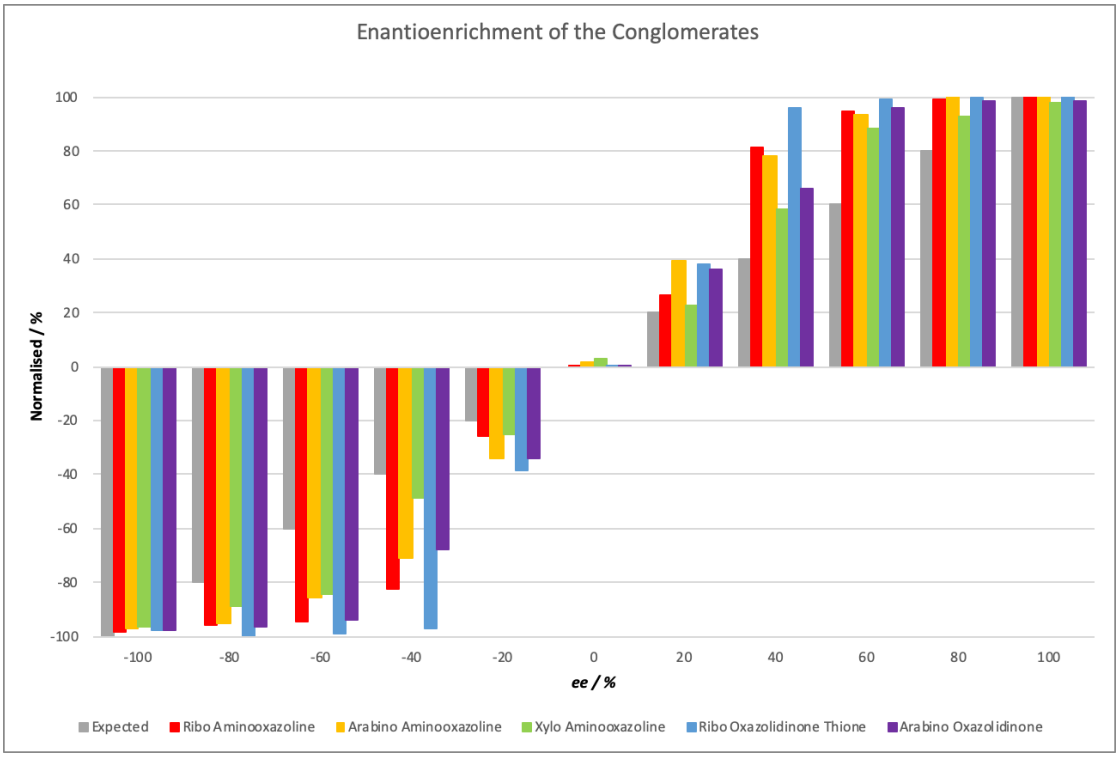

*Figure 79: Normalised enantioenrichment of compounds that formed conglomerates throughout the research. Showing the change in optical rotation of the crystals of **RAO** (0.25 M, H_2O), **AAO** (1.00 M, H_2O), **XAO** (1.00 M, H_2O), **ROT** (1.50 M, H_2O) and **AOX** (5.00 M, H_2O/ethanol (1:1)) for a range of ee values.*

What is also of note is that at 20% *ee* there are a number of compounds that in fact show enantiomeric amplification, particularly **AAO**, **ROT** and additionally **AOX**. However, it is worth noting that **AOX** was not carried out in water and was crystallised using a H_2O/ ethanol (1:1) solvent combination.

3.9 Conglomerate vs Racemic Crystals – Crystal Structure Comparison

Over the course of the research the compounds synthesised are presented below (Figure 80), the crystals obtained at 0% *ee* were collected and these were analysed and confirmed by SXRD or PXRD.

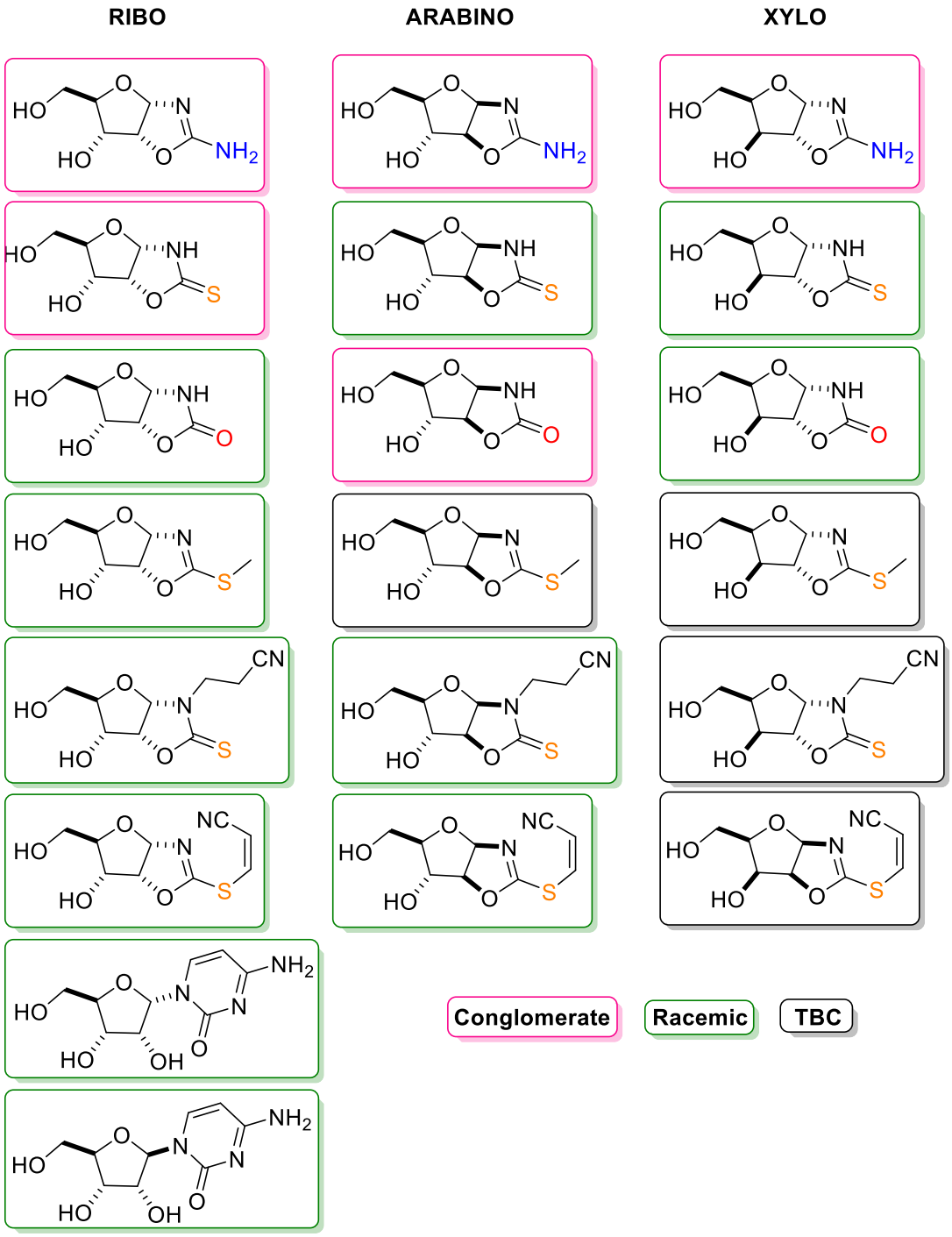

Figure 80: Summary of investigated prebiotically relevant molecules and their crystallisation. Pink represents conglomerate formation, green represents racemic crystal formation and black represents crystals that were unable to be identified.

The crystal structures obtained were investigated within a series (i.e. aminooxazolines (**AO**), oxazolidinone thiones (**OT**) etc) and also within diastereoisomers (i.e. *ribo*-, *arabino*-, *xylo*-). The *ribo*- series collected the most amount of data for the various compounds investigated

and it was revealed that there are possibly some favourable interactions that take place in either the homochiral compound, or ones that form in the racemic compound that therefore lead to either conglomerate or racemic formation. These will be described below, starting with the aminooxazolines (**AO**), and continuing throughout the *ribo*- series.

The notable interactions take place when each molecule has two hydrogen bonds to that same other molecule (i.e. molecule A has two hydrogen bonds to molecule B). In *ribo*-aminooxazoline (**RAO**), which forms conglomerate crystals, this is highlighted within the homochiral crystals by interactions between **N1** ··· C5'-O**H** and **O1** ··· C3'-O**H** that is illustrated in Figure 81 by a pink circle.

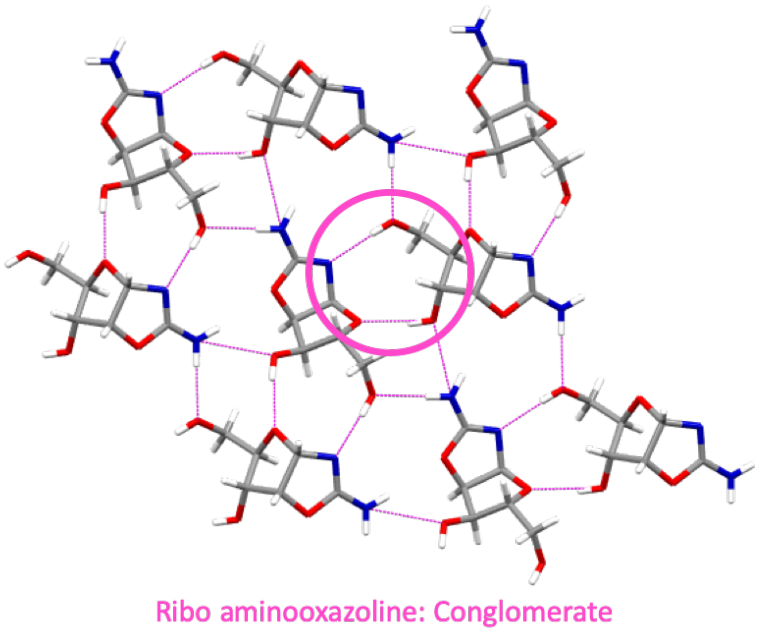

*Figure 81: Homochiral D **RAO** key interactions highlighted by a pink ring.*

Ribo-oxazolidinone thione (**ROT**) also forms conglomerate crystals, therefore when examining the homochiral, D **ROT** also exhibits the **N1** ··· C5'-O**H** and **O1** ··· C3'-O**H** interactions are seen as shown in Figure 82.

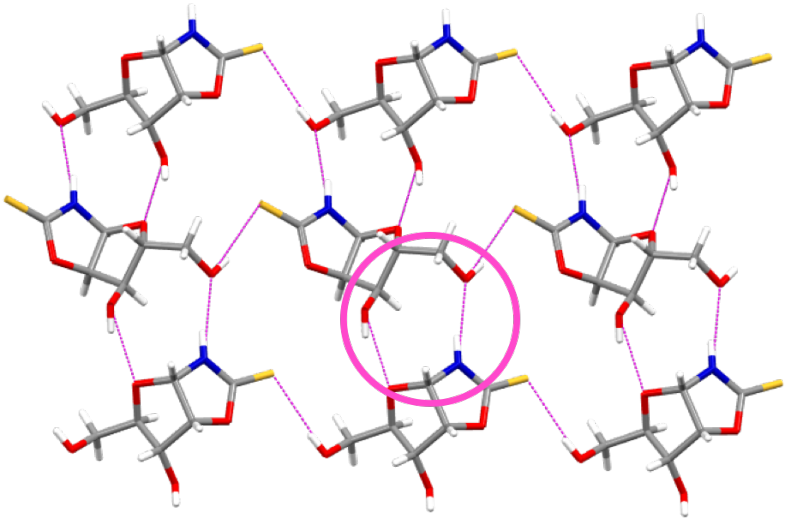

*Figure 82: D **ROT** key interactions highlighted by a pink circle.*

Ribo-oxazolidinone (**ROX**) has been noted of forming racemic crystals at 0% *ee*, therefore through examining the racemic crystal structure, it can be observed that one molecule interacts to another molecule through **N1** ··· C5'-O**H** and **O3** ··· C3'-O**H** interactions shown in Figure 83.

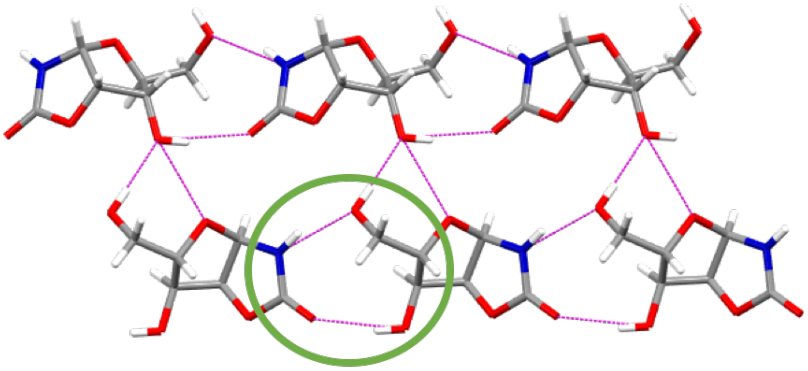

*Figure 83: Racemic **ROX** key interactions highlighted by a green circle.*

However, whilst traditionally both enantiomers show the exact same crystal structure, including the same space group, this has not proved to be the case for **ROX**. This can possibly be explained by polymorphism, however was not fully explored. What makes this also of particular interest is that in the L- enantiomer, the key interactions mentioned previously is also noted, however are not present in the highlighted D- enantiomer (Figure 84).

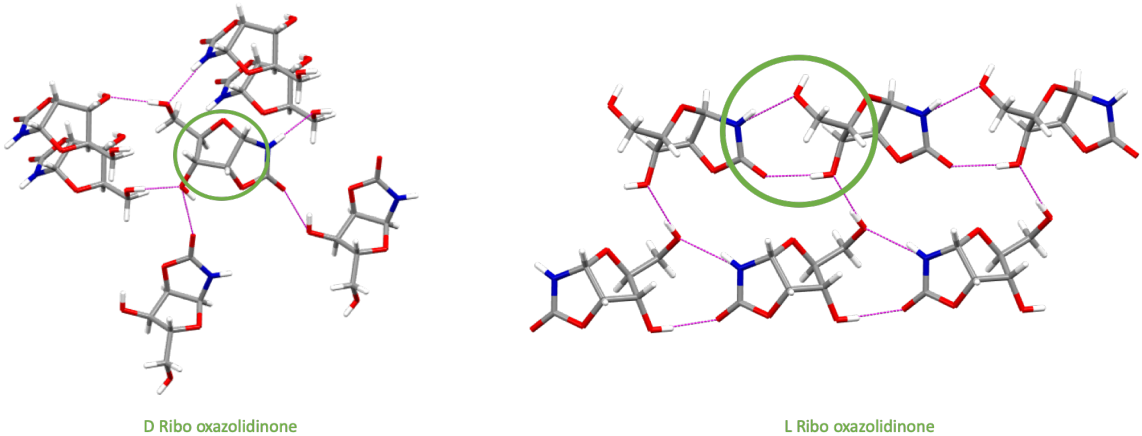

*Figure 84: D **ROX** and L **ROX***

Ribo methyl-oxazolidinone thione (**RMOT**) also presented with racemic crystals at 0% *ee*, it can be seen that within the homochiral structures there is a large 3D structure with no dimer-like interactions, however in the racemic crystal, there are the favourable interactions mentioned previously. In this structure two molecules interact *via* **N1** ··· C5'-O**H** and **O3** ··· C3'-O**H** as seen in Figure 85.

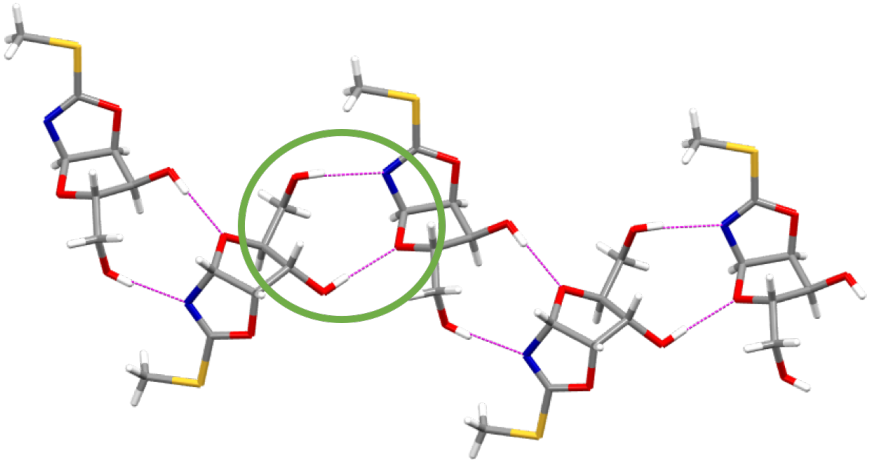

*Figure 85: Racemic ribo methyl-oxazolidinone thione (**RMOT**) favourable interactions indicated by green circle.*

Ribo N-cyanoethyl oxazolidinone thione (**RCEOT**) formed racemic crystals from 0% *ee* solutions of **RCEOT**. In these crystals, the dimer type motif is however, not observed (Figure 86).

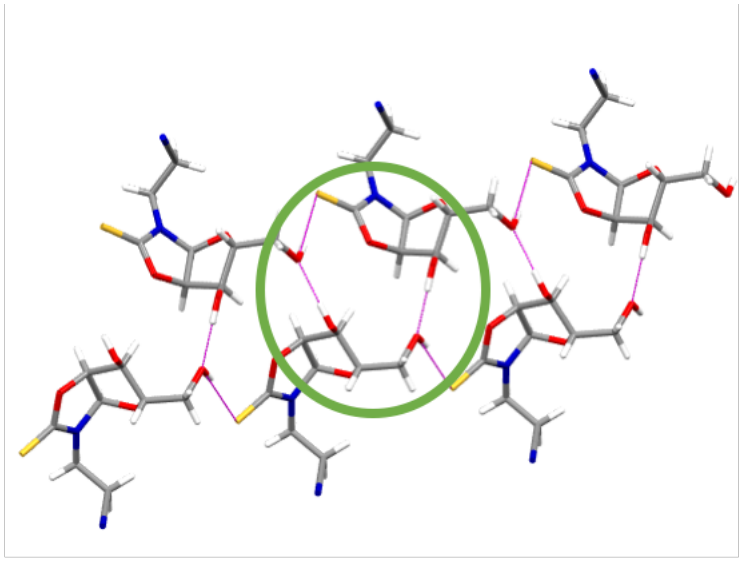

Ribo N-cyanoethyl oxazolidinone thione: Racemic

*Figure 86: Racemic ribo N-cyano ethyl-oxazolidinone thione (**RCEOT**) favourable interactions indicated by green circle.*

In order to consistently define and classify the hydrogen-bonded synthons, graph set analysis was performed in the methodology of Bernstein et al and is described within.[245] Further graph set analysis was performed (See experimental section 6.16). This was to investigate the possibility that conglomerate formation was in-fact guided by the formation of particular hydrogen bond patterns. If this could be better understood, could this assist in future explorations to finally better understand the origin of life.

Initially, graph set analysis was performed on the molecules at hand, which was the aminooxazolines (**AO**). Within these molecules it could be seen that the oxygen within the ring (O1) and the nitrogen within the ring (N1) were used to form rings with itself in conglomerate forming crystal structures. In **RAO** this was seen as $R\frac{2}{2}(10)$, however in **AAO** this was observed as $R\frac{4}{4}(21)$, and in **XAO** it was $R\frac{4}{4}(22)$. We then looked at other molecules as they

were obtainable to look for interactions in this manner, and whilst this was occasionally present, it did not correlate to whether the molecule formed conglomerate or racemic crystals.

The conglomerate forming: **RAO**, **AAO**, **XAO**, **ROT**, and **AOX** were compared. The graph set $C\frac{1}{1}(7)$ was noted to be forming within all the conglomerate crystals, which is between the 5'-OH to N1. However, when looking at the racemic forming crystals with available crystal structures: **AOT**, **XOT**, **ROX**, **XOX**, **RMOT**, **RCEOT** the $C\frac{1}{1}(7)$ was also present in multiple of the racemic structures. Therefore, not considered to be a reason for the formation of conglomerate forming crystals.

This therefore concluded that from this investigation, that there are no hydrogen bonding patterns which dictate the formation of conglomerate or racemic formation. This leads onto the future work, such as more advanced methods which may be able to uncover what molecular descriptor, or energy which encourages the crystals to form in the manners that they do.

3.10 Racemic vs Conglomerate Crystal Selectivity and the Effect on Rate of Formation

Some crystallisations occur over a matter of hours, whereas others are much slower - sometimes taking weeks to complete. We found that compounds that show a tendency to form conglomerate crystals will crystallise faster at high ee's and those which prefer to form

racemic crystals will crystallise quicker at lower ee's (Table 10). The crystals rate presented in Table 10 are at the same concentrations used for the enantioenrichment scalemic reactions presented earlier in each respective section.

Table 10: Analysis into how quickly different prebiotically relevant compounds crystallise, measured in days at the described concentrations for the scalemic experiments.

Days Taken	ee / %											Observed
	-100	-80	-60	-40	-20	0	20	40	60	80	100	
Ribo Aminooxazoline	1	1	2	3	4	7	4	3	2	1	1	Conglomerate
Arabino Aminooxazoline	2	3	4	7	8	8	8	7	4	3	2	Conglomerate
Xylo Aminooxazoline	3	4	4	7	8	9	8	7	4	4	3	Conglomerate
Ribo Oxazolidinone Thione	1	1	2	4	8	8	8	4	2	1	1	Conglomerate
Arabino Oxazolidinone Thione	7	6	5	4	3	3	3	4	5	6	7	Racemic
Xylo Oxazolidinone Thione	11	9	7	5	4	3	4	5	7	9	11	Racemic
Ribo Oxazolidinone	14	12	8	3	3	3	3	3	8	12	14	Racemic
Arabino Oxazolidinone	6	8	8	10	14	15	14	10	8	8	6	Conglomerate
Xylo Oxazolidinone	14	13	10	8	5	4	5	8	10	13	14	Racemic
Ribo Methyl Oxazolidinone Thione	18	16	14	12	10	8	10	12	14	16	18	Racemic

We can explain this observation thus: conglomerate crystals are enantiomerically pure, i.e. each individual crystal is either D- or L-. Therefore, in a solution of a compound that selectively form conglomerate rather than racemic crystals, D will bond with D, until all D has been crystallised. L will also bind preferentially with L. D- will not bond with L- and vice versa. In a racemic or low ee solution, it is just as likely that D will 'meet' another molecule of D as it will 'meet' a molecule of L and so it takes longer for the conglomerate crystal to form. However, at higher ee's, such as over 60%, it is far more likely that D will 'meet' another D and form a conglomerate crystal, so the crystals can form much faster.

For molecules that prefer to form racemic crystals, in a low ee solution of that compound, it is highly likely that L will meet D and readily start to form crystals. At high ee's it is much less likely that D will meet L and so crystal formation is slowed. In this scenario, crystallisations take much longer.

We can therefore infer that when crystals form quickly from a solution, then if that solution is high ee, we are observing conglomerate crystal formation, and if the solution is of a lower ee, we are observing racemic crystals being formed. We can also infer, that if crystals rapidly form at high ee's the compound has a preference for conglomerate crystal formation. Conversely, when crystals rapidly form from low ee or racemic mixtures, that compound has a preference to form racemic crystals.

It is worth highlighting that this effect is relative within a series at a certain concentration. That is to say that if, for example, a *ribo*- compound takes a week to form, we can only deem that to be slow or fast compared to other crystallisations of the same ribo compound at the same concentrations. I.e. 'fast' for one compound may seem very slow compared to another.

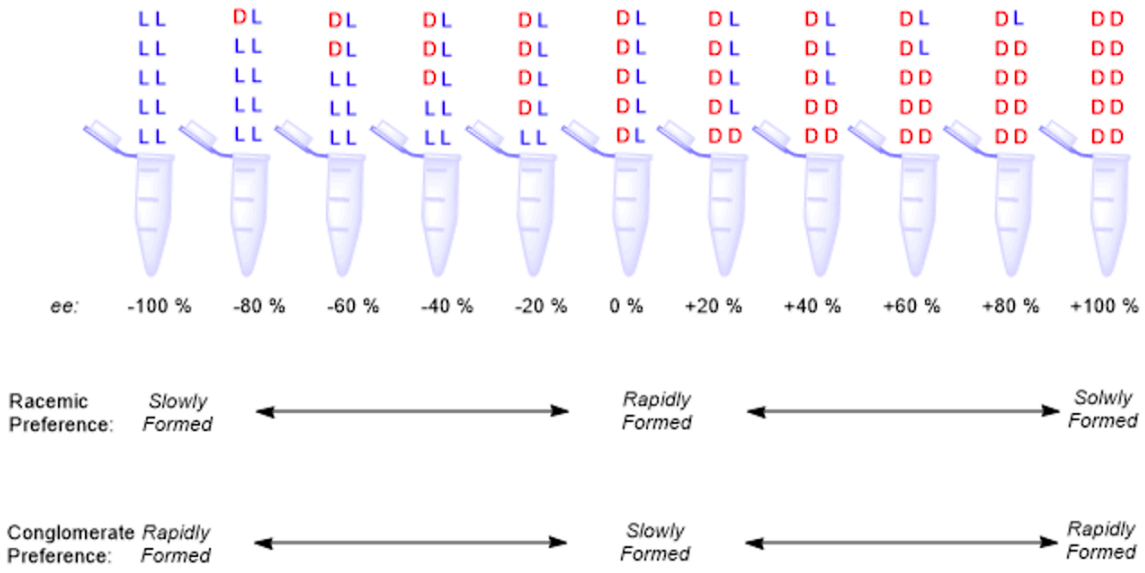

Figure 87: The effect of crystallisation preference on the rate of crystal formation.

3.11 Competition Experiments

During the course of this research, it became an interest to know whether we might use crystal engineering techniques to change the preference that a compound shows from forming, for example, racemic crystals to forming conglomerate crystals. I.e. could we find conditions under which **ROT** (which tends to form conglomerate crystals) can be 'persuaded' to form racemic or vice versa. Or if such conditions exist under which **AOT** will form conglomerate crystals rather than its preferred racemic crystals. It was also useful to understand the crystallisation of these prebiotic compounds in an environment that may be plausible, i.e. one in which there isn't just the one compound in solution, and there are multiple compounds. However, it is obviously not possible to re-create conditions for the purpose of confirming or disproving a hypothesis. It isn't necessary or reasonable to expect to recreate the 'primordial soup' exactly as it may have existed on the early Earth due to the myriad variables, compounds and fluxional conditions. Having said that these experiments provide a good approximation of those conditions and give us insight into how enantiomeric selectivity arose. It may be, and probably is, the case that there are other effects we do not yet know of or fully understand which will be revealed as research in this area continues, and it is an exciting notion that this work has contributed in a meaningful way to those investigations.

It was quickly realised that due to the high concentrations required for crystallisation therefore large amounts of solid needed, and the small-scale reaction conditions meant that the initial concentration required was reduced, often significantly to allow both compounds to dissolve completely.

As such, an initial crystallisation experiment was carried out in which homochiral D-**ROT** (1 M) was mixed with homochiral D- **AOT** (1 M) in a 1:1 ratio in water (1 mL) and allowed to crystallise

at low temperature (−4° C). An aliquot of the solution was taken at 0, 24 h and 1 week and analysed by NMR against a known concentration of standard (4,4- dimethyl-4-silapentane-1-sulfonic acid (DSS), 200 mM) to see how the ratio had changed. Based on our findings, we would expect D- **ROT** to form conglomerate crystals and D- **AOT** to form racemic crystals.

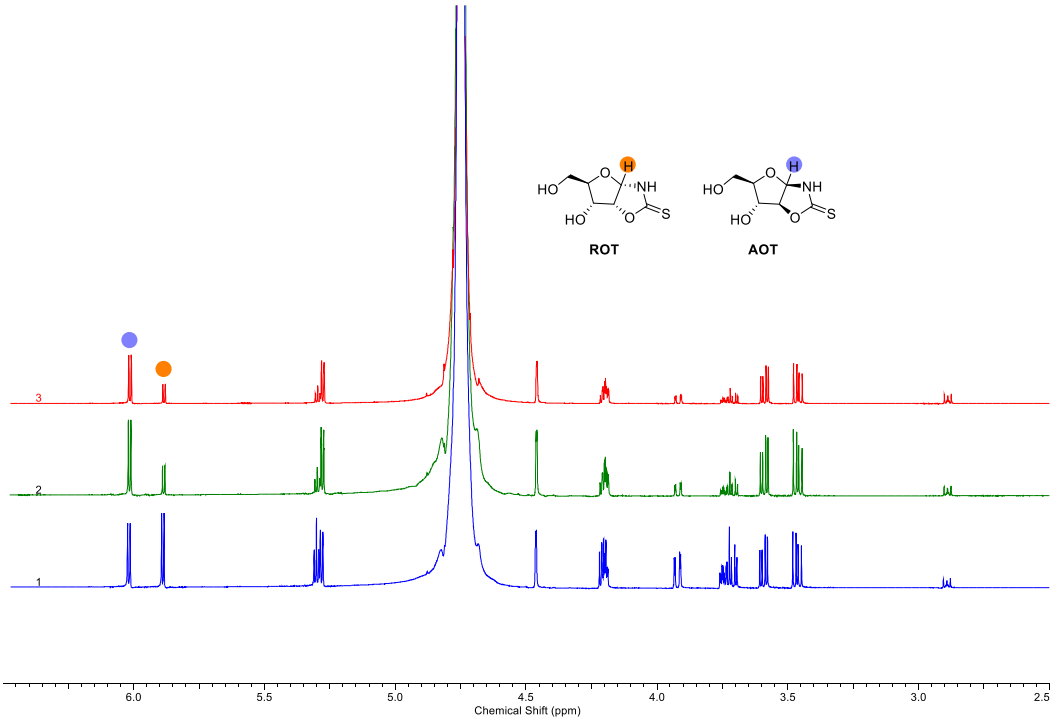

*Figure 88: D- **ROT** (1M) vs D- **AOT** (1M) in water. (1) 0 h. (2) 24 h. (3) 1 week.*

As the ee is 100%, we would therefore expect to see homochiral **ROT** crystals form quicker than the **AOT** crystals. Looking at the NMR over time (Figure 88), we do indeed see that the concentration of **ROT** in solution is decreasing relative to the **AOT** as it is crystallising out of solution. In this case, the presence of the **AOT** does not affect the expected outcome of the crystallisation.

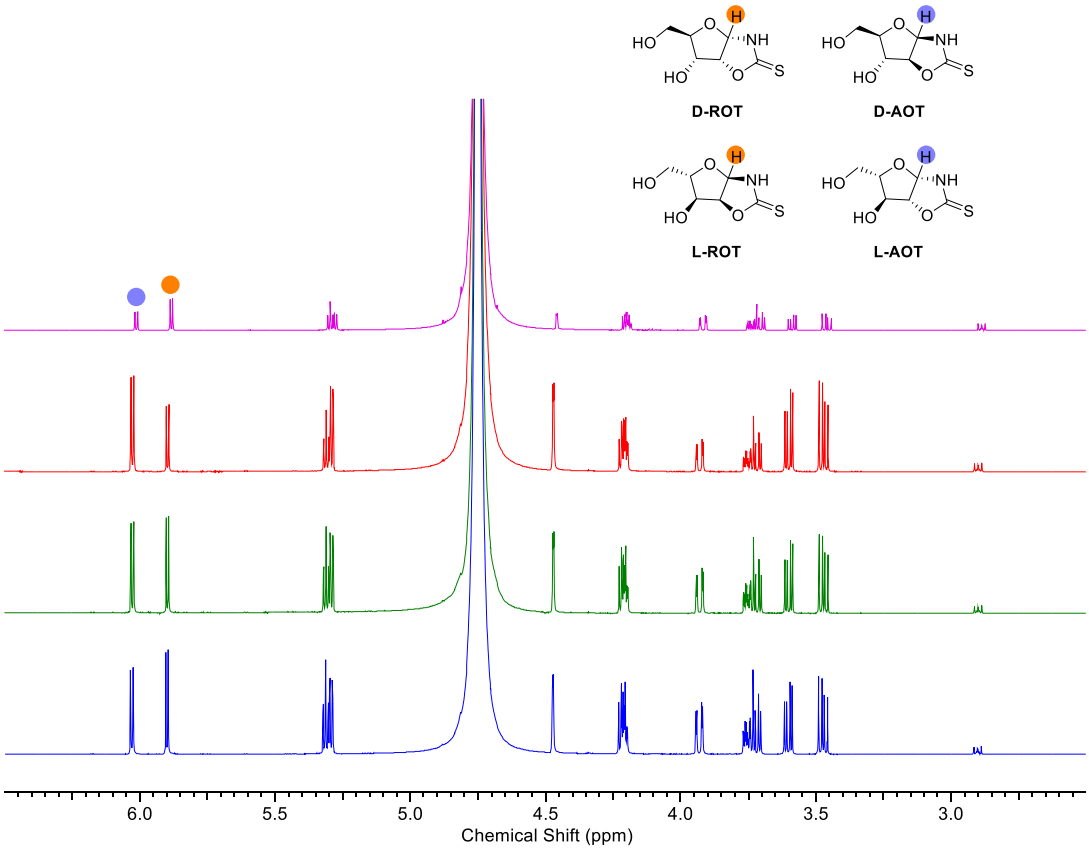

*Figure 89: D/L **ROT** (1M: 0.5 M of each enantiomer) vs D/L **AOT** (1M: 0.5 M of each enantiomer) in water. (Blue) 0 h. (Green) 24 h. (Red) 1 week. (Pink) 2 weeks.*

In this experiment, the **ROT** begins to slowly crystallise initially. As **ROT** tends to favour conglomerate formation that would account for the slow rate of crystallisation. Surprisingly, however, as **AOT** would ordinarily favour racemic we should expect to see this crystallise more readily from solution since the racemic mixture favours it. As shown in the NMR **AOT** crystallises much slower, even than the **ROT** up until 1-2 weeks when we see both have crystallised out more substantially. It may therefore be the case that the presence of **ROT** appears to have slowed the formation of racemic crystals. Alternatively, it could be the case that **AOT** needs to be present at higher concentration in order to crystallise faster. It was therefore attempted to prepare a more concentrated solution, but it wasn't possible to get higher than the 1 M solution (with respect to each compound) used here, as the solid would not dissolve.

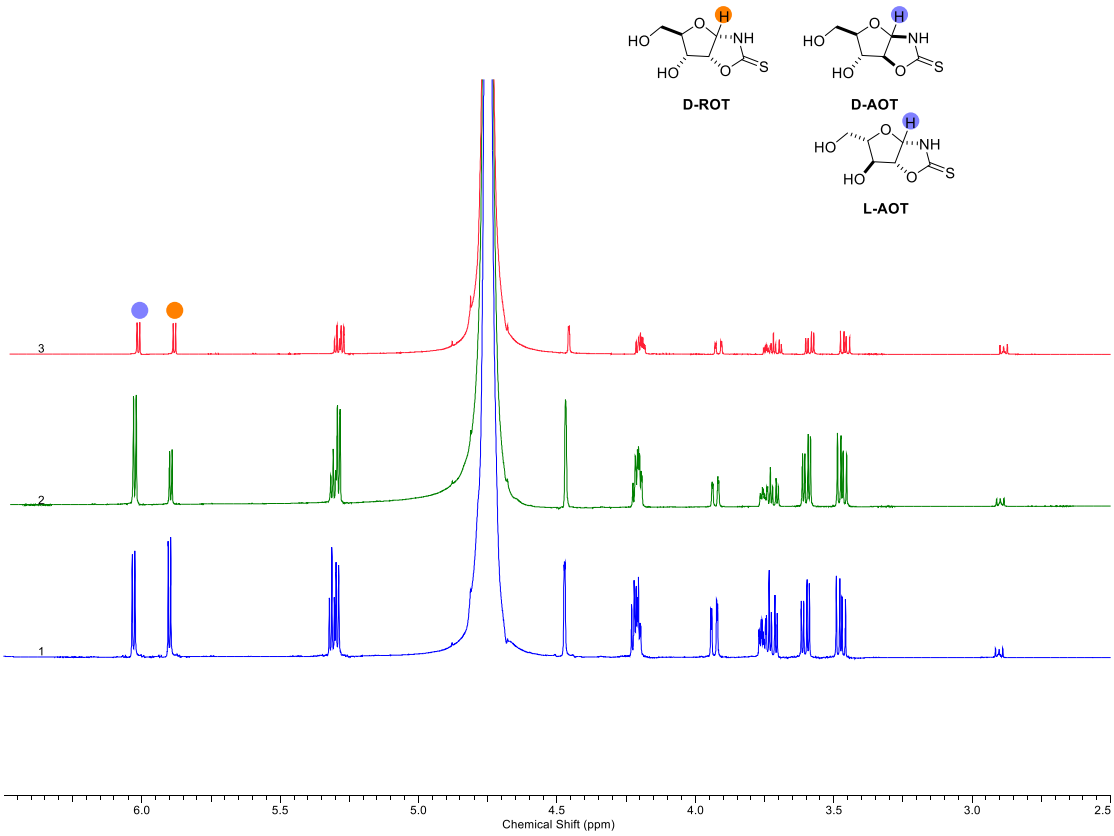

*Figure 90: D/D **ROT** (2 M) vs D/L **AOT** (1 M of each enantiomer) crystallised in water. (1) 0 h. (2) 24 h (3) 1 week.*

To test the crystallisation rates at this concentration, since it is not feasible to increase above this, a mixture was prepared that gives each compound equal chance to crystallise. As **ROT** seeks to form conglomerates, it should crystallise faster in the presence of only one enantiomer. Therefore, only D-ribo was added. As **AOT** seeks to form racemic, it should crystallise fastest when there is a mixture of D- and L- enantiomers, so a 1:1 mixture of this was added. The concentration is the same as the first two experiments. The crystallisation was monitored by NMR (Figure 90).

Once again, the **ROT** conglomerates form fastest and after 24 h the crystallisation rate has plateaued. As in the last experiment, the **AOT** crystals form much slower, though after one

week the concentration of **ROT** and **AOT** is almost the same in solution, and all crystallisation has equilibrated. Polarimetry and PXRD confirmed the crystal forms present. From these experiments, it would appear therefore, that the presence of each compound does not affect the crystal forms (conglomerate vs racemic).

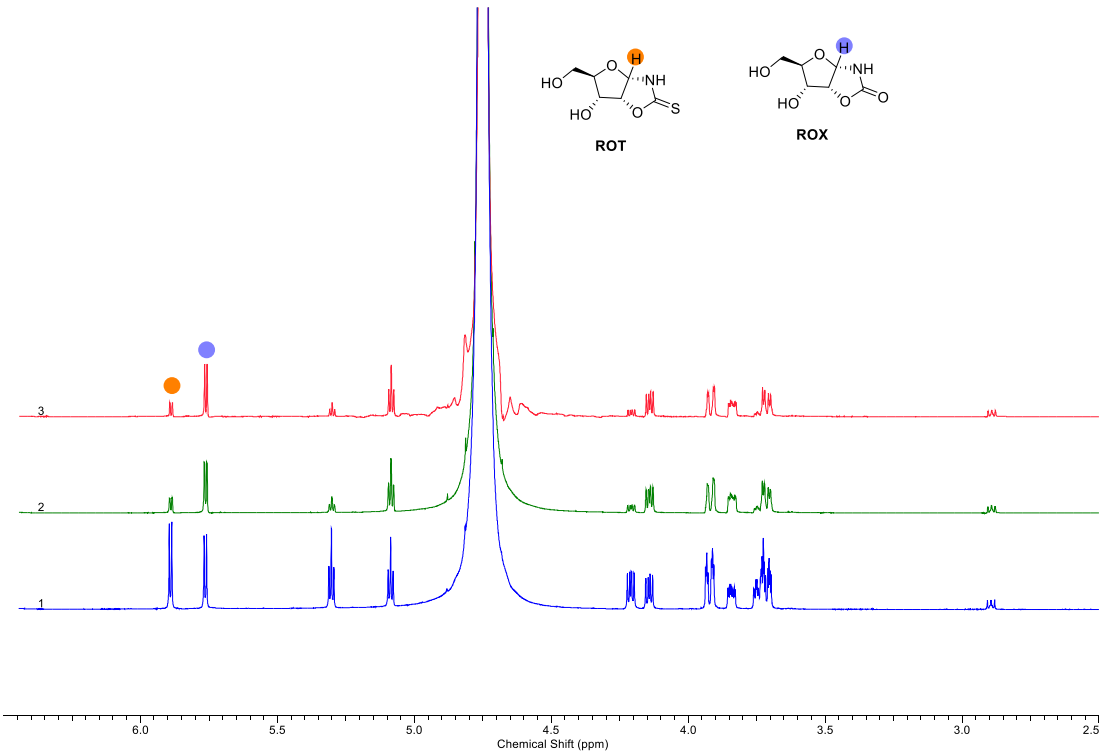

*Figure 91: D **ROT** (1M) vs D **ROX** (1M) crystallisation in water. (1) 0 h. (2) 24 h. (3) 1 week.*

Ribo oxazolidinone thione (**ROT**) was also investigated against another prebiotically relevant compound, ribo oxazolidinone (**ROX**). In the previous experiments, **ROT** was found to be forming conglomerate crystals, whereas **ROX** was found to form racemic crystals. This crystallisation was initially investigated with the homochiral enantiomers (Figure 91). When 1 M of **ROT** and 1 M of **ROX** are crystallised from water, it can be seen from the NMR that **ROT** crystallises initially after 24 h where the crystallisation plateaus. The **ROX** does not form any crystals over this time.

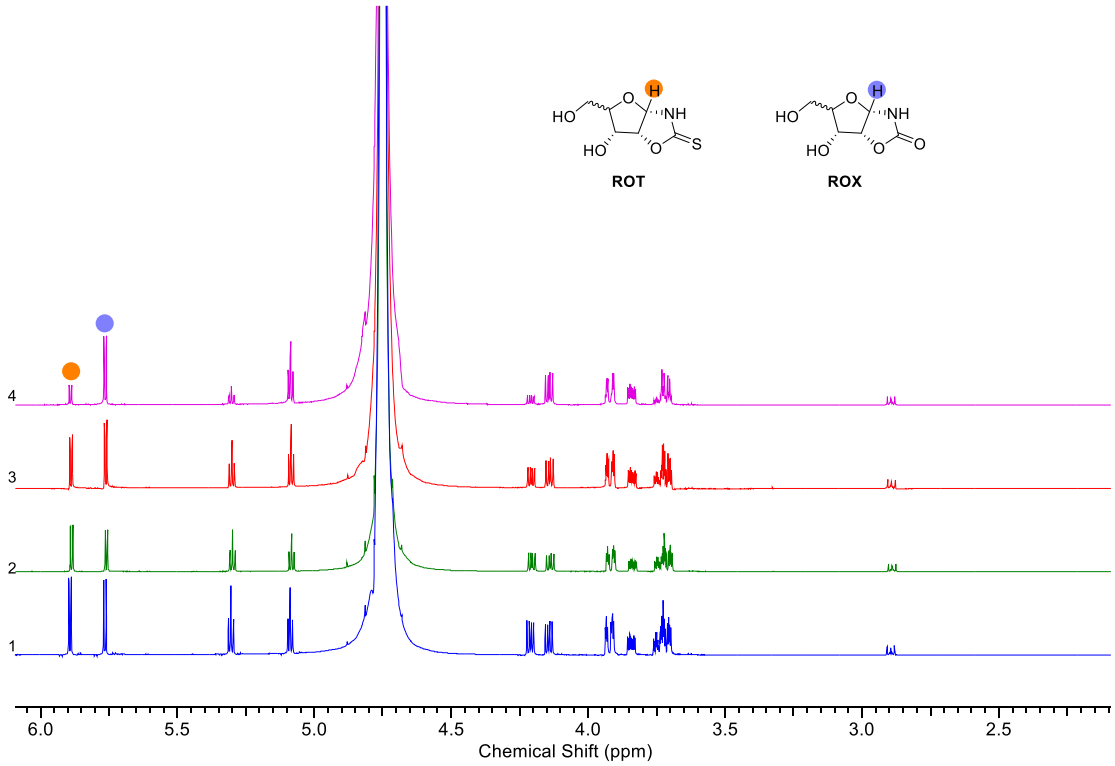

*Figure 92: D/L **ROT** (0.5M each enantiomer, total 1M), D/L **ROX** (0.5M each enantiomer, total 1M). (1) 0 h. (2) 24 h. (3) 1 week. (4) 2 weeks.*

Further to that experiment, the racemic mixture D/L of **ROT** and D/L **ROX** with 0.5 M of each enantiomer (1 M total of each compound) were dissolved in water and allowed to crystallise. From Figure 92 it can be seen that crystallisation takes place for the **ROT**, however only takes place after 2 weeks. This is to be expected as whilst the overall molarity of the **ROT** is the same, the available concentration is lower (due to the desire for D to bond with D, and vice versa with L). The crystals obtained were analysed by PXRD and were confirmed to be conglomerate crystals. The concentration for the oxazolidinone to crystallise does not appear to be low enough, however this could not be increased as the solids would not dissolve due to the quantity of solid required for the molarity.

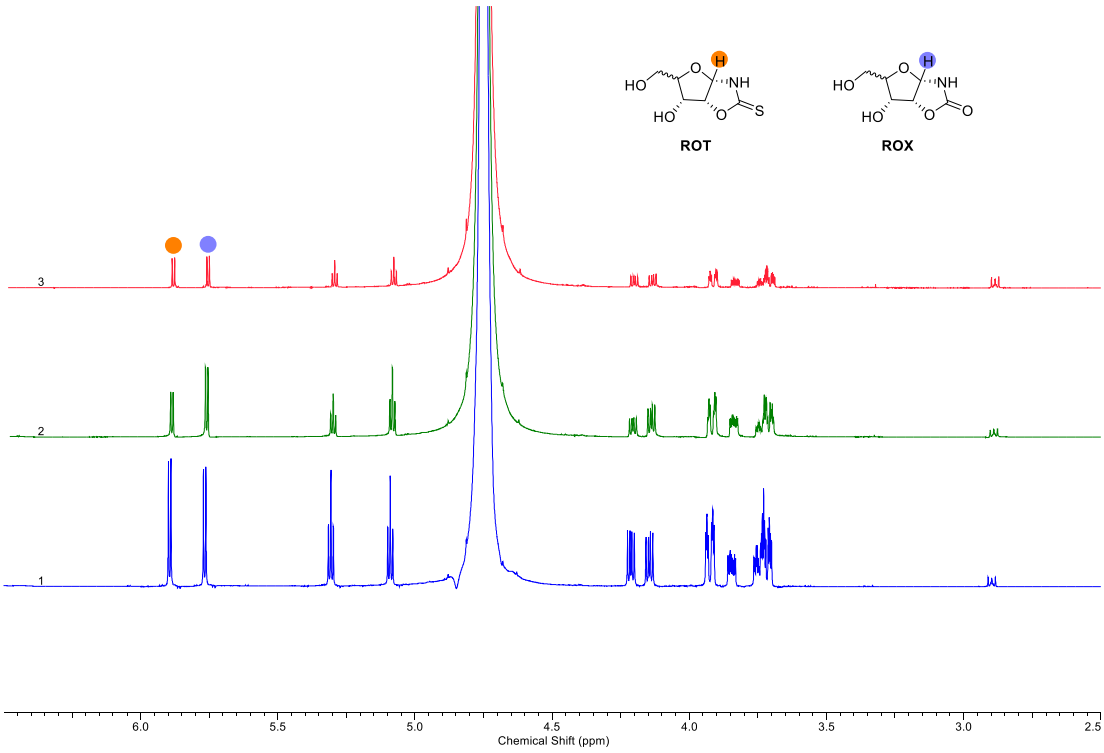

*Figure 93: D **ROT** (2M) vs D/L **ROX** (1M of each enantiomer). (1) 0 h. (2) 24 h. (3) 1 week.*

In this final experiment, homochiral D **ROT** (2 M) was dissolved in water along with D/L **ROX** with 1 M of each enantiomer (Figure 93). Due to the conglomerate forming preference of **ROT** this gives the compound equal chance as the preferentially forming racemic **ROX**. In this experiment, it is seen that after 24 h the **ROT** forms faster, however by 1 week, there is equal amount of **ROT** and **ROX** in solution and therefore has also crystallised.

4 Crystal Engineering towards the Prebiotic Aminal

4.1 Introduction

The proposed prebiotic route to access the pyrimidine ribonucleotides necessitates the synthesis of the pentose aminooxazolines (**AO**) discussed earlier. However, the syntheses of these important intermediates have questions around their plausibility due to the requisite strict sequential, step-wise process by which they are assembled. Beginning with the addition of cyanamide (**6**) to glycolaldehyde (**13**) to produce 2-aminooxazole (**15**), immediately followed by reaction with glyceraldehyde to furnish the target pentose aminooxazoline (**AO**). However, if this is not carried out such a direct manner, side products are created due to the lack of selectivity in each step (Scheme 35).

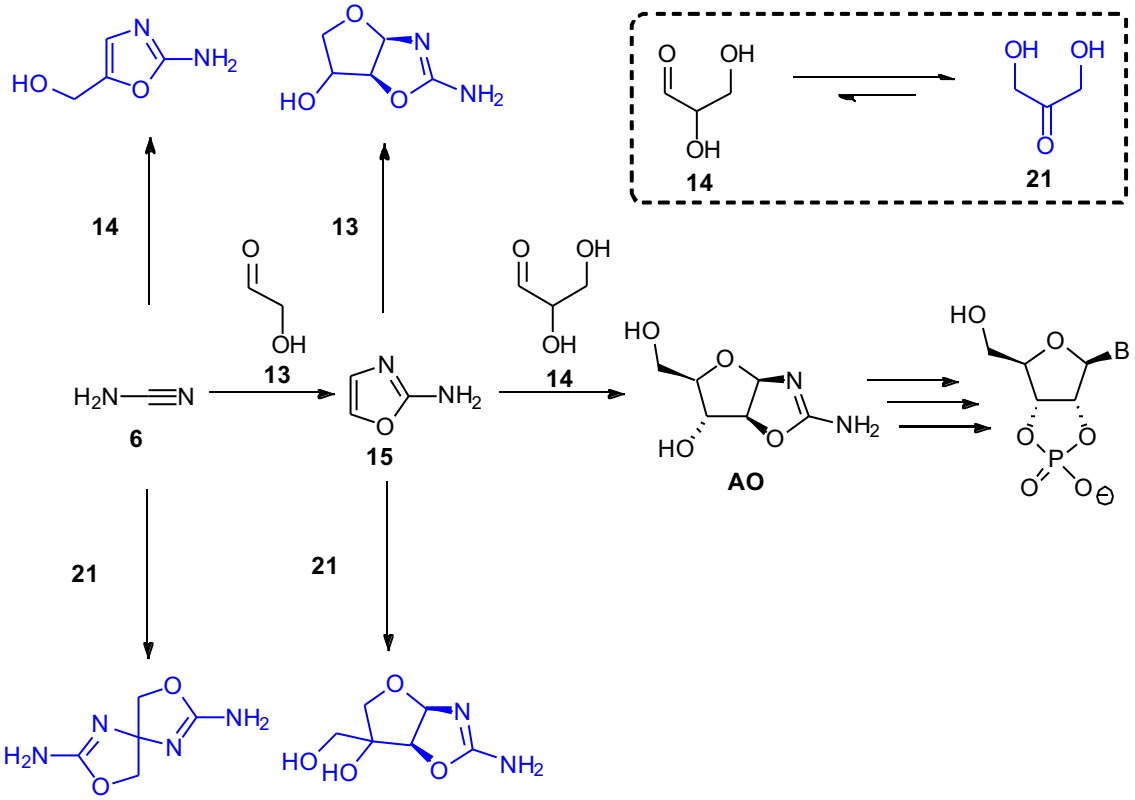

Scheme 35: Stepwise synthesis of ribonucleotides from the pure reagents (black) along with the undesirable side products created if the sequential addition is not achieved (blue).

In 2017 Islam et al. demonstrated that 2-aminothiazole (**23**), a prebiotically-plausible molecule, can selectively react with two- and three-carbon sugars (glycolaldehyde (**13**) and glyceraldehyde (**14**) respectively) which results in crystalline aminal (Scheme 36). This not only achieves a method of purification, it also allows ribonucleotide synthesis starting from a large and complex mixture of sugars. Further, aminal formation also has the added benefit that it is able to inhibit the thermodynamically-favoured isomerisation of glyceraldehyde (**14**) into dihydroxyacetone (**21**) by forming the glyceraldehyde aminal (**25**), which removes glyceraldehyde (**14**) from the system and drives the equilibrium of the reaction. Furthermore, this method is additionally time-resolved whereby separation of the crystal reservoirs are achieved through the rate of formation of the glycolaldehyde aminal (**24**) being more rapid than that of the glyceraldehyde aminal (**25**) (Scheme 36).

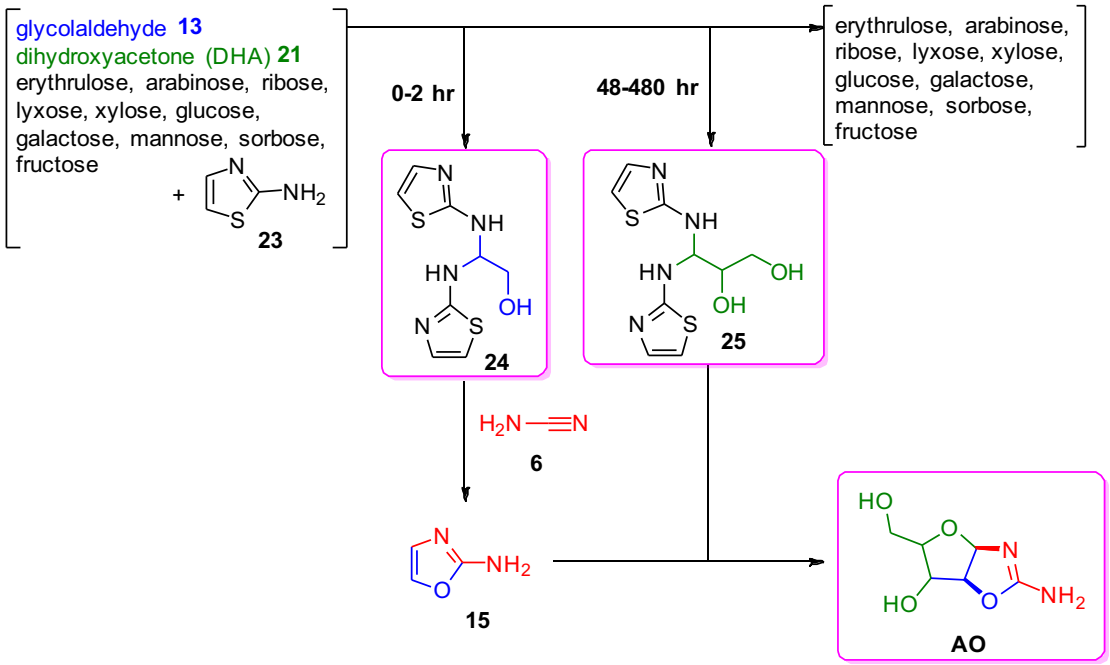

*Scheme 36: Synthesis of ribo-aminooxazoline (**RAO**) from a complex sugar mixture and 2-aminothiazole (**23**). Pink: compounds obtained as crystals.*

Whilst this impressive method overcomes many of the issues (such as; overcoming the thermodynamically favoured isomerisation of glyceraldehyde (**14**) into DHA (**21**) and the required sequential addition) with the previous syntheses, the discussion of homochirality is still unanswered. The crystals obtained are racemic when starting from racemic starting materials (SMs) or homochiral if starting from enantiopure SMs. So, with this in mind, is it possible to stereoselectively form the aminal precursor and carry that stereochemistry through to the aminooxazoline (**AO**)? By using crystal engineering techniques, we anticipated that it would be possible to isolate the chiral precursor as a conglomerate co-crystal if the suitable candidate molecule could be found.

4.2 Crystal Engineering

Crystal engineering is a subdiscipline within supramolecular chemistry at the intersection of organic, inorganic, and physical chemistry; rooted in the study of non-covalent interactions that are observed in crystals; focussed on understanding and using those interactions to control how substances crystallise, and thus exploit novel behaviours and create new materials.[246] The phrase 'crystal engineering' was coined by Pepinsky and later elaborated upon by Schmidt who described the relationship between the crystal structure of trans-cinnamic acids and their reactivity.[247,248] Since then, the ways in which crystals form, their constituent synthons[3], and the subtle ways in which the chemist can substitute them to access alternative crystal forms has been developed into a craft of its own to design and prepare new solids with novel physical and chemical properties.[249]

[3] Structural units within molecules which can be formed and/ or assembled by known or conceivable synthetic operations – Corey's definition of a synthon.[257]

Hydrogen bonded networks of 2-aminothiazoles (**23**) have received notable interest due to the predictable way in which they crystallise with carboxylic acids and/or carboxylate ions.[250] There are four likely synthons that can be used to design various supramolecular assemblies with a range of dimensionalities (Scheme 37).

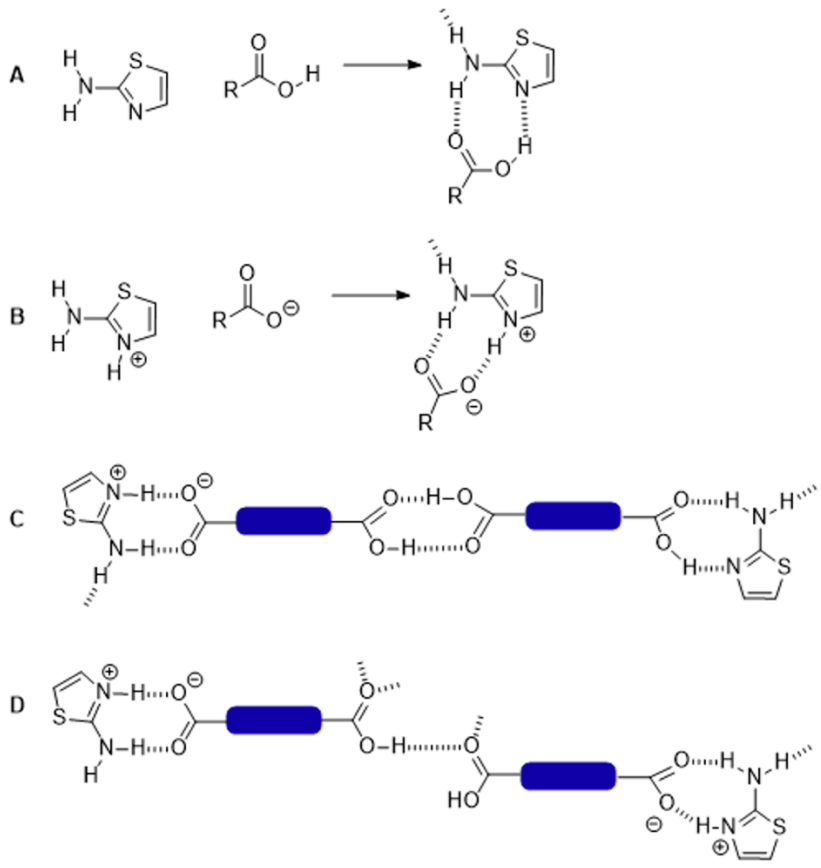

*Scheme 37: Possible supramolecular synthons for 2-aminothiazole (**23**). A) 2-aminothiazole with a monocarboxylic acid forming a cocrystal. B) 2-aminothiazole monocarboxylate salt. C) 2 aminothiazolium hydrogen dicarboxylate (1:1 organic salt). D) 2-aminothiazolium hydrogen dicarboxylate (1:1 organic salt).Redrawn from Yadav et al.*[250]

2-aminothiazole (**23**) and mono-carboxylic acids can form zero-dimensional network when prepared in a 1:1 ratio, giving the cyclic H-bonded motif shown in A and 1-dimensional B above. Dicarboxylate forms the dimer synthon shown in C leading to 2-dimensional structures and the catemer synthon shown in D results in 3-dimensional structures.[250]

By understanding the aminal's binding and crystal behaviour, we can gain a deeper understanding of how the constituent building blocks connect and then in turn try to control the crystalline preferences. In each case, the connections need to be analysed, this is mainly achieved by observing the hydrogen bonding.

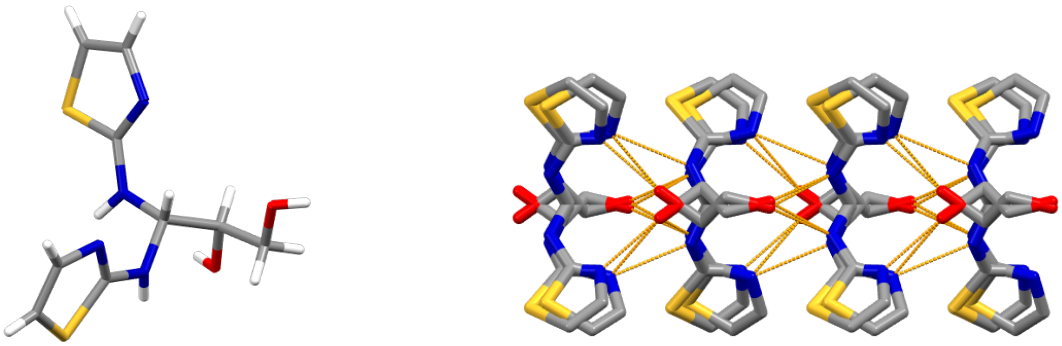

*Figure 94: (Left) Crystal structure of glyceraldehyde aminal (**25**) obtained from SXRD (CSD 1477045). (Right) Interactions of the aminal – each aminal position within the crystal is occupied by both the D- and L- isomer.*

As seen in Figure 94, the racemic crystal of glyceraldehyde aminal (**25**) is characterised by multiple hydrogen bonds in the crystal. Each aminal position within the crystal is occupied by both the D- and L- isomer. The C2-OH forms intramolecular H-bonds with the –NH groups of the imine, which holds the molecule in the conformer shown. The –OH on C3 is therefore potentially free to form intermolecular H-bonds with the polar imine protons.

There is literature precedent demonstrating that 2-aminothiazole co-crystallises with a range of compounds including octanedioic (CCD 964476) and decanedioic (CCD 930266) acid, 6-methylimidazo(2,1-b)thiaole (CCD 248171), and 5-chloro-N-(2-chloro-4-dinitrophenyl)-2-hydroxybenzamide (CCD 1437254) shown with their key interactions in Figure 95. Therefore,

suitable conformers were chosen based on the presence of specific functional groups in the attempt to form cocrystals with the aminal.

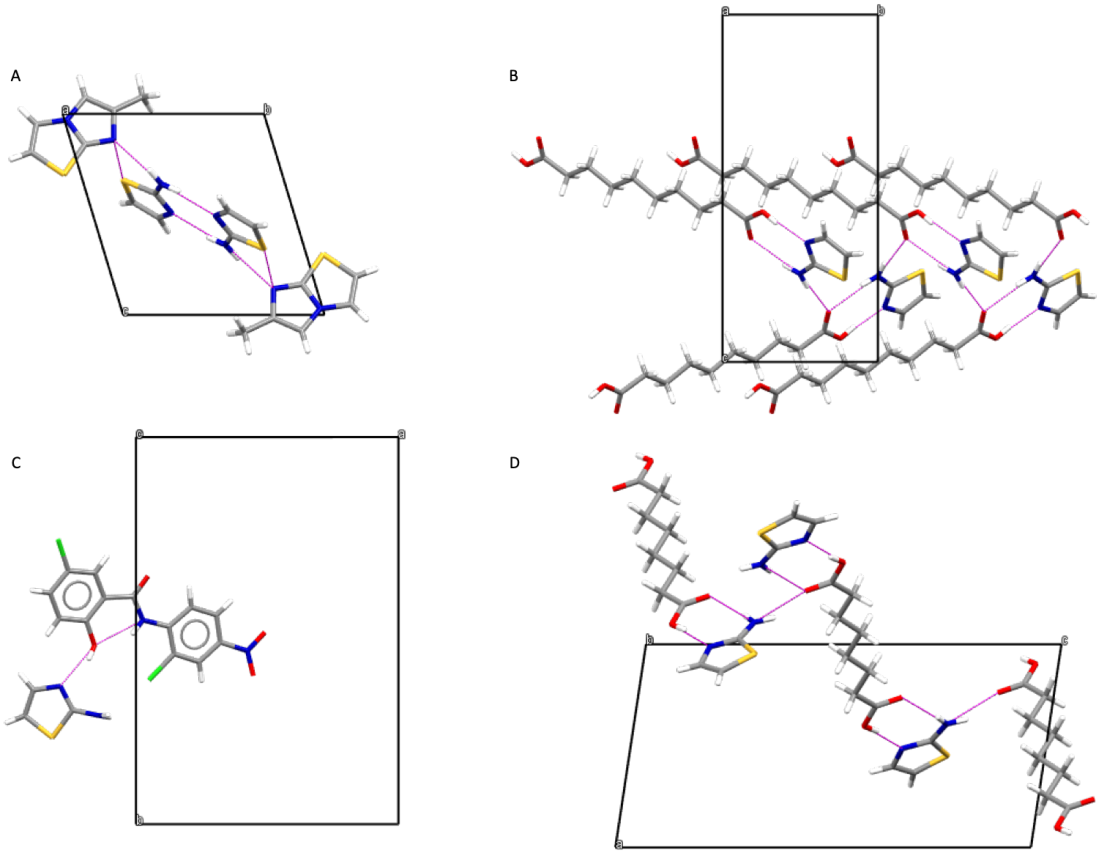

Figure 95:2-aminothiazole with A) 6-methylimidazo(2,1-b)thiaole (CCD 248171), B) decanedioic acid (CCD 930266) C) 5-chloro-N-(2-chloro-4-dinitrophenyl)-2-hydroxybenzamide (CCD 1437254) D) and octanedioic acid (CCD 964476).

Using this methodology and based on the established proclivity for H-bonding moieties to incorporate into novel crystal structures with 2-aminothiazoles that may otherwise be inaccessible, we predicted that small molecules containing carboxylate groups, including amino acids, as well as carbonyls and substituted phenols & pyridines would be suitable candidates for crystal engineering and so were selected as the candidate additives for co-crystallisation. The projected H-bonding motifs are shown in Figure 96.

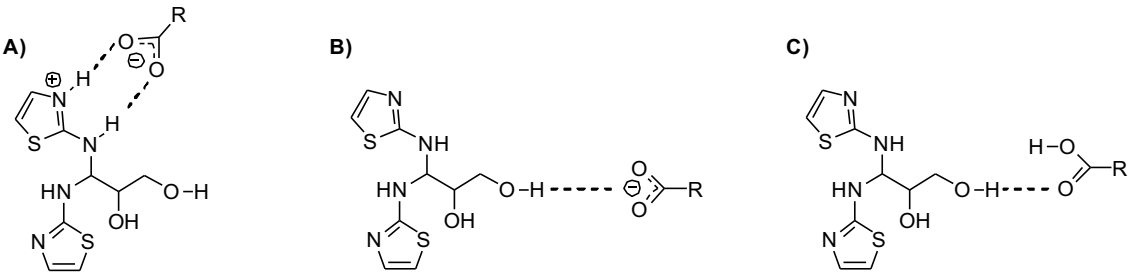

Figure 96: A,B,C: anticipated hydrogen bond interactions for the glyceraldehyde aminal cocrystal.

In the first example (Figure 96 A), the N-protonated thiazolium moiety is coordinated by the carboxylate anion. In Figure 96 B, the primary alcohol on the aminal's terminal carbon is involved in H-bonding with the carboxyl group of the additive and finally in C, the C=O group is hydrogen bonding with the alcoholic proton.

The additives chosen for screening are shown below:

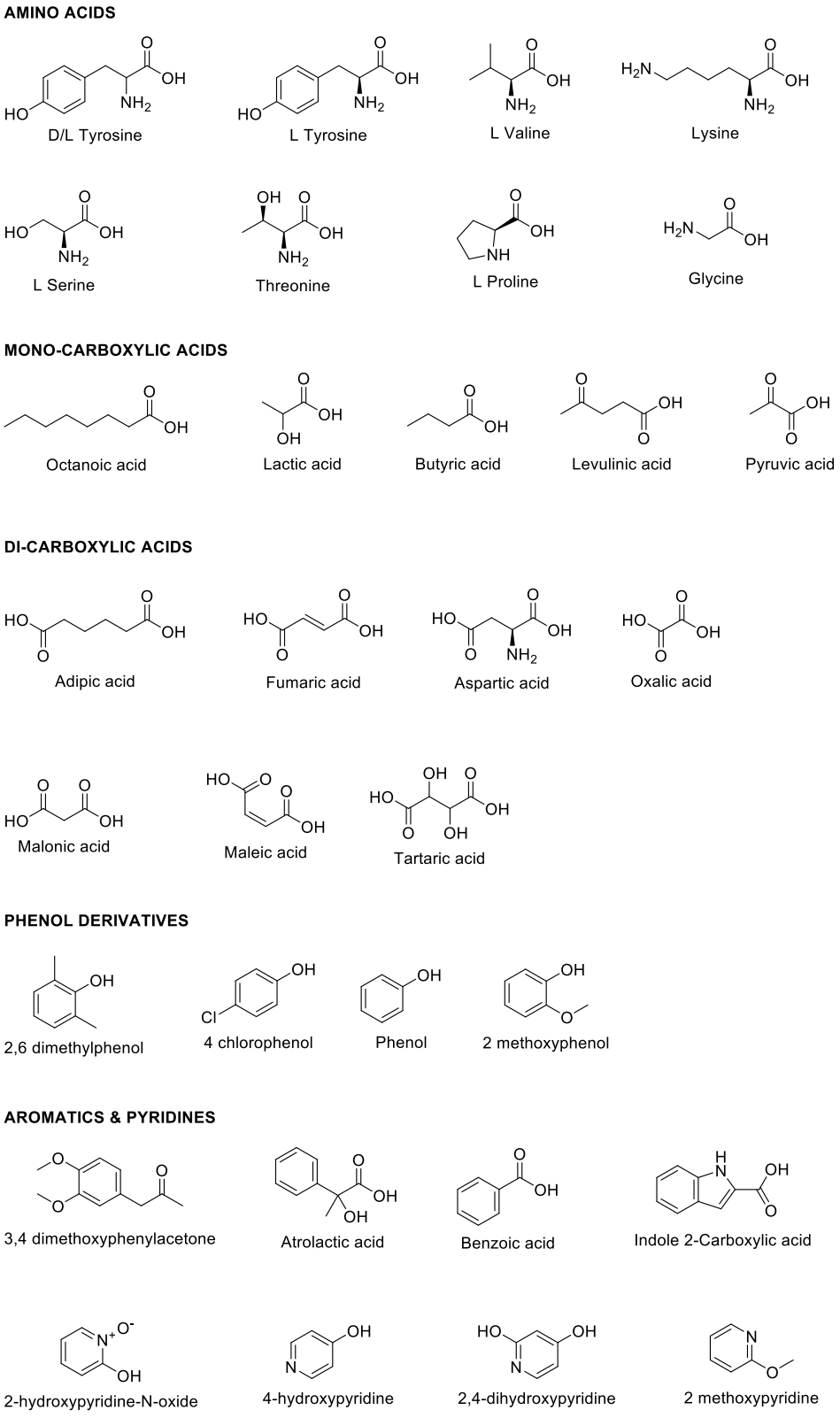

Figure 97: Additives chosen for potential co-crystallisation coformers with the aminal.

Aside from simply choosing H-bond donor/acceptors, amino acids were selected due to their potential prebiotic availability. Further, three amino acids have been noted to form conglomerate crystals, these are asparagine (Asn, glutamic acid (Glu) and threonine (Thr) which may induce conglomerate formation within the aminal.[1,175] Blackmond and Breslow have noted enantiomeric amplification based on the equilibrium solid-liquid phase behaviour of amino acids in solution which operates in aqueous systems, which was an ideal starting point for these screenings..[184,185,251]

Organic acids were selected as they have been shown to provide the bulk of adduct structures with 2-aminothiazole (**23**). Several di-acids were also selected due to their success in co-crystallising with 2-aminothiazole.[250] Equimolar amounts of the additives were used, or a 1:2 ratio was used (solubility permitted) in order to encourage co-crystallisation and provide enough opportunity for hydrogen bonding patterns to emerge.

4.3 Method

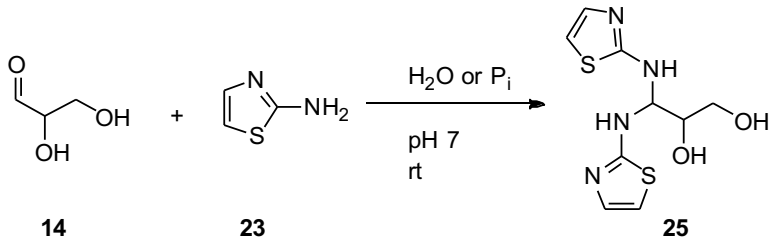

14 **23** **25**

*Scheme 38: Synthesis of glyceraldehyde aminal (**25**) from glyceraldehyde (**14**) and 2-aminothiazole (**23**).*

The aminal formation proceeds with glyceraldehyde (**14**, 1 equiv.) and 2-aminothiazole (**23**, 2 equiv.) in water or phosphate buffer (pH 7), at room temperature for 24 hours.[63] This synthesis has been noted to have an increased rate of reaction in phosphate buffer (1 M, pH 7) than in

water, and the crystals used for single x-ray crystal structures obtained previously for the aminal were slowly grown from water. [63] The previous success of crystal growth from water, the known water-solubility of all compounds involved, and the likelihood that such reactions could have taken place concomitant with prebiotic environments, therefore meant that performing the crystallisations from water was the obvious choice. Moreover, from a purely practical point of view, solution chemistry was easier and more expedient for screening the original additives as a starting point, before optimising the conditions.

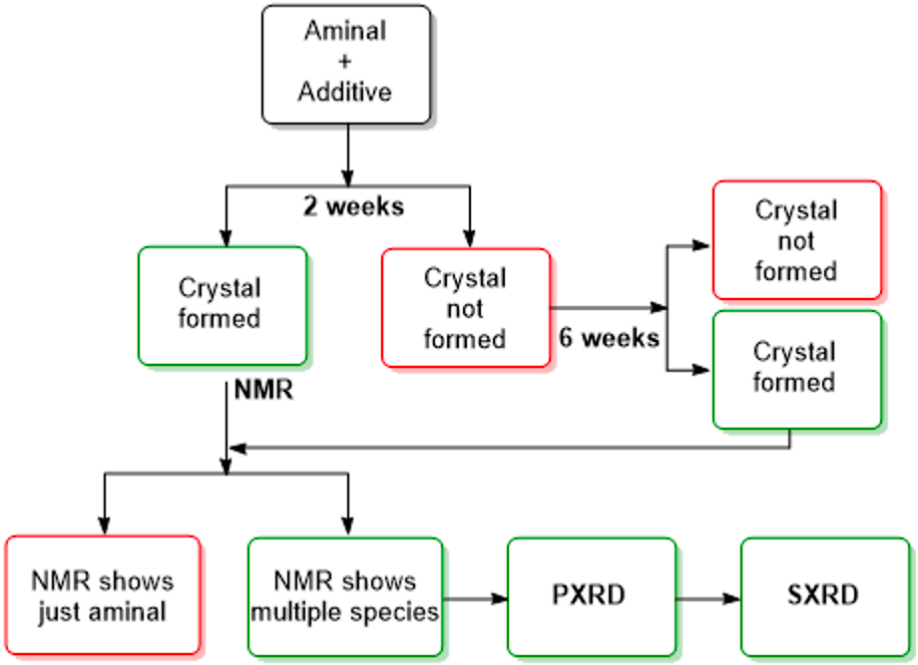

Figure 98: Flow chart illustrating the method used to analyse the co-crystallisation screening. Red boxes indicate negative results, green boxes indicate positive results in which the appearance of cocrystals is possible.

The workflow for selecting the method of analysis following crystal formation is shown in Figure 98. This procedure starts with the crystallisation taking place over a period of 2 weeks. If crystals were not formed the crystallisation screen was left for a further 4 weeks, or indefinitely if no still no crystallisation was found after that time. If crystals were seen to have formed after 2 or 6 weeks, they were collected and washed with ice cold water (0 °C), and a

small amount analysed by ^{1}H NMR in $CDCl_3$. If the NMR analysis indicated there was just aminal present in the NMR, the experiment was deemed to not have incorporated an additive into the crystal structure. However, if there were multiple species in the NMR that would indicate that co-crystallisation may have occurred: a positive result. If that was the case, the solid would be taken for PXRD analysis to confirm whether the additive was incorporated into the crystal structure of the aminal. If that was seen to be the case then a suitable crystal would be analysed by SXRD to obtain the crystal structure of the newly-obtained compound, and hence be able to investigate the interactions therein. The reason for using NMR analysis as a first step of analysis meant it was not necessary to have to perform dozens of PXRD experiments if no co-crystallisation had occurred – thus saving much time and resource.

4.4 Results and Discussion

Initially the reaction was explored without the additive present. Glyceraldehyde (0.5 M) was added with 2-aminothiazole (**23**, 1 M) in phosphate buffer (1 M, pH 7) and stirred at room temperature for 24 h. First the 2-aminothiazole (**23**) had to be recrystallised as when it was received from the supplier it was a dark brown solid. However, through recrystallisation using petroleum ether (40-60%) it is possible to gain a white crystalline solid which was used to produce visually superior crystals. It became apparent that 2-aminothiazole (**23**) has poor solubility in water at pH 7 and so the reaction mixture must first be made acidic and the glyceraldehyde (**14**) added. Finally, the solution was neutralised by addition of NaOH (4 M). The yield is drastically affected by moving away from neutral pH and the reaction would not produce enough aminal to investigate the crystallisation therefore this step was crucial. It was further confirmed that using phosphate buffer (1 M, pH 7) increased the yield significantly (83%) rather than using water (pH 7) (65%). The crystals were separated from the supernatant and then washed with ice cold water (0 °C) to remove any of the remaining supernatant liquid.

For the purpose of this investigation into the co-crystallisation of the glyceraldehyde aminal (**25**) with additives, it isn't necessary to perform the crystallisation from the reaction mixture in one step. Therefore, the aminal (**25**) was pre-formed on a large scale (5 g) and isolated separately to the crystallisation experiments being performed. The benefits of this are to overcome the yield challenges and to reduce the amount of waste that would be generated by inefficient synthesis and the possibility an impure mixture hinders the crystallisation. The crystallisation experiments were then set up in a falcon tube containing the aminal at the required concentration in water or phosphate buffer as specified. The pH was reduced until the aminal fully dissolved (between pH 3 and pH 4), the additive was added directly, and the pH was raised back to 7 and the solution was left for a week to allow crystallisation. The crystals were collected, washed and then dissolved in deuterated chloroform for analysis by ^{1}H NMR to allow quantification of the ratio of additive and aminal (**25**) within the crystals.

4.4.1 Aminal and Amino Acids

The first group of additives that were investigated was amino acids. Based on Blackmond's work, we believed that their H-bond donor/acceptor properties as well as the potential amplification demonstrated in the literature, make them attractive candidates from crystal engineering of the aminal. Moreover, their prebiotic availability and the potential that they may have existed with a measurable *ee* already (as seen on various aforementioned meteorites)[25], and thus that they could potentially confer that stereochemistry to the crystals formed.

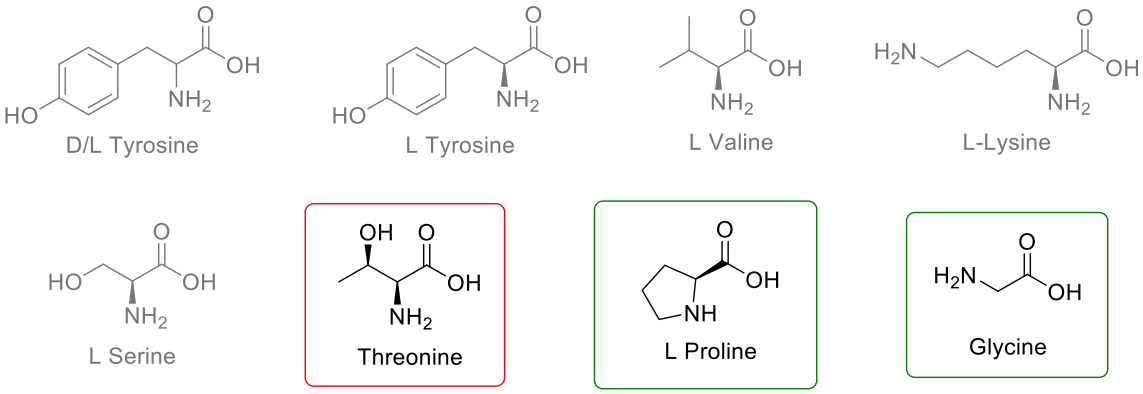

Figure 99: Amino acid additives chosen. Greyed out: issue with solubility. Red: Dissolved, however not formed crystals. Green: Formed crystals, however both components were not observed in the NMR.

The amino acids chosen are shown in Figure 99. Of these, rac-tyrosine, L-tyrosine, L-valine, L-lysine, and L-serine would not dissolve in the reaction mixture which precluded them from investigation. Threonine would dissolve, but no crystals were formed after2 years. The mixture with L-proline (0.25 and 0.5 M) did form crystals from a 1:1 mixture (aminal: additive) in water and in phosphate buffer (1 M, pH 7). It did not form crystals when mixed in a 1:2 ratio (aminal: additive). Analysis by ^{1}H NMR showed the presence of only aminal in the crystals with no proline detected. The mixture with glycine (0.25 and 0.5 M) also formed crystals from a 1:1 mixture (aminal: additive) in water and phosphate in buffer (1 M, pH 7). Likewise, it did not form any crystals when mixed in a 1:2 ratio (aminal: additive). Again, the crystals were isolated and analysed by ^{1}H NMR, showing no presence of glycine in the spectrum.

4.4.2 Aminal and Mono-carboxylic Acids

The next group of additives to be investigated was mono-carboxylic acids. As shown, they have a tendency to form multi-dimensional structures with 2-aminothiazole (**23**) in crystals as both the acid and the 2-aminothiaolium-carboxylate complex (see Figure 95). The acids chosen are shown below (Figure 100).

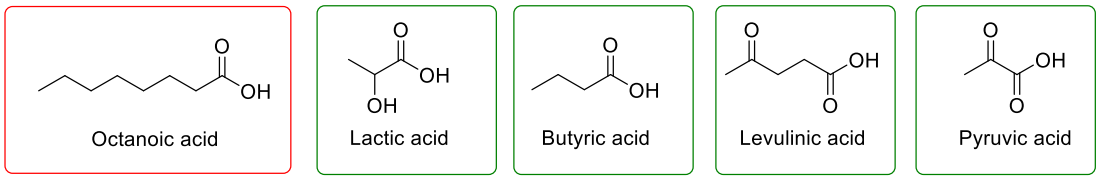

Figure 100: Mono-carboxylic acids chosen for screening. Red: The additive dissolved, however no crystals were formed. Green: Additive dissolved, crystals were observed, however the additive was not observed in the NMR.

Of the carboxylic acids chosen, octanoic acid (0.25 M, 0.5 M and 1 M) failed to produce any crystals for mixtures in water with ratios of 1:1 and 1:2 (aminal: additive). A mixture of lactic acid (1 M) in water or phosphate buffer (1 M, pH 7) at ratio of 1:1 formed crystals after two weeks which were isolated. Analysis by ^{1}H NMR showed only presence of aminal in the dissolved crystals, no lactic acid was seen in the spectrum. The separate mixtures of butyric acid (0.5 M and 1 M) in water, levulinic acid (0.5 M and 1 M) in water, and pyruvic acid (0.5 M and 1 M) in water, all in a ratio of 1:1 with the aminal, produced crystals after 2 weeks. Again, these were isolated and analysed by ^{1}H NMR, but none were present in their respective crystals' spectra which showed only presence of aminal. When these carboxylic acids were mixed in a 1:2 ratio (aminal: aditive) would not dissolve sufficiently to continue.

4.4.3 Aminal and Dicarboxylic Acids

Next, we investigated the propensity of glyceraldehyde aminal (**25**) to co-crystallise with seven readily available carboxylic acids (Figure 101).

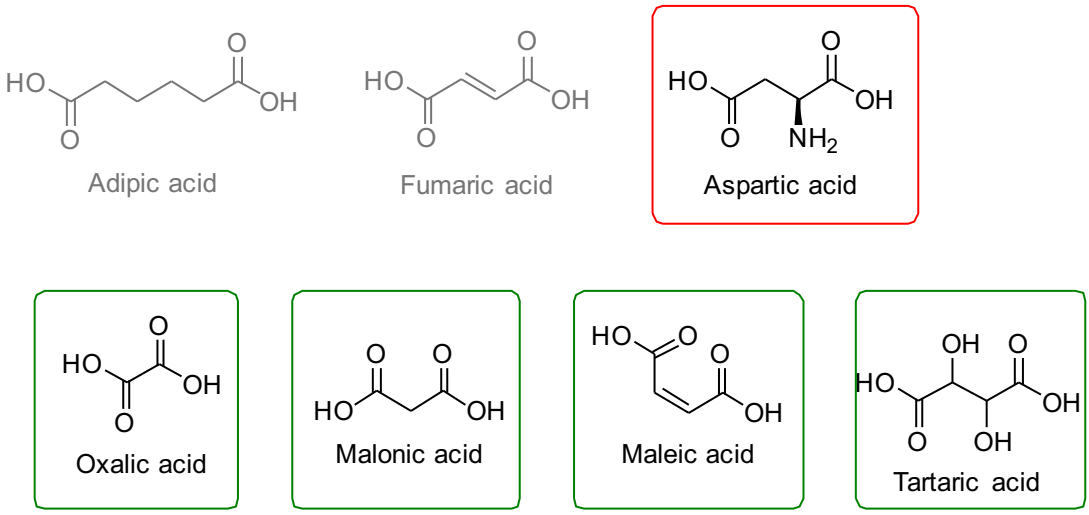

*Figure 101: Di-carboxylic acids chosen for screening. Grey: Additive struggled dissolving. Red: The additive dissolved, however no crystals were formed. Green: Additive dissolved, crystals were observed, however the additive not observed in the NMR. *Oxalic acid is not possible to be observed by NMR.*

Of these, adipic acid and fumaric acid failed to dissolve sufficiently from 0.25 M down to 0.1 M. These were excluded from further investigation for this reason. Aspartic acid (0.5 M) more readily dissolved in water (but not in phosphate buffer solution (1 M, pH 7) and would not form crystals after an indefinite period of time.

The mixture of oxalic acid (1 M) in a ratio of 1:1 and 1:2 (aminal: additive) in water produced crystals after 2 weeks which were isolated and analysed by ^{1}H NMR. However, oxalic acid lacks a detectable proton in ^{1}H NMR, so this result is not conclusive and in the future IR should be taken to confirm. The mixture of malonic acid (1 M) in a ratio of 1:1 and 1:2 (aminal: additive) in water produced crystals, again ^{1}H NMR analysis of which did not show presence of the additive. Mixture of maleic acid (1 M) in phosphate buffer (1 M, pH 7) in a ratio of 1:1 produced crystals after 6 weeks which did not contain additive, as shown by ^{1}H NMR. The equivalent crystallisation did not proceed from water. The mixture of tartaric acid (1 M) in water and also in phosphate buffer (1 M, pH7) produced crystals from a 1:1 ratio after 2 weeks. No tartaric acid was detected in the NMR of those crystals.

4.4.4 Aminal and Phenols

The aforementioned acids that were screened have a low pKa and are therefore relatively strong acids that would affect the pH of the solution. Due to the pH-sensitivity of the aminal reaction, the use of a weaker acids was considered, e.g. phenol (pKa = 10). Following initial investigations into each of these candidate additives (amino acids, carboxylic acids and dicarboxylic acids), we expanded the scope beyond the commonly-accepted prebiotic feedstock to test whether phenol might work due to its solubility in water and acidic proton that may become involved in H-bonding, and the possibility that it may pi-stack with the aminothiazole ring in the crystal packing.

It was found that phenol (0.5 M and 1 M) in a 1:1 and 1:2 ratio (aminal: additive) in water produced crystals after 2 weeks. These were isolated and analysed by ^{1}H NMR and the presence of phenol along with the aminal was detected in the spectrum in a ratio of 1:1 (Figure 102). Additional unreacted 2-aminothiazole (**23**) was also observed.

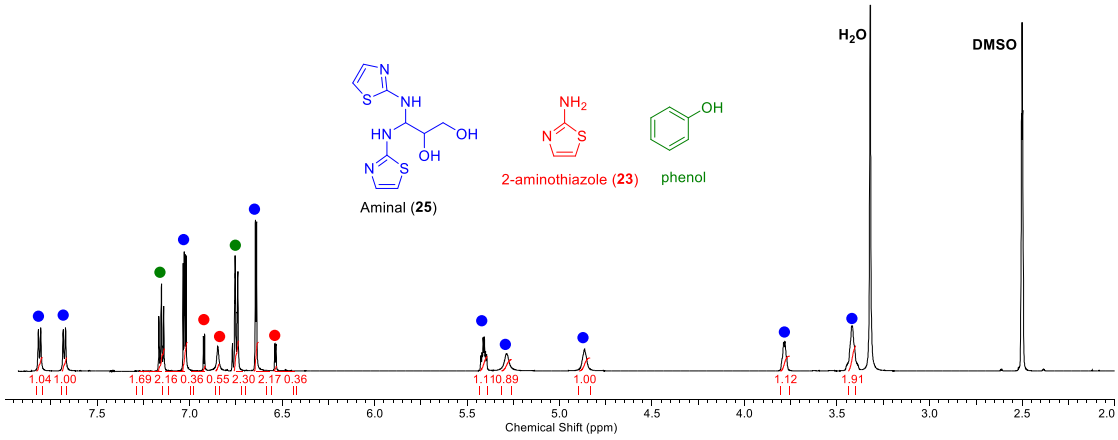

*Figure 102: ^{1}H NMR of the result of the co-crystallisation experiment of aminal (**25**, 1 M) with phenol (1M) in water. Illustrating the aminal (**25**, blue), phenol (green) and un-reacted 2-aminothaizole (**23**,red).*

This encouraging result meant that next we analysed the crystals by PXRD. Unfortunately, this showed that no phenol had been incorporated into a new aminal (**25**) crystal as the PXRD showed the aminal crystal in the original state (Figure 103). It appears that phenol and the aminal (**25**) had simply crystallised out independently from solution but no co-crystals were formed.

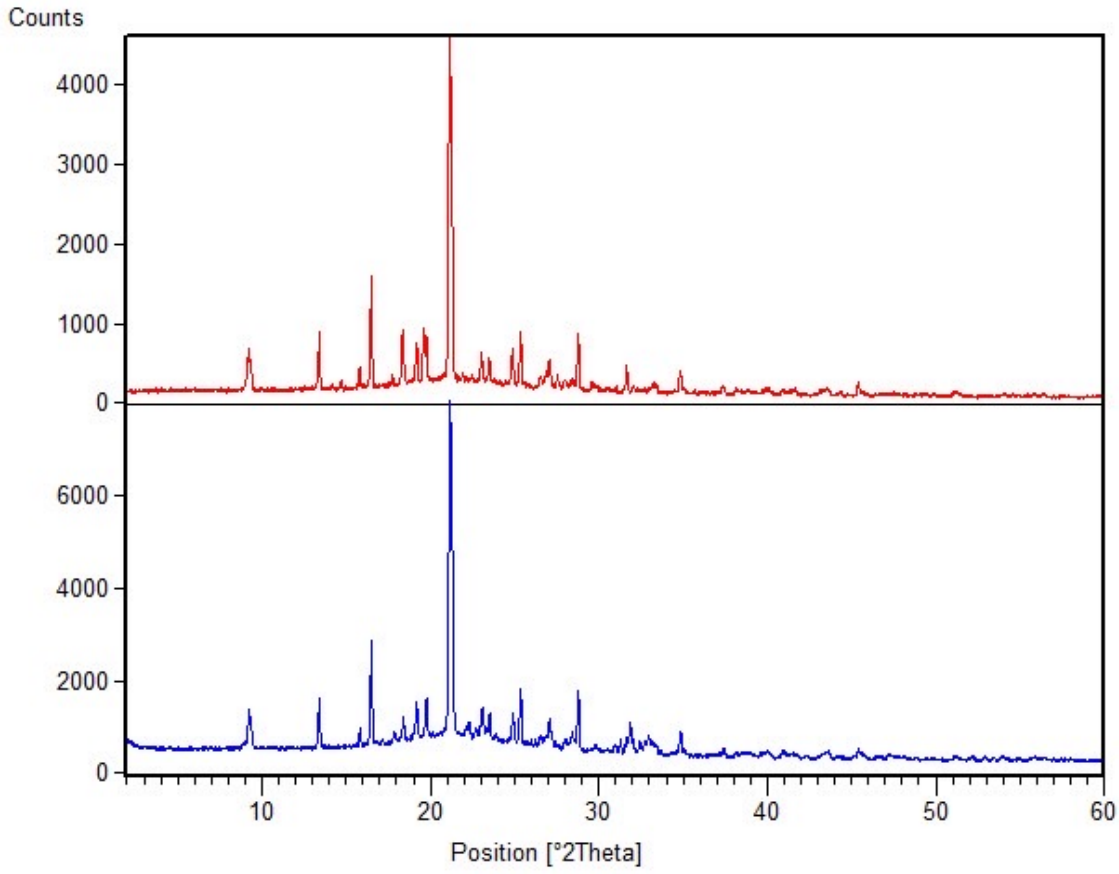

*Figure 103: PXRD (blue) of aminal (**25**), PXRD (red) of the crystals obtained from the co-crystallisation experiment of aminal (**25**) and phenol showing that the crystals are the same as the starting material.*

Based on these results, it would appear that the presence of the additive actually solubilises the aminal, inhibiting the crystallisation or preventing it from crystallising at all. This is not entirely surprising due to the H-bonding nature of the additive/aminal, and the naturally low solubility of the aminal, so if the additive is more soluble in water than the aminal it may form a complex in solution which is more soluble than the aminal on its own. Seemingly, by introducing a small polar molecule to the mixture, the tendency is for the aminal to remain in solution rather than precipitate out. This is a different result to that reported for co-crystallisations of simple 2-aminothiazole (**23**), but likewise the molecule in question is much different – containing two aminothiazole rings and an alkyl chain which we would naturally expect to reduce the polarity of the molecule and thus reduce its solubility in water.

Having achieved this result, it was thought that more phenol-based compounds should be investigated (Figure 104). 2,6-dimethylphenol and 4-chlorophenol were unable to dissolve at the concentrations required for the crystallisation, neither in water nor phosphate buffer. However, 2 methoxyphenol (0.5 and 1 M) dissolved in water and crystals formed after 2 weeks. These were analysed by ^{1}H NMR, however illustrated only the aminal within the solid.

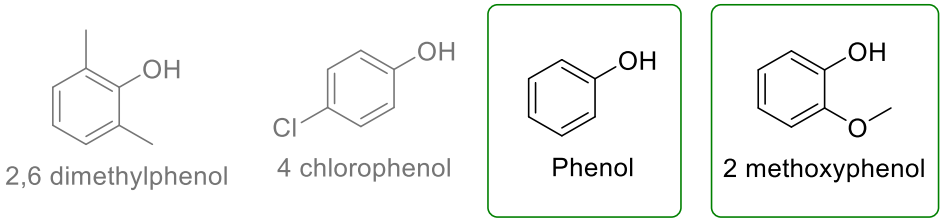

Figure 104: Phenol based compounds chosen for co-crystallisation with the aminal. Grey: Unable to dissolve. Green: Produced crystals.

4.4.5 Aminal, Aromatics and Pyridines

Broadening the candidate molecule scope further, it was speculated that using other pyridine compounds and other aromatic compounds may lead to co-crystals forming (Figure 105). The chosen 3,4 dimethoxyphenylacetone, atrolactic acid, benzoic acid, 2-hydroxypyridine-N-oxide and 4-hydroxypyridine all showed limited solubility in water and so no further crystallisations experiments could be investigated with these compounds.

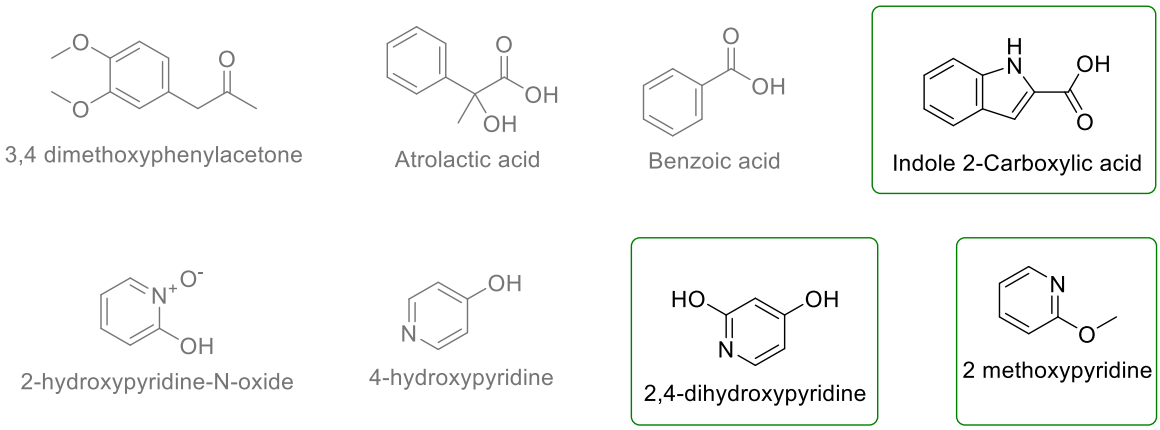

Figure 105: Aromatic and pyridine-based compounds chosen for co-crystallisation with the aminal. Grey: Unable to dissolve. Green: Produced crystals but no co-crystal detected within the ^{1}H NMR.

It was found that indole 2-carboxylic acid (1 M) in water in a ratio of 1:1 (aminal: additive) produce crystals after 2 weeks, however even after 6 weeks, a ratio of 1:2 (aminal: additive) did not. The 2,4-dihydroxypyridine (0.5 and 1 M) and 2 methoxypyridine (0.5 and 1 M) in water in a 1:1 ratio (aminal: additive) also both produced crystals after 2 weeks. However, when the ^{1}H NMR were analysed for these three compounds, only the aminal was present in the spectra.

Nonetheless, it is very encouraging to have found additives that allows the aminal to crystallise after screening such a wide selection with little other success. It is hoped that this first step

forward will open the door to find a likely candidate additive that, via co-crystallisation, will allow amplification of the aminal to occur, and thus grant access to enantiopure aminooxazolines, and beyond to the corresponding nucleosides.

Moving on, due to the sensitivity of the aminal reaction, it is also suspected that other aminals that form under the same conditions could potentially induce or assist the co-crystallisation of the key glyceraldehyde aminal to result in the homochirality that is required.

4.5 Co-crystallisation of Aminals

Another way to approach co-crystallisation for the purposes of enantio-enrichment was to investigate other prebiotically-available aminals. D-glyceraldehyde (**25**) is the precursor to the natural sugars, and L-lactaldehyde is the precursor to the amino acid (L-threonine). Therefore, we questioned if there is a way to use co-crystallisation of their aminal-derivatives as a method to join the sugar synthesis stream with the amino acid synthesis stream. As both groups of compounds must have arisen for life to flourish, perhaps they had a role to play in each other's homochirality by way of co-crystallisation.

Using aminal formation, rac-lactaldehyde (**rac-43**) and D-glyceraldehyde (**D-14**) were reacted with 2-aminothiazole (**24**) to give the corresponding aminals (Scheme 39). It was proposed that the L-lactaldehyde aminal (**L-44**) might co-crystallise with the D-glyceraldehyde aminal (**D-25**) to form an L:D co-crystal. The remaining unreacted D-lactaldehyde aminal (**D-44**) in solution could then be washed away from the co-crystal. This would successfully achieve kinetic resolution of lactaldehyde (**43**), as it preferentially isolates one enantiomer out of the racemic mixture (Scheme 39). The L:D co-crystal could be reacted with cyanide to gain direct

access to the resultant cyanohydrins (**45** and **46**). The cyanohydrins can then undergo a Strecker reaction in the presence of ammonia. The D-glyceraldehyde cyanohydrin (**46**) would be unable to achieve this step due to an intermolecular reaction, which leads to hydrolysis.[51] By producing L-threonine specifically, this demonstrates the viability of aminal formation as a candidate for the origin of homochirality in amino acids.

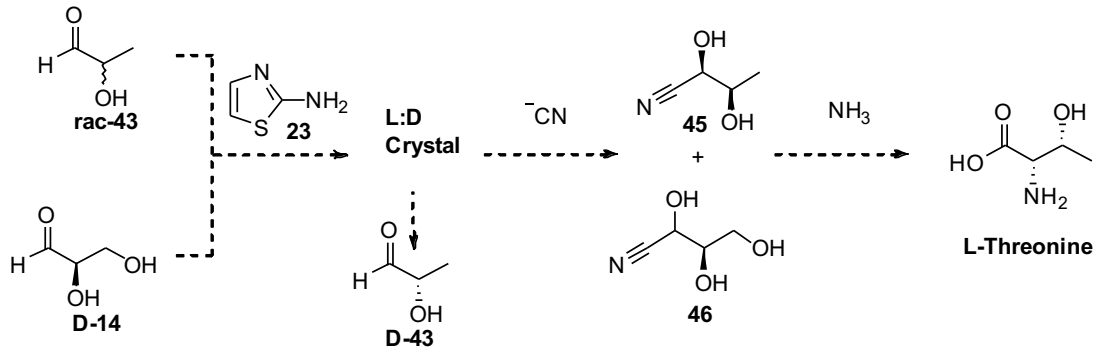

*Scheme 39: Proposed route from glyceraldehyde (**14**) and racemic lactaldehyde (**43**) to enantiopure amino acid (**L-Threonine**).*

We therefore pursued the aminal crystallisation of lactaldehyde (**43**) as required. Despite lactaldehyde's (**43**) diminutive molecular weight, it is prohibitively expensive to source (£91 mL^{-1}). Consequently, (rac-**43**) was prepared using the two-step route described in Scheme 40. Starting with a sodium borohydride reduction of pyruvic aldehyde dimethyl acetal (**47**), followed by acetal de-protection using DOWEX (H^+) affords the desired product (**rac-48**) in good yield (75%) without the need for further purification. Note: in order to avoid intermolecular aldol reactions upon concentration of (**rac-43**), the product was found to be best stored as a dilute (0.5 M) stock solution at 4 °C in water. Racemic-lactaldehyde (**rac-43**) was reacted with 2-aminothiazole (**23**) to form the racemic lactaldehyde aminal (**rac-44**) in good yield (75%).

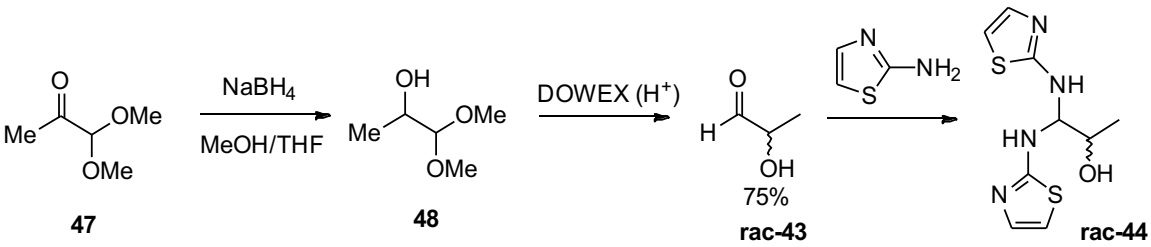

*Scheme 40: Synthesising racemic lactaldehyde aminal (**rac-44**)*

In order to test the viability of the hypothesis outlined above, the synthesis was first performed on racemic starting materials. Racemic lactaldehyde aminal (**rac-44**) was incubated with cyanide to produce diastereoisomers of the lactaldehyde cyanohydrin (**45**), and the remaining 2-aminothiazole (**23**). It has already been noted that 2-aminothiazole (**23**) does not participate in this formation.[63] This proved to be an efficient and clean synthesis that goes to completion within 24 hours (Figure 106).

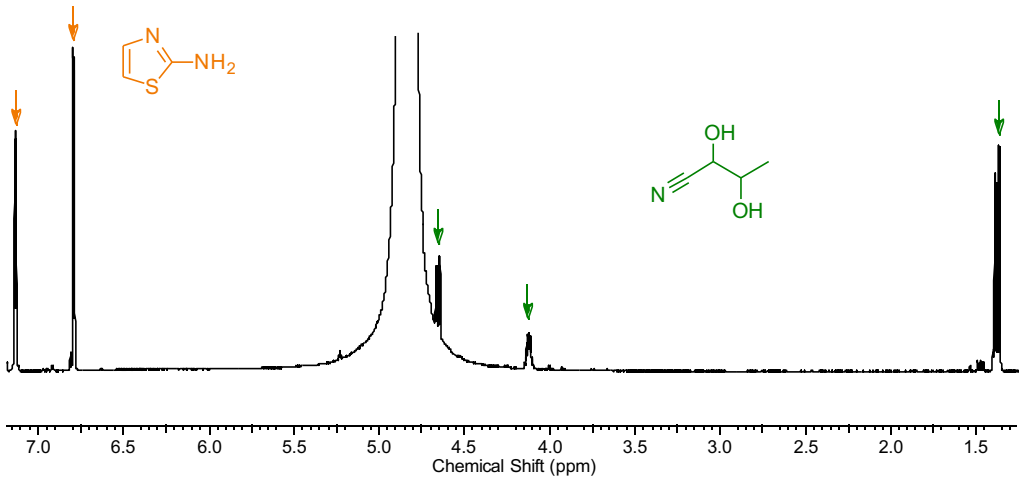

*Figure 106: Crude ^{1}H NMR of the lactaldehyde aminal (**44**) reaction with potassium cyanide to form the cyanohydrin (**45**) and 2-aminothiazole (**23**).*

This experiment was repeated using glyceraldehyde aminal (**25**) and cyanide, forming the cyanohydrin (**46**) with complete conversion (observed by ^{1}H NMR). Following addition of ammonia, the glyceraldehyde cyanohydrin (**46**) undergoes quantitative hydrolysis of the amidine group (**49**) to give the amide (**50**), and subsequently the target compound acid (**51**) (Scheme 41).[63] This demonstrates that this is a potential route to obtain L-threonine, provided a suitable co-crystal can be acquired.

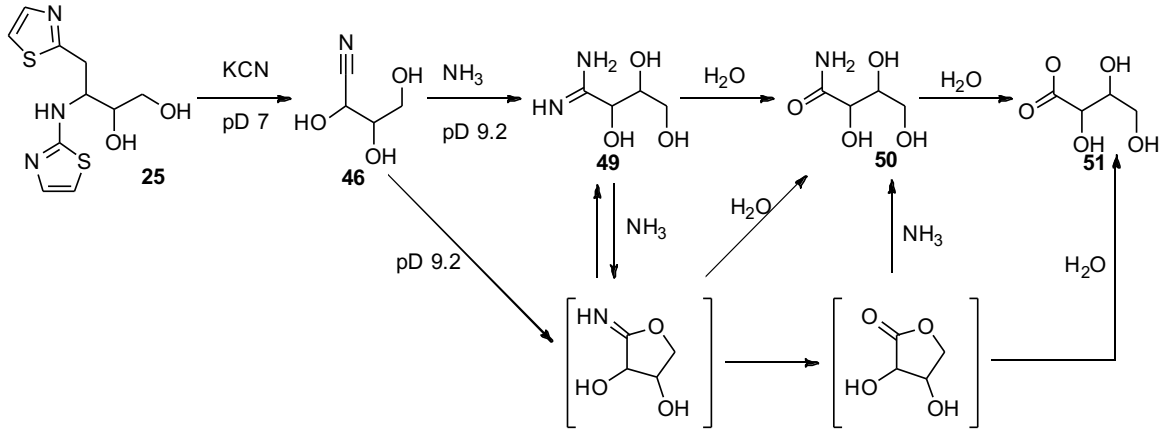

*Scheme 41: Decomposition of glyceraldehyde cyanohydrin (**46**) via hydrolysis (redrawn)*[51]

With regards to performing the synthesis on homochiral lactaldehyde (**43**), the L-lactaldehyde (**L-43**) itself was first prepared by a three-step route following literature procedure (Scheme 42).[252] The protected ester (**53**) was synthesised good yield (74%) by reaction with TBSCl. Reduction of the ester group to the corresponding aldehyde (**54**) was performed using diisobutylaluminium hydride (DIBAL) as the reducing agent. Following the failed reactions using DIBAL in hexane, which is the reducing agent stipulated in the literature procedure, alternative sources of DIBAL were investigated (Table 11). Following repeated iterations of each of the entries, it was determined that the reaction's extreme sensitivity to water was the most likely source of the problem – this was overcome by significantly increasing the scale of the reaction and using freshly-distilled ether as the solvent. After performing this reaction on

the literature precedent of 7 g scale using fresh diethyl ether distilled from sodium metal, the product (**L-43**) was eventually isolated in good yield (75%).

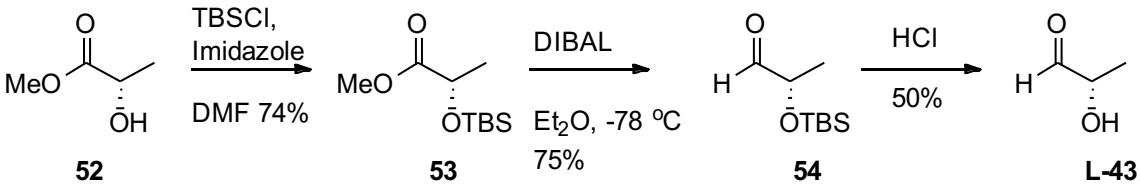

*Scheme 42: Synthetic route to chiral lactaldehyde (**L-43**)*[252]

*Table 11: Reduction methods used to gain access to the protected aldehyde (**54**)*

Entry	Scale / g	Reducing Agent	Solvent	Temperature /°C	Yield / %
1	0.1	$LiAlH_4$ (THF)	THF	RT	0 %
2	0.1	$LiAlH_4$ (THF)	THF	0	0 %
3	0.5	DIBAL (hexane)	DCM	–78	0 %
4	0.5	DIBAL (hexane)	DCM	–98	0 %
5	0.5	DIBAL (hexane)	Toluene	–78	0 %
6	1	DIBAL (THF)	Et_2O	–78	0 %
7	1	DIBAL (THF)	Et_2O	–98	0 %
8	1	DIBAL	Et_2O	–98	0 %
9	7	DIBAL	Et_2O	–78	75%

There is not an abundance of reliable literature precedent for this specific TBS de-protection step. As such, conditions were screened for optimisation purposes. It was found that, whilst the starting material (**54**) was soluble in organic solvents, the product (**L-43**) was not, necessitating the use of a biphasic reaction.

*Table 12: Routes to deprotect lactaldehyde (**L-43**)*

Entry	Acid	Solvent System	Time / h	Result
1	HCl (1 M)	HCl (aq)	2	16% yield
2	HCl (2 M)	HCl (aq)	2	7% yield
3	Methanolic HCl	HCl/ MeOH	4	Complete decomposition
4	AcOH	H_2O/ THF (50:50)	4	0% yield
5	50% aq HF	MeCN	2	10% yield
6	HCl (to pH 3)	D_2O/ Acetonitrile (50:50)	4	Trace
7	HCl (to pH 3 at 60 °C)	D_2O/ Acetonitrile (50:50)	4	50% yield

The deprotection was first attempted with HCl (1 and 2 M) (Table 2). Lowering the pH using HCl was found to be a clean route to deprotection, however the yield was only 16%. Methanolic HCl was then used in order to dissolve the starting material (**L-54**) and the product (**L-43**), however this failed to result in any deprotection. Finally, a multi-solvent system consisting of D_2O/ Acetonitrile (50:50) was used, and the pH adjusted to 3 by dropwise addition of HCl 3 M. The progress was monitored by TLC and at room temperature the reaction's progress found to be very sluggish. However, heating at 60 °C for 4 hours gave the desired product (**L-43**) in 50% yield. The target aminal **L-44** was formed cleanly by reaction of L-lactaldehyde (**L-43**) with 2-aminothiazole (**23**) to produce **L-44** in good yield (75%).

A slurry of L-lactaldehyde aminal (**L-44**) and D-glyceraldehyde aminal (**D-25**) in water was stirred left for 2 weeks to form crystals. The crystals were isolated and washed and sent for PXRD analysis. The results of these are being waited-on at the time of writing.

The conditions for lactaldehyde aminal (**44**) and glyceraldehyde aminal (**25**) to enable co-crystallisation are still being investigated within the group and have led to the exploration of the use of grinding experiments to build upon the findings reported here with the hope of achieving homochirality in these two crucial prebiotic intermediates.

4.6 Aminal Synthesis using Proline Derivatives

Another route to accessing enantiomeric precursors of ribo-nucleotides could be by establishing stereospecificity early in the synthetic route described by Powner *et al.*, which is discussed in this section.[52]

Phosphates, phosphonic acids and phosphonic acids have been detected in carbonaceous meteorites and would have been available in prebiotic environments.[82] It is, therefore, reasonable to expect that these species and their analogues /derivatives would have a key role to play in the development of RNA in the RNA World.

Considering the role of phosphate within the context of this piece of work: it has been demonstrated that using phosphate buffer increases the rate of aminal formation, as it is able to act as a good general acid/base catalyst.[63] Therefore, exploring different phosphate derivatives that drive the aminal formation is worth understanding, particularly if the phosphate derivatives could influence the crystallisation. Further, chirality can potentially be introduced through a chiral phosphate derivative transferring its stereochemistry to the products. Furthermore, as phosphonic acids maintain close pK_a-relationship to phosphoric acid, which is known to be effective catalysts for the conversion of DHA (**21**) to glyceraldehyde

(**14**)(which is the precursor to glyceraldehyde aminal (**25**)), we suspected them to be equally efficient catalysts in this department.[63]

Two simple phosphate derivatives, methyl phosphonic acid (**55**) and ethyl phosphonic acid (**56**), were selected to investigate the role of the buffer in this reaction, and 1-amino-1-phenylmethyl phosphonic acid (**56**) to establish the importance of steric hindrance on the yield of the reaction (Scheme 43).

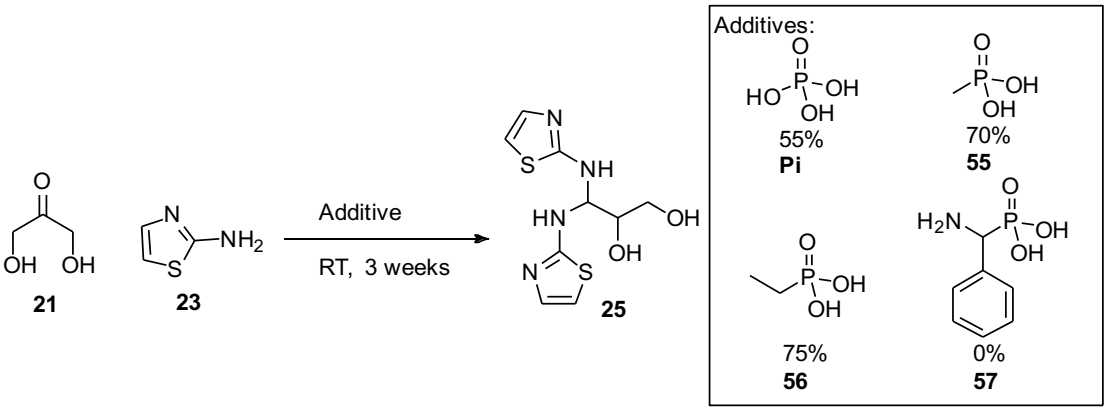

*Scheme 43: 1 M DHA (**21**),2 M 2-aminothiazole (**23**),1M of additives; phosphate buffer (**Pi**), methyl-phosphonic acid (**55**), ethyl-phosphonic acid (**56**),1 amino-1-phenylmethyl phosphonic acid (**57**) to form the aminal (**25**).*

A mixture of DHA (**21**, 1 M) and 2-aminothiazole (**23**, 2 M) in phosphate buffer (P_i, pH 7) was left for 3 weeks at room temperature, after which time, aminal (**25**) was determined to have formed in 55% yield. Next, the reaction was repeated using methyl phosphonic acid (**55**) in place of the buffer, producing the aminal in higher yield (70%). The phosphonic acid was observed to be an efficient proton shuffle in this reaction and capable of replacing the phosphate buffer. Using ethyl phosphonic acid (**56**) the aminal (**25**) yield was 75%, under comparable conditions. The reaction involving the highly sterically-hindered 1-amino-1-phenylmethyl phosphonic acid (**57**) gave no aminal product. The zwitterionic properties of 1-

amino-1-phenylmethyl phosphonic acid (**57**) may account for the low activity of this phosphate reducing the capability of the phosphonate as a general acid-base.

Following the success of the experiments involving methyl- and ethyl phosphonic acids, the use of chiral phosphate buffers was explored in order to establish whether chirality could be induced in aminal (**25**). The phosphate analogue of proline (**S-59**, **R-59**) (Figure 107) was chosen because of the pivotal role proline has played in the development of organocatalysis.[253] Moreover, L-proline (**L-58**) is a natural proteinogenic amino acid that is believed to be prebiotic and a small but not insignificant L-enantiomeric excess of such amino acids have been found in carbonaceous meteorites, which could indicate that this may have been the origin of biological homochirality on Earth.[254] These small enantiomeric excesses could provide chiral preference (or imbalance) that could have led to chiral amplification and ultimately homochiral biopolymers, if these carbonaceous chondrites are representative of the materials that would have been present on the early Earth.[40,65]

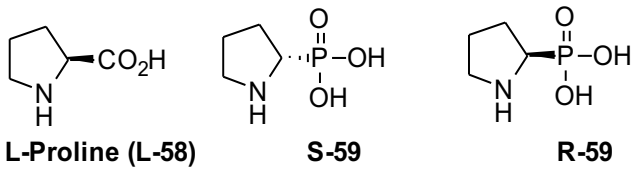

L-Proline (L-58) **S-59** **R-59**

Figure 107: Proline and the proline phosphonic acid-based derivatives

It was also particularly encouraging to explore proline phosphate derivatives (**59**) thanks to Breslow's work that described how chiral amino acids (and in particular proline (**58**)) can influence the stereochemistry in the product of the aldol reaction between glycolaldehyde (**13**) and formaldehyde (**32**) leading to glyceraldehyde (**14**).[100,255] Blackmond's group exploited

proline (**58**) to confer a chiral imbalance in Powner's prebiotic nucleotide synthesis from racemic glyceraldehyde (**14**) and 2-aminooxazole (**15**).[255] They demonstrated a notable enantiomeric excess when proteinogenic L-amino acids were present in the reaction and particularly, L-proline (**L-58**) led to an enantiomeric excess of 80% ee favouring the D-nucleoside precursor.[255] The chiral transfer from proline (**58**) to D-nucleoside precursor can be explained by a non-catalytic kinetic resolution model, where a multicomponent by-product of this reaction acts to selectively sequester the natural amino acid and the unnatural sugar. This means that the D-glyceraldehyde (**D-14**) is stereoselectively incorporated into the corresponding aminooxazoline (**D-AO**). By the same reasoning, then, we aimed use a similar strategy when forming the corresponding aminals stereoselectively.

The first step in the preparation of the proline-based phosphonate proceeded smoothly (Scheme 44). This method was previously demonstrated by Kaboudin to access α-aminophosphonates by a decarboxylative coupling of amino acids with aldehydes and H-dialkylphosphites.[256]

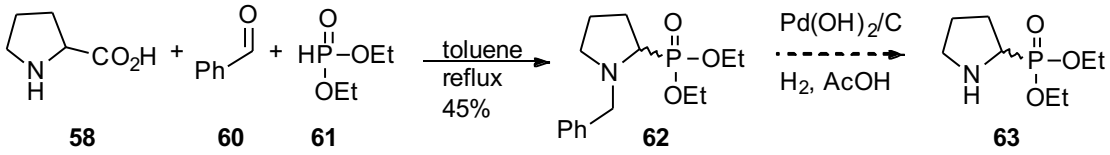

Scheme 44:Synthesis towards preparing the proline phosphate derivative.

A mixture of proline (**58**), benzaldehyde (**60**) and diethyl phosphite (**61**) underwent a one-pot decarboxylation-phosphonylation reaction in refluxing toluene under an argon atmosphere. The reaction was monitored by ^{1}H NMR spectroscopy. After 3 hours, the ^{31}P NMR spectra indicated a mixture of products had been formed – the predominance of resonances at 20

ppm indicated significant quantities of intermediate products (Figure 108). However, after 18 hours, 6 hours longer than literature procedure a single peak in the ^{31}P NMR was observed the reaction was worked up and the desired product (**63**) isolated in 45% yield. Though further optimisation would likely improve this reaction, these studies were deemed to fall outside the scope of this project.

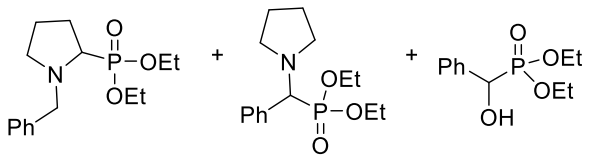

Figure 108: Likely intermediate by-products

Hydrogenative debenzylation of the product (**63**) was attempted using $Pd(OH)_2/C$, but was unsuccessful after multiple attempts. The most likely cause was that the catalyst had expired, and the reaction was re-attempted using new stock. This was still unsuccessful. Moving forward, racemic pyrolidine-2-phosphonate (**63**) would be reacted with the resolving agent affording diastereomeric amides (**64**) that can be separated and acidified to furnish the single enantiomeric product (**59**).

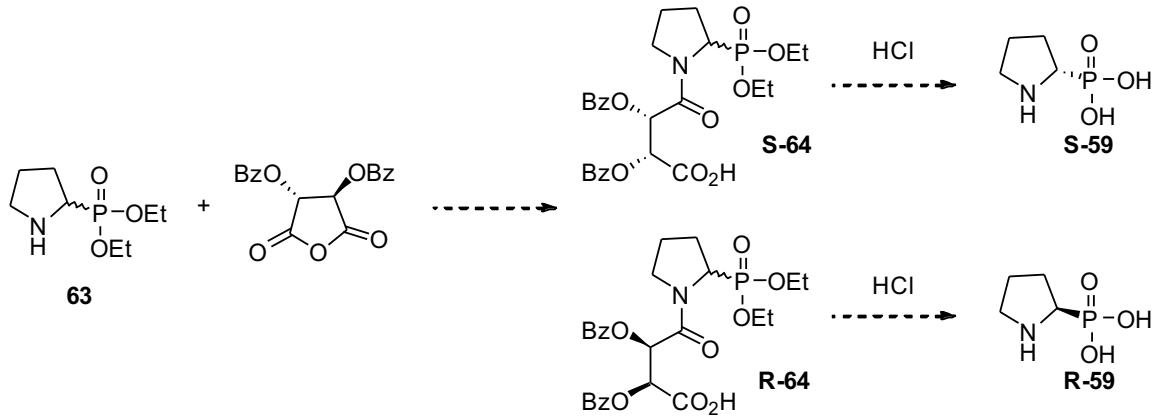

*Scheme 45: Synthesis of (**R-59**)- and (**S-59**)- pyrolidine-2-phosphonic acids*

The lack of success in the initial reaction steps precluded the synthesis of the proline phosphonate derivatives for use in the catalytic experiments. It is hoped that overcoming this synthetic challenge will eventually allow further investigation into the behaviour of these catalysts which still hold much promise.

5 Conclusion and Future Work

5.1 Chapter 1: Crystallisation Properties of Pentose Oxazoline Derivatives

During our investigations into prebiotic chemistry, we have built upon the previous work in the group which has identified prebiotically-plausible pathways to synthesise biological polymers (Scheme 46). The seminal synthetic routes presented in that previous work was missing the crucial piece of the jigsaw, which is and explanation as to how the homochirality of the polymers that we see on Earth today arose from and why.

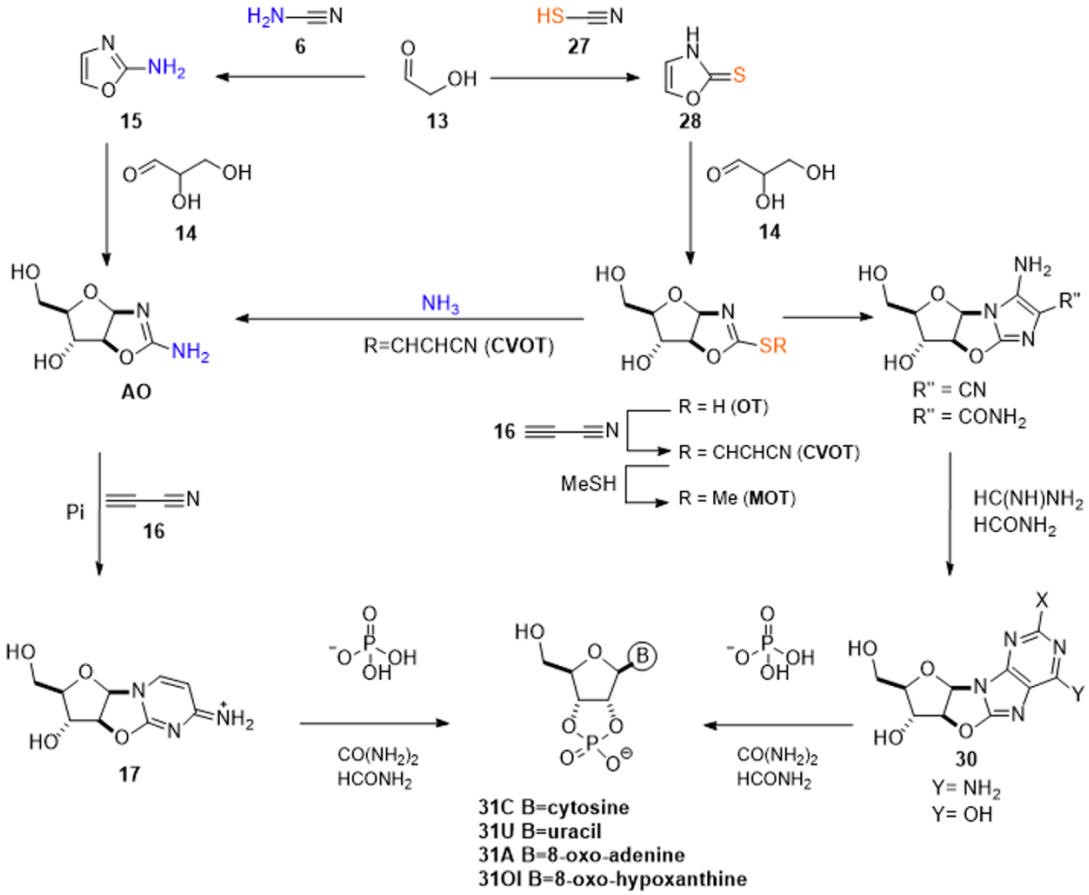

Scheme 46: Powner et al synthesis of ribonucleotides by a divergent synthesis from glycolaldehyde (13).

Initially, we investigated how the enantioenrichment of close-to-racemic mixtures of aminooxazoline (**AO**), oxazolidinone thione (**OT**) and oxazolidinone (**OX**) compounds *via* enantiomeric amplification in solution. Moreover, we showed that formation of conglomerate crystals was the root of this effect and illustrated that by collecting single x-ray crystal structures of all these structures.

On the basis that **RAO** was known to both form conglomerate crystals and exhibit enantioenrichment behaviour under prebiotic conditions, this work involved further investigation that established that such behaviour is also observed across the series (**RAO**, **AAO**, **XAO** and additionally to other prebiotically relevant compounds) and can be used to

obtain significantly enantioenriched these precursors (Figure 109). **RAO**, **AAO**, **XAO**, were all shown to form conglomerate crystals, as confirmed by SXRD. Scalemic mixtures were formed of these compounds and it was interesting to note that at 20% *ee*, **AAO** was amplified the greatest compared to all other compounds investigated, suggesting that only a small *ee* is required for substantial enantio-amplification to occur. This is significant in context of the emergence of homochirality, as this is the required diastereomer, so one could imagine that if **AAO** was able to be amplified in some way, it could lead to significant enantiomeric excess that would lead to homochirality in RNA. This, however, would only occur in >1M solution, therefore the viability of that occurrence should be considered.

With these positive results, oxazolidinone thiones (**OT**) were investigated. Extraordinarily, a novel conglomerate crystal was formed for the prebiotically-important **ROT**. Enantioenrichment for **ROT** is significant at 40% *ee*, where it shows the greatest enantiomeric amplification of all the compounds investigated, forming almost homochiral conglomerates. This is a remarkable result yet again indicating that a small amount of *ee* which could feasibly arise by symmetry breaking can be significantly amplified under the right conditions to produce homochirality. This however is achieved at even higher concentration (>3M). This is interesting in terms of a mixed pool of substrates, whereby in relation to the **AO**, the concentrations required for crystallisation is significantly higher for the **OT**.

Common side-products in many prebiotic reactions are oxazolidinones (**OX**). For **AOX** specifically, unreported conglomerate formation was noted. This was achieved in a water/ ethanol (1:1) solvent system. It is the only compound in this series for which conglomerate crystallisation was observed.

For those compounds which preferentially formed racemic crystals, enrichment in the supernatant liquid was observed. Therefore, regardless of how a compound tends to crystallise, enantioenrichment is possible through crystallisation as a purification method – this is important as we can therefore justify the homochirality in a greater number of derivatives.

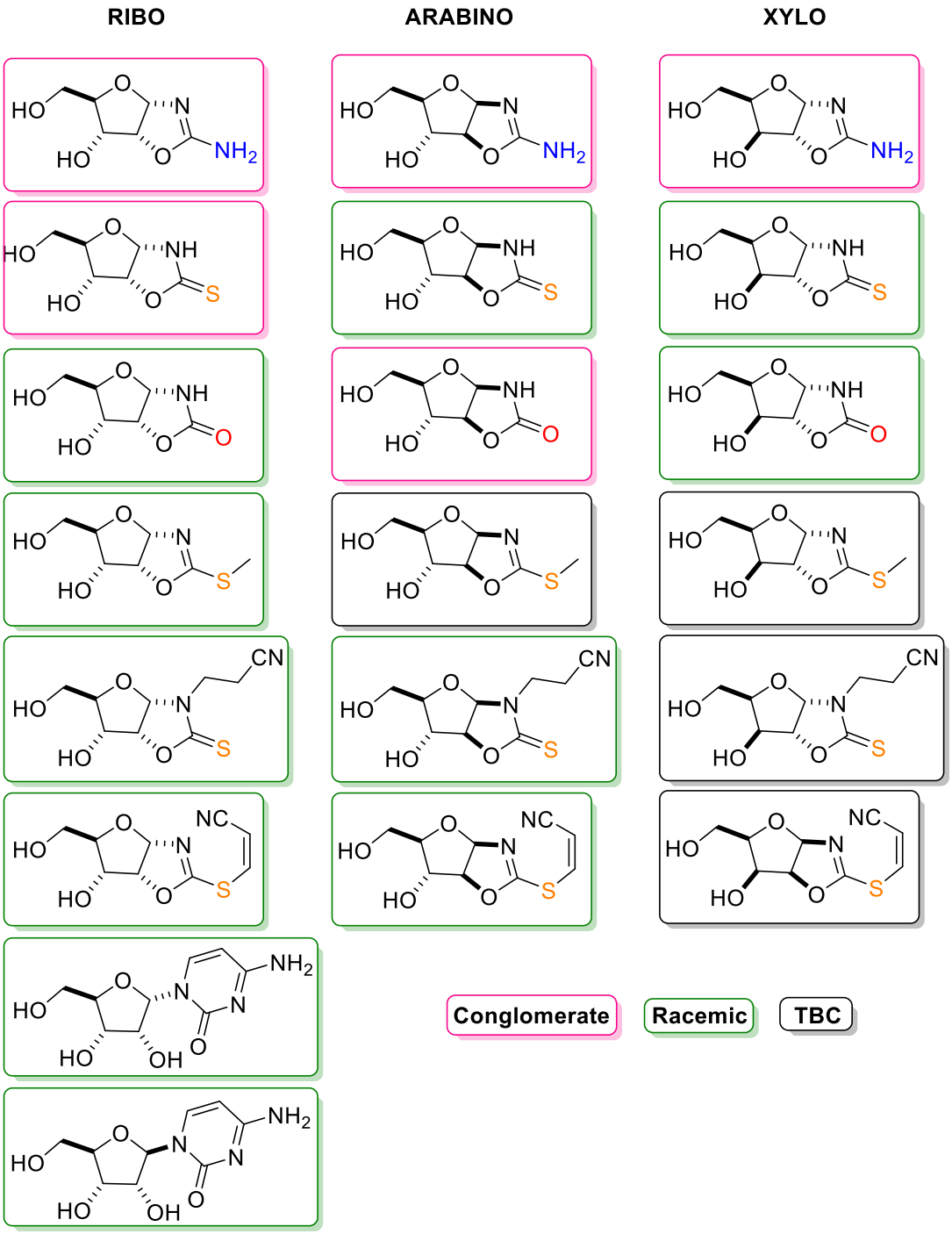

Figure 109: Summary of the crystal properties of the compounds studied in this work.

We also noted that compounds that are likely to form conglomerate crystals will do so rapidly in solutions of high enantiomeric excess relative to in close-to-racemic solutions where formation is much slower. Conversely, we also showed that the opposite is also true:

compounds which readily form racemic crystals will crystallise out rapidly from racemic solutions and crystallise significantly slower from solutions with moderate to high enantiomeric excesses. We discovered that we could use this insight as a useful guide for whether we have formed conglomerate or racemic crystals based on the *ee* of the mixture and the tendency of the molecule to form one or the other type of crystal.

Of course, in the prebiotic world, we would expect to find a complex mixture of these compounds in any one place. And so, to reinforce the prebiotic credentials of this methodology, competition experiments were carried which illustrated that the crystallisation occur in the same manner as they did previously (albeit at lower concentrations to accommodate the greater amount of material in solution). For example, a mixture of homochiral ROT with homochiral AOT still leads to the preferential formation of ROT as a conglomerate crystal where AOT remains entirely in solution. This therefore validates our method by which to purify these important compounds.

Following these positive results, other relevant intermediates (**MOT**, **CEOT**, **CVOT**, **a-ribo-42**, and **B-ribo-42**) were crystallised at -100, 0, +100% *ee* solutions in a variety of solvents to form racemic crystals. The crystal structure patterns for all of the above were obtained and elucidated showing many different H-bonding motifs and synthons. It is not yet clear what the underlying reason is for why some compounds form conglomerate crystals whilst others do not, nor if there is a single explanation. But due to the variety in structures formed, this opens a window into many more crystal structures that must be explored and there is a great deal more new knowledge to be gained towards understanding at a molecular level to produce such structures, which is extremely exciting.

The major hurdle for these investigations was the large amount of highly pure material required, therefore, repeated synthesis on a much larger scale would facilitate many more iterations of the experiments. This would enable us to try to understand how their crystallisation properties could be beneficial to design crystal engineering experiments and develop greater control over conglomerate formation and additionally enantiomeric amplification. We would also be able to perform more combinations of competition experiments to test the hypothesis that crystal engineering can grant access to homochirality. It is possible that through these experiments, we might find that preferential crystallisation of one compound will stimulate the crystallisation of another in conditions where it normally would remain in solution. That therefore would grant us enormous amounts of control over which compounds we choose to access.

This study would benefit from more sophisticated methods to use molecular descriptors and statistical methods which could allow the identification of chemical properties that contribute to conglomerate forming behaviour. These properties may relate to lattice energy calculations, densities, hydrogen bond donors/ acceptors or simple molecular properties such as shape, size and polarity. It is likely to be a combination of factors which ultimately influence the crystal structure preference and the initial behaviours found within this thesis will assist in the learning and understanding that can be gained from alternative methods.

5.2 Chapter 2: Crystal Engineering towards the Prebiotic Aminal

This work built upon another further route which accesses the aminooxazolines (**AO**) *via* crystallisation of aminals (Scheme 47). Glyceraldehyde aminal (**25**) has been noted to have

interesting crystallisation properties, where the aminal forms in a racemic manner solving many problems with the strict addition required for the previous synthesis (Scheme 47). It was hypothesised that in order to achieve homochirality in the nucleosides, enantiomeric excess could be introduced at the aminal stage of the synthesis using selective crystallisation of one enantiomer using additives, which could prove to be invaluable if homochirality could be introduced.

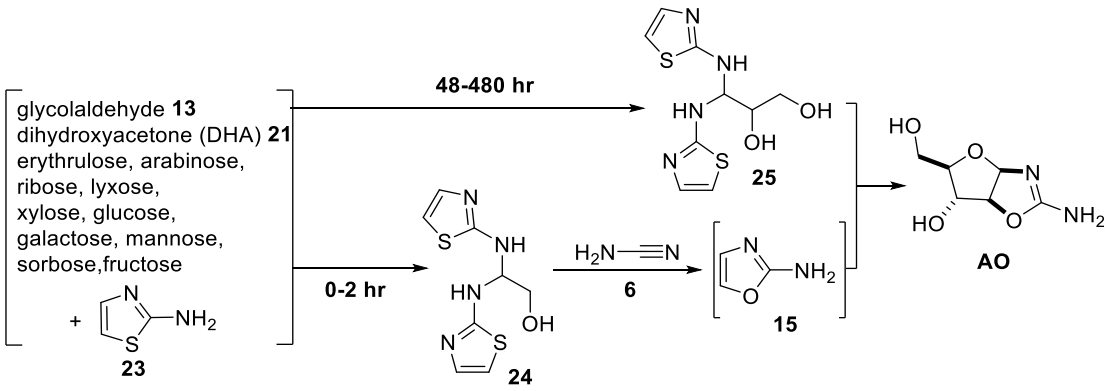

Scheme 47: Islam et al. synthesis of aminals from simple prebiotic starting materials.

To test this theory, co-crystallisation experiments with thirty-four different additives, in over a hundred sets of conditions of solution-based crystallisation, were performed. When crystallisation did occur, no incorporation of the additive into the aminal crystal lattice was observed. We believe this is due to the sensitive nature of the aminal formation. Resulting from these experiments, a collaboration is ongoing involving mechanochemistry rather than wet chemical techniques to try to force co-crystallisation through this alternative technique. Statistical analysis of cocrystal formation could additionally lead to a greater understanding of the observed relationships between molecule and co-former which may form the basis to a predictive model.

5.3 Summary

The value of crystal engineering in the discovery of new materials and unusual reaction pathways, prompted us to explore these techniques in the context of the origins of life. Solid-state chemistry and crystallisation have already attracted the attention of origin of life researchers, and seminal studies in the 1950s demonstrated that 'molecular dissymmetry' could be achieved by chiral-seeded crystallization strategies. More recently a dynamic process of crystal dissolution and growth enhanced by mechanical attrition (Viedma ripening) has enabled reliable access to enantiopure crystals through crystal grinding, offering a viable hypothesis for the chiral-amplification en route to biological homochirality. Chiral discrimination through Viedma ripening can, however, only occur with molecules that form racemic conglomerate crystals. Although only about 10% of chiral molecules are observed to crystallise as conglomerates, it is of note **RAO**, **AAO**, **XAO**, **ROT** and **AOX** have been found to do so in this work which allows chiral resolution of these compounds (and others, through preferential racemic formation leading to enantioenrichment in the solution) relevant to the origins of life which would be a major step towards understanding the chemical origins of biological homochirality. It is concluded that through this work, homochirality can be achieved using the conglomerate forming molecules to enable access to homochiral RNA when combined with a method of initial symmetry breaking.

Although we were not able to identify suitable co-crystallisation additive candidates for crystallisation with the aminal within this work, it may be possible, by leveraging techniques such as high-throughput crystallisation screening to more rapidly investigate a greater variety of additives and identify which can be used to produce conglomerates from compounds that usually form racemic crystals.

What this work demonstrates, then, is that it is indeed possible to utilise the physical properties of these intermediates' crystals to achieve the homochirality required for life, through a multitude of imaginable scenarios. The full appreciation for this is yet to be fully established but this work demonstrates the exciting prospect that further investigations are very likely to lead to a scientifically sound synthesis of homochiral RNA precursors in laboratory conditions that mimic those of the primordial Earth, and such a demonstration is within reach.

6 Experimental

6.1 General

Reagents and solvents were obtained and used without further purification, unless specified, from the following commercial sources: Alfa Aesar, Acros Organics, BDH, Carbosynth, Fisher Scientific, Fluorochem, Manchester Organics, Merck, Santa Cruz Biotechnology, Sigma Aldrich and VWR International. Deionized water was obtained from an Elga Option 3 purification system. ^{1}H, ^{13}C and ^{31}P NMR spectra were recorded on Bruker NMR spectrometers AVANCE III 600, AVANCE III 400 equipped with a Bruker 5 mm cryoprobe (600 MHz) and a gradient probe (400). All chemical shifts (δ) are reported in parts per million (ppm) relative to residual solvent peaks, and ^{1}H and ^{13}C chemical shifts relative to TMS and were calibrated using the residual solvent peak. When a mixed H_2O/D_2O solvent system was used a solvent suppression pulse sequence (noesygppr1d, Bruker) was used to obtain ^{1}H NMR spectra. Coupling constants are reported in Hertz (Hz). Spin multiplicities are indicated by symbols: s (singlet); d (doublet); t (triplet); q (quartet); m (multiplet); obs. (obscured/coincidental signals), or a combination of these. Diastereotopic geminal (AB) spin systems coupled to one or two additional nuclei are reported as ABX and ABXY, respectively. NMR data are reported as follows: chemical shift (number of nuclei, multiplicity, coupling constants (J), nuclear assignment). Spectra were recorded at 298 K. Melting points were determined using an Electrothermal standard digital apparatus for all solids and are quoted to the nearest ºC and are uncorrected. Infrared spectra (IR) were recorded on a Shimadzu IR Tracer 100 FTIR spectrometer. Absorption maxima are reported in wavenumber (cm^{-1}). Mass spectra and accurate mass measurements were recorded on a VG70-SE, Waters LCT Premier XE or Thermo Finnigan MAT 900XP instrument at the Department of Chemistry, University College London. Optical rotation was measured by Perkin Elmer Polarimeter Model 343 using a 1 dm polarimeter cell. Flash Column Chromatography (FCC) was carried out on a Biotage Isolera One purification platform using

either Biotage SNAP or Kinesis TELOS cartridges unless stated otherwise. HPLC was carried out on an Agilent 1260 Infinity LC system. Solution pH values were measured using a Mettler Toledo Seven Compact or a Corning 430 pH meter equipped with either a Mettler Toledo InLab semi-micro pH probe or a Fisherbrand FB68801 semi-micro pH probe.

6.2 General Synthesis of Pentose Aminooxazolines

Pentose (**40**, 5.00 g, 33.3 mmol) was dissolved in aqueous ammonia solution (3.5%, 50 mL). Cyanamide (**6**, 2.28 g, 54.2 mmol) was added and the solution was heated at 60 °C for 1 h, then allowed to cool to room temperature, followed by the addition of MeOH (100 mL) to promote crystallisation. After 16 h at 4 °C the crystals were collected by filtration and washed with ice-cold methanol and dried under vacuum. Further crops of the crystals were obtained from the filtrate.

6.2.1 D-ribo- aminooxazoline (D-RAO)

Starting from D-ribose (**D-*ribo*-40**, 5.00 g, 33.3 mmol) yielded D-ribo aminooxazoline (D-**RAO**; 4.52 g, 78%) as a fine white powder. M.p. 185 – 187 °C (Lit. 195 °C)[45]. IR (Solid, cm^{-1}) 3426 (NH_2), 3150 (OH), 2913 (CH), 1663 (C=N). ^{1}H NMR (600 MHz, D_2O) 5.97 (1H, d, J = 5.3 Hz, H1'), 5.38 (1H, t, J = 5.3 Hz, H2'), 4.21 (1H, dd, J = 9.6, 5.3 Hz, H3'), 3.87 (1H, ABX, J = 12.8, 2.3 Hz, H5'), 3.79 (1H, ddd, J = 9.4, 4.8, 2.3 Hz, H4'), 3.66 (1H, ABX, J = 12.8, 4.8 Hz, H5''). ^{13}C NMR (151 MHz, D_2O) 164.0 (C2), 88.5 (C1'), 86.2 (C4'), 79.4 (C2'), 70.1 (C3'), 59.9 (C5'). HRMS (m/z) calculated for $C_6H_{10}N_2O_4$ $[M+H^+]^+$; 175.0719 found, 175.0713. $[\alpha]_D^{20.0}$ (*c* = 1.00, H_2O) 120.1.

6.2.2 L-ribo aminooxazoline (L-RAO)

Starting from L- ribose (**L-*ribo*-40**, 5.00 g, 33.3 mmol) yielded L-ribo aminooxazoline (**L-RAO**; 4.17 g, 72%) as a fine white powder. M.p. 187 – 189 °C (Lit. 195 °C)[45]. IR (Solid, cm^{-1}) 3430 (NH_2), 3160 (OH), 2921 (CH), 1660 (C=N). ^{1}H NMR (600 MHz, D_2O) 5.97 (1H, d, J = 5.3 Hz, H1'), 5.38 (1H, t, J = 5.3 Hz, H2'), 4.20 (1H, dd, J = 9.6, 5.3 Hz, H3'), 3.86 (1H, ABX, J = 12.8, 2.3 Hz, H5'), 3.78 (1H, ddd, J = 9.6, 4.8, 2.3 Hz, H4'), 3.65 (1H, ABX, J = 12.8, 4.8 Hz, H5''). ^{13}C NMR (151 MHz, D_2O) 164.0 (C2), 88.5 (C1'), 86.1 (C4'), 79.4 (C2'), 70.1 (C3'), 59.9 (C5'). HRMS (m/z) calculated for $C_6H_{10}N_2O_4$ $[M+H^+]^+$; 175.0719 found, 175.0722. $[\alpha]_D^{20.0}$ (*c* = 1.00, H_2O) -119.4.

6.2.3 D-arabino- aminooxazoline (D-AAO)

Starting from D- arabinose (**D-arabino-40**, 5.00 g, 33.3 mmol) yielded D- arabino aminooxazoline (**D-AAO**; 3.59 g, 62%) M.p. 183 – 185 °C (Lit. 175 °C)[45]. IR (Solid, cm^{-1}) 3410 (NH_2), 3151 (OH), 2922 (CH), 1658 (C=N). ^{1}H NMR (600 MHz, D_2O) 6.09 (1H, d, J = 5.6 Hz, H1'), 5.31 (1H, dd, J = 5.6, 0.6 Hz, H2'), 4.50 (1H, m, H3'), 4.18 (1H, ddd, J =5.6, 4.2, 2.7 Hz, H4'), 3.65 (1H, ABX, J = 12.6, 4.2 Hz, H5'), 3.57 (1H, ABX, J = 12.6, 5.6 Hz, H5''). ^{13}C NMR (151 MHz, D_2O) 165.6 (C2), 99.4 (C1'), 89.3 (C4'), 85.0 (C2'), 75.9 (C3'), 62.0 (C5'). HRMS (m/z) calculated for $C_6H_{10}N_2O_4$ $[M+H^+]^+$; 175.0719 found, 175.0723. $[\alpha]_D^{20.0}$ (*c* = 1.00, H_2O) 30.2.

6.2.4 L-arabino- aminooxazoline (L-AAO)

Starting from L- arabinose (**L-arabino-40**, 5.00 g, 33.3 mmol) yielded L- arabino aminooxazoline (**L-AAO**; 3.36 g, 58%). M.p. 183 – 184 °C (Lit. 175 °C)[45]. IR (Solid, cm^{-1}) 3405 (NH_2), 3142 (OH), 2919 (CH), 1659 (C=N). ^{1}H NMR (600 MHz, D_2O) 5.97 (1H, d, J = 5.6 Hz, H1'), 5.31 (1H, dd, J = 5.6, 1.0 Hz, H2'), 4.39 (1H, ddd, J = 3.1, 1.0, 0.5, H3'), 4.07 (1H, ddd, J =6.2, 4.8, 3.1 Hz, H4'), 3.59 (1H, ABX, J = 12.4, 4.8 Hz, H5'), 3.57 (1H, ABX, J = 12.4, 6.2 Hz, H5'').). ^{13}C NMR (151 MHz,

D_2O) 165.6 (C2), 99.4 (C1'), 89.4 (C4'), 85.1 (C2'), 76.0 (C3'), 61.9 (C5'). HRMS (m/z) calculated for $C_6H_{10}N_2O_4$ $[M+H^+]^+$; 175.0719 found, 175.0721. $[\alpha]_D^{20.0}$ (*c* = 1.00, H_2O) -29.8.

6.2.5 D-xylo aminooxazoline (D-XAO)

Starting from D- xylose (**D-xylo-40**, 5.00 g, 33.3 mmol) yielded D- xylo- aminooxazoline (**D-XAO**; 3.77 g, 65%) M.p. 188 – 191 °C (Lit. 185 °C)[45]. IR (Solid, cm^{-1}) 3412 (NH_2), 3194 (OH), 2946 (CH), 1664 (C=N). ^1H NMR (600 MHz, D_2O) 5.99 (1H, d, J = 5.2 Hz, H1'), 5.03 (1H, d, J = 5.2 Hz, H2'), 4.40 (1H, d, J = 2.8, H3'), 3.92 (1H, ddd, J =7.2, 4.5, 2.8 Hz, H4'), 3.87 (1H, ABX, J = 12.0, 4.5 Hz, H5'), 3.77 (1H, ABX, J = 12.0, 7.2 Hz, H5''). ^{13}C NMR (151 MHz, D_2O) 165.0 (C2), 94.8 (C1'), 89.1 (C2'), 80.0 (C4'), 79.9 (C3'), 59.7 (C5'). HRMS (m/z) calculated for $C_6H_{10}N_2O_4$ $[M+H^+]^+$; 175.0719 found, 175.0724. $[\alpha]_D^{20.0}$ (*c* = 1.00, H_2O) 31.9.

6.2.6 L-xylo aminooxazoline (L-XAO)

Starting from L- xylose (**L-xylo-40**, 5.00 g, 33.3 mmol) yielded L- xylo- aminooxazoline (**L-XAO**; 3.48 g, 60%) M.p. 186 – 190 °C (Lit. 185 °C)[45]. IR (Solid, cm^{-1}) 3419 (NH_2), 3197 (OH), 2951 (CH), 1659 (C=N). ^1H NMR (600 MHz, D_2O) 5.98 (1H, d, J = 5.2 Hz, H1'), 5.01 (1H, d, J = 5.2 Hz, H2'), 4.39 (1H, d, J = 2.8, H3'), 3.91 (1H, ddd, J =7.1, 4.5, 2.8 Hz, H4'), 3.86 (1H, ABX, J = 11.8, 4.5 Hz, H5'), 3.77 (1H, ABX, J = 11.8, 7.1 Hz, H5''). ^{13}C NMR (151 MHz, D_2O) 165.1 (C2), 95.1 (C1'), 89.0 (C2'), 79.9 (C4'), 73.7 (C3'), 59.7 (C5'). HRMS (m/z) calculated for $C_6H_{10}N_2O_4$ $[M+H^+]^+$; 175.0719 found, 175.0723. $[\alpha]_D^{20.0}$ (*c* = 1.00, H_2O) -31.4.

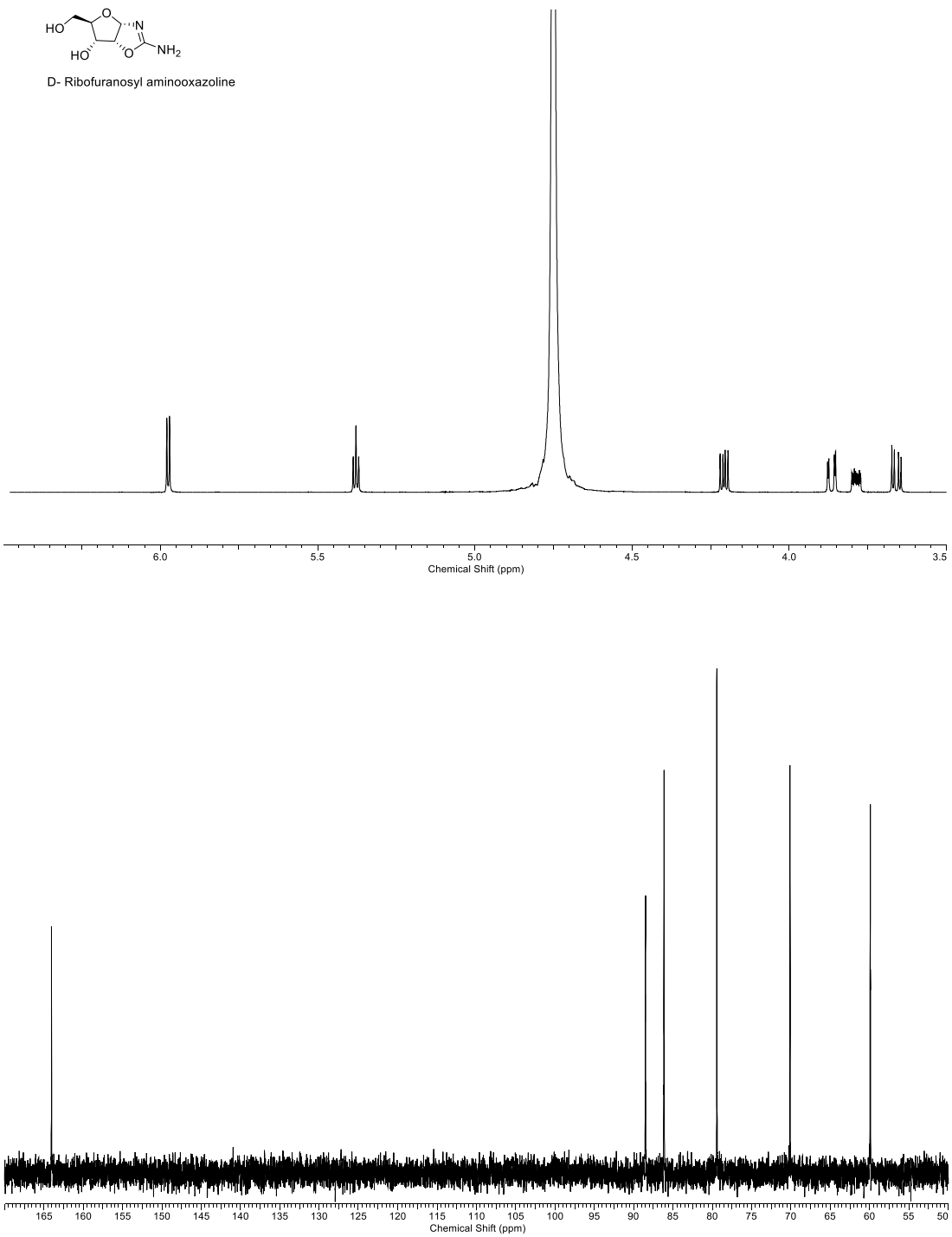

Figure 110: ^{1}H NMR (600 MHz, D_2O, 3.5-6.5 ppm, Top) and ^{13}C NMR (151 MHz, D_2O, 50-170 ppm, Bottom) spectra of D- ribo aminooxazoline (**D-RAO**).

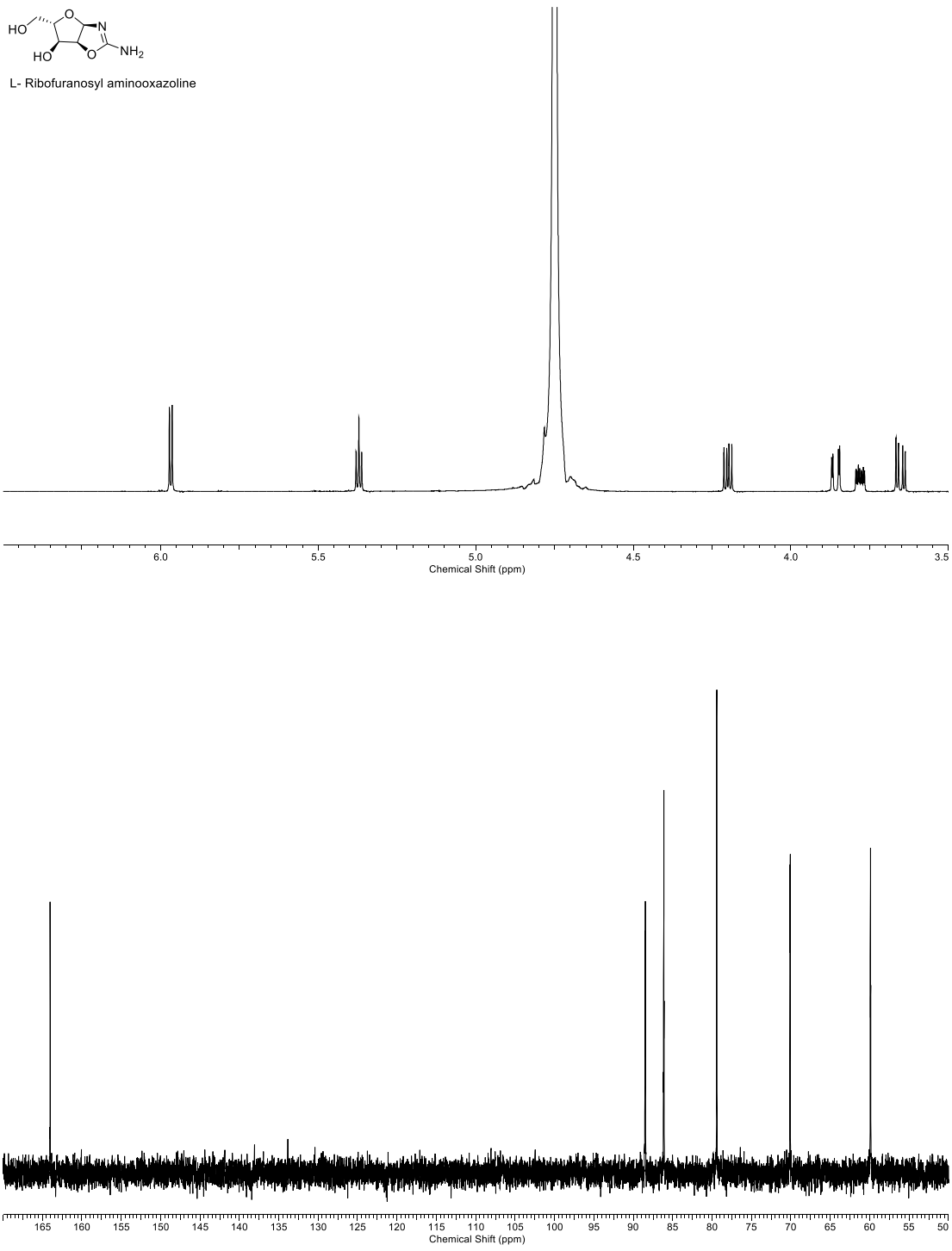

Figure 111: ^{1}H NMR (600 MHz, D_2O, 3.5-6.5 ppm, Top) and ^{13}C NMR (151 MHz, D_2O, 50-170 ppm, Bottom) spectra of L- ribo aminooxazoline (**L-RAO**).

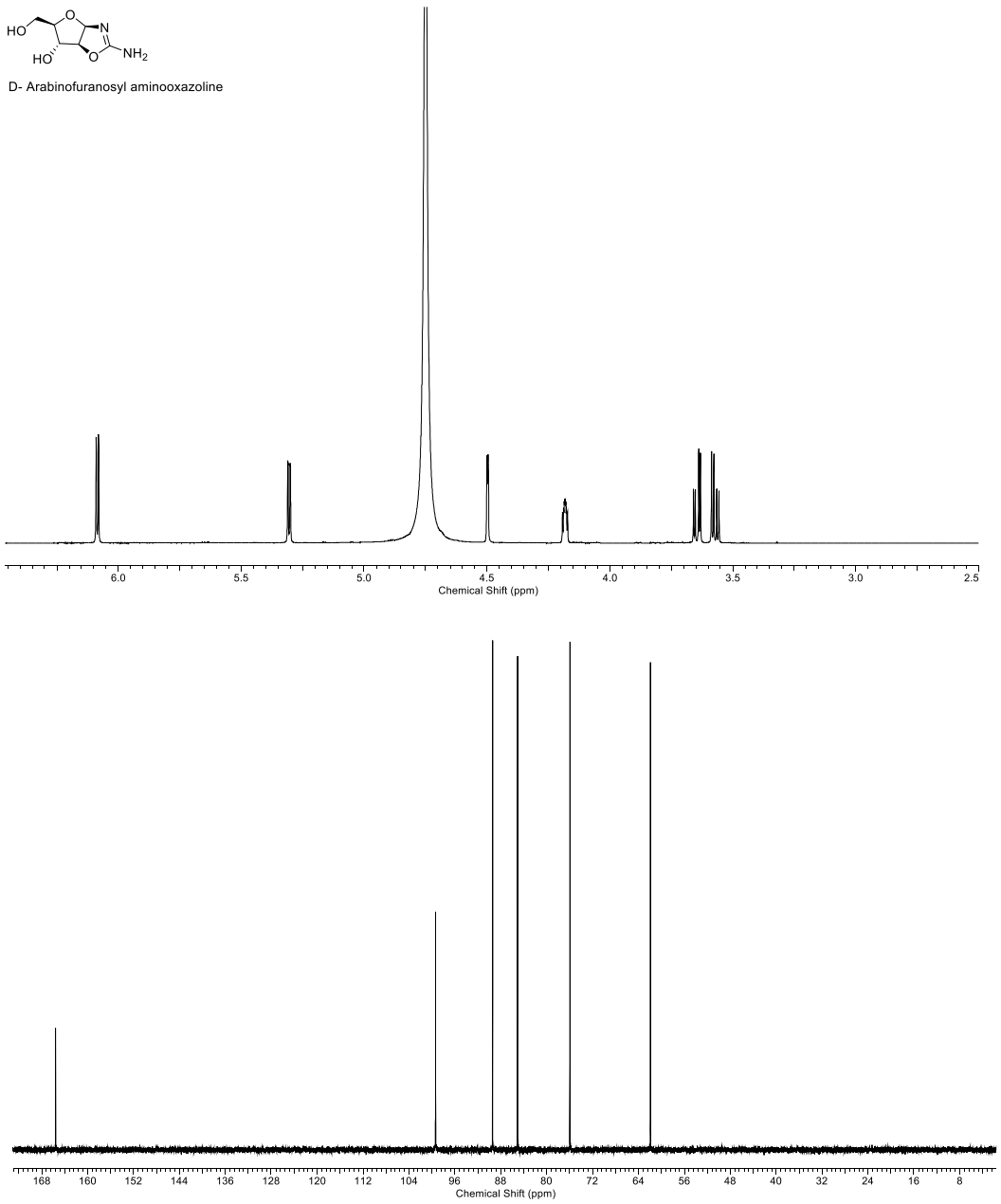

Figure 112: ^{1}H NMR (600 MHz, D_2O, 3.5-6.5 ppm, Top) and ^{13}C NMR (151 MHz, D_2O, 0-170 ppm, Bottom) spectra of D- arabino aminooxazoline (**D-AAO**).

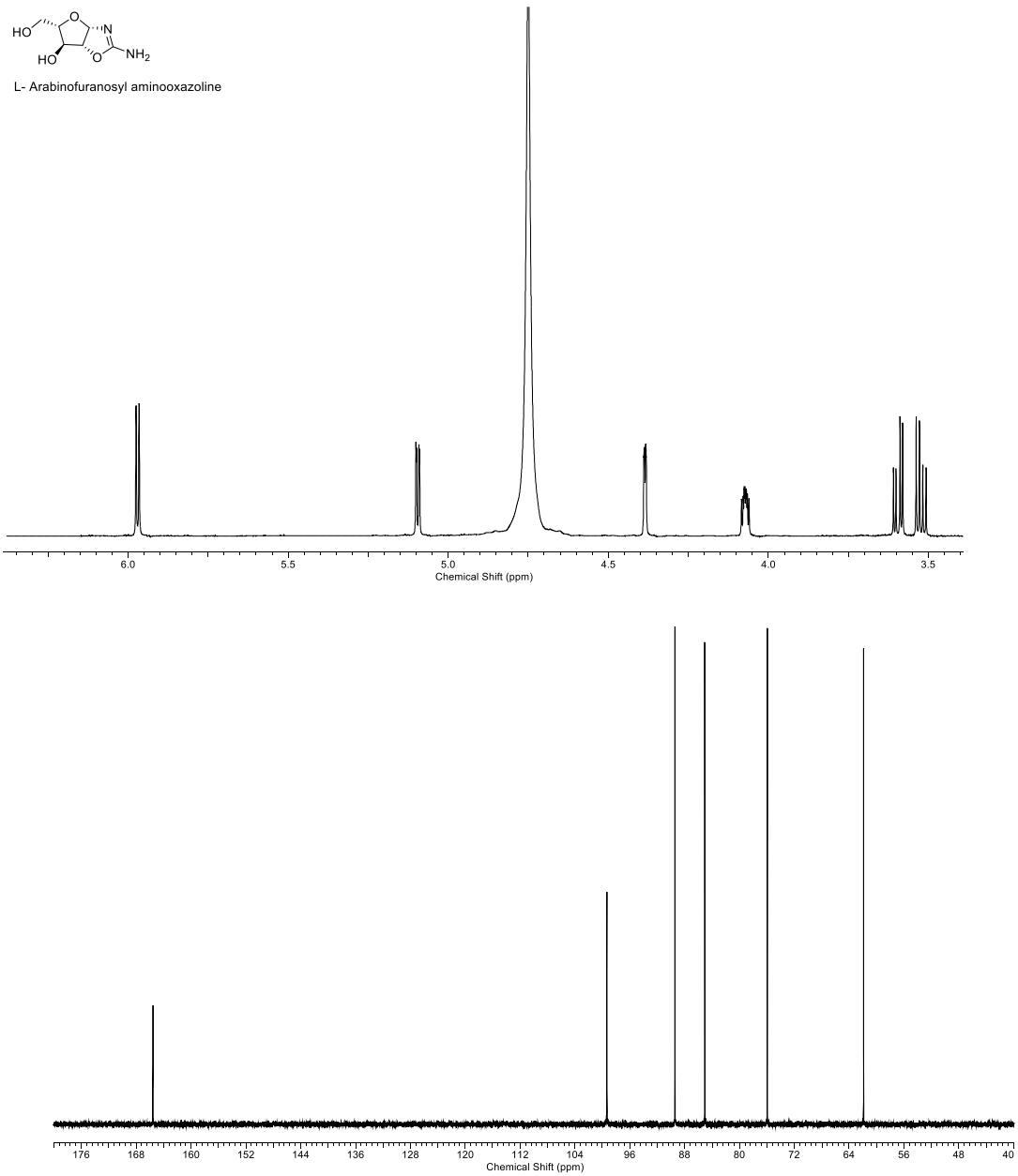

*Figure 113: ^{1}H NMR (600 MHz, D_2O, 3.5-6.5 ppm, Top) and 13C NMR (151 MHz, D_2O, 0-170 ppm, Bottom) spectra of L- arabino aminooxazoline (**L-AAO**).*

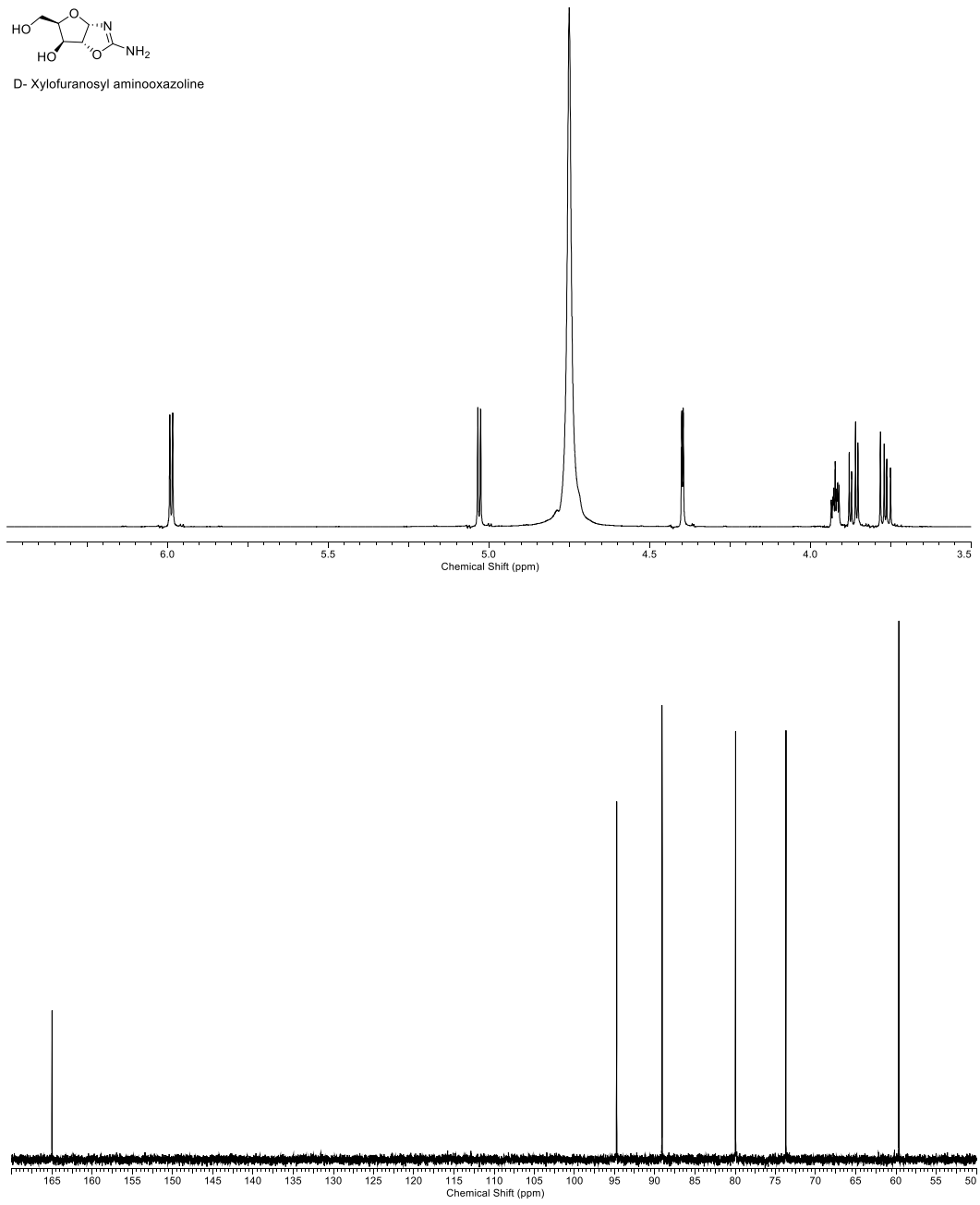

*Figure 114: ^{1}H NMR (600 MHz, D_2O, 3.5-6.5 ppm, Top) and ^{13}C NMR (151 MHz, D_2O, 50-170 ppm, Bottom) spectra of D- xylo aminooxazoline (**D-XAO**).*

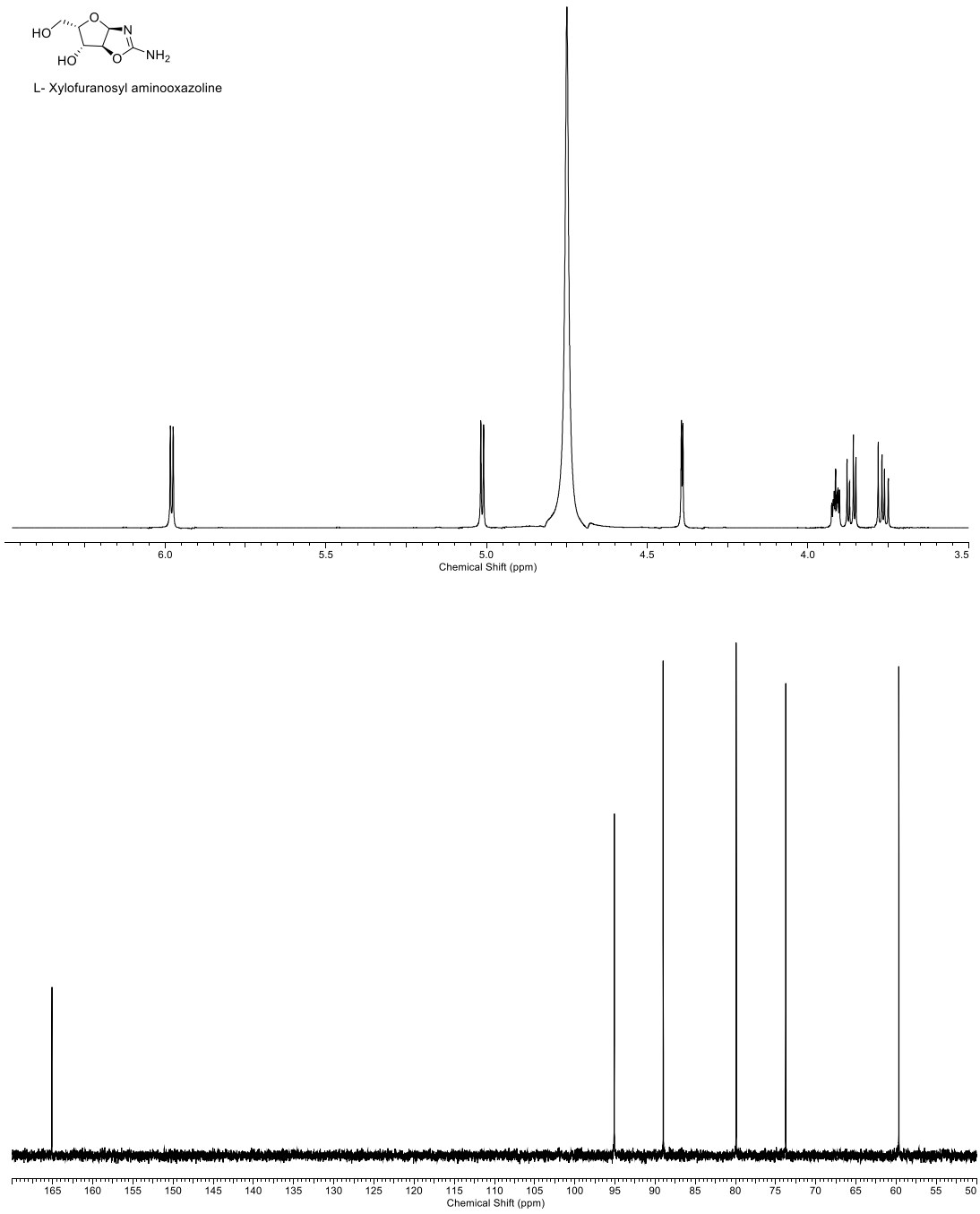

*Figure 115: ^{1}H NMR (600 MHz, D_2O, 3.5-6.5 ppm, Top) and ^{13}C NMR (151 MHz, D_2O, 50-170 ppm, Bottom) spectra of L- xylo aminooxazoline (**L-XAO**).*

6.3 General Synthesis of Pentose Oxazolidinone Thiones (OT)

General procedure was used from Stairs *et al.*[64] Pentose (**40**, 6.00 g, 39.9 mmol), potassium thiocyanate (7.77 g, 79.8 mmol) were dissolved in water (36 mL). Followed by hydrochloric acid (37%, 6.90 mL) that was added dropwise over 5 minutes, then incubated at 60 °C for 24 h. The resultant solution was concentrated in vacuo with silica gel (dry). The powder was then purified by FCC, eluting with EtOAc / MeOH 0-10%. The product was then recrystallized from $CHCl_3$/ EtOH to yield the desired oxazolidinone thione.

6.3.1 D-ribo oxazolidinone thione (D-ROT)

Starting from D-ribose (**D-ribo-40**, 6.00 g, 39.9 mmol) yielded D-ribo oxazolidinone thione (**D-ROT**; 4.80 g, 63%). M.p. 175 – 177 °C decomp. (Lit 167 – 168 °C i). IR (Solid, cm^{-1}) 3440 (NH), 3328 (OH), 2993, 2929, 2902 (CH), 1521 (C=S). ^{1}H NMR (600 MHz, D_2O) 5.89 (1H, d, J = 5.4 Hz, H1'), 5.30 (1H, t, J = 5.4 Hz, H2'), 4.21 (1H, dd, J = 9.4, 5.4 Hz, H3'), 3.92 (1H, ABX, J = 12.5, 2.0 Hz, H5'), 3.75 (1H, ddd, J = 9.4, 4.8, 2.0 Hz, H4'), 3.71 (1H, ABX, J = 12.5, 4.8 Hz, H5'). ^{13}C NMR (151 MHz, D_2O) 191.2 (C2), 89.0 (C1'), 85.9 (C2'), 79.3 (C4'), 70.9 (C3'), 60.0 (C5'). HRMS (m/z) calculated for $C_6H_{10}NO_4S$ [M+H+], 192.0331; found 192.0336. $[\alpha]_D^{20.0}$ (*c* = 1.00, H_2O) -140.1.

6.3.2 L-ribo oxazolidinone thione (L-ROT)

Starting from L-ribose (**L-ribo-40**, 6.00 g, 39.9 mmol) yielded L-ribo oxazolidinone thione (**L-ROT**; 4.42 g, 58%). M.p. 170 – 175 °C decomp. (Lit 167 – 168 °C i). IR (Solid, cm^{-1}) 3439 (NH), 3330 (OH), 2994, 2920, 2902 (CH), 1520 (C=S). ^{1}H NMR (600 MHz, D_2O) 5.89 (1H, d, J = 5.4 Hz, H1'), 5.30 (1H, t, J = 5.4 Hz, H2'), 4.21 (1H, dd, J = 9.4, 5.4 Hz, H3'), 3.92 (1H, ABX, J = 12.5, 2.0 Hz, H5'), 3.75 (1H, ddd, J = 9.4, 4.8, 2.0 Hz, H4'), 3.71 (1H, ABX, J = 12.5, 4.8 Hz, H5''). ^{13}C NMR

(151 MHz, D_2O) 191.2 (C2), 89.0 (C1'), 85.9 (C2'), 79.3 (C4'), 70.9 (C3'), 60.0 (C5'). HRMS (m/z) calculated for $C_6H_{10}NO_4S$ [M+H+], 192.0331; found .192.0338. $[\alpha]_D^{20.0}$ (*c* = 1.00, H_2O) -139.5.

6.3.3 D-arabino oxazolidinone thione (D-AOT)

Starting from D-arabinose (**D-*arabino*-40**, 6.00 g, 39.9 mmol) yielded D-arabino oxazolidinone thione (**D-AOT**; 4.50 g, 59%). M.p. 138 – 142 °C (Lit 132 – 133 °C i). IR (Solid, cm^{-1}) 3390 (NH), 3403 (OH), 2944, 2931, 2871 (CH), 1481 (C=S). ^1H NMR (600 MHz, D_2O) 6.01 (1H, d, J = 5.8 Hz, H1'), 5.28 (1H, dt, J = 5.8, 0.8 Hz, H2'), 4.46 (1H, dt, J = 1.9, 0.8 Hz, H3'), 4.20 (1H, ddd, J = 7.5, 5.2, 1.9 Hz, H4'), 3.59 (1H, ABX, J = 12.3, 5.2 Hz, H5'), 3.46 (1H, ABX, J = 12.3, 7.5 Hz, H5''). ^{13}C NMR (151 MHz, D_2O) 191.2 (C2), 89.0 (C2'), 85.9 (C1'), 79.3 (C4'), 70.9 (C3'), 60.0 (C5'). HRMS (m/z) calculated for $C_6H_{10}NO_4S$ [M+H+], 192.0331; found 192.0338. $[\alpha]_D^{20.0}$ (*c* = 1.00, H_2O) -10.9.

6.3.4 L-arabino oxazolidinone thione (L-AOT)

Starting from L-arabinose (**L-*arabino*-40**, 6.00 g, 39.9 mmol) yielded L-arabino oxazolidinone thione (**L-AOT**; 4.50 g, 59%). M.p. 133 – 134 °C (Lit 132 – 133 °C i). IR (Solid, cm^{-1}) 3389 (NH), 3403 (OH), 2940, 2929, 2870 (CH), 1481 (C=S). ^1H NMR (600 MHz, D_2O) 6.02 (1H, d, J = 5.8 Hz, H1'), 5.29 (1H, dt, J = 5.8, 0.7 Hz, H2'), 4.47 (1H, dt, J = 1.8, 0.7 Hz, H3'), 4.21 (1H, ddd, J = 7.5, 5.3, 1.8 Hz, H4'), 3.60 (1H, ABX, J = 12.3, 5.3 Hz, H5'), 3.46 (1H, ABX, J = 12.3, 7.5 Hz, H5''). ^{13}C NMR (151 MHz, D_2O) 191.1 (C2), 92.6 (C2'), 90.5 (C1'), 87.8 (C4'), 75.3 (C3'), 61.7 (C5'). HRMS (m/z) calculated for $C_6H_{10}NO_4S$ [M+H+], 192.0331; found 192.0331. $[\alpha]_D^{20.0}$ (*c* = 1.00, H_2O) 11.6.

6.3.5 D-xylo oxazolidinone thione (D-XOT)

Starting from D-xylose (**D-*xylo*-40**, 6.00 g, 39.9 mmol) yielded D-xylo oxazolidinone thione (**D-XOT**; 3.05 g, 40%). M.p. 134 – 136 °C (Lit 129 – 130 °C i). IR (Solid, cm^{-1}) 3250 (OH), 2980, 2966 (CH), 1485 (C=S). ^{1}H NMR (600 MHz, D_2O) 6.03 (1H, d, J = 5.5 Hz, H1'), 5.30 (1H, dd, J = 5.5, 0.5 Hz, H2'), 4.48 (1H, d, J = 2.8 Hz, H3'), 4.00 (1H, m, H4'), 3.91 (1H, ABX, J = 12.0, 4.2 Hz, H5'), 3.80 (1H, ABX, J = 12.0, 7.3 Hz, H5''). ^{13}C NMR (151 MHz, D_2O) 190.4 (C2), 91.2 (C2'), 89.6 (C1'), 80.9 (C4'), 73.6 (C3'), 59.6 (C5'). HRMS (m/z) calculated for $C_6H_{10}NO_4S$ [M+H+], 192.0331; found 192.0325. $[\alpha]_D^{20.0}$ (*c* = 1.00, H_2O) 11.9.

6.3.6 L-xylo oxazolidinone thione (L-XOT)

Starting from L-xylose (**L-*xylo*-40**, 6.00 g, 39.9 mmol) yielded L-xylo oxazolidinone thione (**L-XOT**; 3.28 g, 43%). M.p. 133 – 136 °C (Lit 129 – 130 °C i). IR (Solid, cm^{-1}) 3250 (OH), 2980, 2966 (CH), 1485 (C=S). ^{1}H NMR (600 MHz, D_2O) 6.03 (1H, d, J = 5.5 Hz, H1'), 5.30 (1H, dd, J = 5.5, 0.5 Hz, H2'), 4.48 (1H, d, J = 2.8 Hz, H3'), 4.00 (1H, m, H4'), 3.91 (1H, ABX, J = 12.0, 4.2 Hz, H5'), 3.80 (1H, ABX, J = 12.0, 7.3 Hz, H5''). ^{13}C NMR (151 MHz, D_2O) 191.2 (C2), 89.0 (C2'), 85.9 (C1'), 79.3 (C4'), 70.9 (C3'), 60.0 (C5'). HRMS (m/z) calculated for $C_6H_{10}NO_4S$ [M+H+], 192.0331; found 192.0338. $[\alpha]_D^{20.0}$ (*c* = 1.00, H_2O) -11.5.

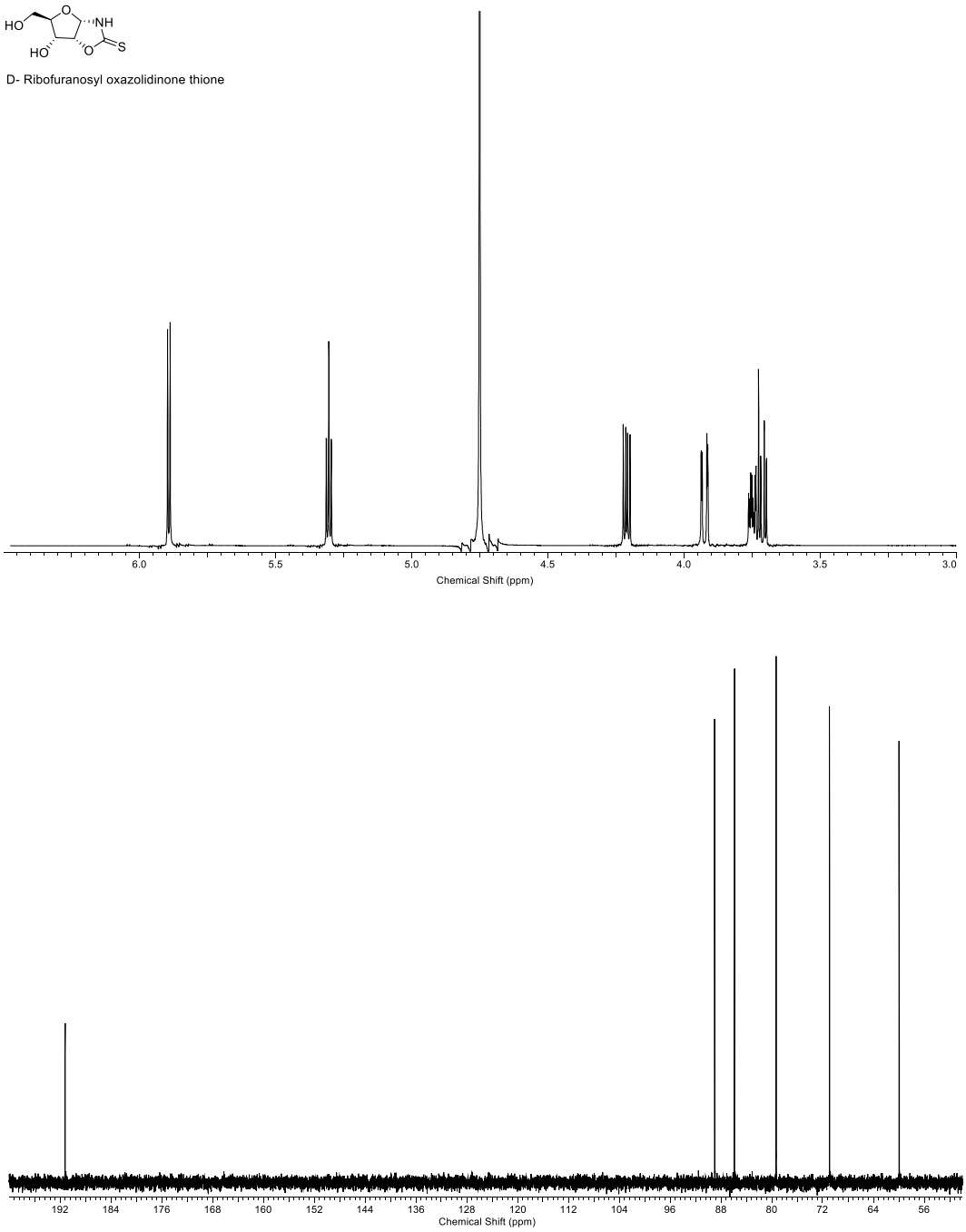

*Figure 116: ^{1}H NMR (600 MHz, D_2O, 3.0-6.5 ppm, Top) and ^{13}C NMR (151 MHz, D_2O, 50-200 ppm, Bottom) spectra of D-ribo oxazolidinone thione (**D-ROT**).*

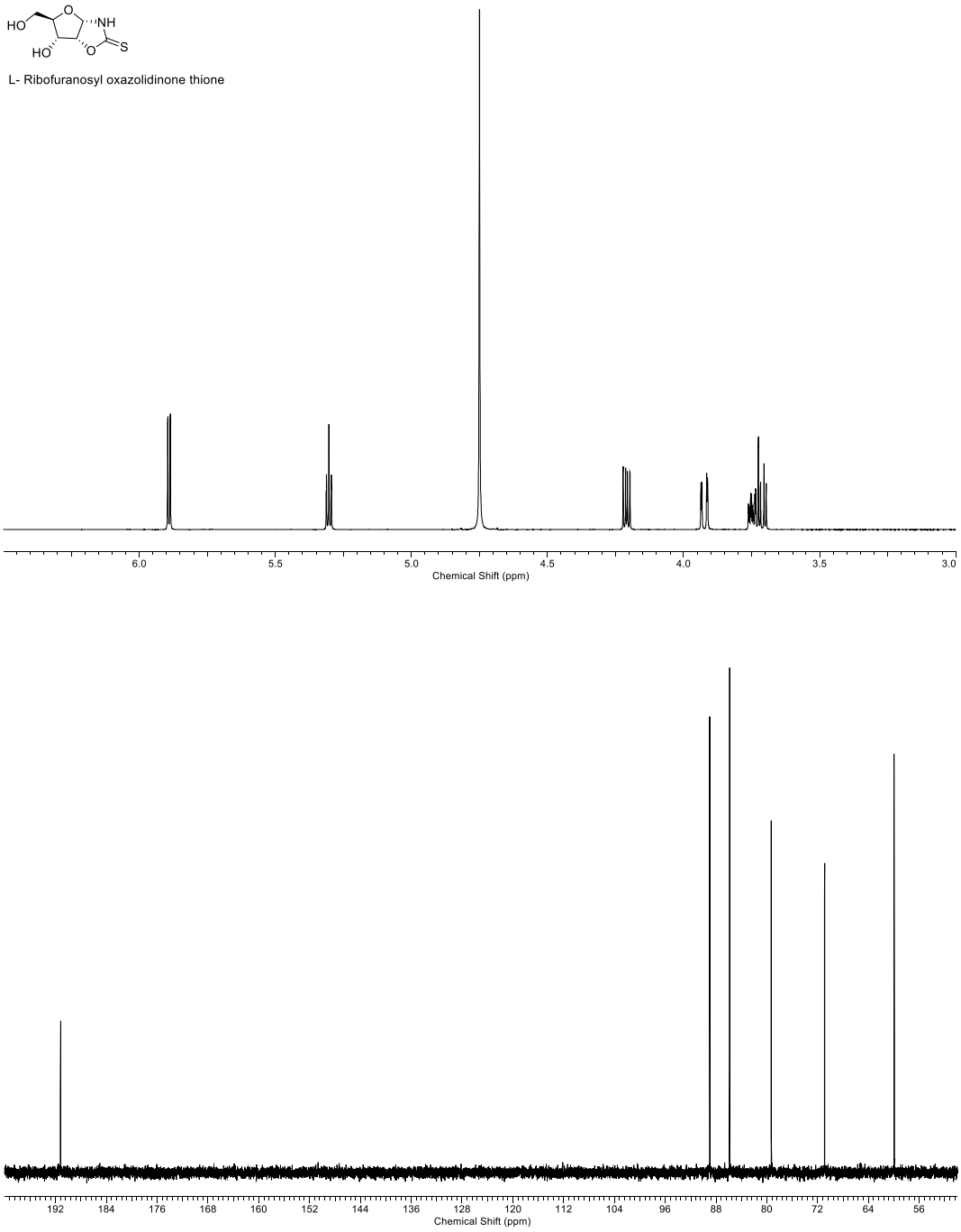

*Figure 117: ^{1}H NMR (600 MHz, D_2O, 3.0-6.5 ppm, Top) and ^{13}C NMR (151 MHz, D_2O, 50-200 ppm, Bottom) spectra of L-ribo oxazolidinone thione (**L-ROT**).*

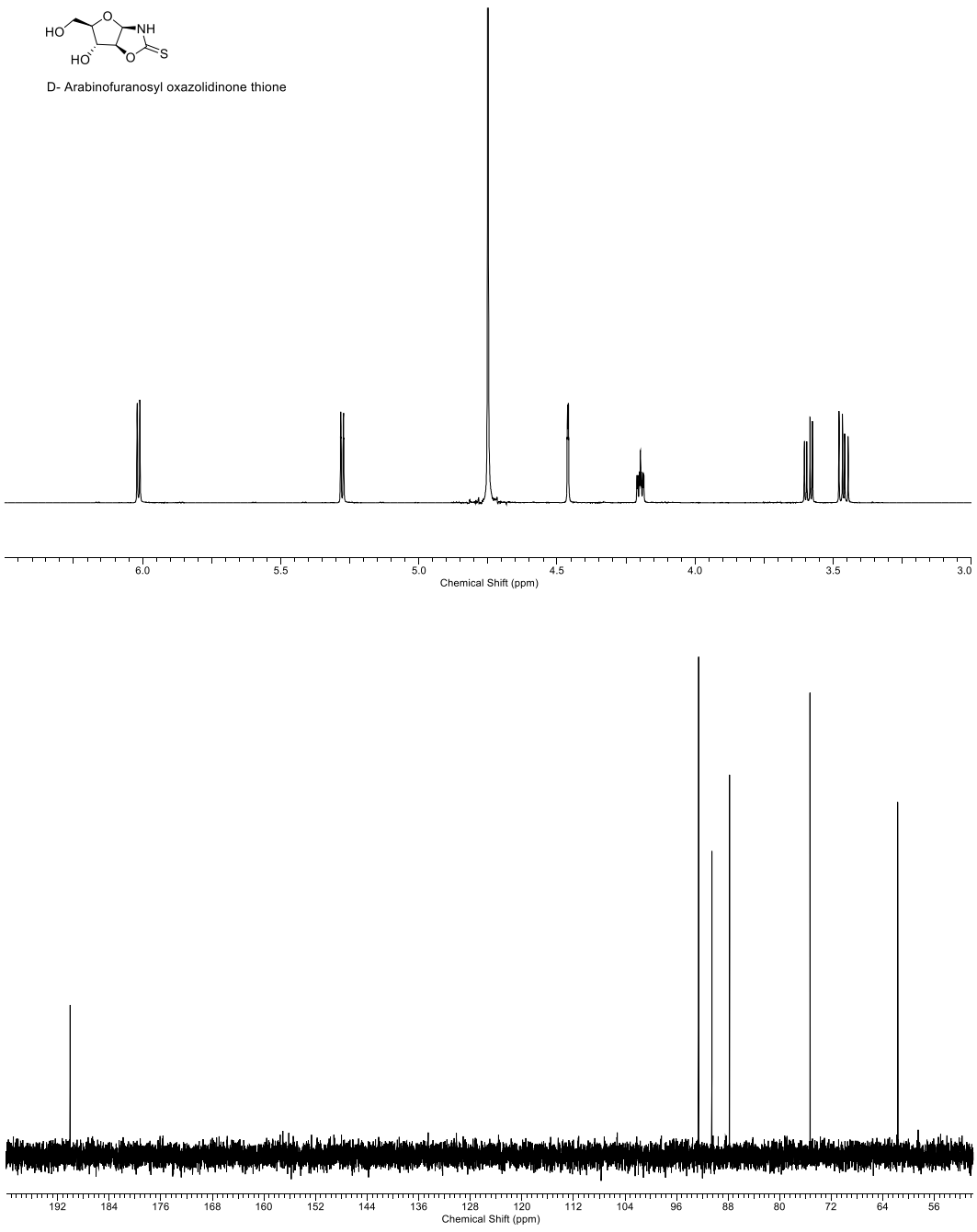

*Figure 118: ^{1}H NMR (600 MHz, D_2O, 3.0-6.5 ppm, Top) and ^{13}C NMR (151 MHz, D_2O, 50-200 ppm, Bottom) spectra of D-arabino oxazolidinone thione (**D-AOT**).*

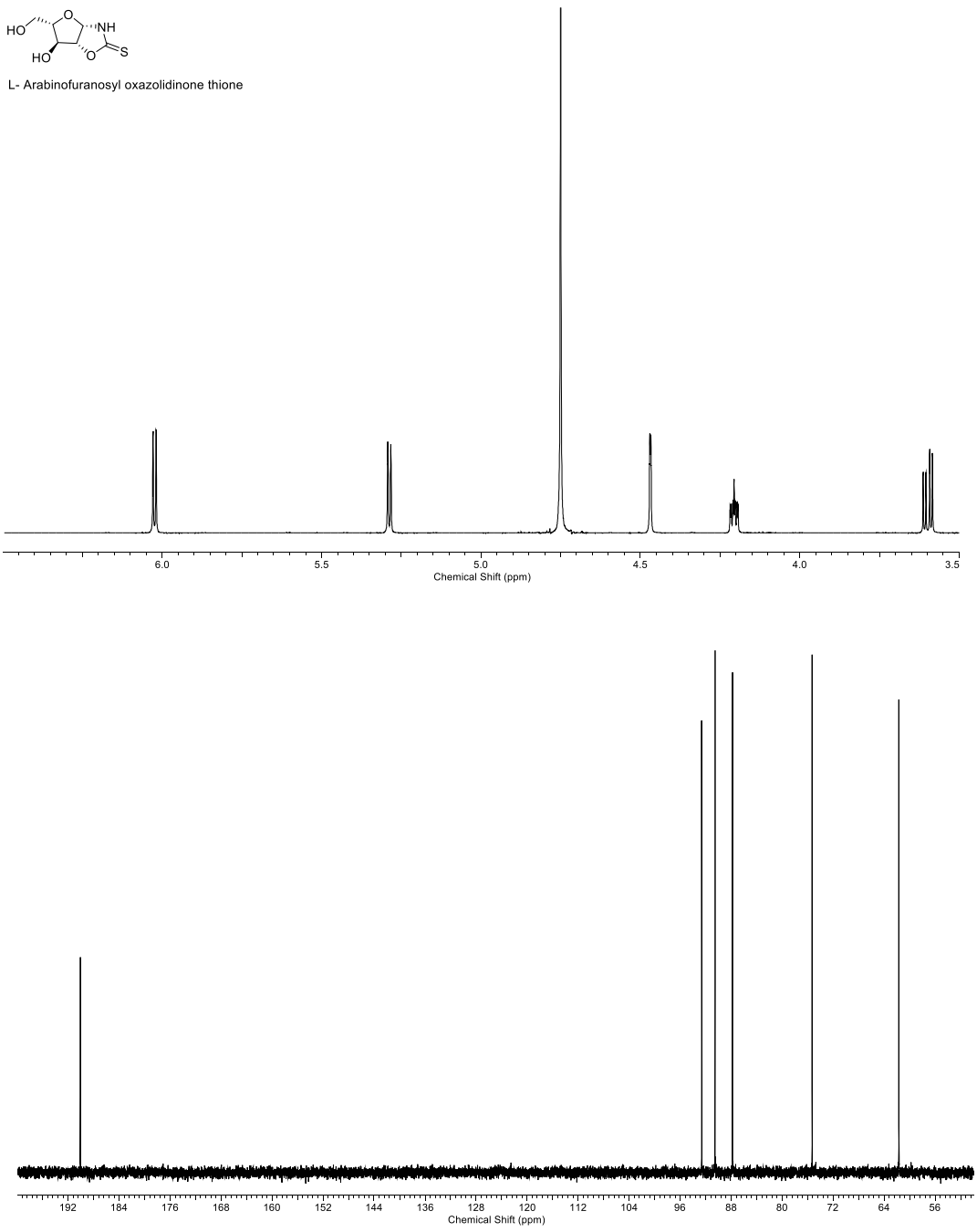

*Figure 119: ^{1}H NMR (600 MHz, D_2O, 3.0-6.5 ppm, Top) and ^{13}C NMR (151 MHz, D_2O, 50-200 ppm, Bottom) spectra of L-arabino oxazolidinone thione (**L-AOT**).*

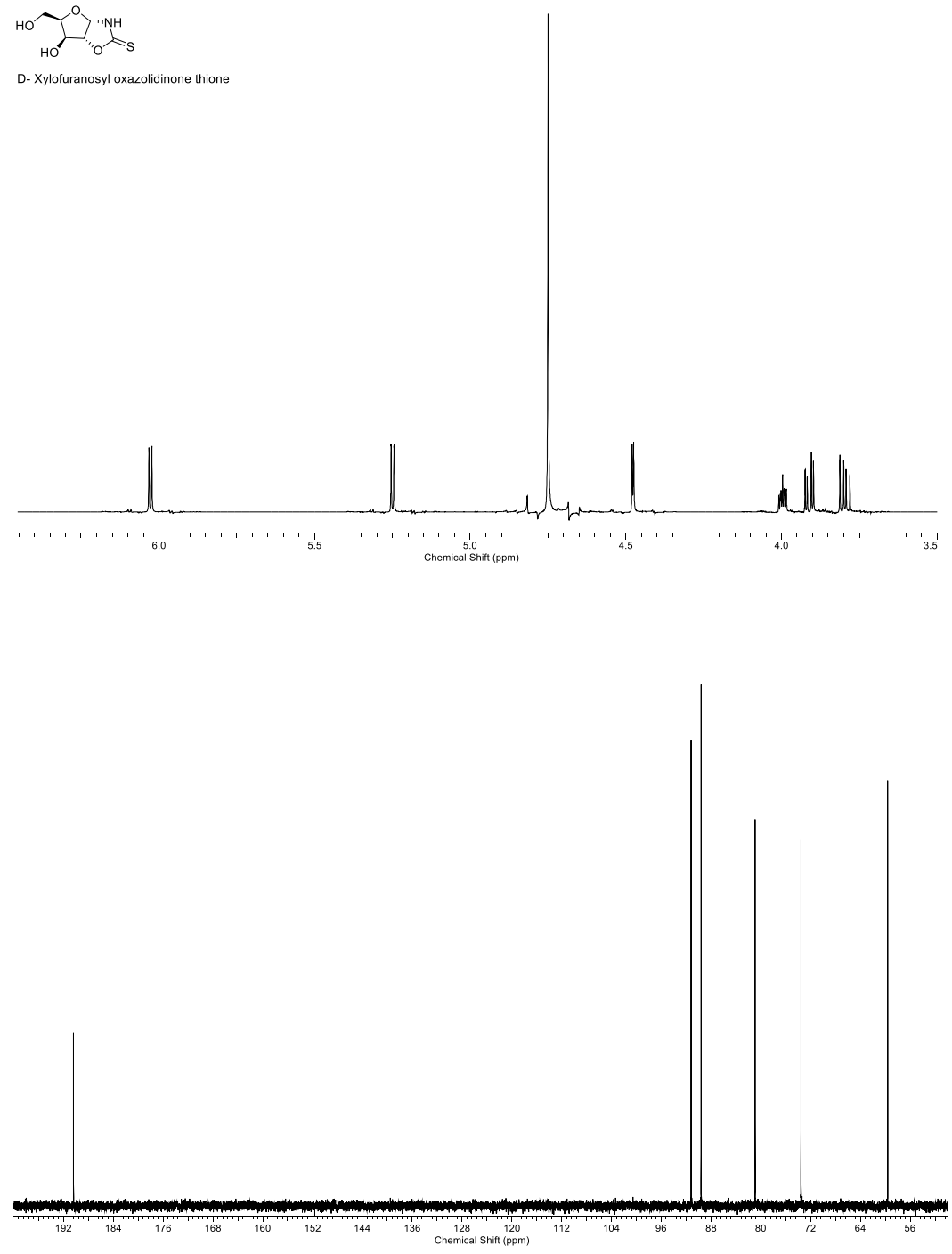

*Figure 120: ^{1}H NMR (600 MHz, D_2O, 3.0-6.5 ppm, Top) and ^{13}C NMR (151 MHz, D_2O, 50-200 ppm, Bottom) spectra of D-xylo oxazolidinone thione (**D-XOT**).*

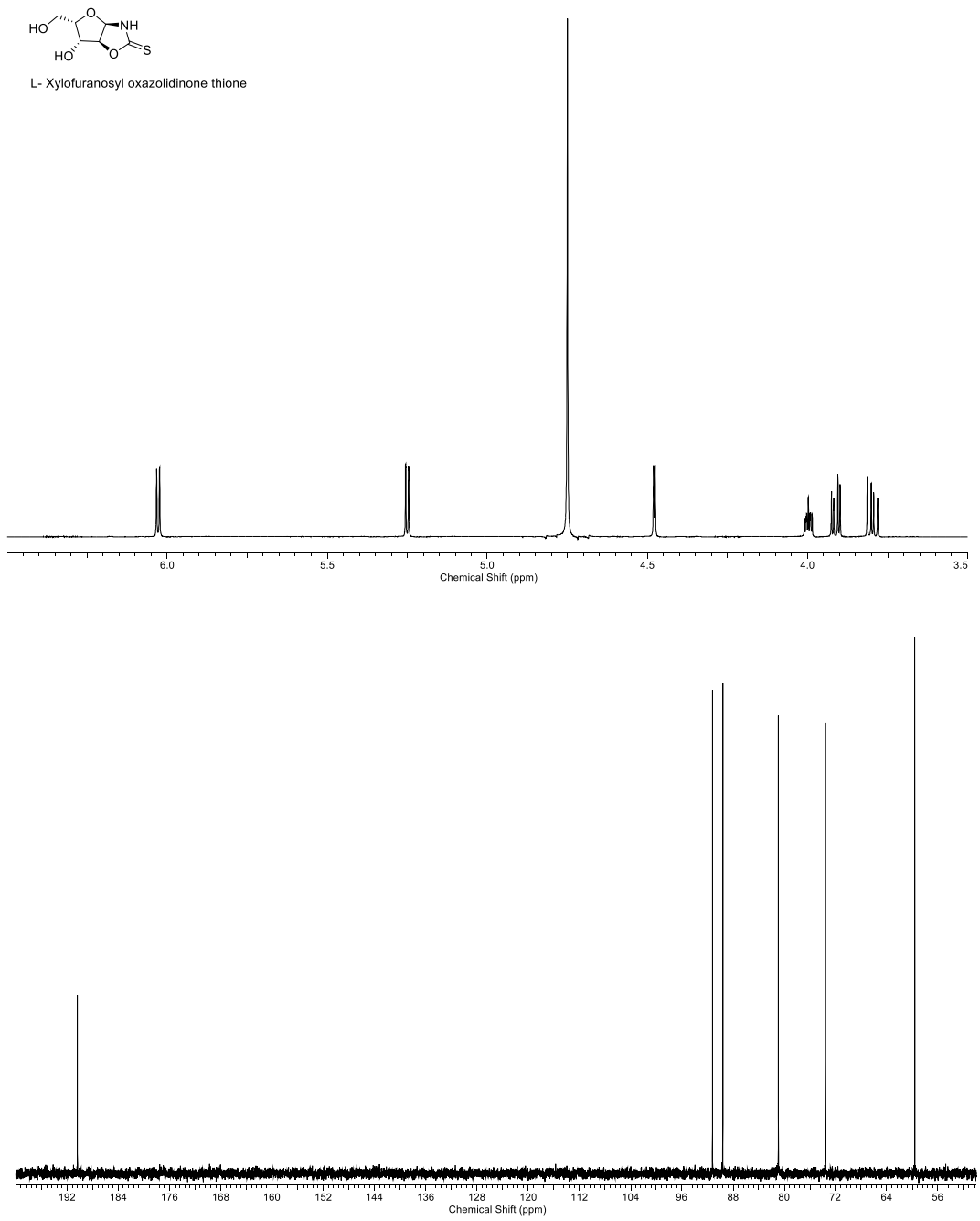

*Figure 121: ^{1}H NMR (600 MHz, D_2O, 3.0-6.5 ppm, Top) and ^{13}C NMR (151 MHz, D_2O, 50-200 ppm, Bottom) spectra of L-xylo oxazolidinone thione (**L-XOT**).*

6.4 General Synthesis of Pentose Oxazolidinones (OX)

Pentose (**40**, 10.00 g, 66.6 mmol) was dissolved in water (65 mL) followed by the addition of potassium cyanate (8.10 g, 100.1 mmol) and NH_4Cl (5.40 g, 100.1 mmol). The resultant solution was heated at 60 °C for 8 h and allowed to cool to room temperature. Silica gel (dry) was then added to result in a free-flowing powder. The powder was then purified by silica gel FCC hand column eluting with EtOAc/ MeOH (99:1), resulting in a white powder.

6.4.1 D-ribo oxazolidinone (D-ROX)

Starting from D-ribose (**D-*ribo*-40**, 10.00 g, 66.6 mmol) yielded D-*ribo* oxazolidinone (**D-ROX**; 4.43 g, 38%). M.p. 124–126 °C. IR (solid, cm^{-1}) 3340 (NH), 3214 (OH), 3002, 2880 (CH), 1712 (C=O). ^1H NMR (600 MHz, D_2O) 5.76 (1H, d, J = 5.4 Hz, H1'), 5.09 (1H, t, J = 5.4 Hz, H2'), 4.14 (1H, dd, J = 9.5, 5.4 Hz, H3'), 3.92 (1H, ABX, J = 12.7, 2.3 Hz, H5'), 3.84 (1H, ddd, J = 9.5, 4.8, 2.3 Hz, H4'), 3.72 (1H, ABX, J = 12.7, 4.8 Hz H5''). ^{13}C NMR (151 MHz, D_2O) 161.2 (C2), 86.0 (C1'), 80.5 (C4'), 78.7 (C2'), 70.5 (C3'), 60.2 (C5'). HRMS (m/z) calculated for $C_6H_9NO_5$ $[M+H^+]^+$ 176.0559; found, 176.0551. $[\alpha]_D^{20.0}$ (*c* = 1.00, H_2O) -113.9.

6.4.2 L-ribo oxazolidinone (L-ROX)

Starting from L-ribose (**L-*ribo*-40**, 10.00 g, 66.6 mmol) yielded L-*ribo* oxazolidinone (**L-ROX**; 5.25 g, 45%). M.p. 125–128 °C. IR (solid, cm^{-1}) 3339 (NH), 3212 (OH), 3005, 2879 (CH), 1714 (C=O). ^1H NMR (600 MHz, D_2O) 5.76 (1H, d, J = 5.4 Hz, H1'), 5.09 (1H, t, J = 5.4 Hz, H2'), 4.14 (1H, dd, J = 9.5, 5.4 Hz, H3'), 3.92 (1H, ABX, J = 12.7, 2.3 Hz, H5'), 3.84 (1H, ddd, J = 9.5, 4.8, 2.3 Hz, H4'), 3.72 (1H, ABX, J = 12.7, 4.8 Hz H5''). ^{13}C NMR (151 MHz, D_2O) 161.2 (C2), 86.0 (C1'), 80.5 (C4'),

78.7 (C2'), 70.5 (C3'), 60.2 (C5'). HRMS (m/z) calculated for $C_6H_9NO_5$ $[M+H^+]^+$ 176.0559; found, 176.0548. $[\alpha]_D^{20.0}$ (*c* = 1.00, H_2O) -115.0.

6.4.3 D-arabino oxazolidinone (D-AOX)

Starting from D-arabino (**D-*arabino*-40**, 10.00 g, 66.6 mmol) yielded D-arabino oxazolidinone (**D-AOX**; 2.44 g, 21%). M.p. 159–162 °C. IR (solid, cm^{-1}) 3400 (NH), 3235 (OH), 2956, 2937, 2895 (CH), 1747 (C=O). ^{1}H NMR (600 MHz, D_2O) 5.92 (1H, d, J = 5.7 Hz, H1'), 5.08 (1H, d, J = 5.7 Hz, H2'), 4.44 (1H, d, J = 2.4 Hz, H3'), 4.16 (1H, ddd, J = 7.0, 4.9, 2.4 Hz, H4'), 3.70 (1H, ABX, J = 12.4, 4.9 Hz, H5'), 3.60 (1H, ABX, J = 12.4, 6.0 Hz, H5''). ^{13}C NMR (151 MHz, D_2O) 160.1 (C2), 87.4 (C1'), 87.3 (C4'), 87.0 (C3'), 75.2 (C2'), 63.0 (C5'). HRMS (m/z) calculated for $C_6H_9NO_5$ $[M+H^+]^+$ 176.0559; found, 176.0559. $[\alpha]_D^{20.0}$ (*c* = 1.00, H_2O) -60.2.

6.4.4 L-arabino oxazolidinone (L-AOX)

Starting from L-arabino (**L-*arabino*-40**, 10.00 g, 66.6 mmol) yielded L-arabino oxazolidinone (**L-ROX**; 2.92 g, 25%). M.p. 160–162 °C. IR (solid, cm^{-1}) 3399 (NH), 3232 (OH), 2934, 2892 (CH), 1745 (C=O). ^{1}H NMR (600 MHz, D_2O) 5.92 (1H, d, J = 5.7 Hz, H1'), 5.08 (1H, d, J = 5.7 Hz, H2'), 4.44 (1H, d, J = 2.4 Hz, H3'), 4.16 (1H, ddd, J = 7.0, 4.9, 2.4 Hz, H4'), 3.70 (1H, ABX, J = 12.4, 4.9 Hz, H5'), 3.60 (1H, ABX, J = 12.4, 6.0 Hz, H5''). ^{13}C NMR (151 MHz, D_2O) 160.4 (C2), 87.6 (C1'), 87.3 (C4'), 86.9 (C3'), 75.5 (C2'), 62.0 (C5'). HRMS (m/z) calculated for $C_6H_9NO_5$ $[M+H^+]^+$ 176.0559; found, 176.0557. $[\alpha]_D^{20.0}$ (*c* = 1.00, H_2O) 59.3.

6.4.5 D-xylo oxazolidinone (D-XOX)

Starting from D-xylo (**L-*xylo*-40**, 10.00 g, 66.6 mmol) yielded D-xylo oxazolidinone (**D-XOX**; 3.50 g, 30%). M.p. 126– 130 °C. IR (solid, cm^{-1}) 3429 (NH), 3268 (OH), 2991 (CH), 1722 (C=O). ^{1}H

NMR (600 MHz, D_2O) 5.86 (1H, d, J = 5.4 Hz, H1'), 4.98 (1H, d, J = 5.4 Hz, H2'), 4.38 (1H, d, J = 2.8 Hz, H3'), 4.07 (1H, ddd, J = 7.3, 4.2, 2.8 Hz, H4'), 3.87 (1H, ABX, J = 11.9, 4.2 Hz, H5'), 3.77 (1H, ABX, J = 11.9, 7.3 Hz, H5''). ^{13}C NMR (151 MHz, D_2O) 160.1 (C2), 86.5 (C1'), 85.9 (C4'), 80.0 (C3'), 73.5 (C2'), 59.6 (C5'). HRMS (m/z) calculated for $C_6H_9NO_5$ $[M+H^+]^+$ 176.0559; found, 176.0561. $[\alpha]_D^{20.0}$ (*c* = 1.00, H_2O) 56.3.

6.4.6 L-xylo oxazolidinone (L-XOX)

Starting from L-xylo (**L-*xylo*-40**, 10.00 g, 66.6 mmol) yielded L-xylo oxazolidinone (**L-XOX**; 3.50 g, 30%). M.p. 128– 131 °C. IR (solid, cm^{-1}) 3370 (NH), 3283 (OH), 2964, 2944 (CH), 1723 (C=O). ^1H NMR (600 MHz, D_2O) 5.92 (1H, d, J = 5.7 Hz, H1'), 5.08 (1H, d, J = 5.7 Hz, H2'), 4.44 (1H, d, J = 2.4 Hz, H3'), 4.16 (1H, ddd, J = 7.0, 4.9, 2.4 Hz, H4'), 3.70 (1H, ABX, J = 12.4, 4.9 Hz, H5'), 3.60 (1H, ABX, J = 12.4, 6.0 Hz, H5''). ^{13}C NMR (151 MHz, D_2O) 160.1 (C2), 86.5 (C1'), 86.0 (C4'), 80.0 (C3'), 73.6 (C2'), 59.6 (C5'). HRMS (m/z) calculated for $C_6H_9NO_5$ $[M+H^+]^+$ 176.0559; found, 176.0558. $[\alpha]_D^{20.0}$ (*c* = 1.00, H_2O)– 55.5.

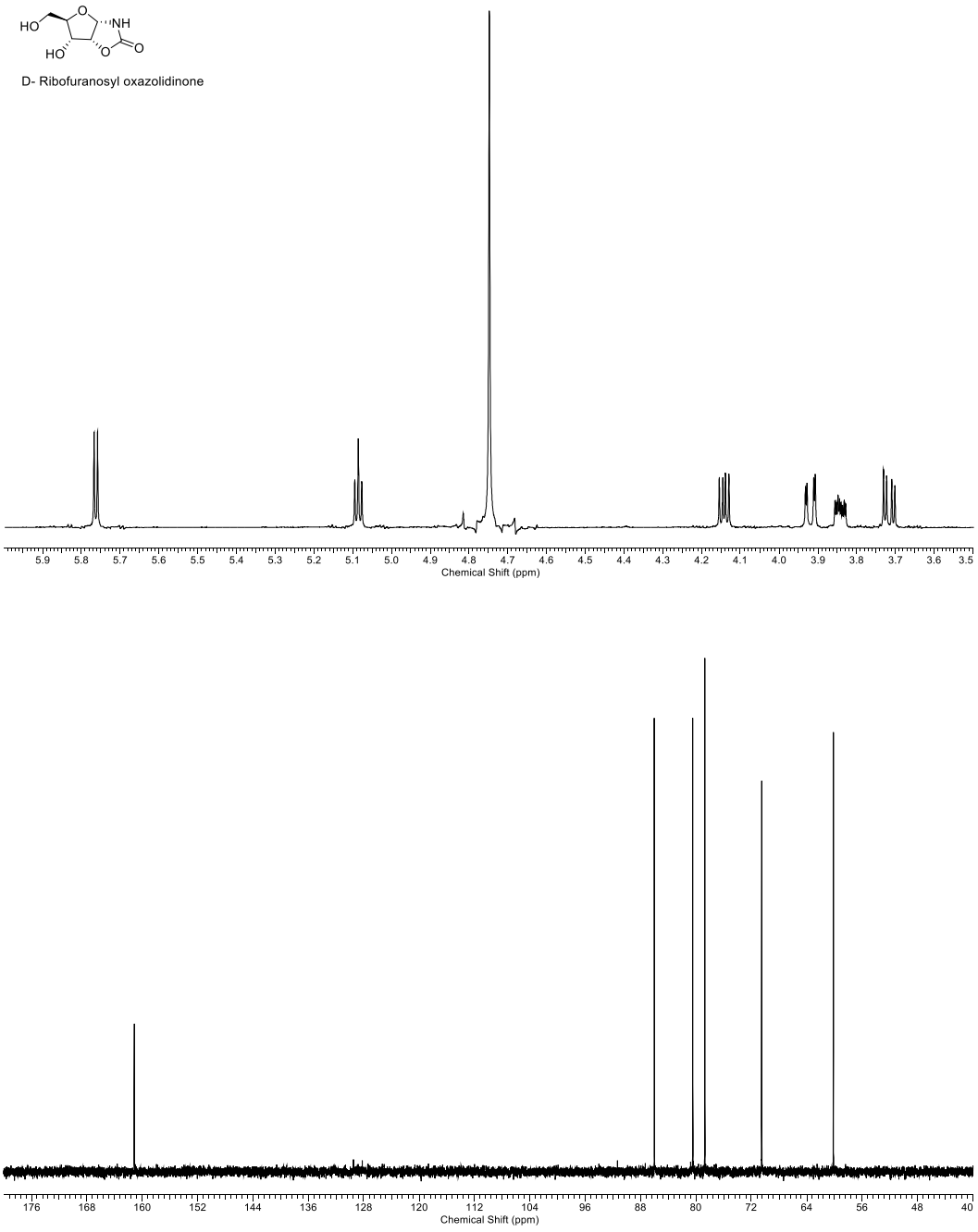

*Figure 122: ^{1}H NMR (600 MHz, D_2O, 3.5-6.0 ppm, Top) and ^{13}C NMR (151 MHz, D_2O, 40-180 ppm, Bottom) spectra of D- ribo oxazolidinone (**D-ROX**).*

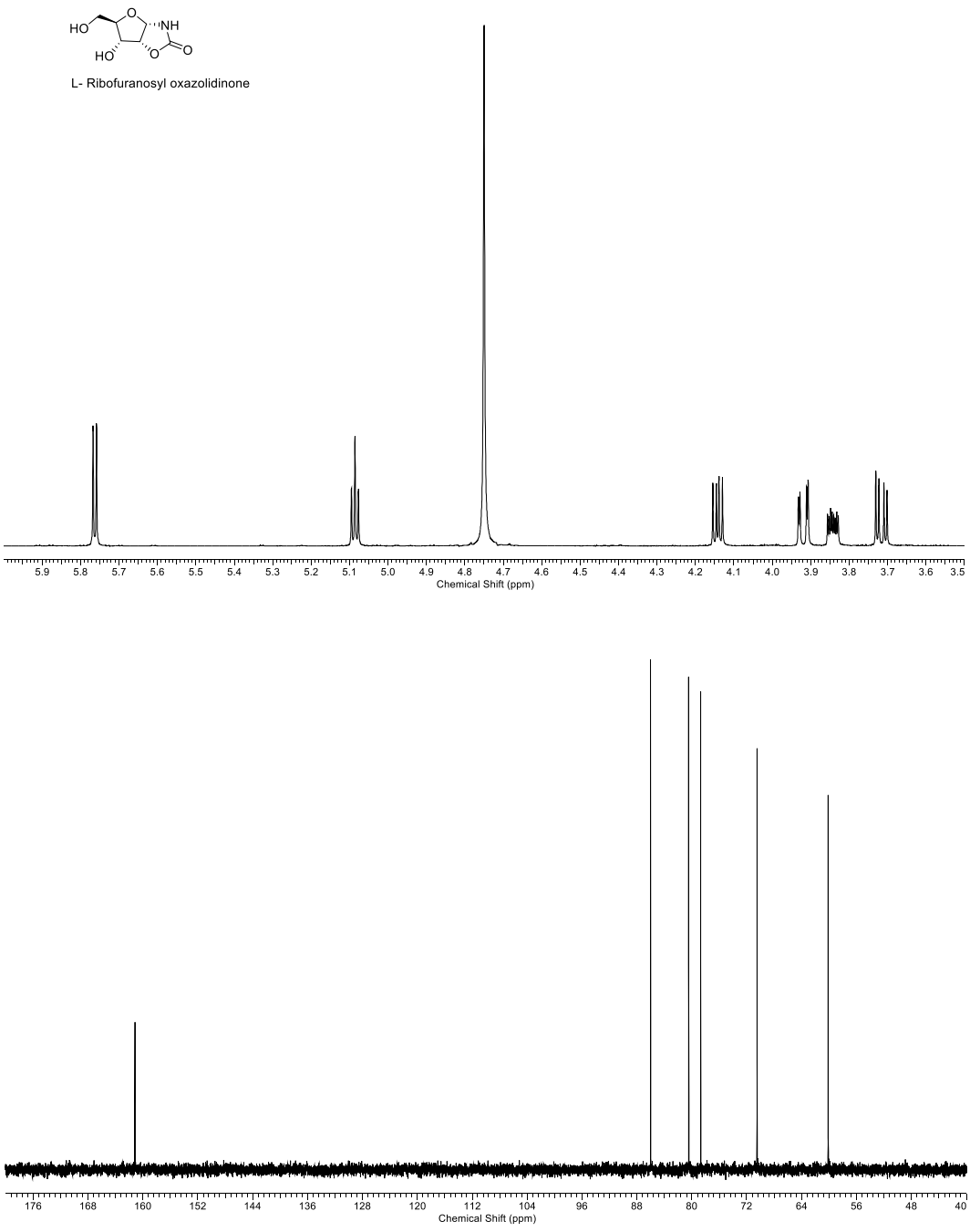

*Figure 123: ^{1}H NMR (600 MHz, D_2O, 3.5-6.0 ppm, Top) and ^{13}C NMR (151 MHz, D_2O, 40-180 ppm, Bottom) spectra of L- ribo oxazolidinone (**L-ROX**).*

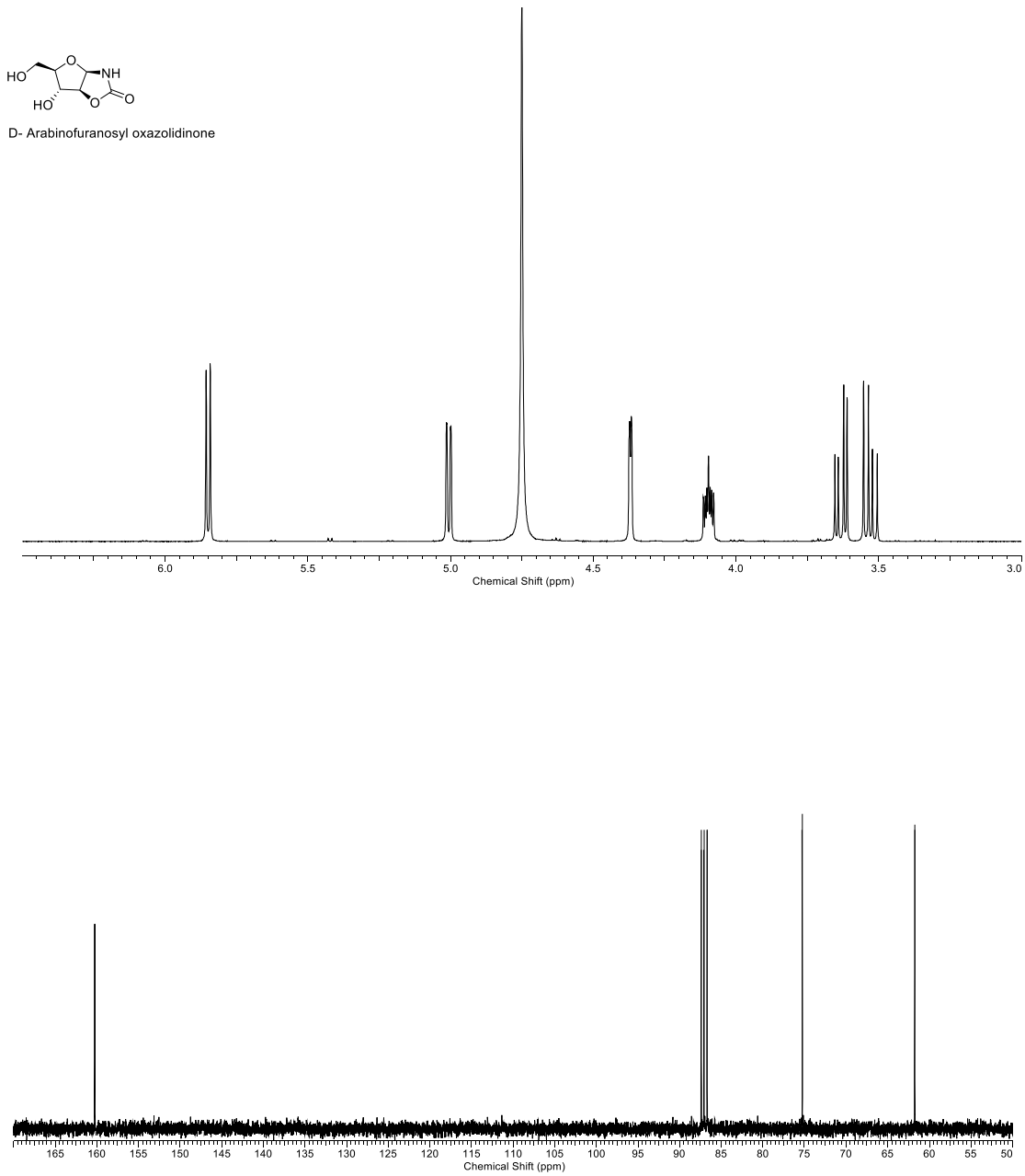

*Figure 124: ^{1}H NMR (600 MHz, D_2O, 3.0-6.5 ppm, Top) and ^{13}C NMR (151 MHz, D_2O, 50-170 ppm, Bottom) spectra of D- arabino oxazolidinone (**D-AOX**).*

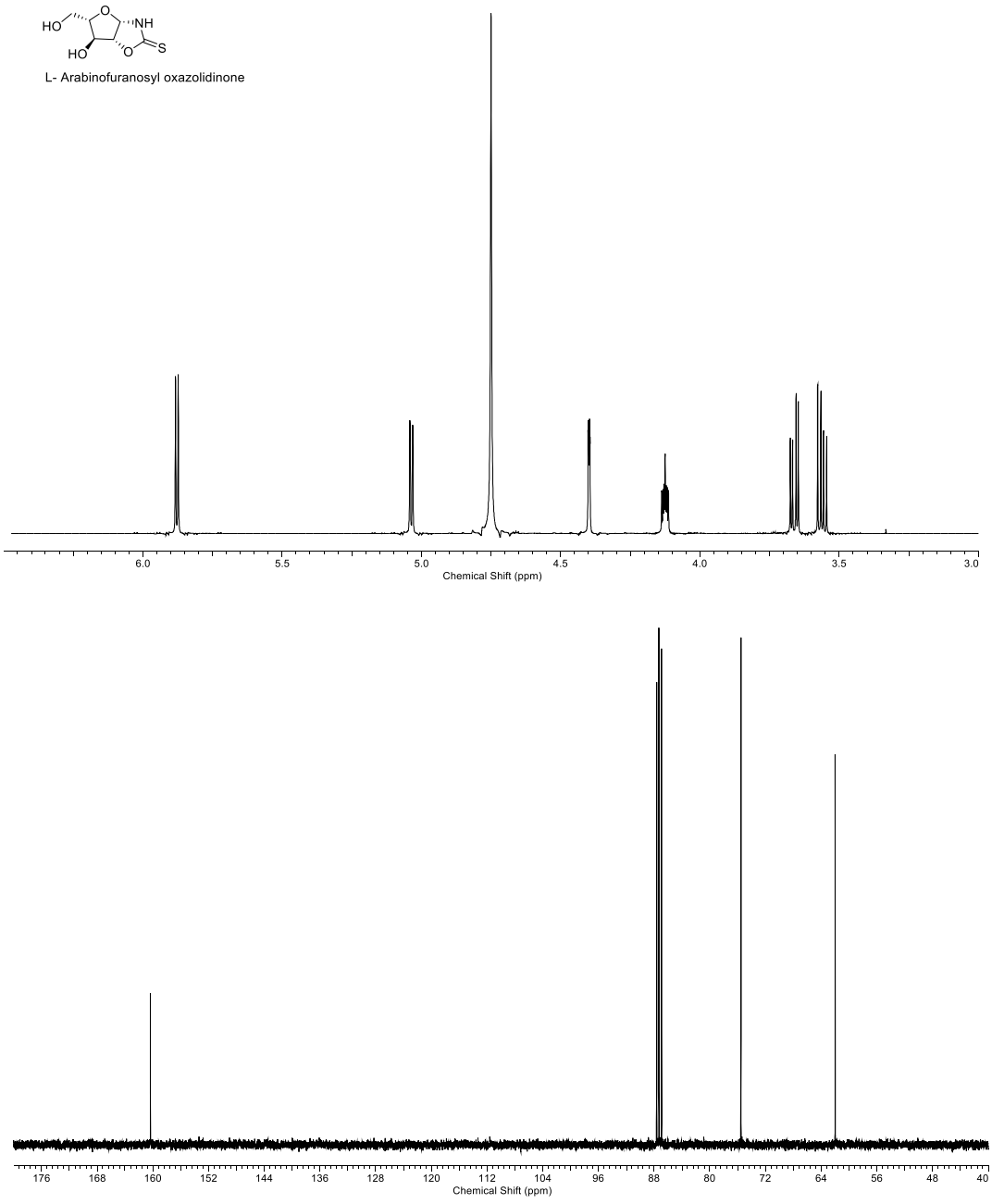

*Figure 125: ^{1}H NMR (600 MHz, D_2O, 3.0-6.5 ppm, Top) and ^{13}C NMR (151 MHz, D_2O, 50-180 ppm, Bottom) spectra of L- arabino oxazolidinone (**L-AOX**).*

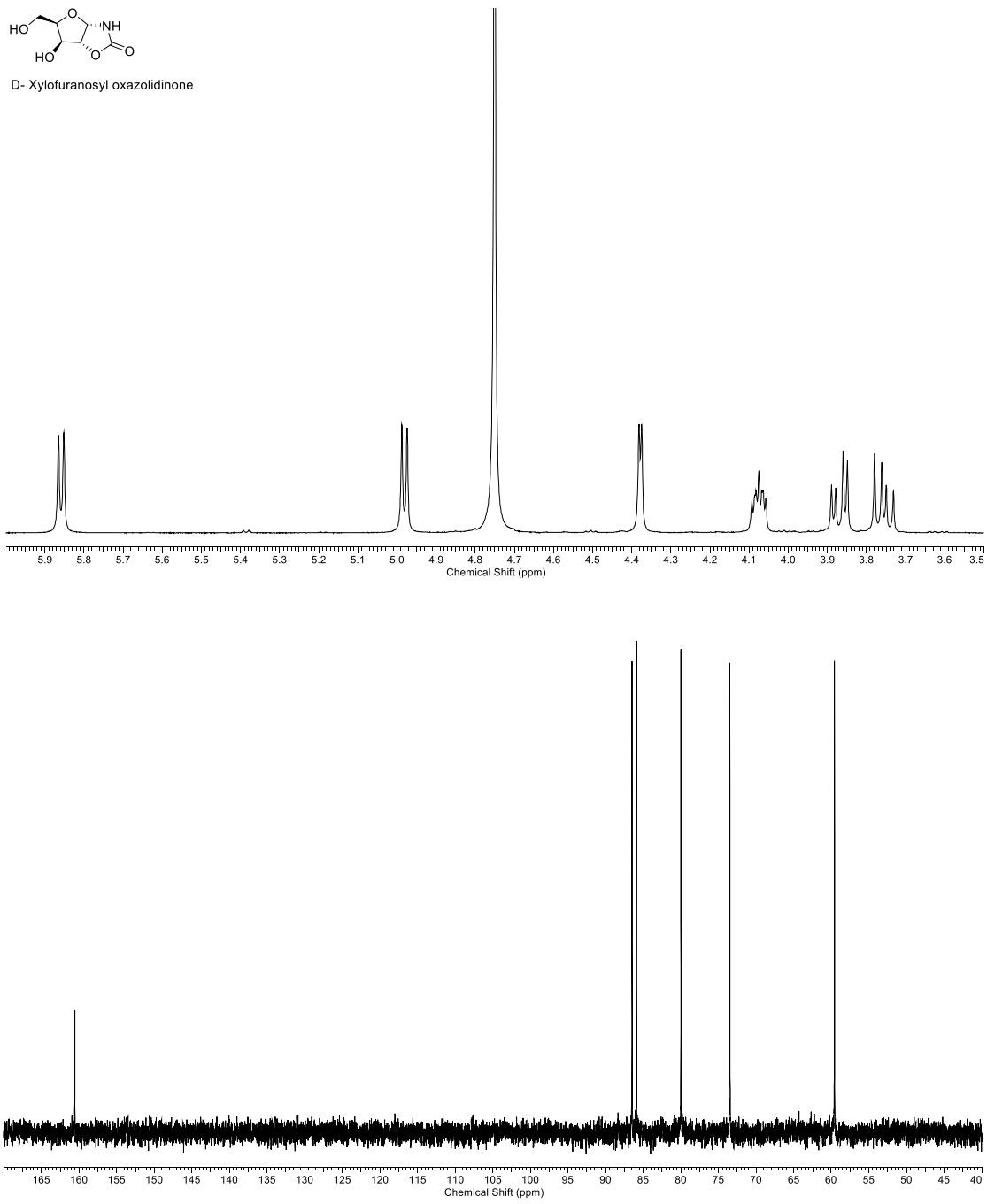

*Figure 126: ^{1}H NMR (600 MHz, D_2O, 3.5-6.0 ppm, Top) and ^{13}C NMR (151 MHz, D_2O, 40-170 ppm, Bottom) spectra of D- xylo oxazolidinone (**D-XOX**).*

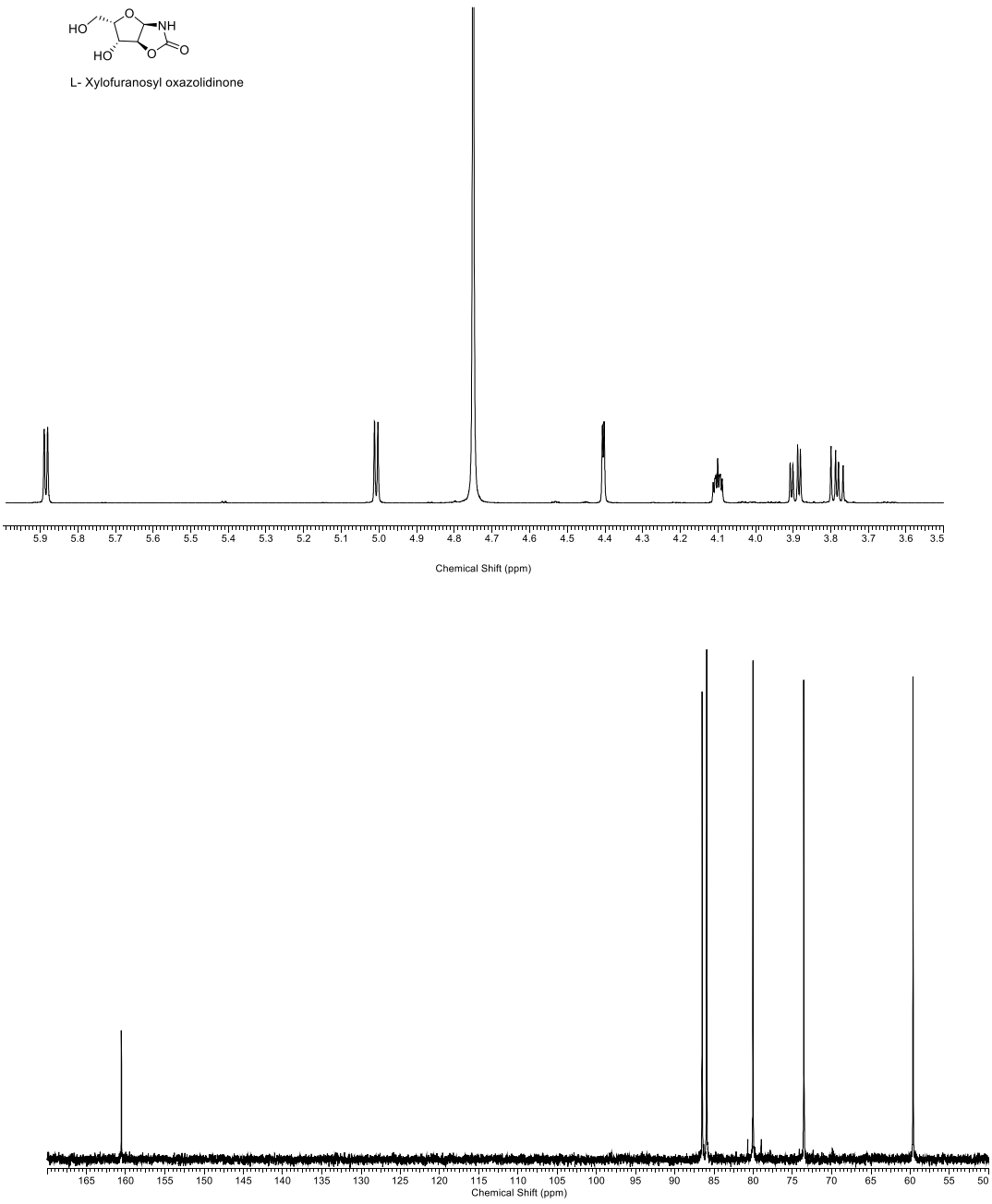

*Figure 127: ^{1}H NMR (600 MHz, D_2O, 3.5-6.0 ppm, Top) and ^{13}C NMR (151 MHz, D_2O, 50-170 ppm, Bottom) spectra of L- xylo oxazolidinone (**L-XOX**).*

6.5 Synthesis of Cyanoacetylene

6.5.1 Propiolamide

Liquid ammonia (150 mL) was cooled to -78 °C and methyl propiolate (19.7 g, 20.0 mL, 224 mmol) was added and stirred for 1h. The solution was then warmed to room temperature and co-evaporated with chloroform (100 mL), resulting in a white solid. This was then recrystallised with hot chloroform and left at -18 °C to give propiolamide (11.1 g, 72%) as colourless needles. M.p. 60-63 °C. ^{1}H NMR (600 MHz, D_2O) 3.48 (1H, s, H-(C3)).

6.5.2 Cyanoacetylene

Propiolamide (11.0 g, 159 mmol) and oven dried sand (30.0 g) were mixed together with a pestle and mortar. P_2O_5 (30.0 g, 211 mmol) was added and transferred to a dry flask under argon atmosphere. Cyanoacetylene was then distilled from this mixture at 130 °C and 100 torr over 1 h. A white solid (6.4 g, 79%) was collected at -78 °C. The solid was immediately dissolved in water (125 mL) to yield a 1 M aqueous solution of cyanoacetylene. ^{1}H NMR (600 MHz, D_2O) 3.46 (1H, s, H-(C3)). ^{13}C NMR (151 MHz, D_2O) 106.0 (C1), 78.3 (C3), 57.1 (C2).

6.6 General Synthesis of Pentose Cyanovinyl Oxazolidinone Thione (CVOT)

The synthetic protocol was followed as in Stairs et al.[64] oxazolidinone thione (**OT**, 660 mg, 3.46 mmol) was added to an aqueous solution of cyanoacetylene (**6**, 20 mL, 0.4 M, 9.80 mmol) and stirred at rt for 1 h. The resulting solution was lyophilized to yield the cyanovinyl oxazolidinone thione (**CVOT**) which was used without further purification.

6.6.1 D- (S-Z-cyanovinyl)-ribo oxazolidinone thione (D-RCVOT)

Starting from D-ribo oxazolidinone thione (**D-ROT**, 660 mg, 3.46 mmol) yielded D- (S-Z-cyanovinyl)-ribo oxazolidinone thione (**D-RCVOT**, 800 mg, 3.30 mmol, 95%). M.p. 190-193 °C. IR (solid, cm^{-1}) 3448 (OH), 3277, 2993, 2881 (CH), 2214 (C≡N), 1639(C=N), 1604(C=C). ^{1}H NMR (600 MHz, D_2O) 7.83 (1H, d, J=10.5 Hz, H4), 6.06 (1H, t, J=5.4 Hz, H1'), 5.95 (1H, J=10.5 Hz, H5), 5.17 (1H, t, J= 5.4 Hz, H2'), 4.22 (1H, dd, J=9.5, 5.4, H3'), 3.91 (1H, J=12.8, 2.3 Hz, H5'), 3.71 (1H, dd, J=12.8, 4.8 Hz, H5''), 3.56 (1H, ddd, J=9.5, 4.8, 2.3 Hz, H4'). ^{13}C NMR (151 MHz, D_2O) 168.3 (C2), 143.8 (C5), 116.1 (C6), 100.4 (C4), 99.0 (C1'), 84.8 (C2'), 79.0 (C4'), 71.0 (C3'), 60.0 (C5'). $[\alpha]_D^{20.0}$ (*c* = 1.00, H_2O) 90.1

6.6.2 L- (S-Z-cyanovinyl)-ribo oxazolidinone thione (L-RCVOT)

Starting from L-ribo oxazolidinone thione (**L-ROT**, 660 mg, 3.46 mmol) yielded L- (S-Z-cyanovinyl)-ribo oxazolidinone thione (**D-RCVOT** 780 mg, 3.22 mmol, 93%). M.p. 184-190 °C. IR (solid, cm^{-1}) 3388 (OH), 3104, 2963, 2832 (CH), 2218 (C≡N), 1653(C=N), 1599(C=C). ^{1}H NMR (600 MHz, D_2O) 7.82 (1H, d, J = 10.4 Hz, H4), 6.05 (1H, t, J = 5.4 Hz, H1'), 5.94 (1H, J = 10.4 Hz, H5), 5.16 (1H, t, J = 5.4 Hz, H2'), 4.21 (1H, dd, J = 9.4, 5.4, H3'), 3.90 (1H, J = 12.8, 2.4 Hz, H5'), 3.70 (1H, dd, J = 12.8, 4.7 Hz, H5''), 3.56 (1H, ddd, J = 9.5, 4.7, 2.4 Hz, H4'). ^{13}C NMR (151 MHz, D_2O) 168.4 (C2), 144.0 (C5), 116.1 (C6), 100.5 (C4), 99.0 (C1'), 85.1 (C2'), 79.2 (C4'), 71.2 (C3'), 60.3 (C5'). $[\alpha]_D^{20.0}$ (*c* = 1.00, H_2O) -91.4

6.6.3 D- (S-Z-cyanovinyl)-arabino oxazolidinone thione (D-ACVOT)

BM615 Starting from D-arabino oxazolidinone thione (**D-AOT**, 660 mg, 3.46 mmol) yielded D-(S-Z-cyanovinyl)-arabino oxazolidinone thione (**D-ACVOT**,820 mg, 3.90 mmol, 98%). M.p. 200–207 °C. IR (solid, cm^{1}) 3370 (OH), 3056 (CH), 2,196 (C≡N), 1,601 (C=N), 1,597 (C=C). ^{1}H NMR (600 MHz, D_2O) 7.79 (1H, d, J=10.5 Hz, H4), 6.13 (1H, d, J=6 Hz, H1'), 5.94 (1H, d, J=10.5 Hz,

H5), 5.15 (1H, d, J=5.9 Hz, H2'), 4.37 (1H, m, H3'), 4.09 (1H, m, H4'), 3.57 (1H, ABX, J=12.4, 4.7 Hz, H5'), 3.48 (1H, ABX, J=12.4, 6.3 Hz, H5''). ^{13}C NMR (151 MHz, D_2O) 177.2 (C2), 143.5 (C5), 115.2 (C6), 100.3 (C4, C1'), 91.5 (C2'), 86.4 (C4'), 76 (C3'), 61.5 (C5'). $[\alpha]_D^{20.0}$ (*c* = 1.00, H_2O) 22.1.

6.6.4 L- (S-Z-cyanovinyl)-arabino oxazolidinone thione (L-ACVOT)

BM616 Starting from L-arabino oxazolidinone thione (**L-AOT**, 660 mg, 3.46 mmol) yielded L-(S-Z-cyanovinyl)-arabino oxazolidinone thione (**L-ACVOT**, 825 mg, 3.30 mmol, 99%). M.p. 204–210 °C. IR (solid, cm ^{1}) 3372 (OH), 3068, 3056, 2956 (CH), 2212 (C≡N), 1601 (C=N). ^{1}H NMR (600 MHz, D_2O) 7.80 (1H, d, J=10.5 Hz, H4), 6.13 (1H, d, J=6 Hz, H1'), 5.93 (1H, d, J=10.5 Hz, H5), 5.17 (1H, d, J=6 Hz, H2'), 4.40 (1H, m, H3'), 4.10 (1H, m, H4'), 3.60 (1H, ABX, J=12.3, 4.4 Hz, H5'), 3.54 (1H, ABX, J=12.3, 6.3 Hz, H5''). ^{13}C NMR (151 MHz, D_2O) 176.9 (C2), 143.6 (C5), 114.1 (C6), 100.4 (C4, C1'), 91.6 (C2'), 86.5 (C4'), 76.1 (C3'), 61.6 (C5'). $[\alpha]_D^{20.0}$ (*c* = 1.00, H_2O) 21.8.

6.6.5 D- (S-Z-cyanovinyl)-xylo oxazolidinone thione (D-XCVOT)

Starting from D-xylo oxazolidinone thione (**D-XOT**, 660 mg, 3.46 mmol) yielded L- (S-Z-cyanovinyl)-xylo oxazolidinone thione (**D-XCVOT**, 794 mg, 3.28 mmol, 95%). M.p.175-178 °C. IR (solid, cm^{-1}) 3448 (OH), 3277, 2993, 2881 (CH), 2214 (C≡N), 1639(C=N), 1604(C=C). ^{1}H NMR (600 MHz, D2O) 7.78 (1H, d, J = 10.3 Hz, H4), 6.18 (1H, t, J = 5.3 Hz, H1'), 5.92 (1H, J = 10.3 Hz, H5), 5.08 (1H, d, J = 5.3 Hz, H2'), 4.41 (1H, d, J = 2.3, H3'), 3.88 (1H, ddd, J = 7.3, 2.3, 0.4 Hz, H5'), 3.71 (1H, m, H5''). $[\alpha]_D^{20.0}$ (*c* = 1.00, H_2O) - 36.3.

6.6.6 L- (S-Z-cyanovinyl)-xylo oxazolidinone thione (L-XCVOT)

Starting from L-xylo oxazolidinone thione (**L-XOT**, 660 mg, 3.46 mmol) yielded L- (S-Z-cyanovinyl)-xylo oxazolidinone thione (**L-XCVOT**,820 mg, 3.38 mmol, 98%). M.p. °C. IR (solid, cm-1) 3448 (OH), 3277, 2993, 2881 (CH), 2214 (C≡N), 1639(C=N), 1604(C=C). ^{1}H NMR (600 MHz, D_2O) 7.78 (1H, d, J = 10.5 Hz, H4), 6.18 (1H, t, J = 5.5 Hz, H1'), 5.93 (1H, J = 10.5 Hz, H5), 5.08 (1H, dd, J = 5.4, 0.4 Hz, H2'), 4.41 (1H, d, J = 2.6, H3'), 3.88 (1H, ddd, J = 7.3, 2.6, 0.4 Hz, H5'), 3.71 (1H, dd, J = 12.8, 4.8 Hz, H5''), 3.56 (1H, ddd, J = 9.5, 4.8, 2.3 Hz, H4'). ^{13}C NMR (151 MHz, D_2O) 167.5 (C2), 143.7 (C5), 116.0 (C6), 100.4 (C4), 99.4 (C1'), 89.8 (C2'), 80.4 (C4'), 73.8 (C3'), 59.6 (C5'). $[\alpha]_D^{20.0}$ (*c* = 1.00, H_2O) 35.6.

6.7 General Synthesis of Pentose (2-thiomethyl)-oxazolidinone (MOT)

The synthetic protocol was followed as in Stairs et al. Oxazolidinone thione (**OT**, 2.50 g, 13.0 mmol), methyl iodide (1.84 g, 14.7 mmol) and NaOH (0.59 g, 14.7 mmol) was stirred at room temperature for 30 minutes in EtOH (100 mL) and H_2O (50 mL). The resulting solution was concentrated and purified by silica gel FCC eluting with $CHCl_3$/ MeOH (9:1) resulting in a white solid. The solid was recrystallised with EtOAc/Pet Ether to yield large plate like crystals.

6.7.1 D-ribo (2-thiomethyl)-oxazolidinone (D-RMOT)

Starting from D-ribo oxazolidinone thione (**D-ROT** 2.50 g, 13.0 mmol) yielded D-ribo (2-thiomethyl)-oxazolidinone (**D-RMOT**; 2.08 g, 78%). M.p. 76-83 ^{o}C ^{1}H NMR (600 MHz, D_2O) 5.95 (1H, d, J = 5.4 Hz, H1'), 5.05 (1H, t, J = 5.4Hz, H2'), 4.15 (1H, dd, J = 9.5, 5.4 Hz, H3'), 3.89 (1H, ABX, J = 12.8, 2.3 Hz, H5'), 3.69 (1H, ABX, J = 12.8, 4.7 Hz, H5''), 3.51 (1H, ddd, J = 9.5, 4.7, 2.3 Hz, H4'), 2.48 (3H, s, CH_3). ^{13}C NMR (151 MHz, D_2O) 175.6 (C2), 98.8 (C1'), 84.0 (C2'), 78.7 (C4'),

71.1 (C3'), 60.1 (C5'), 14.5 (C4). HRMS (m/z) calculated for $C_7H_{12}NO_4S$ $[M+H^+]^+$, 206.0487; found, 206.0481. $[\alpha]_D^{20.0}$ (*c* = 1.00, H_2O) 35.2.

6.7.2 L-ribo (2-thiomethyl)-oxazolidinone (L-RMOT)

Starting from L-ribo oxazolidinone thione (**L-ROT**,2.50 g, 13.0 mmol) yielded L-ribo (2-thiomethyl)-oxazolidinone (**L-RMOT**; 1.66 g, 62%). M.p. 78-86 °C. ^{1}H NMR (600 MHz, D_2O) 5.95 (1H, d, J = 5.3 Hz, H1'), 5.05 (1H, t, J = 5.4Hz, H2'), 4.15 (1H, dd, J = 9.5, 5.6 Hz, H3'), 3.89 (1H, ABX, J = 12.7, 2.1 Hz, H5'), 3.69 (1H, ABX, J = 12.8, 4.6 Hz, H5''), 3.51 (1H, ddd, J = 9.5, 4.6, 2.1 Hz, H4'), 2.49 (3H, s, CH_3). ^{13}C NMR (151 MHz, D_2O) 175.5 (C2), 98.8 (C1'), 84.1 (C2'), 78.7 (C4'), 71.2 (C3'), 60.2 (C5'), 14.5 (C4). HRMS (m/z) calculated for $C_7H_{12}NO_4S$ $[M+H^+]^+$, 206.0487; found, 206.0475. $[\alpha]_D^{20.0}$ (*c* = 1.00, H_2O) -34.9.

6.7.3 D-arabino (2-thiomethyl)-oxazolidinone (D-AMOT)

Starting from D-arabino oxazolidinone thione (**D-AOT**, 2.50 g, 13.0 mmol) yielded D-arabino (2-thiomethyl)-oxazolidinone thione (**D-AMOT**; 1.45 g, 54%). M.p. 80–84 °C. IR (solid, cm^{-1}) 3285 (OH), 2889 (CH), 1579 (C=N). ^{1}H NMR (600 MHz, D_2O) 5.99 (1H, d, J = 5.9 Hz, H1'), 4.98 (1H, dd, J = 5.9, 1 Hz, H2'), 4.27 (1H, dd, J = 3.2, 1 Hz, H3'), 4.00 (1H, ddd, J = 6.7, 5.2, 3.2 Hz, H4'), 3.47 (1H, ABX, J = 12.2, 5.2 Hz, H5'), 3.40 (1H, ABX, J = 12.2, 6.7 Hz, H5''), 2.40 (3H, s, CH_3). ^{13}C NMR (151 MHz, D_2O) 174.5 (C2), 100.2 (C1'), 90.9 (C2'), 86.2 (C4'), 77.3 (C3'), 62.0 (C5'), 14.3 (C4). $[\alpha]_D^{20.0}$ (*c* = 1.00, H_2O) - 9.1.

6.7.4 L-arabino (2-thiomethyl)-oxazolidinone (L-AMOT)

Starting from L-arabino oxazolidinone thione (**L-AOT**, 2.50 g, 13.0 mmol) yielded L-arabino (2-thiomethyl)-oxazolidinone thione (**L-AMOT**; 1.69g, 63%). M.p. 79–86 °C. IR (solid, cm^{-1}) 3301

(OH), 2797 (CH), 1579 (C=N). ^{1}H NMR (600 MHz, D_2O) 6.00 (1H, d, J = 5.9 Hz, H1'), 4.99 (1H, dd, J = 5.9, 0.9 Hz, H2'), 4.27 (1H, m, H3'), 4.00 (1H, ddd, J = 7.0, 5.1, 3.2 Hz, H4'), 3.48 (1H, ABX, J = 12.1, 5.1 Hz, H5'), 3.39 (1H, ABX, J = 12.1, 7.0 Hz, H5''), 2.51 (3H, s, CH_3). ^{13}C NMR (151 MHz, D_2O) 174.5 (C2), 100.2 (C1'), 90.9 (C2'), 86.2 (C4'), 76.1 (C3'), 61.7 (C5'), 14.2 (C4). $[\alpha]_D^{20.0}$ (*c* = 1.00, H_2O) 9.1.

6.7.5 D-xylo (2-thiomethyl)-oxazolidinone (D-XMOT)

Starting from D-xylo oxazolidinone thione (**D-XOT**,2.50 g, 13.0 mmol) yielded D-xylo (2-thiomethyl)-oxazolidinone thione (**D-XMOT**, 1.45 g, 54%). M.p. 81–84 °C. IR (solid, cm^{-1}) 3280 (OH), 2900 (CH), 1602 (C=N). ^{1}H NMR (600 MHz, D_2O) 6.08 (1H, d, J = 5.4 Hz, H1'), 4.97 (1H, d, J = 5.4 Hz, H2'), 4.35 (1H, m, H4'), 4.00 (1H, m, H3'), 3.47 (1H, m H5''), 3.40 (1H, m, H4'), 2.46 (3H, s, CH_3). ^{13}C NMR (151 MHz, D_2O) 174.6 (C2), 99.2 (C1'), 89.2 (C2'), 80.0 (C4'), 74.0 (C3'), 59.6 (C5'), 14.2 (C4). $[\alpha]_D^{20.0}$ (*c* = 1.00, H_2O) 4.3.

6.7.6 L-xylo (2-thiomethyl)-oxazolidinone

Starting from D-xylo oxazolidinone thione (**D-XOT**, 2.50 g, 13.0 mmol) yielded D-arabino (2-thiomethyl)-oxazolidinone thione (**D-XMOT**; 1.45 g, 54%). M.p. 77–82 °C. IR (solid, cm^{-1}) 3286 (OH), 2896 (CH), 1597 (C=N). ^{1}H NMR (600 MHz, D_2O) 6.09 (1H, d, J = 5.4 Hz, H1'), 4.97 (1H, d, J = 5.4, 1 Hz, H2'), 4.35 (1H, d, J = 2.00 Hz, H3'), 3.86 (1H, m, H4'), 3.76 (1H, m, H5'), 3.40 (1H, ABX, J = 12.2, 6.7 Hz, H5''), 2.46 (3H, s, CH_3). ^{13}C NMR (151 MHz, D_2O) 174.6 (C2), 99.2 (C1'), 89.2 (C2'), 80.0 (C4'), 73.9 (C3'), 59.6 (C5'), 14.3 (C4), 14.3. $[\alpha]_D^{20.0}$ (*c* = 1.00, H_2O) - 4.2.

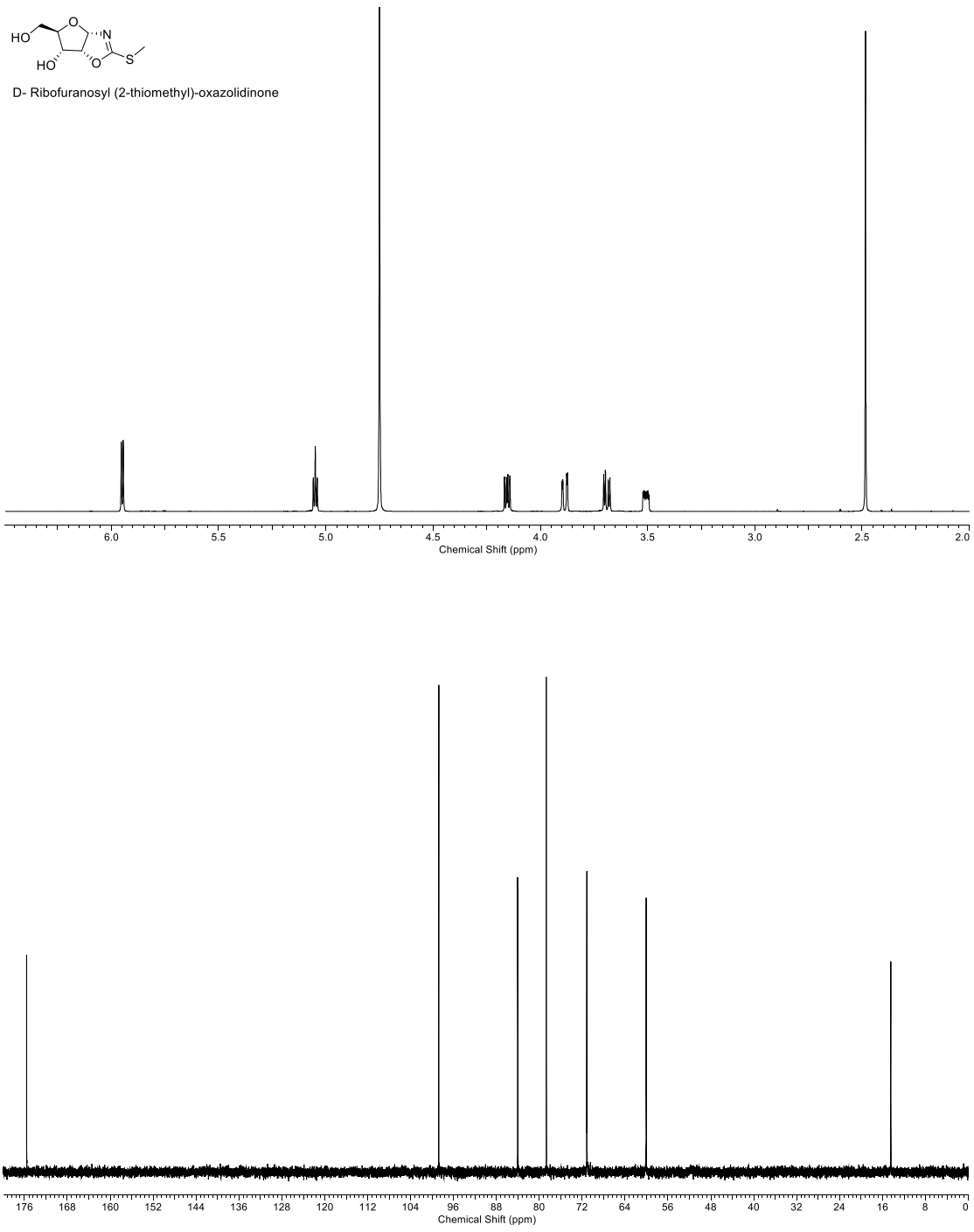

*Figure 128: ^{1}H NMR (600 MHz, D_2O, 2.0-6.5 ppm, Top) and ^{13}C NMR (151 MHz, D_2O, 0-180 ppm, Bottom) spectra of D- ribo (2-thiomethyl)-oxazolidinone (**D-RMOT**).*

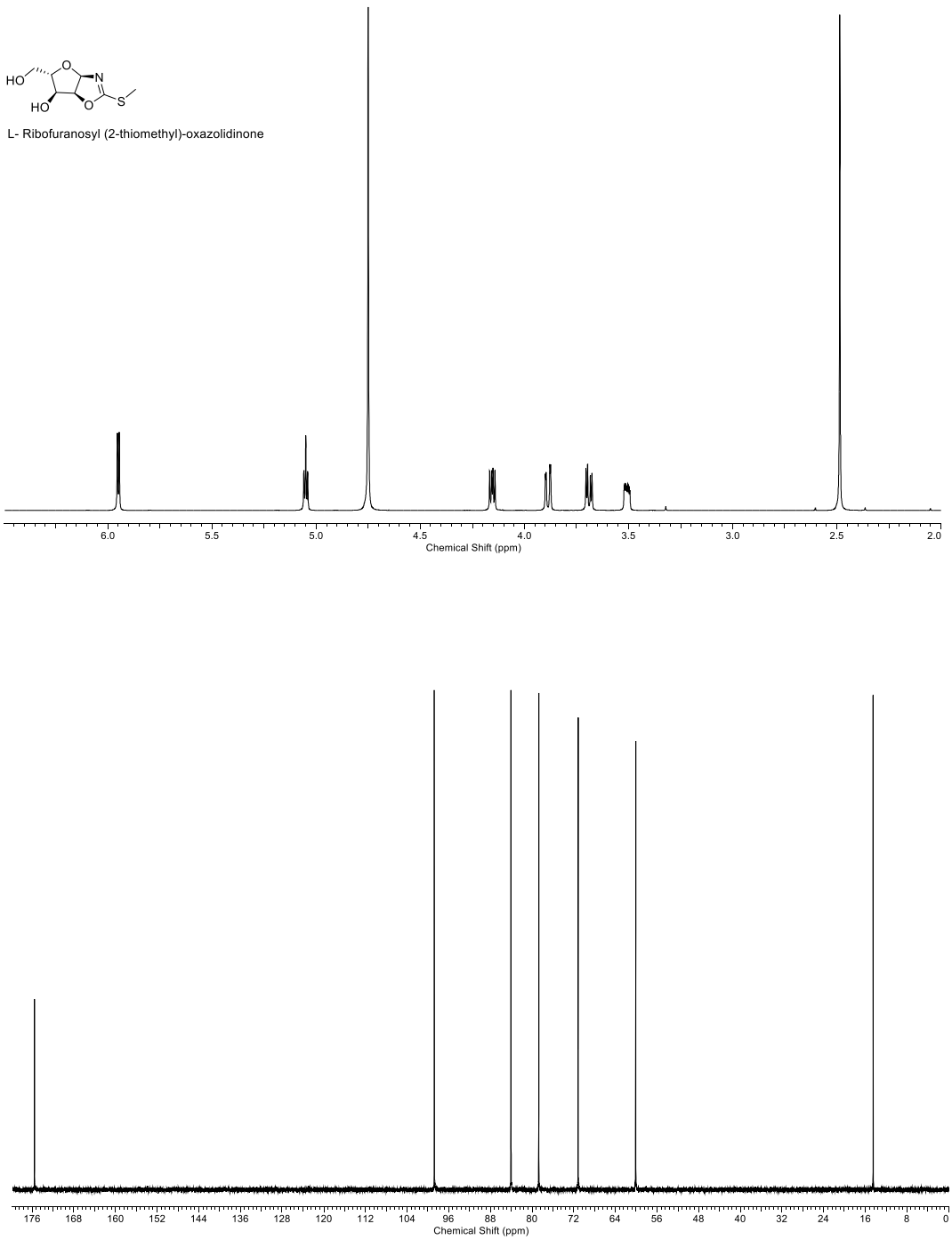

*Figure 129: ^{1}H NMR (600 MHz, D_2O, 2.0-6.5 ppm, Top) and ^{13}C NMR (151 MHz, D_2O, 0-180 ppm, Bottom) spectra of L- ribo (2-thiomethyl)-oxazolidinone (**L-RMOT**).*

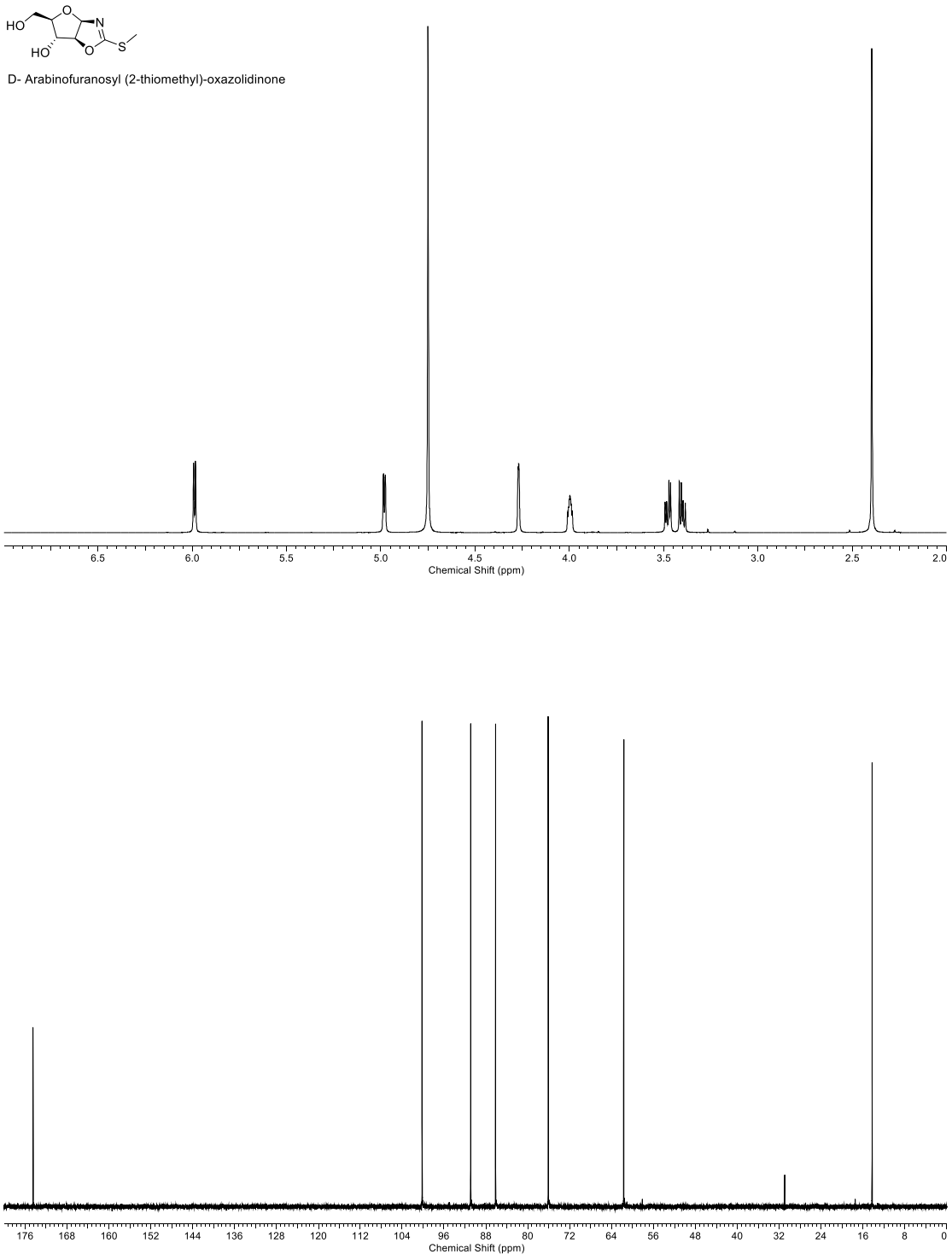

*Figure 130: ^{1}H NMR (600 MHz, D_2O, 2.0-7.0 ppm, Top) and ^{13}C NMR (151 MHz, D_2O, 0-180 ppm, Bottom) spectra of D- arabino (2-thiomethyl)-oxazolidinone (**D-AMOT**).*

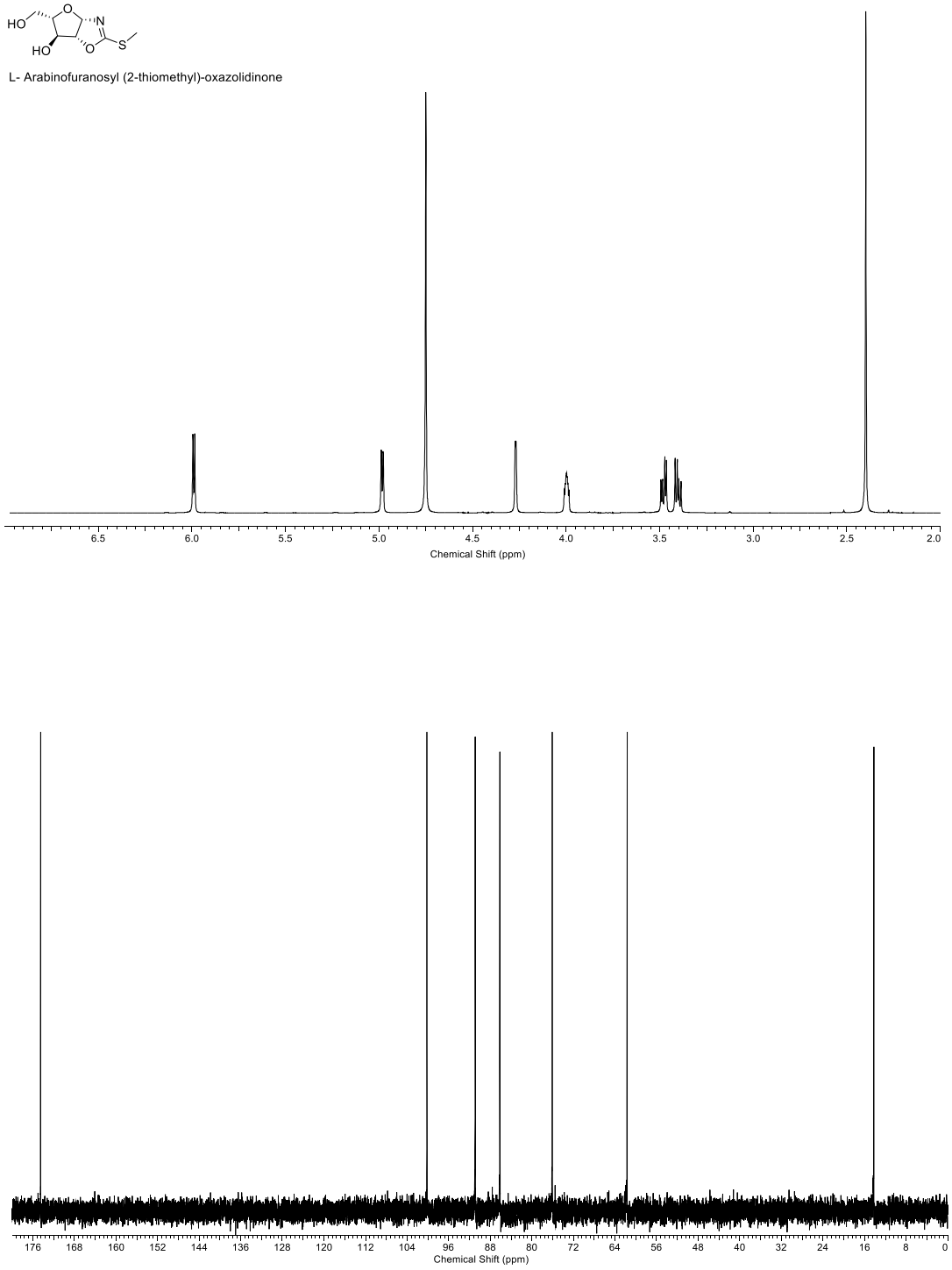

*Figure 131: ^{1}H NMR (600 MHz, D_2O, 2.0-7.0 ppm, Top) and ^{13}C NMR (151 MHz, D_2O, 0-180 ppm, Bottom) spectra of L- arabino (2-thiomethyl)-oxazolidinone (**L-AMOT**).*

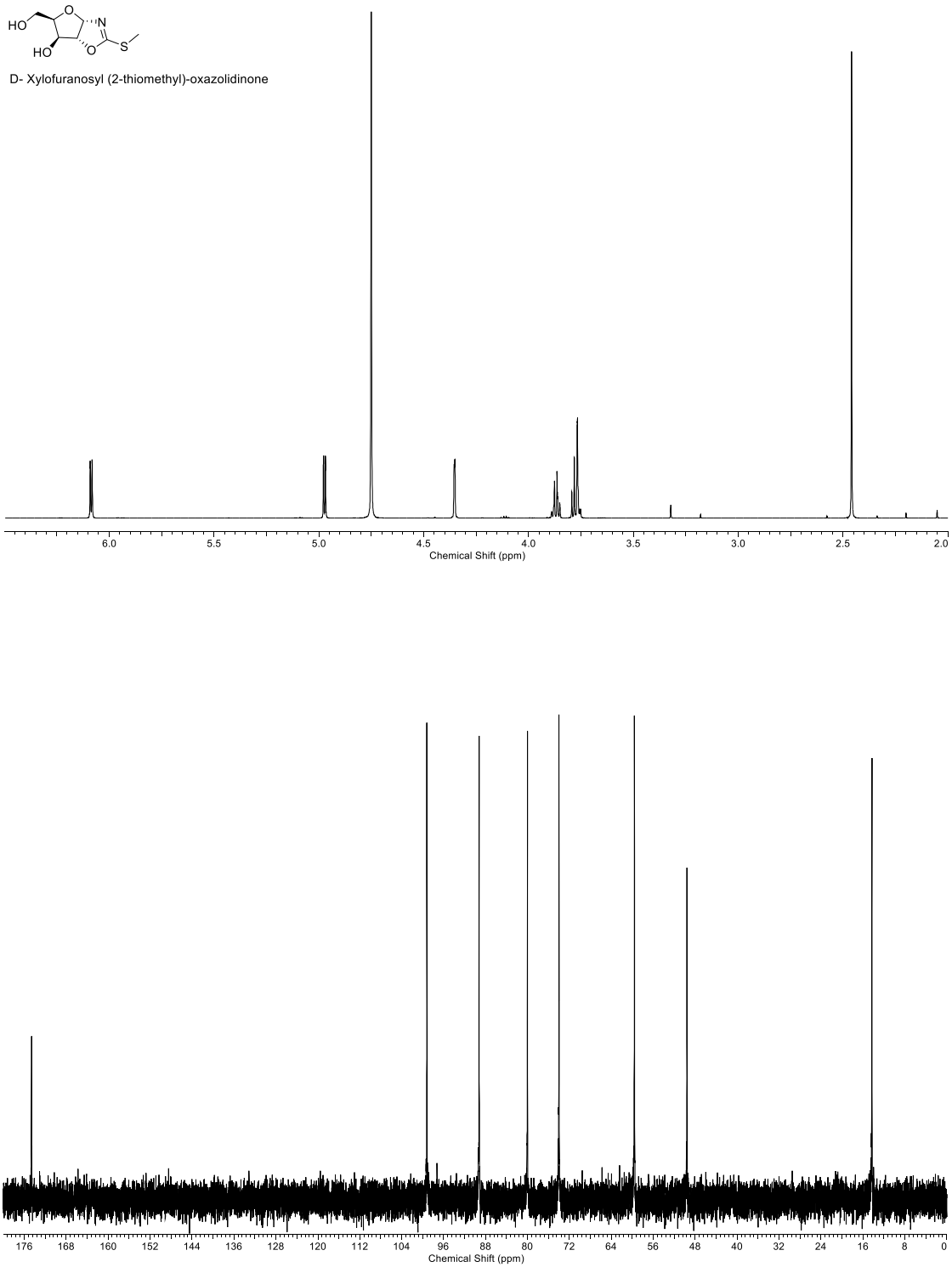

*Figure 132: ^{1}H NMR (600 MHz, D_2O, 2.0-6.5 ppm, Top) and ^{13}C NMR (151 MHz, D_2O, 0-180 ppm, Bottom) spectra of D- xylo (2-thiomethyl)-oxazolidinone (**D-XMOT**).*

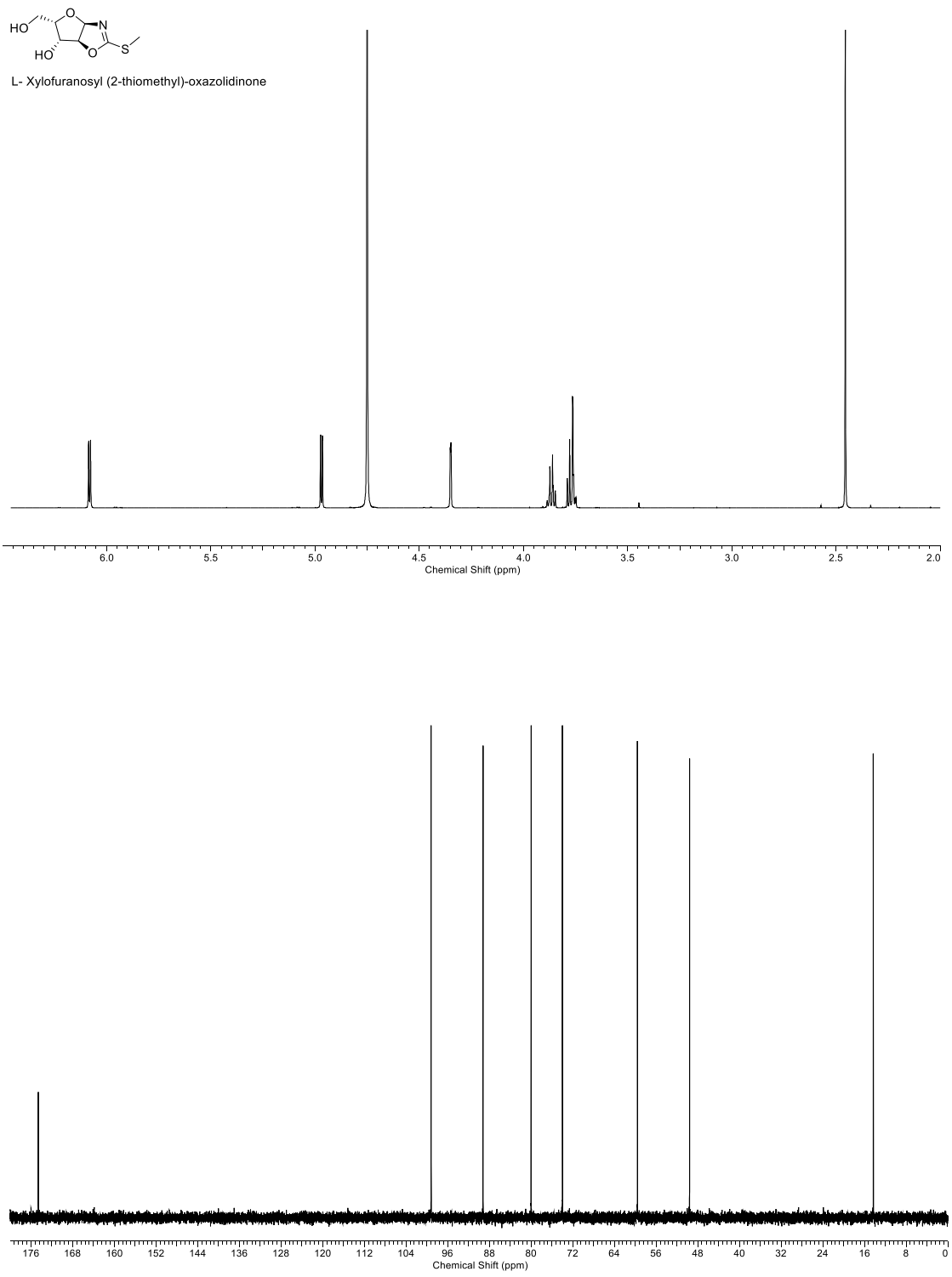

*Figure 133: ^{1}H NMR (600 MHz, D_2O, 2.0-6.5 ppm, Top) and ^{13}C NMR (151 MHz, D_2O, 0-180 ppm, Bottom) spectra of L- xylo (2-thiomethyl)-oxazolidinone (**L-XMOT**).*

6.8 General Synthesis of Pentose N-cyanoethyl Oxazolidinone Thiones (CEOT)

Oxazolidinone thione (**OT**, 500 mg, 2.60 mmol), acrylonitrile (2.68 mL, 26.00 mmol), H_2NaPO_4 (2.40 g, 20.0 mmol) was dissolved in water (28.0 mL) and stirred at pH 9 overnight. The solution was then lyophilised and purified with flash column chromatography eluting with EtOAc/ MeOH (9:1) to yield the product N-cyanoethyl oxazolidinone thione.

6.8.1 D-ribo N-cyanoethyl oxazolidinone thione (D-RCEOT)

Starting from D-*ribo* oxazolidinone thione (**D-ROT**, 500 mg, 2.60 mmol) yielded D-*ribo* N cyanoethyl oxazolidinone thione (**D-RCEOT**; 591 mg, 93%). IR (solid, cm^{-1}) 3280 (OH), 3002, 2970, 2919 (CH), 2245 (C≡N), 1500 (C=S). ^1H (600 MHz, D_2O) 5.98 (1H, d, J = 5.6 Hz, H1'), 5.20 (1H, t, J = 5.6 Hz, H2'), 4.24 (1H, dd, J=9.3, 5.6 Hz, H3'), 4.12 (2H, m, H4'), 3.92 (2H,m, H5), 3.73 (2H, m, H4), 3.00 (2H, m, H5''). ^{13}C NMR (151 MHz, D_2O) 189.8 (C2), 120.0 (C6), 92.6 (C1'), 82.2 (C4'), 79.7 (C2'), 71.0 (C3'), 60.0 (C5'), 42.7 (C4), 16.8 (C5). $[\alpha]_D^{20.0}$ (*c* = 1.00, H_2O) 45.5.

6.8.2 L-ribo N-cyanoethyl oxazolidinone (L-CEOT)

Starting from L-*ribo* oxazolidinone thione (**L-ROT**, 500 mg, 2.60 mmol) yielded D-*ribo* N cyanoethyl oxazolidinone thione (**L-RCEOT**; 611 mg, 96%). IR (solid, cm^{-1}) 3292 (OH), 3011, 2984, 2895 (CH), 2223 (C≡N), 1510 (C=S). ^1H (600 MHz, D_2O) 5.98 (1H, d, J = 5.5 Hz, H1'), 5.19 (1H, t, J = 5.5 Hz, H2'), 4.24 (1H, dd, J=9.3, 5.5 Hz, H3'), 4.13 (2H, m, H4'), 3.91 (2H,m, H5), 3.72 (2H, m, H4), 3.00 (2H, m, H5''). ^{13}C NMR (151 MHz, D_2O) 189.8 (C2), 120.1 (C6), 92.7 (C1'), 82.2 (C4'), 79.6 (C2'), 70.9 (C3'), 59.9 (C5'), 42.6 (C4), 16.7 (C5). $[\alpha]_D^{20.0}$ (*c* = 1.00, H_2O) -46.9.

6.8.3 D-arabino N-cyanoethyl oxazolidinone thione (D-ACEOT)

Starting from D-*arabino* oxazolidinone thione (**D-AOT**, 500 mg, 2.60 mmol) yielded D-*arabino* N cyanoethyl oxazolidinone thione (**D-ACEOT**; 607 mg, 96%). IR (solid, cm^{-1}) 3290 (OH), 3022, 3009, 2994 (CH), 2263 (C≡N), 1542 (C=S). ^{1}H (600 MHz, D_2O) 5.98 (1H, d, J = 5.6 Hz, H1'), 5.20 (1H, t, J = 5.6 Hz, H2'), 4.24 (1H, dd, J=9.3, 5.6 Hz, H3'), 4.12 (2H, m, H4'), 3.92 (2H,m, H5), 3.73 (2H, m, H4), 3.00 (2H, m, H5''). ^{13}C NMR (151 MHz, D_2O) 188.7 (C2), 120.1 (C6), 93.9 (C1'), 89.2 (C4'), 88.4 (C2'), 75.6 (C3'), 61.7 (C5'), 42.7 (C4), 16.5 (C5). $[\alpha]_D^{20.0}$ (*c* = 1.00, H_2O) 28.7.

6.8.4 L-arabino N-cyanoethyl oxazolidinone thione (L-ACEOT)

Starting from D-*arabino* oxazolidinone thione (**L-AOT**, 500 mg, 2.60 mmol) yielded D-*arabino* N cyanoethyl oxazolidinone thione (**L-ACEOT**; 614 mg, 97%). IR (solid, cm^{-1}) 3305 (OH), 3007, 2999, 2992 (CH), 2273 (C≡N), 1552 (C=S). ^{1}H (600 MHz, D_2O) 5.99 (1H, d, J = 5.7 Hz, H1'), 5.20 (1H, d, J = 5.7 Hz, H2'), 4.34 (1H, m, H3'), 4.26 (1H, ddd, J= 7.0, 5.9, 1.6 Hz, H3'), 4.05 (1H,m, H4), 3.98 (1H, m, H4), 3.56 (1H, m, H5') 3.47 (1H, dd, J=12.2, 7.0 Hz, H5'), 2.99 (2H, m, H5''). ^{13}C NMR (151 MHz, D_2O) 188.8 (C2), 120.1 (C6), 92.8 (C1'), 89.2 (C4'), 88.5 (C2'), 75.7 (C3'), 61.7 (C5'), 42.8 (C4), 16.5 (C5). $[\alpha]_D^{20.0}$ (*c* = 1.00, H_2O) - 30.4.

6.8.5 D-xylo N-cyanoethyl oxazolidinone thione (D-XCEOT)

Starting from D-*xylo* oxazolidinone thione (**D-XOT**, 500 mg, 2.60 mmol) yielded D-*xylo* N cyanoethyl oxazolidinone thione (**D-XCEOT**; 592 mg, 93%). IR (solid, cm^{-1}) 3260 (OH), 2998, 2965, 2939 (CH), 2225 (C≡N), 1489 (C=S). ^{1}H (600 MHz, D_2O) 6.10 (1H, d, J = 5.6 Hz, H1'), 5.14 (1H, d, J = 5.6 Hz, H2'), 4.49 (1H, d, J=2.7 Hz, H3'), 4.12 (2H, m, H4), 3.96 (1H,m, H4'), 3.92 (2H, m, H5), 3.82 (2H, m, H5''). ^{13}C NMR (151 MHz, D_2O) 189.8 (C2), 122.5 (C6), 93.9 (C1'), 84.6 (C4'), 82.4 (C2'), 75.6 (C3'), 65.3 (C5'), 48.4 (C4), 18.1 (C5). $[\alpha]_D^{20.0}$ (*c* = 1.00, H_2O) 29.3

6.8.6 L-xylo N-cyanoethyl oxazolidinone (L-XCEOT)

Starting from L-*xylo* oxazolidinone thione (**L-XOT**, 500 mg, 2.60 mmol) yielded D-*xylo* N cyanoethyl oxazolidinone thione (**L-XCEOT**; 611 mg, 96%). IR (solid, cm^{-1}) 3262 (OH), 2991, 2964, 2945 (CH), 2223 (C≡N), 1490 (C=S). ^{1}H (600 MHz, D_2O) 6.12 (1H, d, J = 5.4 Hz, H1'), 5.16 (1H, d, J = 5.5 Hz, H2'), 4.52 (1H, d, J=2.8 Hz, H3'), 4.13 (2H, m, H4), 3.95 (2H,m, H4'), 3.90 (2H, m, H5), 3.86 (2H, m, H5''). ^{13}C NMR (151 MHz, D_2O) 190.2 (C2), 123.0 (C6), 93.8 (C1`), 84.2 (C4`), 82.3 (C2'), 75.6 (C3`), 65.5(C5`), 48.7 (C4), 18.3 (C5). $[\alpha]_D^{20.0}$ (*c* = 1.00, H_2O) - 24.2

6.9 Enantioenrichment Experiments

6.9.1 General Procedure

Solutions of D-, L- and scalemic (sca-) of the desired compound were set up with a range of different *ee* values with intervals of 20% *ee* from -100 % *ee* (pure L-) to +100 % *ee* (pure D-).

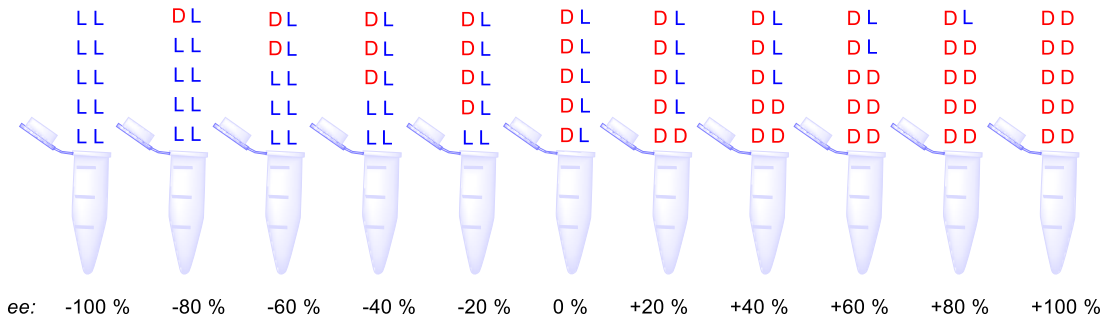

Figure 134: How the scalemic crystallisations were set up with the relative amount of D and L starting materials.

Following 2 weeks, the crystals obtained were separated, washed with ice cold water and dried. They were then analysed by optical polarimetry. If racemic growth was observed

through these crystals, the supernatant remaining was lyophilised and analysed in the same manner.

6.9.2 Aminooxazolines (AO)

6.9.2.1 Ribo aminooxazoline (RAO)

*Table 13: Table showing the change in optical rotation of the crystals formed from solutions of **RAO** (0.25 M, H_2O). Of ee's ranging from -100 % (L) to +100 % (D). The experiment was triplicated with the measurements recorded, the average calculated and the standard deviation shows the associated error.*

ee / %	D / µL	L / µL	Expected α_D/ °	α_{D1}/ °	α_{D2}/ °	α_{D3}/ °	Average α_D/ °	Standard Deviation
-100	0	1000	-119.4	-119.8	-124.3	-110.9	-118.3	5.57
-80	100	900	-94.2	-116.2	-118.6	-109.4	-114.7	3.90
-60	200	800	-64.1	-117.2	-113.6	-110.2	-113.7	2.86
-40	300	700	-41.5	-111.0	-92.0	-94.4	-99.1	8.45
-20	400	600	-19.8	-32.4	-23.4	-36.0	-30.6	5.30
0	500	500	0.5	0.4	0.8	1.0	0.7	0.25
20	600	400	21.2	39.6	32.2	34.7	35.5	6.08
40	700	300	43.2	110.4	92.1	91.0	97.8	8.90
60	800	200	64.3	111.9	119.2	109.3	113.5	4.19
80	900	100	93.4	122.2	121.1	114.4	119.2	3.45
100	1000	0	120.1	120.7	123.4	114.7	119.6	2.07

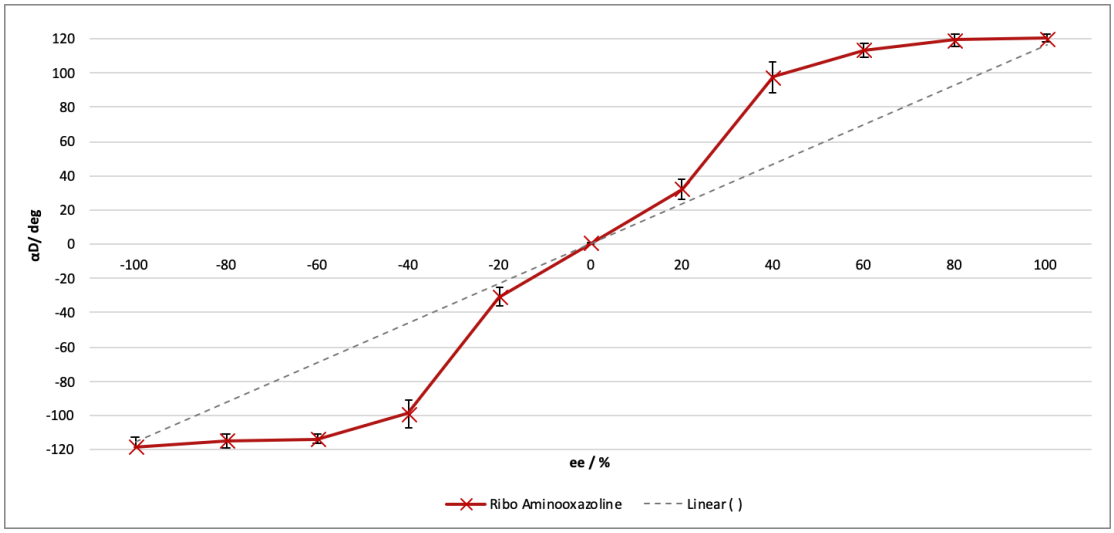

*Figure 135: Enantio-amplification of **RAO** (0.25 M, H_2O). The results were triplicated, and the average plotted along with the expected ee value. The dotted line shows the optical rotation that would be expected if the crystals possessed the same ee value as the starting solution.*

6.9.2.2 Arabino aminooxazoline (AAO)

*Table 14: Table showing the change in optical rotation of the crystals formed from solutions of **AAO** (1.00 M, H_2O). Of ee's ranging from -100 % (L) to +100 % (D). The experiment was triplicated with the measurements recorded, the average calculated and the standard deviation shows the associated error.*

ee / %	D / µL	L / µL	Expected α_D/ °	α_{D1}/ °	α_{D2}/ °	α_{D3}/ °	Average α_D/ °	Standard Deviation
-100	0	1000	-29.8	-28.9	-30.0	-29.3	-29.4	0.45
-80	100	900	-23.3	-28.2	-29.2	-28.9	-28.8	0.42
-60	200	800	-16.8	-24.1	-27.0	-26.4	-25.8	1.25
-40	300	700	-10.4	-22.2	-21.2	-20.8	-21.4	0.59
-20	400	600	-5.2	-9.0	-7.0	-14.5	-10.2	3.17
0	500	500	0.2	0.7	1.0	-0.3	0.5	0.56
20	600	400	5.9	12.4	13.2	9.8	11.8	1.45
40	700	300	11.1	25.1	27.8	18.1	23.7	4.09
60	800	200	16.6	25.7	30.2	28.9	28.3	1.89
80	900	100	23.4	29.8	31.8	30.6	30.7	0.82
100	1000	0	30.2	32.1	31.2	28.4	30.6	1.58

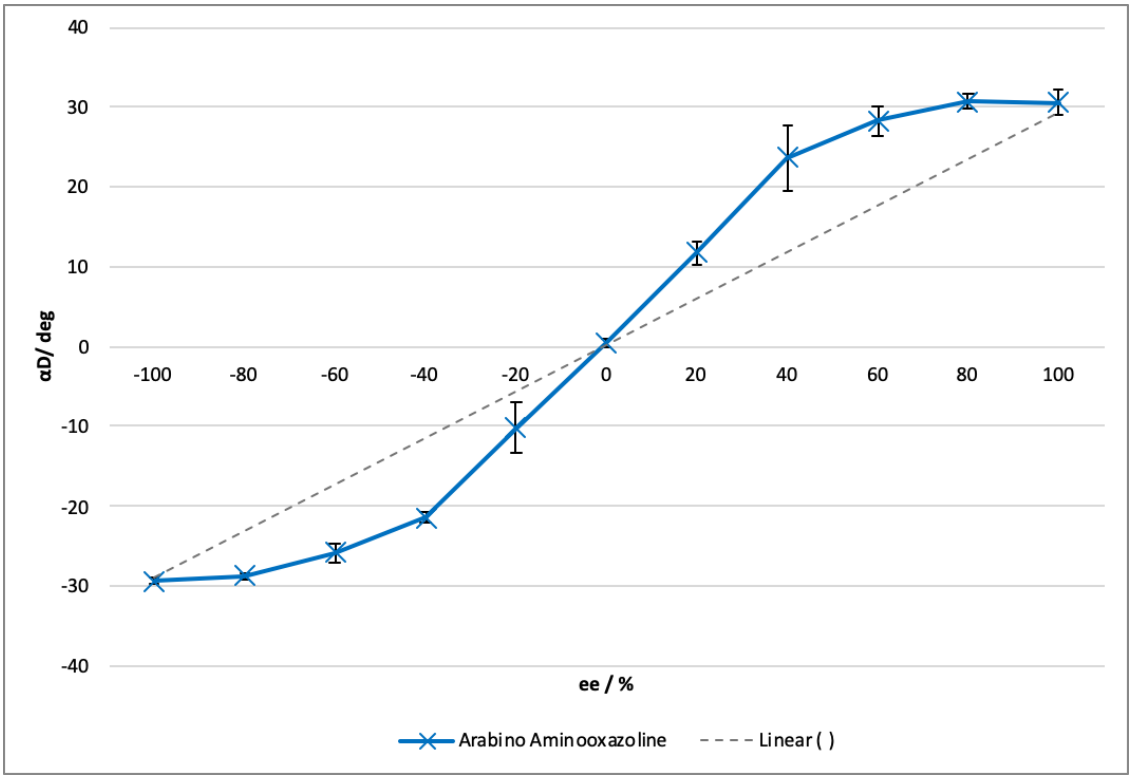

*Figure 136: Enantio-amplification of **AAO** (1.00 M, H_2O). The results were triplicated, and the average plotted along with the expected ee value. The dotted line shows the optical rotation that would be expected if the crystals possessed the same ee value as the starting solution.*

6.9.2.3 Xylo aminooxazoline (XAO)

*Table 15: Table showing the change in optical rotation of the crystals formed from solutions of **XAO** (1.00 M, H_2O). Of ee's ranging from -100 % (L) to +100 % (D). The experiment was triplicated with the measurements recorded, the average calculated and the standard deviation shows the associated error.*

ee / %	D / µL	L / µL	Expected α_D/ °	α_{D1}/ °	α_{D2}/ °	α_{D3}/ °	Average α_D/ °	Standard Deviation
-100	0	1000	-31.4	-31.4	-29.9	-31.2	-30.8	0.81
-80	100	900	-24.2	-25.4	-27.1	-32.4	-28.3	3.65
-60	200	800	-18.9	-21.9	-29.9	-28.7	-26.8	4.31
-40	300	700	-12.9	-14.3	-12.0	-20.0	-15.4	4.12
-20	400	600	-7.1	-6.9	-11.1	-5.8	-7.9	2.80
0	500	500	-0.1	1.8	1.0	0.2	1.0	0.80
20	600	400	5.5	9.2	8.2	4.5	7.3	2.48
40	700	300	12.7	15.9	20.9	18.8	18.5	2.51
60	800	200	18.2	24.4	28.7	31.3	28.1	3.48
80	900	100	24.8	27.2	29.7	32.1	29.7	2.45
100	1000	0	31.9	31.7	30.1	31.8	31.2	0.95

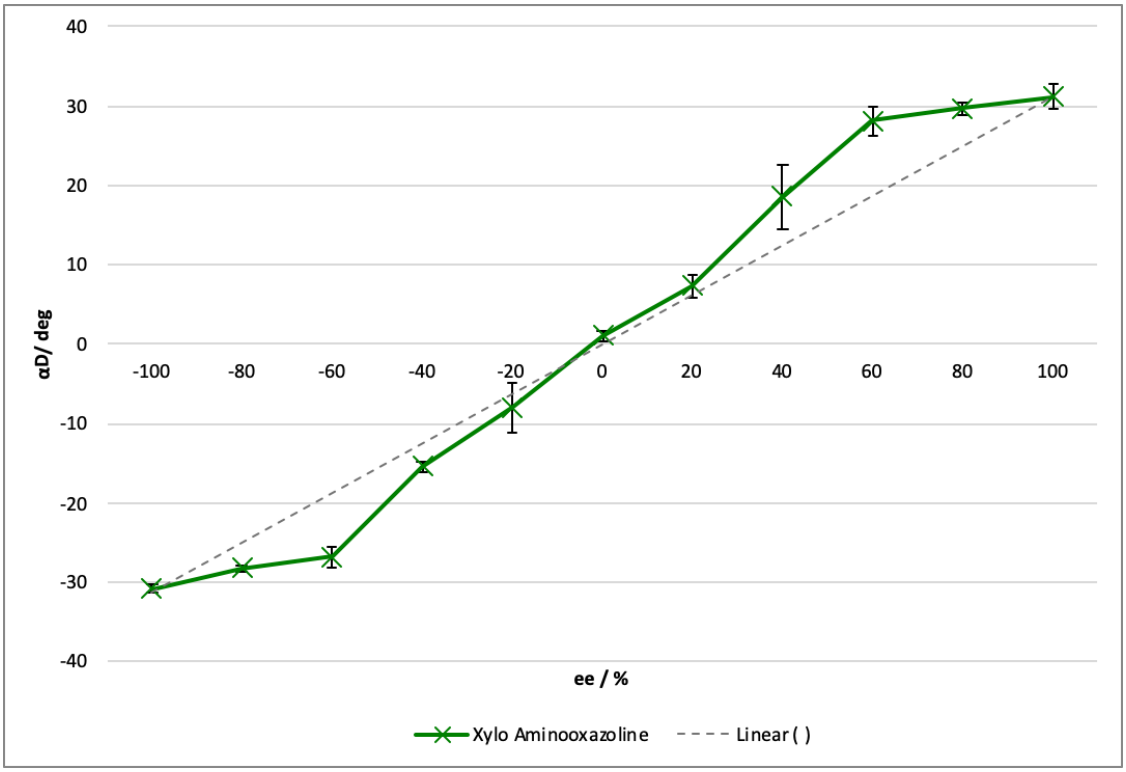

*Figure 137: Enantio-amplification of **XAO** (1.00 M, H_2O). The results were triplicated, and the average plotted along with the expected ee value. The dotted line shows the optical rotation that would be expected if the crystals possessed the same ee value as the starting solution.*

Table 16:Table showing the solution α_D, the measured crystal α_D and that normalised by comparison for **RAO** (0.25 M), **AAO** (1 M) and **XAO** (1 M) in H_2O.

ee / %	Expected RAO α_D/ °	RAO α_D/ °	Normalised RAO α_D/ °	Expected AAO α_D/ °	AAO α_D/ °	Normalised AAO α_D/ °	Expected XAO α_D/ °	XAO α_D/ °	Normalised XAO α_D/ °
-100	-119.4	-118.3	-98.5	-29.8	-29.4	-97.4	-31.4	-30.8	-96.7
-80	-94.2	-114.7	-95.5	-23.3	-28.8	-95.3	-24.2	-28.3	-88.7
-60	-64.1	-113.7	-94.6	-16.8	-25.8	-85.5	-18.9	-26.8	-84.1
-40	-41.5	-99.1	-82.5	-10.4	-21.4	-70.9	-12.9	-15.4	-48.4
-20	-19.8	-30.6	-25.5	-5.2	-10.2	-33.7	-7.1	-7.9	-24.9
0	0.5	0.7	0.6	0.2	0.5	1.5	-0.1	1.0	3.1
20	22.2	32.2	26.8	5.9	11.8	39.1	5.5	7.3	22.9
40	45.2	97.8	81.5	11.1	23.7	78.4	12.7	18.5	58.1
60	66.3	113.5	94.5	16.6	28.3	93.6	18.2	28.1	88.2
80	92.4	119.2	99.3	23.4	30.7	101.8	24.8	29.7	93.0
100	120.1	120.5	100.3	30.2	30.6	101.2	31.9	31.2	97.8

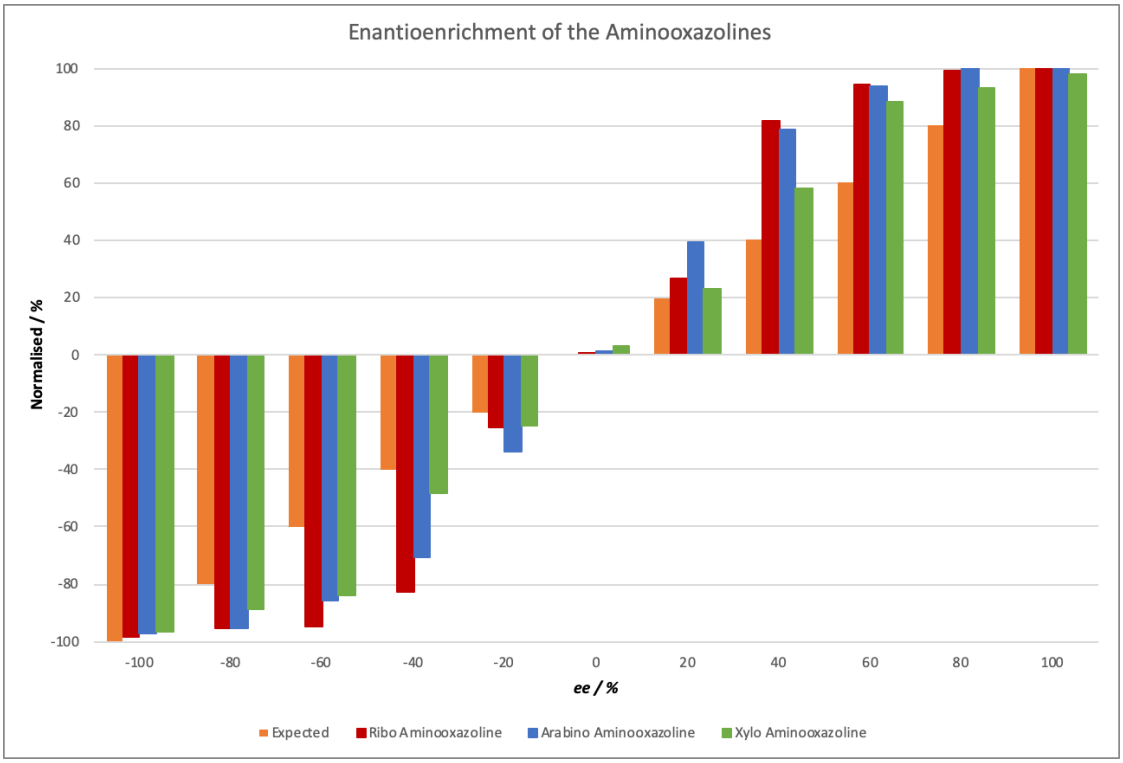

*Figure 138: Graph illustrating the normalised α_D obtained for **RAO** (0.25 M), **AAO** (1 M) and **XAO** (1 M) in H_2O.*

6.9.3 Oxazolidinone Thiones (OT)

6.9.3.1 Ribo oxazolidinone thione (ROT)

*Table 17: Table showing the change in optical rotation of the crystals formed from solutions of **ROT** (1.50 M, H_2O). Of ee's ranging from -100 % (L) to +100 % (D). The experiment was triplicated with the measurements recorded, the average calculated and the standard deviation shows the associated error.*

ee / %	D / µL	L / µL	Expected α_D/ °	α_{D1}/ °	α_{D2}/ °	α_{D3}/ °	Average α_D/ °	Standard Deviation
-100	0	1000	-139.5	-138.6	-135.3	-136.4	-136.8	1.37
-80	100	900	-109.3	-139.4	-140.7	-140.9	-140.3	0.66
-60	200	800	-81	-140.2	-139.3	-137.2	-138.9	1.26
-40	300	700	-53.4	-138.0	-130.1	-139.0	-135.7	3.98
-20	400	600	-26.7	-62.8	-48.3	-50.7	-53.9	6.35
0	500	500	0.3	1.2	-0.8	-0.2	0.1	0.84
20	600	400	25.4	49.5	56.8	53.3	53.2	2.98
40	700	300	52.8	138.3	135.9	130.2	134.8	3.40
60	800	200	80.4	138.7	140.9	136.7	138.8	1.72
80	900	100	109.4	143.1	139.1	137.2	139.8	2.46
100	1000	0	140.1	142.0	144.3	142.6	143.0	0.97

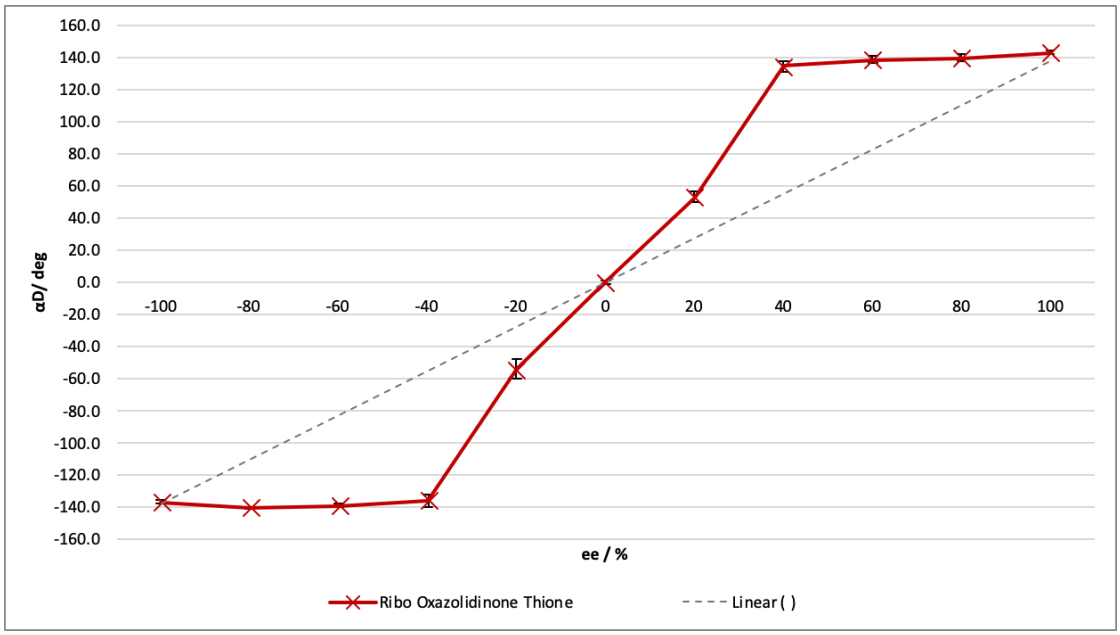

*Figure 139: Enantio-amplification of **ROT** (1.50 M, H_2O). The results were triplicated, and the average plotted along with the expected ee value. The dotted line shows the optical rotation that would be expected if the crystals possessed the same ee value as the starting solution.*

6.9.3.2 Arabino oxazolidinone thione (AOT)

*Table 18: Table showing the change in optical rotation of the crystals formed from solutions of **AOT** (3.00 M, H_2O). Of ee's ranging from -100 % (L) to +100 % (D). The experiment was triplicated with the measurements recorded, the average calculated and the standard deviation shows the associated error.*

ee / %	D / µL	L / µL	Expected α_D/ °	Crystal α_{D1}/ °	Crystal α_{D2}/ °	Crystal α_{D3}/ °	Average α_D/ °	Standard Deviation
-100	0	1000	11.6	10.2	10.9	11.6	10.9	0.57
-80	100	900	9.2	6.9	5.4	5.2	5.8	0.76
-60	200	800	7	1.6	1.2	0.5	1.1	0.44
-40	300	700	4.5	1.4	0.7	0.4	0.8	0.41
-20	400	600	2.4	1.2	0.2	0.2	0.5	0.46
0	500	500	0	0.1	0.0	-0.1	0.0	0.08
20	600	400	-2.5	-0.2	-0.3	-0.2	-0.2	0.08
40	700	300	-4.4	-0.3	-0.9	-0.4	-0.5	0.29
60	800	200	-6.5	-0.2	-1.8	-0.5	-0.8	0.70
80	900	100	-9	-5.3	-8.1	-7.6	-7.0	1.22
100	1000	0	-10.9	-10.1	-11.3	-9.9	-10.4	0.63

*Table 19: Table showing the change in optical rotation of the supernatant remaining from solutions of **AOT** (3.00 M, H_2O) once crystals were removed. Of ee's ranging from -100 % (L) to +100 % (D). The experiment was triplicated with the measurements recorded, the average calculated and the standard deviation shows the associated error.*

ee / %	Expected α_D/ °	Supernatant α_{D1}/ °	Supernatant α_{D2}/ °	Supernatant α_{D3}/ °	Average α_D/ °	Standard Deviation
-100	11.6	11.2	10.5	10.8	10.8	0.34
-80	9.2	11.6	10.0	10.6	10.7	0.79
-60	7	10.1	10.3	9.9	10.1	0.20
-40	4.5	8.5	9.9	8.7	9.0	0.76
-20	2.4	6.7	7.5	6.0	6.7	0.77
0	0	-0.6	-0.5	0.5	-0.2	0.57
20	-2.5	-6.9	-8.4	-8.0	-7.8	0.80
40	-4.4	-8.7	-9.8	-10.1	-9.5	0.71
60	-6.5	-10.1	-10.1	-10.9	-10.4	0.44
80	-9	-11.4	-9.6	-11.1	-10.7	0.93
100	-10.9	-10.9	-10.5	-10.8	-10.7	0.21

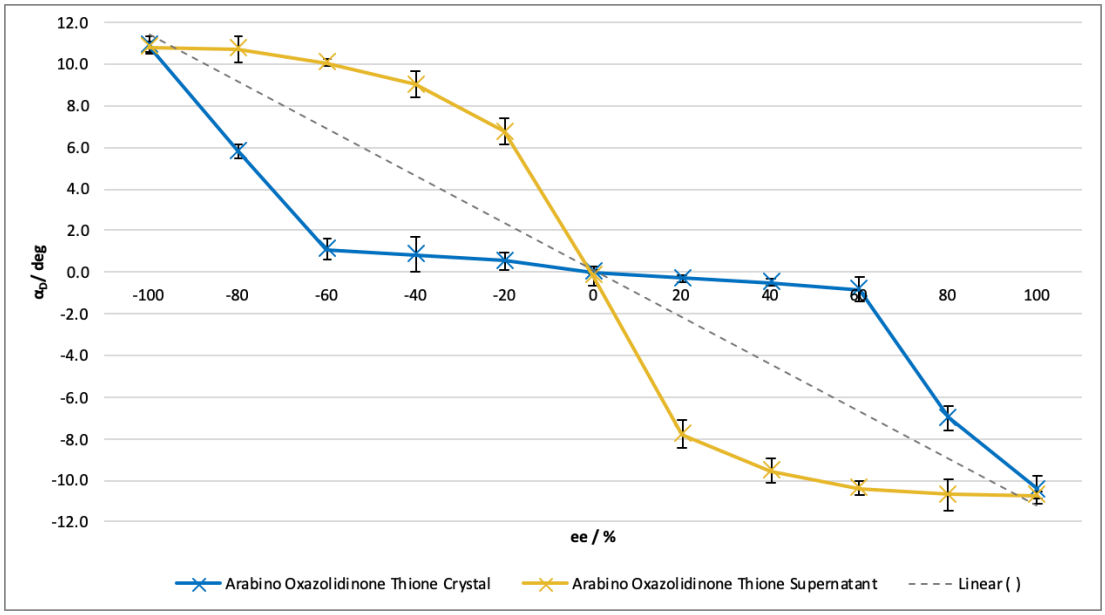

*Figure 140: Enantio-amplification of **AOT** (3.00 M, H_2O). Blue: measurement of the crystals obtained. Yellow: measurement of the supernatant. The results were triplicated, and the average plotted along with the expected ee value. The dotted line shows the optical rotation that would be expected if the crystals possessed the same ee value as the starting solution.*

6.9.3.3 Xylo oxazolidinone thione (XOT)

*Table 20: Table showing the change in optical rotation of the formed from solutions of **XOT** (3.00 M, H_2O). Of ee's ranging from -100 % (L) to +100 % (D). The experiment was triplicated with the measurements recorded, the average calculated and the standard deviation shows the associated error.*

ee / %	D / µL	L / µL	Expected α_D/ °	α_{D1}/ °	α_{D2}/ °	α_{D3}/ °	Average α_D/ °	Standard Deviation
-100	0	1000	-11.54	-10.97	-11.23	-11.93	-11.38	0.50
-80	100	900	-9.85	-4.36	-5.21	-4.69	-4.75	0.43
-60	200	800	-7.32	-1.17	-1.86	-2.40	-1.81	0.62
-40	300	700	-4.72	-0.60	-0.93	1.02	-0.17	1.04
-20	400	600	-2.28	-0.56	-0.41	0.39	-0.19	0.51
0	500	500	0.10	0.05	-0.13	-0.06	-0.05	0.09
20	600	400	2.42	0.79	0.39	0.46	0.55	0.21
40	700	300	4.79	1.12	0.78	0.81	0.90	0.19
60	800	200	7.08	2.90	1.98	1.53	2.14	0.70
80	900	100	9.71	4.23	4.83	3.45	4.17	0.69
100	1000	0	11.90	11.86	10.59	12.11	11.52	0.82

*Table 21: Table showing the change in optical rotation of the supernatant remaining from solutions of **XOT** (3.00 M, H_2O) once crystals were removed. Of ee's ranging from -100 % (L) to +100 % (D). The experiment was triplicated with the measurements recorded, the average calculated and the standard deviation shows the associated error.*

ee / %	Expected α_D/ °	Supernatant α_{D1}/ °	Supernatant α_{D2}/ °	Supernatant α_{D3}/ °	Average α_D/ °	Standard Deviation
-100	-11.54	-11.61	-11.20	-11.49	-11.43	0.21
-80	-9.85	-11.52	-11.22	-11.15	-11.30	0.20
-60	-7.32	-10.93	-11.40	-10.57	-10.97	0.42
-40	-4.72	-10.02	-10.26	-10.92	-10.40	0.47
-20	-2.28	-8.52	-9.47	-8.20	-8.73	0.66
0	0.10	1.10	0.28	-0.30	0.36	0.70
20	2.42	8.35	9.24	8.91	8.83	0.45
40	4.79	10.70	9.43	9.88	10.00	0.64
60	7.08	10.52	11.22	11.04	10.93	0.36
80	9.71	10.90	11.52	11.42	11.28	0.33
100	11.90	11.47	11.35	11.91	11.58	0.29

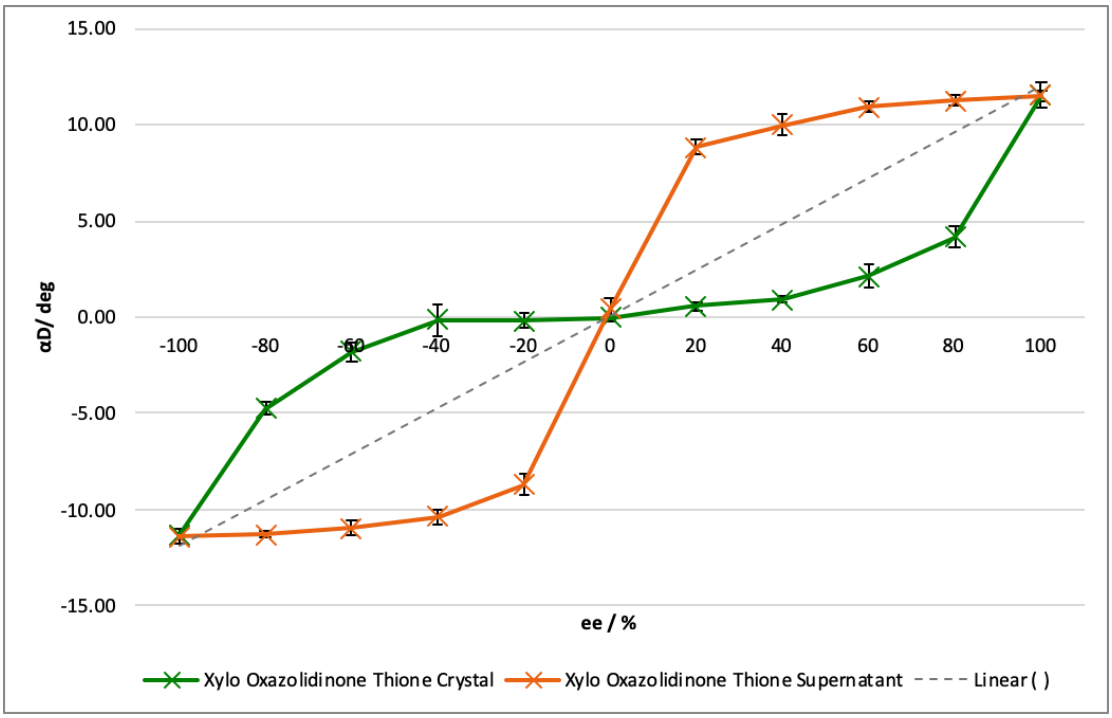

*Figure 141: Enantio-amplification of **AOT** (3.00 M, H_2O). Green: measurement of the crystals obtained. Orange: measurement of the supernatant. The results were triplicated, and the average plotted along with the expected ee value. The dotted line shows the optical rotation that would be expected if the crystals possessed the same ee value as the starting solution*

Table 22: Table showing the solution α_D, the measured crystal α_D and that normalised by comparison for **ROT** (1.5 M), **AOT** (3 M) and **XOT** (3 M) in H_2O.

ee / %	**Expected ROT α_D/ °**	**ROT α_D/ °**	**Normalised ROT α_D/ °**	**Expected AOT α_D/ °**	**AOT α_D/ °**	**Normalised AOT α_D/ °**	**Expected XOT α_D/ °**	**XOT α_D/ °**	**Normalised XOT α_D/ °**
-100	-139.5	-136.8	-95.7	11.6	10.9	-100.0	-11.54	-11.4	-95.6
-80	-109.3	-140.3	-98.2	9.2	5.8	-53.5	-9.85	-4.8	-39.9
-60	-81	-138.9	-97.2	7	1.1	-10.2	-7.32	-1.8	-15.2
-40	-53.4	-135.7	-94.9	4.5	0.9	-7.8	-4.72	-0.2	-1.4
-20	-26.7	-53.9	-37.7	2.4	0.6	-5.0	-2.28	-0.2	-1.6
0	0.3	0.1	0.0	0	0.0	0.0	0.1	0.0	-0.4
20	25.4	53.2	37.2	-2.5	-0.3	2.7	2.42	0.5	4.6
40	52.8	134.8	94.3	-4.4	-0.5	4.5	4.79	0.9	7.6
60	80.4	138.8	97.1	-6.5	-0.8	7.6	7.08	2.1	18.0
80	109.4	139.8	97.8	-9	-7.0	64.2	9.71	4.2	35.0
100	140.1	143.0	100.0	-10.9	-10.4	95.6	11.9	11.5	96.8

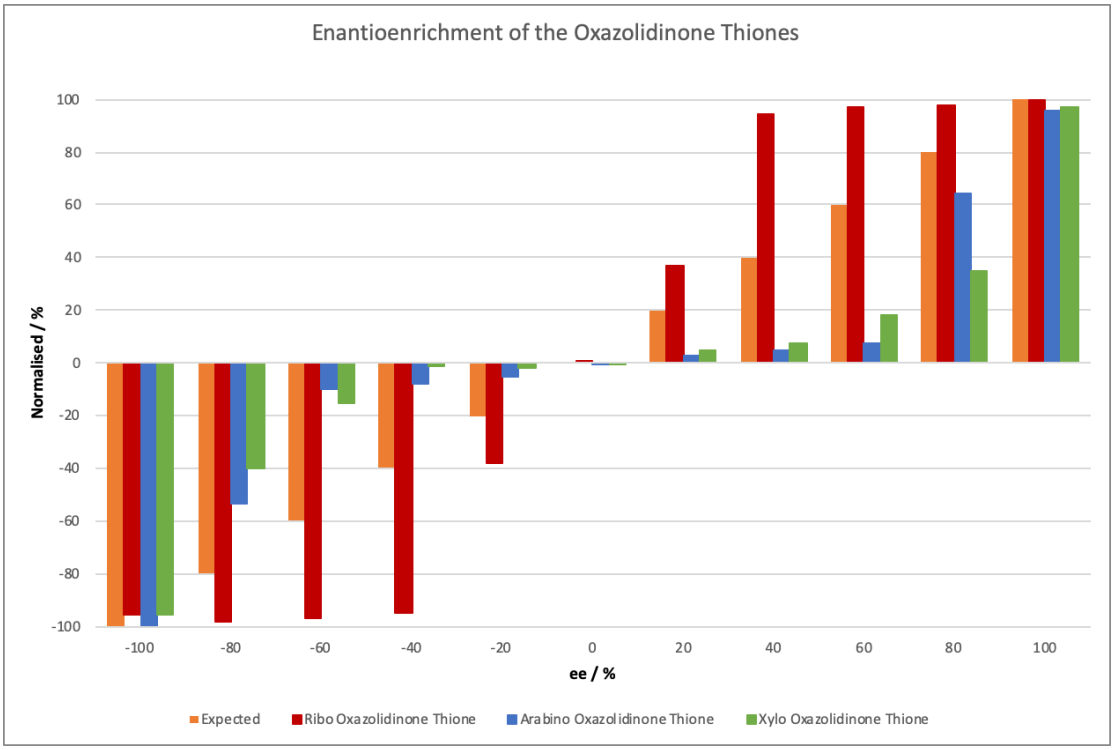

Figure 142: Normalised for comparison of **ROT** (1.5 M), **AOT** (3 M) and **XOT** (3 M) in H_2O.

6.9.4 Oxazolidinones (OX)

6.9.4.1 Ribo oxazolidinone (ROX)

*Table 23: Table showing the change in optical rotation of the crystals formed from solutions of **ROX** (3.00 M, H_2O). Of ee's ranging from -100 % (L) to +100 % (D). The experiment was triplicated with the measurements recorded, the average calculated and the standard deviation shows the associated error.*

ee / %	D / µL	L / µL	Expected α_D/ °	α_{D1}/ °	α_{D2}/ °	α_{D3}/ °	Average α_D/ °	Standard Deviation
-100	0	1000	-115.0	-115.3	-112.5	-111.9	-113.2	1.81
-80	100	900	-91.2	-61.1	-72.3	-66.3	-66.6	5.60
-60	200	800	-67.4	-9.3	-4.9	-6.6	-6.9	2.22
-40	300	700	-43.2	-6.8	-3.1	-6.4	-5.4	2.03
-20	400	600	-21.9	-2.2	-2.0	-1.8	-2.0	0.20
0	500	500	-0.1	0.2	-0.1	0.4	0.2	0.25
20	600	400	22.6	1.9	2.5	2.4	2.3	0.32
40	700	300	46.8	6.2	3.4	7.8	5.8	2.23
60	800	200	69.2	8.7	4.8	7.2	6.9	1.97
80	900	100	90.7	60.4	73.7	64.9	66.3	6.76
100	1000	0	113.9	114.3	112.9	111.2	112.8	1.55

*Table 24: Table showing the change in optical rotation of the supernatant remaining from solutions of **ROX** (3.00 M, H_2O) once crystals were removed. Of ee's ranging from -100 % (L) to +100 % (D). The experiment was triplicated with the measurements recorded, the average calculated and the standard deviation shows the associated error.*

ee / %	Expected α_D/ °	Supernatant α_{D1}/ °	Supernatant α_{D2}/ °	Supernatant α_{D3}/ °	Average α_D/ °	Standard Deviation
-100	-115.0	-115.1	-114.4	-116.8	-115.4	1.23
-80	-91.2	-114.3	-110.1	-115.6	-113.3	2.87
-60	-67.4	-107.5	-97.3	-106.6	-103.8	5.65
-40	-43.2	-100.2	-80.2	-107.3	-95.9	14.05
-20	-21.9	-65.6	-68	-64.9	-66.2	1.63
0	-0.1	1.3	0.4	0.5	0.7	0.49
20	22.6	68.7	61.2	63.4	64.4	3.86
40	46.8	98.3	85.8	100.3	94.8	7.86
60	69.2	103.8	100.7	105.5	103.3	2.43
80	90.7	105.7	110.9	107.2	107.9	2.68
100	113.9	114.2	112.8	115.1	114.0	1.16

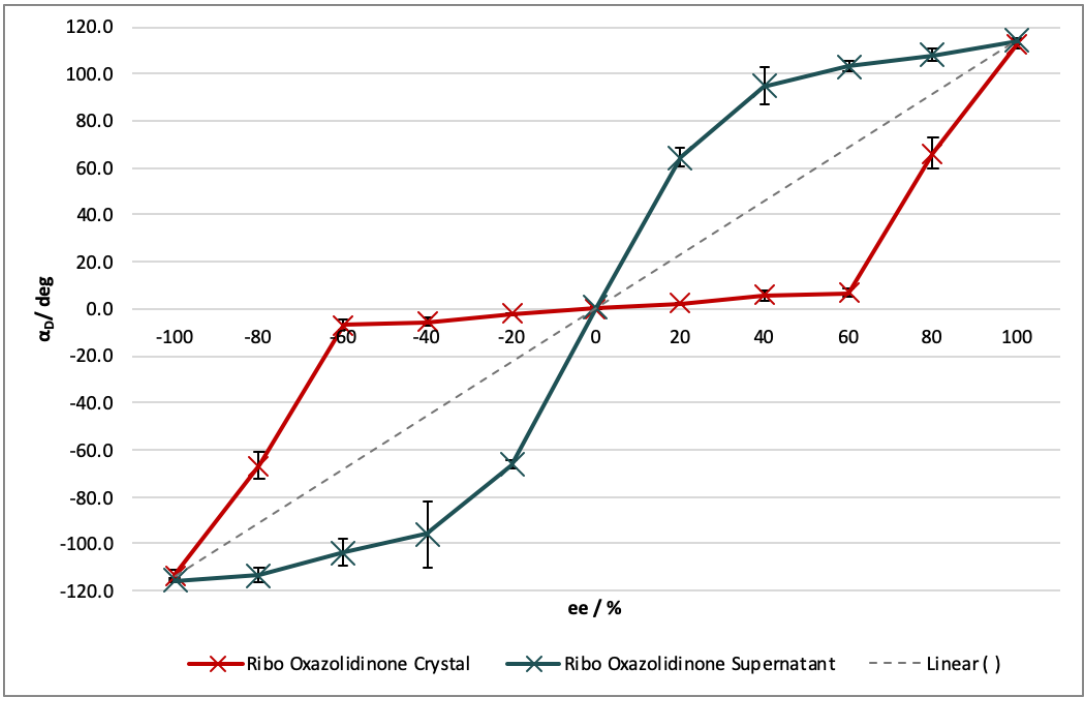

*Figure 143: Enantio-amplification of **ROX** (3.00 M, H_2O). Red: measurement of the crystal. Blue: measurement of the supernatant. The results were triplicated, and the average plotted along with the expected ee value. The dotted line shows the optical rotation that would be expected if the crystals possessed the same ee value as the starting solution.*

6.9.4.2 *Arabino oxazolidinone (AOX)*

*Table 25: Table showing the change in optical rotation of the crystals formed from solutions of **AOX** (5.00 M, H_2O/ethanol (1:1)). Of ee's ranging from -100 % (L) to +100 % (D). The experiment was triplicated with the measurements recorded, the average calculated and the standard deviation shows the associated error.*

ee / %	D / µL	L / µL	Expected α_D/ °	α_{D1}/ °	α_{D2}/ °	α_{D3}/ °	Average α_D/ °	Standard Deviation
-100	0	1000	59.3	59.3	58.3	59.3	59.0	0.47
-80	100	900	44.7	58.2	57.9	58.2	58.1	0.14
-60	200	800	31.9	57.9	58.3	53.1	56.4	2.36
-40	300	700	23.5	37.5	43.6	40.7	40.6	2.49
-20	400	600	12.1	24.3	21.0	16.4	20.6	3.24
0	500	500	0.2	0.2	-0.5	-0.1	-0.1	0.29
20	600	400	-11.7	-21.4	-25.2	-18.2	-21.6	2.86
40	700	300	-24.6	-41.6	-33.4	-43.9	-39.6	4.51
60	800	200	-34.1	-55.7	-59.8	-57.5	-57.7	1.68
80	900	100	-46.7	-59.2	-60.1	-58.3	-59.2	0.73
100	1000	0	-60.2	-61.5	-57.1	-59.0	-59.2	1.80

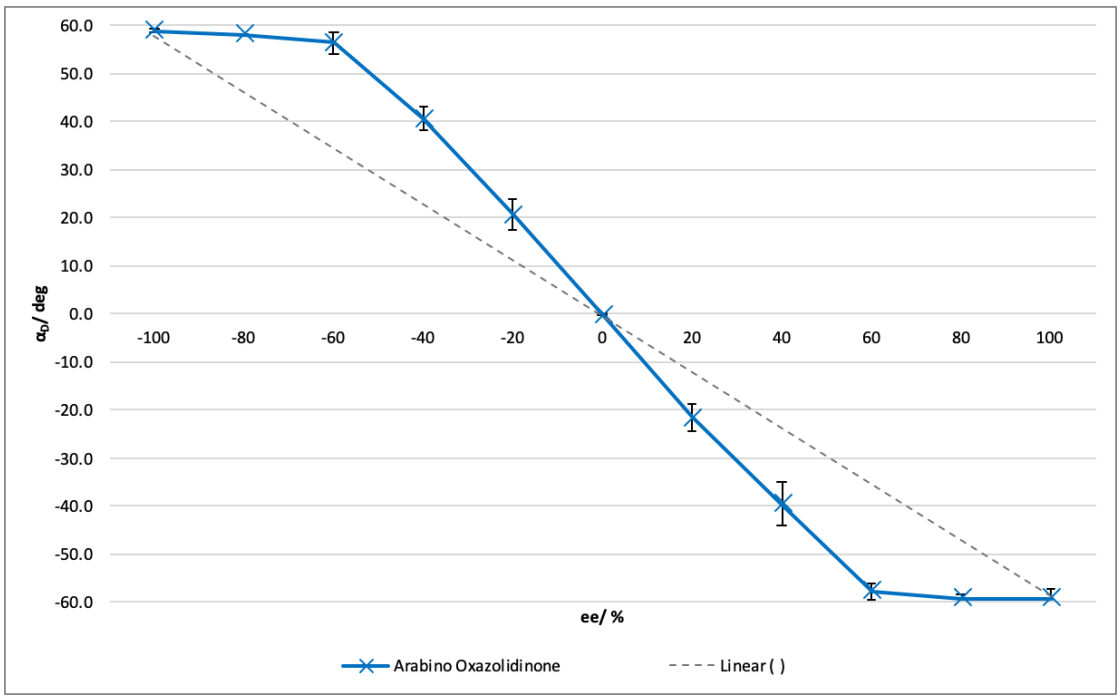

*Figure 144: Enantio-amplification of **AOX** (5.00 M, H_2O/ethanol (1:1)). The results were triplicated, and the average plotted along with the expected ee value. The dotted line shows the optical rotation that would be expected if the crystals possessed the same ee value as the starting solution.*

6.9.4.3 Xylo oxazolidinone (XOX)

*Table 26: Table showing the change in optical rotation of the crystals formed from solutions of **XOX** (6.00 M, H_2O/ethanol (1:1)). Of ee's ranging from -100 % (L) to +100 % (D). The experiment was triplicated with the measurements recorded, the average calculated and the standard deviation shows the associated error.*

ee / %	D / µL	L / µL	Expected α_D/ °	α_{D1}/ °	α_{D2}/ °	α_{D3}/ °	Average α_D/ °	Standard Deviation
-100	0	1000	-55.5	-60.5	-53.5	-55.5	-56.5	2.94
-80	100	900	-44.8	-27.6	-17.9	-21.9	-22.5	3.98
-60	200	800	-30.4	-7.4	-6.4	-16.8	-10.2	4.68
-40	300	700	-19.9	-5.1	-4.2	-2.2	-3.1	1.21
-20	400	600	-9.9	-1.7	-3.3	-3.3	-2.2	0.75
0	500	500	0.1	0.4	0.3	0.3	0.3	0.05
20	600	400	10.4	1.2	2.6	2.6	2.4	0.66
40	700	300	22.3	6.0	2.4	2.4	2.6	1.70
60	800	200	30.8	9.9	5.2	11.2	6.2	2.58
80	900	100	44.3	25.4	17.5	20.5	21.1	3.26
100	1000	0	56.3	56.3	52.3	55.3	54.6	1.70

*Table 27: Table showing the change in optical rotation of the supernatant remaining from solutions of **XOX** (6.00 M, H_2O/ethanol (1:1)) once crystals were removed. Of ee's ranging from -100 % (L) to +100 % (D). The experiment was triplicated with the measurements recorded, the average calculated and the standard deviation shows the associated error.*

ee / %	Expected α_D/ °	Supernatant α_{D1}/ °	Supernatant α_{D2}/ °	Supernatant α_{D3}/ °	Average α_D/ °	Standard Deviation
-100	-55.5	-58.6	-60.3	-59.5	-59.5	0.85
-80	-44.8	-57.4	-59.0	-58.7	-58.4	0.85
-60	-30.4	-52.2	-57.7	-58.2	-56.0	3.33
-40	-19.9	-38.6	-44.2	-46.3	-43.0	3.98
-20	-9.9	-19.1	-24.4	-25.2	-22.9	3.32
0	0.1	-0.2	0.4	0.3	0.2	0.32
20	10.4	18.7	26.3	23.5	22.8	3.84
40	22.3	34.9	40.1	43.9	39.6	4.52
60	30.8	50.3	45.6	54.0	50.0	4.21
80	44.3	57.2	58.6	57.3	57.7	0.78
100	56.3	59.3	60.0	58.2	59.2	0.91

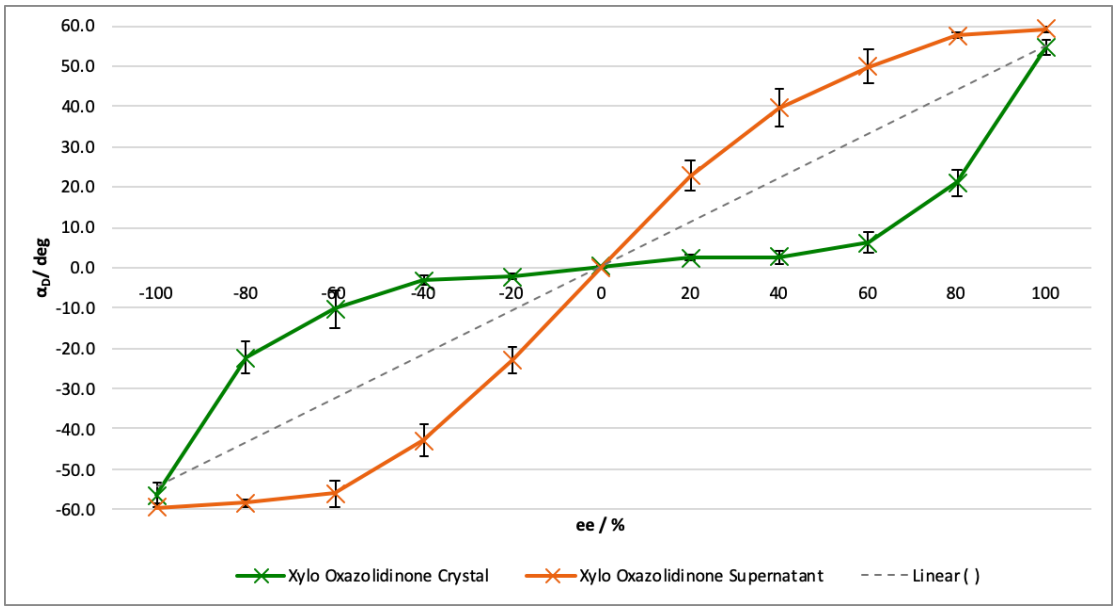

*Figure 145: Enantio-amplification of **XOX** (6.00 M, H_2O/ethanol (1:1)). The results were triplicated, and the average plotted along with the expected ee value. The dotted line shows the optical rotation that would be expected if the crystals possessed the same ee value as the starting solution.*

Table 28: Table showing the solution α_D, the measured crystal α_D and that normalised by comparison for **ROX** (1.5 M, H_2O), **AOX** (5 M, *H_2O/ethanol (1:1)*) and **XOTX** (6 M, *H_2O/ethanol (1:1)*).

ee / %	**Expected ROX α_D/ °**	**ROX α_D/ °**	**Normalised ROX α_D/ °**	**Expected AOX α_D/ °**	**AOX α_D/ °**	**Normalised AOX α_D/ °**	**Expected XOX α_D/ °**	**XOX α_D/ °**	**Normalised XOX α_D/ °**
-100	-115.0	-113.2	-100.4	59.3	59.0	-98.0	-55.50	-56.50	-100.4
-80	-91.2	-66.6	-59.0	44.7	58.1	-96.5	-44.75	-22.47	-39.9
-60	-67.4	-6.9	-6.1	31.9	56.4	-93.7	-30.44	-10.20	-18.1
-40	-43.2	-5.4	-4.8	23.5	40.6	-67.4	-19.86	-3.10	-5.5
-20	-21.9	-2.0	-1.8	12.1	20.6	-34.2	-9.87	-2.20	-3.9
0	-0.1	0.2	0.1	0.2	-0.1	0.2	0.04	0.33	0.6
20	22.6	2.3	2.0	-11.7	-21.6	35.9	10.43	2.40	4.3
40	46.8	5.8	5.1	-24.6	-39.6	65.8	22.30	2.60	4.6
60	69.2	6.9	6.1	-34.1	-57.7	95.8	30.78	6.20	11.0
80	90.7	66.3	58.8	-46.7	-59.2	98.3	44.32	21.13	37.5
100	113.9	112.8	100.0	-60.2	-59.2	98.3	56.30	54.63	97.0

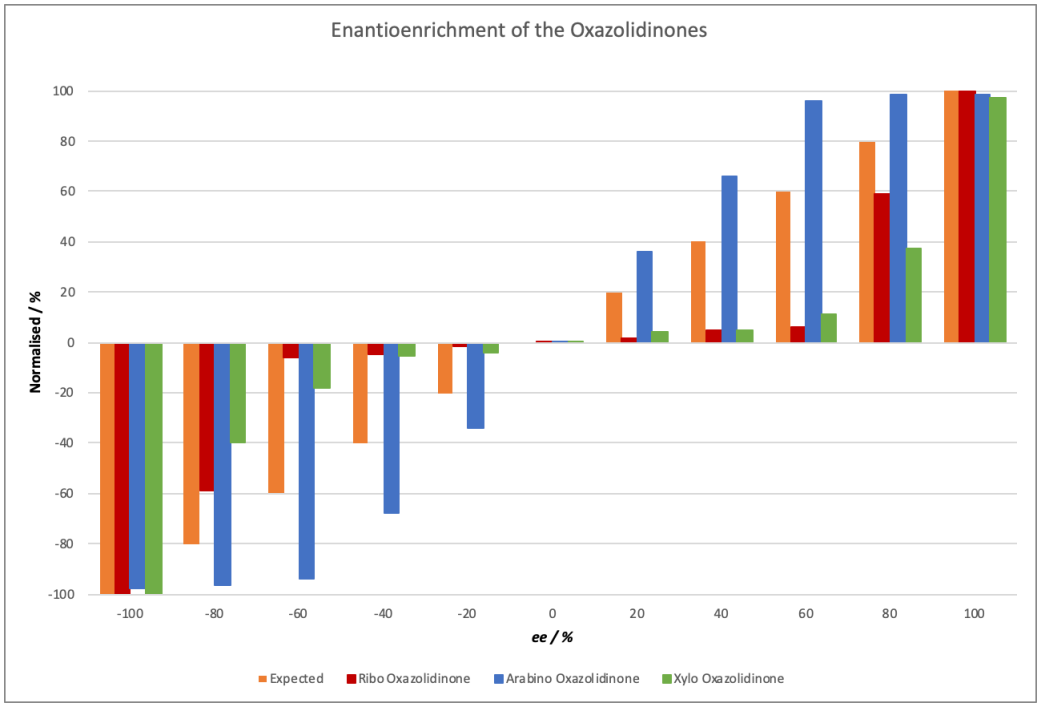

Figure 146: Normalised for comparison of **ROX** (1.5 M, H_2O), **AOX** (5 M, *H_2O/ethanol (1:1)*) and **XOTX** (6 M, *H_2O/ethanol (1:1)*).

6.9.5 Methyl Oxazolidinone Thione (RMOT)

6.9.5.1 Ribo methyl oxazolidinone thione (RMOT)

*Table 29: Table showing the change in optical rotation of the crystals formed from solutions of **RMOT** (5.00 M, H_2O/ethanol (1:1)). Of ee's ranging from -100 % (L) to +100 % (D). The experiment was triplicated with the measurements recorded, the average calculated and the standard deviation shows the associated error.*

ee / %	D / µL	L / µL	Expected α_D/ °	α_{D1}/ °	α_{D2}/ °	α_{D3}/ °	Average α_D/ °	Standard Deviation
-100	0	1000	-34.9	-35.2	-33.8	-36.1	-35.0	1.16
-80	100	900	-27.8	-24.3	-18.6	-17.6	-20.2	3.61
-60	200	800	-21.2	-10	-6.3	-8.8	-8.4	1.89
-40	300	700	-15.1	-4.1	-3.9	-3.2	-3.7	0.47
-20	400	600	-6.8	-2.9	-1.8	-2.3	-2.3	0.55
0	500	500	0.1	0.1	0.4	-0.2	0.1	0.30
20	600	400	7.5	1.9	3.2	2.3	2.5	0.67
40	700	300	13.2	3.2	5.6	4.5	4.4	1.20
60	800	200	20.8	11.5	7.8	6.7	8.7	2.51
80	900	100	28.4	23.7	16.5	21.9	20.7	3.75
100	1000	0	35.2	35	33.2	35.4	34.5	1.17

*Table 30: Table showing the change in optical rotation of the supernatant remaining from solutions of **RMOT** (5.00 M, H_2O/ethanol (1:1)) once crystals were removed. Of ee's ranging from -100 % (L) to +100 % (D). The experiment was triplicated with the measurements recorded, the average calculated and the standard deviation shows the associated error.*

ee / %	Expected α_D/ °	Supernatant α_{D1}/ °	Supernatant α_{D2}/ °	Supernatant α_{D3}/ °	Average α_D/ °	Standard Deviation
-100	-34.9	-34.1	-35.6	-31.2	-33.6	2.24
-80	-27.8	-33.0	-31.0	-32.4	-32.1	1.03
-60	-21.2	-22.5	-31.6	-29.4	-27.8	4.75
-40	-15.1	-23.9	-21.7	-28.2	-24.6	3.31
-20	-6.8	-11.9	-19.0	-17.1	-16.0	3.68
0	0.1	0.9	0.9	-0.9	0.3	1.04
20	7.5	9.3	16.2	18.4	14.6	4.75
40	13.2	19.7	22.1	27.6	23.1	4.05
60	20.8	25.8	28.8	27.8	27.5	1.53
80	28.4	27.3	31.6	32.5	30.5	2.78
100	35.2	32.4	30.1	34.8	32.4	2.35

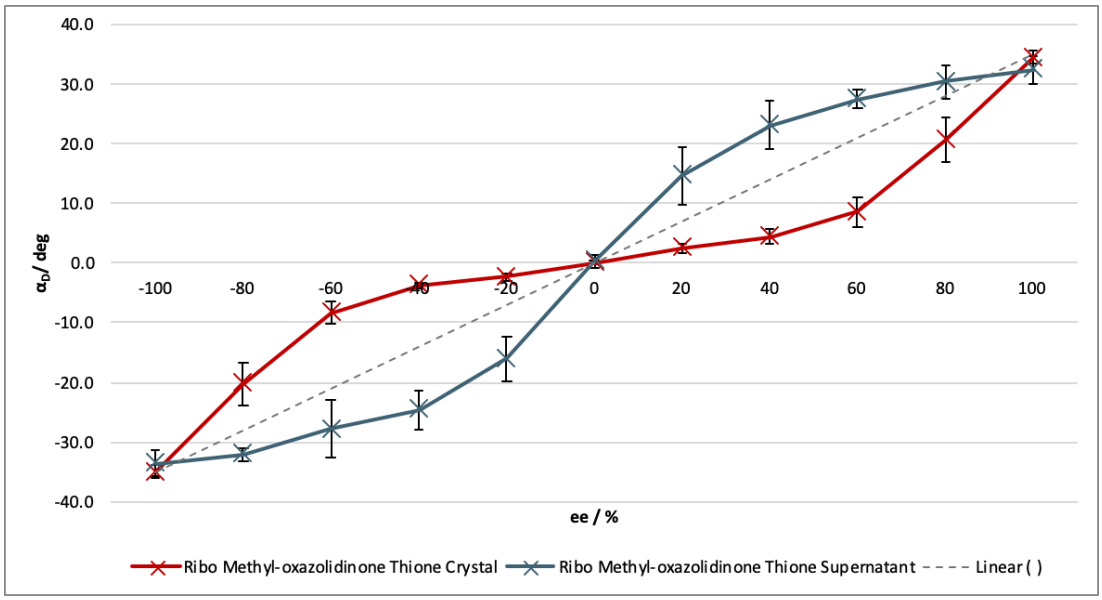

*Table 31: Table showing the change in optical rotation of the crystals of **RAO** (0.25 M, H_2O), **AAO** (1.00 M, H_2O), **XAO** (1.00 M, H_2O), **ROT** (1.50 M, H_2O) and **AOX** (3.00 M, H_2O/ethanol (1:1)). Of ee's ranging from -100 % (L) to +100 % (D). The experiment was triplicated with the measurements recorded, the average calculated and the results normalized to the calculated value of the solution.*

ee **/ %**	**RAO** **α_D/ °**	**Normalised** **RAO α_D/ °**	**AAO** **α_D/ °**	**Normalised** **AAO α_D/ °**	**XAO** **α_D/ °**	**Normalised** **XAO α_D/ °**	**ROT** **α_D/ °**	**Normalised** **ROT α_D/ °**	**AOX** **α_D/ °**	**Normalised** **AOX α_D/ °**
-100	-118.3	-98.5	-29.4	-97.4	-30.8	-96.7	-136.8	-97.6	59.0	-98.0
-80	-114.7	-95.5	-28.8	-95.3	-28.3	-88.7	-140.3	-100.2	58.1	-96.5
-60	-113.7	-94.6	-25.8	-85.5	-26.8	-84.1	-138.9	-99.1	56.4	-93.7
-40	-99.1	-82.5	-21.4	-70.9	-15.4	-48.4	-135.7	-96.9	40.6	-67.4
-20	-30.6	-25.5	-10.2	-33.7	-7.9	-24.9	-53.9	-38.5	20.6	-34.2
0	0.7	0.6	0.5	1.5	1.0	3.1	0.1	0.0	-0.1	0.2
20	32.2	26.8	11.8	39.1	7.3	22.9	53.2	38.0	-21.6	35.9
40	97.8	81.5	23.7	78.4	18.5	58.1	134.8	96.2	-39.6	65.8
60	113.5	94.5	28.3	93.6	28.1	88.2	138.8	99.0	-57.7	95.8
80	119.2	99.3	30.7	101.8	29.7	93.0	139.8	99.8	-59.2	98.3
100	120.5	100.3	30.6	101.2	31.2	97.8	143.0	102.0	-59.2	98.3

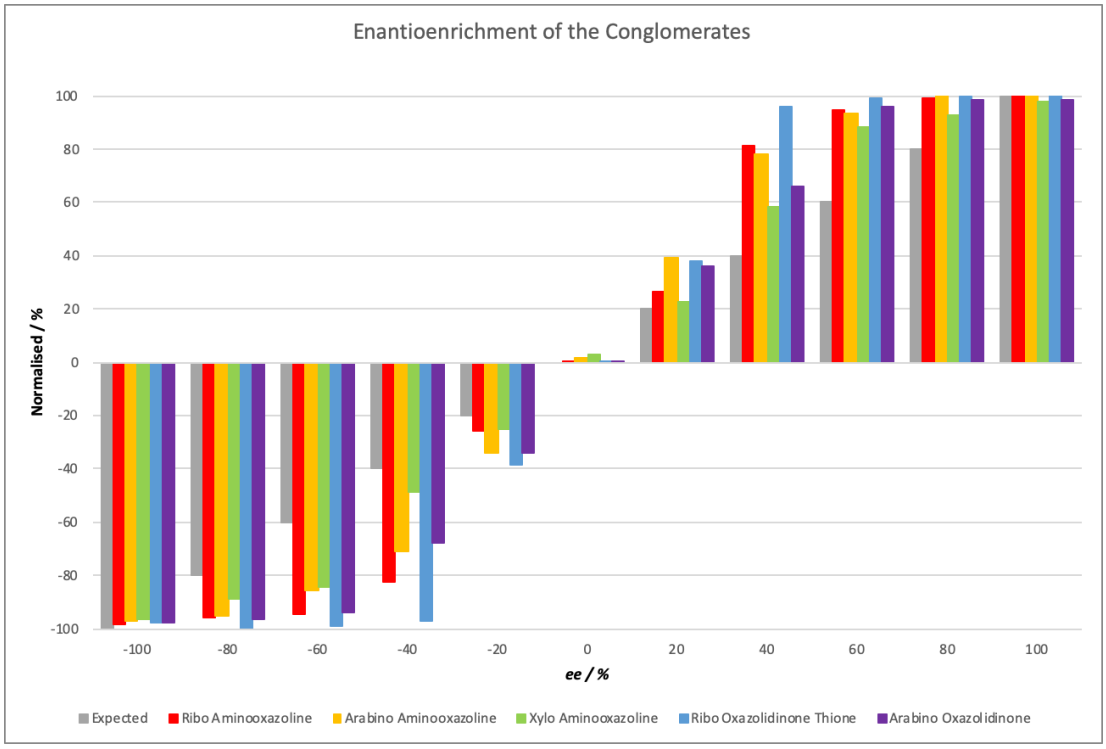

*Figure 147: Showing the change in optical rotation of the crystals of **RAO** (0.25 M, H_2O), **AAO** (1.00 M, H_2O), **XAO** (1.00 M, H_2O), **ROT** (1.50 M, H_2O) and **AOX** (3.00 M, H_2O/ethanol (1:1)). Of ee's ranging from -100 % (L) to +100 % (D). The experiment was triplicated with the measurements recorded, the average calculated and the results normalized to the calculated value of the solution.*

6.10 Lactaldehyde (43)

6.10.1 Rac-lactaldehyde (rac-43)

Pyruvic aldehyde dimethyl acetal (**47**, 1.21 mL, 10 mmol, 1 equiv), was stirred in MeOH (10 mL) at 0 °C. Sodium borohydride (0.38 g, 10 mmol, 1 equiv) was added in portions over 10 minutes. The reaction was then warmed to RT and then stirred for 45 minutes. This was then poured into sat. aq NH_4Cl solution (5 mL), and the aqueous layer extracted with Et_2O (3 x 10 mL). The organic layers were concentrated in vacuo to give a pale-yellow oil. This was then re-dissolved in CH_2Cl_2 (15 mL), washed with brine (5 mL) and dried with Na_2SO_4, filtered and then concentrated to 5 mL in vacuo. This was then re-dissolved in water (10 mL), the pH was adjusted to 1.2 using DOWEX (H+) and stirred for 24 hours followed by filtration. The title compound was stored as a solution at pH 7, 0.5 M. Yield (75% compared to standard in NMR).

^{1}H NMR (400 MHz, D_2O) 3.6 (m, 1H, (C2)-H), 1.2 (d, J=6.5 Hz, 3H, (C3)-H). ^{13}C NMR (151 MHz, D_2O) ppm 190.1, 69.1, 25.9. Data in agreement with published literature data.[55]

6.10.2 Methyl (S)-2-((tert-butyldimethylsilyl)oxy)propanoate (53)

L-methyl lactate (**52**, 1 mL, 10 mmol, 1 equiv) and imidazole (1.0 g, 15 mmol, 1.5 equiv) were stirred in DMF (9 mL). Tert-butylchlorodimethylsilane (1.8 g, 12 mmol, 1.2 equiv) was added and stirred for 30 mins at RT. Water (15 mL) was then added and extracted with Et_2O (3 x 15 mL). The organic layers were combined and washed with brine (15 mL), dried with $MgSO_4$ and concentrated *in vacuo*. The residue was then co-evaporated with heptane to leave colourless oil (1.70g, 7.8 mmol, 78%). ^{1}H NMR (400 MHz, $CDCl_3$) 4.33 (q, J=6.8 Hz, 1H, $CHCH_3$), 3.72 (s, 3H, CH_3O), 1.40 (d, J=6.8 Hz, 3H, CH_3CH), 0.90 (s, 9 H, $SiC(CH_3)_3$), 0.10 (m, 6 H, 2 x $SiCH_3$). ^{13}C NMR (151 MHz, $CDCl_3$) ppm 174.2, 67.1, 50.9, 26.0, 22.4, 18.7, -4.1, -5.1.

6.10.3 Methyl ((S)-2-((tert-butyldimethylsilyl)oxy)propanal (54)

Due to problems occurred during the synthesis, this compound was made on numerous occasions using different methods. Below is a table to summarise the outcome, some reactions were repeated more than once.

General Method

Reducing agent was added dropwise over 2 hours to a stirring solution of methyl (S)-2-((tert butyldimethylsilyl)oxy)propanoate (**53**) in solvent at the temperature listed. After the addition was completed, the reaction was stirred for an additional 30 minutes, then quenched by dropwise addition of MeOH and H_2O. The reaction was then warmed to RT and stirred for 1.5 hours followed by addition of $Na_2SO_4.10H_2O$ and $MgSO_4$ and stirring for an extra 15 mins. The

reaction mixture is then filtered through a short plug of celite and silica eluting with Et_2O. The filtrate was then concentrated in vacuo and purified by short path distillation (100 °C at 20 mm Hg) to give the aldehyde as a colourless oil. (4.5 g, 23.9 mmol, 75%). Bp 84-88 °C (24 Torr). ^1H NMR (400 MHz, $CDCl_3$) 9.58 (d, 1H, J = 1.3 Hz, CHO), 4.06 (qd, 1H, J = 1.3, 6.8 Hz, $CHCH_3$), 1.24 (d, 3H, J = 6.8 Hz, $CHCH_3$), 0.89 (s, 9H, $SiC(CH_3)_3$), 0.08 (s, 3H, $SiCH_3$), 0.06 (s, 3H, $SiCH_3$).

*Table 32: Table showing the routes used to gain access to the protected aldehyde (**54**).*

Entry	Scale / g	Reducing Agent	Solvent	Temperature /°C	Yield / %
1	0.1	$LiAlH_4$ (THF)	THF	RT	0 %
2	0.1	$LiAlH_4$ (THF)	THF	0	0 %
3	0.5	DIBAL (hexane)	DCM	–78	0 %
4	0.5	DIBAL (hexane)	DCM	–98	0 %
5	0.5	DIBAL (hexane)	Toluene	–78	0 %
6	1	DIBAL (THF)	Et_2O	–78	0 %
7	1	DIBAL (THF)	Et_2O	–98	0 %
8	1	DIBAL (cyclohexane)	Et_2O	–98	0 %
9	7	DIBAL (cyclohexane)	Et_2O	–78	75%

6.10.4 Rac-lactaldehyde (rac-43)

(S)-2-((tert-butyldimethylsilyl)oxy)propanal (**54**, 94mg, 0.5 mmol, 0.5 M) was stirred in 1 mL with the solvent system listed. The acid was then added and monitored by NMR every 4 hours up to 48 hours in total. Kept as a solution at pH 7 in -80 °C. ^1H NMR (400 MHz, $CDCl_3$) 3.75 (dq, 1H, J = 5.3, 6.4 Hz, $CHCH_3$), 1.25 (d, 3H, J = 6.4 Hz, CH_3).

Entry	Acid	Solvent System	Time / h	Result
1	HCl (1 M)	HCl (aq)	2	16% yield
2	HCl (2 M)	HCl (aq)	2	7% yield
3	Methanolic HCl	HCl/ MeOH	4	Complete decomposition
4	AcOH	H_2O/ THF (50:50)	4	0% yield
5	50% aq HF	MeCN	2	10% yield
6	HCl (to pH 3)	D_2O/ Acetonitrile (50:50)	4	Trace
7	HCl (to pH 3 at 60 °C)	D_2O/ Acetonitrile (50:50)	4	50% yield

6.11 General procedure A for the synthesis of aminals

The aldehyde (2.5 mmol, 1 equiv, 0.5 M) was stirred at RT with 2-aminothiazole (**23**, 5.0 mmol, 2 equiv, 1 M) in sodium phosphate buffer (1M, pH 7). The resultant suspension was centrifuged, and the supernatant removed. The precipitate was washed with ice cold water. The precipitate was dried to yield the aminal as a white solid in all cases.

6.11.1 Rac-glyceraldehyde aminal (rac-25)

General procedure A was followed using rac-glyceraldehyde (**rac-14**) and 2-aminothiazole (**23**) yielding **rac-25** as a white solid (75%). ^{1}H NMR (400 MHz, DMSO) 7.83 (d, J = 7.6 Hz, 1H, NH), 7.70 (d, J = 7.6 Hz, 1H, NH), 7.02 (d, J = 3.7 Hz, 2H, Ar), 6.64 (d, J = 3.7 Hz, 2H, Ar), 5.41 (td, J = 7.6, 3.7 Hz, 1H, OH), 5.31 (d, J = 5.6 Hz, 1H, C1-H), 4.93 – 4.86 (br. s, 1H, OH), 3.83 – 3.73 (m, 1H, C2-H), 3.41 (m 2H, C3-H). ^{13}C NMR (101 MHz, DMSO-d6) δ 168.2, 167.8, 138.4, 138.2, 107.1, 107.0, 72.4, 66.7, 62.0. IR (solid, cm^{-1}): 3382, 3289, 3150, 3115, 2978, 2866, 1528, 1495, 1452, 1409, 1372. M.p. 121-128 °C (decomposed). $[\alpha]_D^{20.0}$ (*c* = 1.00, H_2O) -0.3

6.11.2 D-glyceraldehyde aminal (D-25)

General procedure A was followed using D-glyceraldehyde (**D-14**) and 2-aminothiazole (**23**) yielding **D-25** as a white solid (68%). ^{1}H NMR (400 MHz, DMSO) 7.83 (d, J = 7.6 Hz, 1H, NH), 7.70 (d, J = 7.6 Hz, 1H, NH), 7.02 (d, J = 3.7 Hz, 2H, Ar), 6.64 (d, J = 3.7 Hz, 2H, Ar), 5.41 (td, J = 7.6, 3.7 Hz, 1H, OH), 5.31 (d, J = 5.6 Hz, 1H, C1-H), 4.93 – 4.86 (br. s, 1H, OH), 3.83 – 3.73 (m, 1H, C2-H), 3.41 (m 2H, C3-H). ^{13}C NMR (101 MHz, DMSO-d_6) δ 168.3, 167.8, 138.4, 138.2, 107.2, 107.0, 72.5, 66.8, 62.2. IR (solid, cm^{-1}): 3382, 3289, 3150, 3115, 2978, 2866, 1528, 1495, 1452, 1409, 1372. M.p. 121-128 °C (decomposed). $[\alpha]_D^{20.0}$ (*c* = 1.00, MeOH) 26.9.

6.11.3 L-glyceraldehyde aminal (L-25)

General procedure A was followed using L-glyceraldehyde (**L-14**) and 2-aminothiazole (**23**) yielding **rac-25** as a white solid (61%). ^{1}H NMR (400 MHz, DMSO) 7.82 (d, J = 7.6 Hz, 1H, NH), 7.71 (d, J = 7.6 Hz, 1H, NH), 7.01 (d, J = 3.6 Hz, 2H, Ar), 6.66 (d, J = 3.6 Hz, 2H, Ar), 5.42 (td, J = 7.6, 3.6 Hz, 1H, OH), 5.30 (d, J = 5.6 Hz, 1H, C1-H), 4.92 – 4.84 (br. s, 1H, OH), 3.83 – 3.72 (m, 1H, C2-H), 3.40 (m 2H, C3-H). ^{13}C NMR (101 MHz, DMSO-d_6) δ 168.2, 167.9, 138.3, 138.0, 107.2, 107.0, 72.5, 66.8, 62.2. IR (solid, cm^{-1}): 3380, 3272, 3145, 3110, 1535, 1490, 1462, 1401, 1367. M.p. 124-129 °C (decomposed). $[\alpha]_D^{20.0}$ (*c* = 1.00, MeOH) -27.1.

6.11.4 Rac-lactaldehyde aminal (rac-44)

General procedure A was followed using rac-lactaldehyde (**rac-43**) and 2-aminothiazole (**23**) yielding **rac-44** as a white solid (72% yield). ^{1}H NMR (400 MHz, DMSO) 7.70 (d, J = 7.5 Hz, 1H, NH), 7.63 (d, J = 7.5 Hz, 1H, NH), 7.00 (m, 2H, Ar), 6.63 (m, 2H, Ar), 5.20 (m, 1H, (C1')–H), 5.09 (br-s, 1H, OH), 3.94 (m, 1H, (C2')–H), 1.11 (d, J = 6.4 Hz, 3H, (C3')–H3). ^{13}C NMR (151 MHz, DMSO) 169.3, 168.1, 141.2, 139.4, 109.3, 106.5, 72.1, 68.0, 20.1. IR (solid, cm^{-1}): 3220, 2963, 1547, 1523, 1505. M.p. 134–142 °C $[\alpha]_D^{20.0}$ (*c* = 1.00, H_2O) 0.2.

6.11.5 L-lactaldehyde aminal (L-44)

General procedure A was followed using L-lactaldehyde (**L-43**) and 2-aminothiazole (**23**) yielding **L-44** as a white solid (68% yield). ^{1}H NMR (400 MHz, DMSO) 7.70 (d, J = 7.4 Hz, 1H, NH), 7.64 (d, J = 7.4 Hz, 1H, NH), 7.01 (m, 2H, Ar), 6.62 (d, J = 3.7, 1H, Ar), 6.62 (d, J = 3.7, 1H, Ar) 5.21 (m, 1H, (C1')–H), 5.10 (br-s, 1H, OH), 3.93 (m, 1H, (C2')–H), 1.10 (d, J = 6.4 Hz, 3H, (C3')–H_3). ^{13}C NMR (151 MHz, DMSO) 169.2, 168.9, 139.2, 137.7, 107.5, 106.7, 70.3, 67.3, 19.1. IR (solid, cm^{-1}): 3224, 2981, 1560, 1524, 1506, 1505. M.p. 126–130 °C $[\alpha]_D^{20.0}$ (*c* = 1.00, H_2O) -17.5

6.12 General procedure B for the synthesis of cyanohydrin from the aminal

Aminal (0.1 mmol) was stirred in H_2O/ D_2O (9:1, 0.5 mL) and the pH was adjusted to 3 using 4 M HCl, where the solution becomes homogenous. The solution was then raised to pH 7 with 4 M NaOH and potassium cyanide was added (9.75 mg, 0.15 mmol). The pH was then raised further to pH 9.2 with 4 M NaOH and then the total volume was adjusted to 1 mL using D_2O. NMR monitored the formation of the cyanohydrin.

6.12.1 Lactaldehyde cyanohydrin (L-45)

General procedure B was followed where NMR monitored the formation of the cyanohydrin as a mixture of diastereoisomers formed, major: minor (53:47). ^{1}H NMR (400 MHz, D_2O) 4.67 (d, J = 4.9 Hz, 1H, (C2)-H minor, 4.65 (d, J = 4.5 Hz, 1H, (C2)-H major), 4.13 (m, 2H, (C3)-H major + minor), 1.39 (d, J = 6.4 Hz, 3H, (C4)-H3, minor), 1.39 (d, J = 6.5 Hz, 3H, (C4)-H3, major).

6.12.2 Glyceraldehyde cyanohydrin (L-46)

General procedure B was followed where NMR monitored the formation of the cyanohydrin as a mixture of diastereoisomers formed, major: minor (54:46). ^{1}H NMR (400 MHz, D_2O) δ ppm 4.78 (d, J = 5.8 Hz, 1H, (C2)-H, major), 4.75 (d, J = 4.6 Hz, 1H, (C2)-H, minor), 4.03 (m, 2H, (C3)-H, major + minor), 3.79 (m, 4H, (C4)-H2, major + minor).

6.13 General procedure C for the co-crystallisation experiments with Glyceraldehyde aminal (rac-25)

Aminal (specified concentration) was stirred in H_2O or phosphate buffer (1 M, pH 7) and the pH was adjusted to 3 using 4 M HCl, where the solution becomes homogenous. The additive (specified concentration and ratio) was added. The solution was then raised to pH 7 with 4 M NaOH and allowed to crystallise for 2 weeks.

*Table 33: Table showing all the attempted co-crystallisations with rac-glyceraldehyde aminal (**25**) at different concentrations, with multiple additives, at multiple ratios. Green tick means yes. Red cross means no. N/A- not applicable.*

Rac-glyceraldehyde aminal (25)/ (M)	Addititive / (M)	Ratio	Solvent System	Key Functional Group	Crystals Formed?	Additive Present in NMR?	PXRD show s incorporation of additive?
0.25	Menthol	1:1	H_2O	Alcohol	N/A	✗	N/A
0.50	Menthol	1:1	H_2O	Alcohol	N/A	✗	N/A
1.00	Menthol	1:1	H_2O	Alcohol	N/A	✗	N/A
1.00	L Serinamide	1:1	H_2O	Amide	N/A	✗	N/A
0.25	L Serinamide	1:1	H_2O	Amide	N/A	✗	N/A
0.50	L Serinamide	1:1	H_2O	Amide	N/A	✗	N/A
0.25	D/L Tyrosine	1:1	H_2O	Amino acid	N/A	✗	N/A
0.50	D/L Tyrosine	1:1	H_2O	Amino acid	N/A	✗	N/A
1.00	D/L Tyrosine	1:1	H_2O	Amino acid	N/A	✗	N/A
0.25	Glycine	1:1	H_2O	Amino acid	✓	✗	N/A

0.50	Glycine	1:1	H_2O	Amino acid	✔	✗	N/A
1.00	Glycine	1:1	H_2O	Amino acid	N/A	✗	N/A
0.25	Glycine	1:1	Pi (1M)	Amino acid	✔	✗	N/A
0.50	Glycine	1:1	Pi (1M)	Amino acid	✔	✗	N/A
1.00	Glycine	1:1	Pi (1M)	Amino acid	N/A	✗	N/A
0.25	Glycine	1:2	Pi (1M)	Amino acid	✗	✗	N/A
0.50	Glycine	1:2	Pi (1M)	Amino acid	N/A	✗	N/A
1.00	Glycine	1:2	Pi (1M)	Amino acid	N/A	✗	N/A
0.25	L Proline	1:1	H_2O	Amino acid	✔	✗	N/A
0.50	L Proline	1:1	H_2O	Amino acid	✔	✗	N/A
1.00	L Proline	1:1	H_2O	Amino acid	N/A	✗	N/A
0.25	L Proline	1:1	Pi (1M)	Amino acid	✔	✗	N/A
0.50	L Proline	1:1	Pi (1M)	Amino acid	✔	✗	N/A
1.00	L Proline	1:1	Pi (1M)	Amino acid	N/A	✗	N/A
0.25	L Proline	1:2	H_2O	Amino acid	N/A	✗	N/A

0.50	L Proline	1:2	H_2O	Amino acid	N/A	✗	N/A
1.00	L Proline	1:2	H_2O	Amino acid	N/A	✗	N/A
0.25	L Serine	1:1	H_2O	Amino acid	N/A	✗	N/A
0.50	L Serine	1:1	H_2O	Amino acid	N/A	✗	N/A
1.00	L Serine	1:1	H_2O	Amino acid	N/A	✗	N/A
0.25	L Tyrosine	1:1	H_2O	Amino acid	N/A	✗	N/A
0.50	L Tyrosine	1:1	H_2O	Amino acid	N/A	✗	N/A
1.00	L Tyrosine	1:1	H_2O	Amino acid	N/A	✗	N/A
0.25	L Valine	1:1	H_2O	Amino acid	N/A	✗	N/A
0.50	L Valine	1:1	H_2O	Amino acid	N/A	✗	N/A
1.00	L Valine	1:1	H_2O	Amino acid	N/A	✗	N/A
0.50	Lysine	1:1	H_2O	Amino acid	✗	✗	N/A
0.50	Lysine	1:2	H_2O	Amino acid	✗	✗	N/A
0.25	Threonine	1:1	Pi (1M)	Amino acid	✗	✗	N/A
0.25	Threonine	1:1	H_2O	Amino acid	✗	✗	N/A

0.25	3,4 dimethoxyphenylacetone	1:1	Pi (1M)	Aromatic	N/A	✗	N/A
0.25	3,4 dimethoxyphenylacetone	1:1	H_2O	Aromatic	N/A	✗	N/A
0.50	3,4 dimethoxyphenylacetone	1:1	H_2O	Aromatic	N/A	✗	N/A
1.00	3,4 dimethoxyphenylacetone	1:1	H_2O	Aromatic	N/A	✗	N/A
1.00	Atrolactic acid	1:1	H_2O	Aromatic	N/A	✗	N/A
0.25	Atrolactic acid	1:1	H_2O	Aromatic	N/A	✗	N/A
1.00	Atrolactic acid	1:2	H_2O	Aromatic	N/A	✗	N/A
0.25	Benzoic acid	1:1	H_2O	Aromatic	N/A	✗	N/A
0.50	Benzoic acid	1:1	H_2O	Aromatic	N/A	✗	N/A
1.00	Benzoic acid	1:1	H_2O	Aromatic	N/A	✗	N/A
0.50	Indole 2-Carboxylic acid	1:1	H_2O	Aromatic	✗	✗	N/A

1.00	Indole 2-Carboxylic acid	1:1	H_2O	Aromatic	✔	✗	N/A
1.00	Indole 2-Carboxylic acid	1:2	H_2O	Aromatic	✗	✗	N/A
0.25	Adipic acid	1:1	Pi (1M)	Di-carboxylic acid	N/A	✗	N/A
0.25	Adipic acid	1:2	H_2O	Di-carboxylic acid	N/A	✗	N/A
0.10	Adipic acid	1:1	H_2O	Di-carboxylic acid	N/A	✗	N/A
0.10	Adipic acid	1:2	H_2O	Di-carboxylic acid	N/A	✗	N/A
0.50	Aspartic acid	1:1	H_2O	Di-carboxylic acid	✗	✗	N/A
0.50	Aspartic acid	1:2	H_2O	Di-carboxylic acid	✗	✗	N/A
0.25	Fumaric acid	1:2	H_2O	Di-carboxylic acid	N/A	✗	N/A
0.10	Fumaric acid	1:0.5	Pi (1M)	Di-carboxylic acid	N/A	✗	N/A
0.10	Fumaric acid	1:0.5	H_2O	Di-carboxylic acid	N/A	✗	N/A
0.10	Fumaric acid	1:1	H_2O	Di-carboxylic acid	N/A	✗	N/A
0.10	Fumaric acid	1:2	H_2O	Di-carboxylic acid	N/A	✗	N/A
1.00	Maleic acid	1:2	H_2O	Di-carboxylic acid	N/A	✗	N/A
1.00	Maleic acid	1:1	H_2O	Di-carboxylic acid	✗	✗	N/A

1.00	Maleic acid	1:1	Pi (1M)	Di-carboxylic acid	✓	✗	N/A
0.10	Maleic acid	1:2	Pi (1M)	Di-carboxylic acid	✗	✗	N/A
0.25	Maleic acid	1:1	Pi (1M)	Di-carboxylic acid	✗	✗	N/A
0.25	Maleic acid	1:1	H_2O	Di-carboxylic acid	✗	✗	N/A
1.00	Malonic acid	1:1	H_2O	Di-carboxylic acid	✓	✗	N/A
1.00	Malonic acid	1:1	Pi (1M)	Di-carboxylic acid	✗	✗	N/A
0.25	Malonic acid	1:1	H_2O	Di-carboxylic acid	✗	✗	N/A
1.00	Malonic acid	1:2	H_2O	Di-carboxylic acid	✓	✗	N/A
0.10	Malonic acid	1:2	Pi (1M)	Di-carboxylic acid	✗	✗	N/A
1.00	Oxalic acid	1:1	H_2O	Di-carboxylic acid	✓	N/A	N/A
1.00	Oxalic acid	1:2	H_2O	Di-carboxylic acid	✓	N/A	N/A
0.50	Oxalic acid	1:1	Pi (1M)	Di-carboxylic acid	✗	N/A	N/A
0.10	Oxalic acid	1:2	H_2O	Di-carboxylic acid	✗	N/A	N/A
0.25	Oxalic acid	1:1	H_2O	Di-carboxylic acid	✗	N/A	N/A
0.10	Tartaric acid	1:2	H_2O	Di-carboxylic acid	✗	✗	N/A

1.00	Tartaric acid	1:1	H_2O	Di-carboxylic acid	✔	✗	N/A
1.00	Tartaric acid	1:1	Pi (1M)	Di-carboxylic acid	✔	✗	N/A
0.25	Tartaric acid	1:1	H_2O	Di-carboxylic acid	✗	✗	N/A
1.00	Tartaric acid	1:2	H_2O	Di-carboxylic acid	N/A	✗	N/A
0.50	Butyric acid	1:1	H_2O	Mono carboxylic acid	✔	✗	N/A
1.00	Butyric acid	1:1	H_2O	Mono carboxylic acid	✔	✗	N/A
1.00	Butyric acid	1:2	H_2O	Mono carboxylic acid	N/A	✗	N/A
1.00	Lactic acid	1:1	H_2O	Mono carboxylic acid	✔	✗	N/A
0.10	Lactic acid	1:2	H_2O	Mono carboxylic acid	✗	✗	N/A
1.00	Lactic acid	1:1	H_2O	Mono carboxylic acid	✔	✗	N/A
0.25	Lactic acid	1:1	H_2O	Mono carboxylic acid	✗	✗	N/A
1.00	Lactic acid	1:2	H_2O	Mono carboxylic acid	N/A	✗	N/A
0.50	Levulinic acid	1:1	H_2O	Mono carboxylic acid	✔	✗	N/A
1.00	Levulinic acid	1:1	H_2O	Mono carboxylic acid	✔	✗	N/A
1.00	Octanoic acid	1:1	H_2O	Mono carboxylic acid	✗	✗	N/A

0.50	Octanoic acid	1:1	H_2O	Mono carboxylic acid	✗	✗	N/A
0.50	Octanoic acid	1:2	H_2O	Mono carboxylic acid	✗	✗	N/A
0.25	Octanoic acid	1:1	H_2O	Mono carboxylic acid	✗	✗	N/A
0.25	Octanoic acid	1:2	H_2O	Mono carboxylic acid	✗	✗	N/A
0.50	Pyruvic acid	1:1	H_2O	Mono carboxylic acid	✓	✗	N/A
1.00	Pyruvic acid	1:1	H_2O	Mono carboxylic acid	✓	✗	N/A
0.50	2 methoxyphenol	1:2	H_2O	Phenol	✗	✗	N/A
1.00	2 methoxyphenol	1:1	H_2O	Phenol	✓	✗	N/A
0.50	2 methoxyphenol	1:1	Pi (1M)	Phenol	✓	✗	N/A
0.50	2 methoxyphenol	1:1	H_2O	Phenol	✓	✗	N/A
1.00	2 methoxyphenol	1:2	H_2O	Phenol	N/A	✗	N/A
0.25	2,6 dimethylphenol	1:1	Pi (1M)	Phenol	N/A	✗	N/A
0.25	2,6 dimethylphenol	1:1	H_2O	Phenol	N/A	✗	N/A
0.50	2,6 dimethylphenol	1:1	H_2O	Phenol	N/A	✗	N/A
1.00	2,6 dimethylphenol	1:1	H_2O	Phenol	N/A	✗	N/A

1.00	3,4 dimethylphenol	1:1	H_2O	Phenol	N/A	✗	N/A
0.50	3,4 dimethylphenol	1:1	H_2O	Phenol	N/A	✗	N/A
0.25	3,4 dimethylphenol	1:1	Pi (1M)	Phenol	N/A	✗	N/A
1.00	4 chlorophenol	1:1	H_2O	Phenol	N/A	✗	N/A
0.50	4 chlorophenol	1:1	H_2O	Phenol	N/A	✗	N/A
0.50	Phenol	1:1	H_2O	Phenol	✓	✓	✗
0.50	Phenol	1:2	H_2O	Phenol	✓	✓	✗
1.00	Phenol	1:1	H_2O	Phenol	✓	✓	✗
1.00	Phenol	1:2	H_2O	Phenol	✓	✓	✗
0.10	Phenol	1:1	H_2O	Phenol	✓	✗	N/A
0.20	Phenol	1:1	H_2O	Phenol	✓	✗	N/A
0.30	Phenol	1:1	H_2O	Phenol	✓	✗	N/A
0.50	2 methoxypyridine	1:1	H_2O	Pyridine	✓	✗	N/A
1.00	2 methoxypyridine	1:1	H_2O	Pyridine	✓	✗	N/A

0.50	2-hydroxypyridine-N-oxide	1:2	H_2O	Pyridine	✓	✗	N/A
0.50	2-hydroxypyridine-N-oxide	1:1	H_2O	Pyridine	✓	✗	N/A
0.50	2,4-dihydroxypyridine	1:1	H_2O	Pyridine	✓	✗	N/A
1.00	2,4-dihydroxypyridine	1:1	H_2O	Pyridine	✓	✗	N/A
0.50	4-hydroxypyridine	1:1	H_2O	Pyridine	✗	✗	N/A
1.00	4-hydroxypyridine	1:1	H_2O	Pyridine	✗	✗	N/A

6.14 Single-crystal X-ray Diffraction

6.14.1 Conditions

The crystallographic data was collected using an Agilent SuperNova (Dual Source) single crystal X-ray diffractometer equipped with an Atlas CCD detector. The data set was collected at 150 K using CuK radiation (= 1.54184). The data was collected and processed using the CrysAlisPro1program. Lorentz and polarization corrections were applied using the same software. Structure solution and refinement were performed using SHELXS2and SHELXL3, respectively. The crystal structure was solved using direct methods. All non-hydrogen atoms were refined anisotropically, while hydrogen atoms associated with carbon and oxygen atoms were refined isotropically in geometrically constrained positions. Hydrogen atoms affiliated with nitrogen atoms were refined isotropically in positions identified in the difference Fourier map. The positions and anisotropic displacement parameter of these hydrogen atoms were constrained in the final refinement cycle.

6.15 Crystallographic data

The crystallographic and refinement parameters are shown in the following tables.

Compound name	L-ribo amino oxazoline	D-ribo amino oxazoline
Identification code	xstr0867new	xstr0812new1
Empirical formula	$C_6H_{10}N_2O_4$	$C_6H_{10}N_2O_4$
Formula weight	174.16	174.16
Temperature/K	153(4)	150.00(10)
Crystal system	orthorhombic	orthorhombic
Space group	$P2_12_12_1$	$P2_12_12_1$
a/Å	8.3865(2)	8.38620(10)
b/Å	8.56606(18)	8.56520(10)
c/Å	10.0464(3)	10.04820(10)
α/°	90	90
β/°	90	90
γ/°	90	90
Volume/Å^3	721.72(3)	721.757(14)
Z	4	4
ρ_{calc}g/cm^3	1.603	1.603
μ/mm^1	1.168	1.168
F(000)	368	368
Crystal size/mm^3	0.112 × 0.097 × 0.072	0.221 × 0.116 × 0.102
Radiation	CuKα (λ = 1.54184)	CuKα (λ = 1.54184)
2Θ range for data collection/°	13.584 to 133.172	13.584 to 147.254

Index ranges	$-9 \leq h \leq 9, -10 \leq k \leq 10, -11 \leq l \leq 11$	$-10 \leq h \leq 10, -10 \leq k \leq 10, -12 \leq l \leq 12$
Reflections collected	23796	24569
Independent reflections	1275 [R_{int} = 0.0589, R_{sigma} = 0.0173]	1461 [R_{int} = 0.0335, R_{sigma} = 0.0096]
Data/restraints/parameters	1275/0/111	1461/0/117
Goodness-of-fit on F^2	1.113	1.072
Final R indexes [I>=2σ (I)]	R_1 = 0.0309, wR_2 = 0.0782	R_1 = 0.0238, wR_2 = 0.0622
Final R indexes [all data]	R_1 = 0.0329, wR_2 = 0.0803	R_1 = 0.0240, wR_2 = 0.0623
Largest diff. peak/hole / e $Å^{-3}$	0.16/-0.28	0.20/-0.19
Flack parameter	-0.05(12)	0.05(4)
CCDC number		

Compound name	L-arabino amino oxazoline	D-arabino amino oxazoline	L-arabino amino oxazoline*
Identification code	xstr0848abscorr	xstr0772	xstr0841-abs
Empirical formula	$C_6H_9N_2O_4$	$C_6H_{10}N_2O_4$	$C_6H_{10}N_2O_4$
Formula weight	173.15	174.16	174.16
Temperature/K	151(1)	150.0(4)	157(6)
Crystal system	monoclinic	monoclinic	monoclinic
Space group	$P2_1$	$P2_1$	$P2_1$
a/Å	6.39170(10)	6.39390(10)	6.39320(10)
b/Å	7.6660(2)	7.66760(10)	7.66910(10)
c/Å	8.29010(10)	8.29250(10)	8.2927(2)
α/°	90	90	90
β/°	110.656(2)	110.681(2)	110.673(2)
γ/°	90	90	90
Volume/Å^3	380.092(13)	380.349(10)	380.411(13)
Z	2	2	2
ρ_{calc}g/cm^3	1.513	1.521	1.52
μ/mm^{-1}	1.109	1.108	1.108
F(000)	182	184	184

Crystal size/mm^3	0.2 × 0.151 × 0.095	? × ? × ?	0.248 × 0.229 × 0.131
Radiation	CuKα (λ = 1.54184)	CuKα (λ = 1.54184)	CuKα (λ = 1.54184)
2Θ range for data collection/°	11.408 to 147.684	11.406 to 132.882	11.404 to 147.442
Index ranges	-7 ≤ h ≤ 7, -8 ≤ k ≤ 9, -10 ≤ l ≤ 10	-7 ≤ h ≤ 7, -9 ≤ k ≤ 9, -9 ≤ l ≤ 9	-7 ≤ h ≤ 7, -9 ≤ k ≤ 9, -10 ≤ l ≤ 9
Reflections collected	12914	12349	13048
Independent reflections	1433 [R_{int} = 0.0297, R_{sigma} = 0.0122]	1340 [R_{int} = 0.0356, R_{sigma} = 0.0134]	1521 [R_{int} = 0.0241, R_{sigma} = 0.0094]
Data/restraints/parameters	1433/1/119	1340/1/119	1521/1/111
Goodness-of-fit on F^2	1.103	1.087	1.146
Final R indexes [I>=2σ (I)]	R_1 = 0.0308, wR_2 = 0.0866	R_1 = 0.0308, wR_2 = 0.0869	R_1 = 0.0265, wR_2 = 0.0692
Final R indexes [all data]	R_1 = 0.0308, wR_2 = 0.0867	R_1 = 0.0308, wR_2 = 0.0869	R_1 = 0.0265, wR_2 = 0.0692
Largest diff. peak/hole / e $Å^{-3}$	0.49/-0.39	0.44/-0.42	0.18/-0.24
Flack parameter	-0.04(9)	-0.10(7)	0.05(4)
CCDC number			

Compound name	L-xylo-amino oxazoline	D-xylo-amino oxazoline
Identification code	xstr0766abs	xstr0764abs
Empirical formula	$C_6H_{11}N_2O_4$	$C_6H_{10}N_2O_4$
Formula weight	175.17	174.16
Temperature/K	150.01(10)	293(2)
Crystal system	orthorhombic	orthorhombic
Space group	$P2_12_12_1$	$P2_12_12_1$
a/Å	6.92338(7)	6.92400(10)
b/Å	9.55543(9)	9.55350(10)
c/Å	10.83670(12)	10.83210(10)
α/°	90	90
β/°	90	90
γ/°	90	90
Volume/Å^3	716.911(12)	716.526(14)
Z	4	4
ρ_{calc}g/cm^3	1.623	1.614
μ/mm^{-1}	1.176	1.177
F(000)	372	368
Crystal size/mm^3	0.155 × 0.139 × 0.093	0.474 × 0.265 × 0.119
Radiation	CuKα (λ = 1.54184)	CuKα (λ = 1.54184)

2Θ range for data collection/°	12.35 to 147.182	12.354 to 133.134
Index ranges	-8 ≤ h ≤ 8, -11 ≤ k ≤ 11, -13 ≤ l ≤ 13	-8 ≤ h ≤ 8, -11 ≤ k ≤ 11, -12 ≤ l ≤ 12
Reflections collected	24943	23438
Independent reflections	1442 [R_{int} = 0.0304, R_{sigma} = 0.0082]	1255 [R_{int} = 0.0224, R_{sigma} = 0.0056]
Data/restraints/parameters	1442/0/111	1255/0/111
Goodness-of-fit on F^2	1.101	1.147
Final R indexes [I>=2σ (I)]	R_1 = 0.0293, wR_2 = 0.0786	R_1 = 0.0247, wR_2 = 0.0665
Final R indexes [all data]	R_1 = 0.0296, wR_2 = 0.0790	R_1 = 0.0247, wR_2 = 0.0666
Largest diff. peak/hole / e Å^{-3}	0.20/-0.58	0.28/-0.24
Flack parameter	-0.02(4)	0.07(3)
CCDC number		

Compound name	L-ribo-oxazolidinone thione	D-ribo-oxazolidinone thione	D-ribo-oxazolidinone thione*
Identification code	xstr0770new	xstr0847new	xstr0686new
Empirical formula	$C_6H_9NO_4S$	$C_6H_9NO_4S$	$C_6H_9NO_4S$
Formula weight	191.2	191.2	191.2
Temperature/K	148(3)	150.00(10)	150.00(10)
Crystal system	orthorhombic	orthorhombic	orthorhombic
Space group	$P2_12_12_1$	$P2_12_12_1$	$P2_12_12_1$
a/Å	8.27000(10)	8.26890(10)	8.27310(10)
b/Å	8.51680(10)	8.52410(10)	8.52060(10)
c/Å	11.13730(10)	11.1339(2)	11.13760(10)
α/°	90	90	90
β/°	90	90	90
γ/°	90	90	90
Volume/Å^3	784.444(15)	784.772(19)	785.109(15)
Z	4	4	4
ρ_{calc}g/cm^3	1.619	1.618	1.618
μ/mm^1	3.521	3.519	3.518
F(000)	400	400	400
Crystal size/mm^3	0.295 × 0.22 × 0.108	0.234 × 0.114 × 0.08	0.232 × 0.18 × 0.113

Radiation	CuKα (λ = 1.54184)	CuKα (λ = 1.54184)	CuKα (λ = 1.54184)
2Θ range for data collection/°	13.086 to 133.158	13.08 to 133.192	13.082 to 133.166
Index ranges	-9 ≤ h ≤ 9, -10 ≤ k ≤ 10, -13 ≤ l ≤ 13	-9 ≤ h ≤ 9, -10 ≤ k ≤ 10, -12 ≤ l ≤ 13	-9 ≤ h ≤ 9, -10 ≤ k ≤ 10, -13 ≤ l ≤ 13
Reflections collected	26083	25546	25834
Independent reflections	1385 [R_{int} = 0.0230, R_{sigma} = 0.0061]	1384 [R_{int} = 0.0377, R_{sigma} = 0.0106]	1387 [R_{int} = 0.0314, R_{sigma} = 0.0076]
Data/restraints/parameters	1385/0/114	1384/0/114	1387/0/114
Goodness-of-fit on F^2	1.112	1.083	1.088
Final R indexes [I>=2σ (I)]	R_1 = 0.0180, wR_2 = 0.0472	R_1 = 0.0201, wR_2 = 0.0532	R_1 = 0.0201, wR_2 = 0.0524
Final R indexes [all data]	R_1 = 0.0180, wR_2 = 0.0472	R_1 = 0.0201, wR_2 = 0.0532	R_1 = 0.0201, wR_2 = 0.0524
Largest diff. peak/hole / e $Å^{-3}$	0.16/-0.21	0.16/-0.19	0.15/-0.20
Flack parameter	-0.004(3)	-0.008(6)	0.143(4)
CCDC number			

Compound name	L-arabino-oxazolidinone thione	rac-arabino-oxazolidinone thione
Identification code	xstr0838new	xstr0688new2
Empirical formula	$C_6H_9NO_4S$	$C_6H_9NO_4S$
Formula weight	191.2	191.2
Temperature/K	151(2)	151(2)
Crystal system	monoclinic	monoclinic
Space group	$P2_1$	$P2_1/c$
a/Å	5.09990(10)	5.27069(4)
b/Å	10.9491(2)	12.65159(11)
c/Å	7.0711(2)	11.70221(11)
α/°	90	90
β/°	91.880(2)	96.3897(8)
γ/°	90	90
Volume/Å^3	394.633(15)	775.486(12)
Z	2	4
ρ_{calc}g/cm^3	1.609	1.638
μ/mm^1	3.499	3.561
F(000)	200	400
Crystal size/mm^3	0.243 × 0.168 × 0.078	0.167 × 0.16 × 0.089

Radiation	CuKα (λ = 1.54184)	CuKα (λ = 1.54184)
2Θ range for data collection/°	12.524 to 133.14	10.332 to 133.182
Index ranges	-6 ≤ h ≤ 6, -13 ≤ k ≤ 13, -8 ≤ l ≤ 8	-6 ≤ h ≤ 6, -15 ≤ k ≤ 15, -13 ≤ l ≤ 13
Reflections collected	12710	24743
Independent reflections	1389 [R_{int} = 0.0346, R_{sigma} = 0.0130]	1368 [R_{int} = 0.0349, R_{sigma} = 0.0099]
Data/restraints/parameters	1389/1/111	1368/1/114
Goodness-of-fit on F^2	1.057	1.079
Final R indexes [I>=2σ (I)]	R_1 = 0.0246, wR_2 = 0.0664	R_1 = 0.0288, wR_2 = 0.0792
Final R indexes [all data]	R_1 = 0.0246, wR_2 = 0.0664	R_1 = 0.0294, wR_2 = 0.0799
Largest diff. peak/hole / e $Å^{-3}$	0.24/-0.19	0.27/-0.31
Flack parameter	-0.007(11)	
CCDC number		

Compound name	L-xylo-oxazolidinone thione	D-xylo-oxazolidinone thione
Identification code	xstr0771	xstr0837
Empirical formula	$C_6H_9NO_4S$	$C_6H_9NO_4S$
Formula weight	191.2	191.2
Temperature/K	150.00(10)	150.2(9)
Crystal system	orthorhombic	orthorhombic
Space group	$P2_12_12_1$	$P2_12_12_1$
a/Å	4.77330(10)	4.77360(10)
b/Å	7.08020(10)	7.08000(10)
c/Å	22.8695(2)	22.8672(2)
α/°	90	90
β/°	90	90
γ/°	90	90
Volume/Å^3	772.90(2)	772.84(2)
Z	4	4
ρ_{calc}g/cm^3	1.643	1.643
μ/mm^1	3.573	3.573
F(000)	400	400
Crystal size/mm^3	0.327 × 0.079 × 0.049	0.165 × 0.162 × 0.092

Radiation	CuKα (λ = 1.54184)	CuKα (λ = 1.54184)
2Θ range for data collection/°	7.732 to 133.126	7.732 to 133.13
Index ranges	-5 ≤ h ≤ 5, -8 ≤ k ≤ 8, -27 ≤ l ≤ 27	-5 ≤ h ≤ 5, -8 ≤ k ≤ 8, -27 ≤ l ≤ 27
Reflections collected	25406	25388
Independent reflections	1361 [R_{int} = 0.0340, R_{sigma} = 0.0105]	1361 [R_{int} = 0.0340, R_{sigma} = 0.0093]
Data/restraints/parameters	1361/1/111	1361/1/114
Goodness-of-fit on F^2	1.095	1.103
Final R indexes [I>=2σ (I)]	R_1 = 0.0214, wR_2 = 0.0540	R_1 = 0.0194, wR_2 = 0.0504
Final R indexes [all data]	R_1 = 0.0217, wR_2 = 0.0544	R_1 = 0.0195, wR_2 = 0.0505
Largest diff. peak/hole / e $Å^{-3}$	0.17/-0.19	0.15/-0.19
Flack parameter	-0.011(6)	-0.020(5)
CCDC number		

Compound name	D-ribo-oxazolidinone	rac-ribo-oxazolidinone
Identification code	xstr0810new1	xstr0833new1
Empirical formula	$C_6H_9NO_5$	$C_6H_9NO_5$
Formula weight	175.14	175.14
Temperature/K	150.1(4)	153(5)
Crystal system	orthorhombic	monoclinic
Space group	$P2_12_12_1$	$P2_1/c$
a/Å	5.07450(10)	7.35610(10)
b/Å	9.27750(10)	11.45320(10)
c/Å	14.7627(2)	8.7299(2)
α/°	90	90
β/°	90	108.207(2)
γ/°	90	90
Volume/Å^3	695.008(18)	698.68(2)
Z	4	4
ρ_{calc}g/cm^3	1.674	1.665
μ/mm^1	1.288	1.281
F(000)	368	368
Crystal size/mm^3	0.113 × 0.1 × 0.092	0.406 × 0.221 × 0.178
Radiation	CuKα (λ = 1.54184)	CuKα (λ = 1.54184)

2Θ range for data collection/°	11.264 to 133.122	12.668 to 132.782
Index ranges	-6 ≤ h ≤ 6, -11 ≤ k ≤ 11, -17 ≤ l ≤ 17	-8 ≤ h ≤ 8, -13 ≤ k ≤ 13, -10 ≤ l ≤ 10
Reflections collected	22635	21965
Independent reflections	1226 [R_{int} = 0.0389, R_{sigma} = 0.0106]	1229 [R_{int} = 0.0228, R_{sigma} = 0.0057]
Data/restraints/parameters	1226/0/111	1229/1/111
Goodness-of-fit on F^2	1.14	1.121
Final R indexes [I>=2σ (I)]	R_1 = 0.0253, wR_2 = 0.0642	R_1 = 0.0335, wR_2 = 0.0851
Final R indexes [all data]	R_1 = 0.0259, wR_2 = 0.0647	R_1 = 0.0337, wR_2 = 0.0852
Largest diff. peak/hole / e $Å^{-3}$	0.18/-0.20	0.24/-0.28
Flack parameter	-0.09(5)	
CCDC number		

Compound name	L-arabino-oxazolidinone
Identification code	xstr0836new1
Empirical formula	C6H9NO5
Formula weight	175.14
Temperature/K	151(2)
Crystal system	orthorhombic
Space group	P212121
a/Å	4.96880(10)
b/Å	9.6148(2)
c/Å	14.4113(2)
α/°	90
β/°	90
γ/°	90
Volume/Å3	688.49(2)
Z	4
ρcalcg/cm3	1.69
μ/mm1	1.3
F(000)	368
Crystal size/mm3	0.217 × 0.133 × 0.101
Radiation	CuKα (λ = 1.54184)
2Θ range for data collection/°	11.062 to 133.188
Index ranges	-5 ≤ h ≤ 5, -11 ≤ k ≤ 10, -17 ≤ l ≤ 17

Reflections collected	22490
Independent reflections	1209 [Rint = 0.0402, Rsigma = 0.0122]
Data/restraints/parameters	1209/0/111
Goodness-of-fit on F2	1.125
Final R indexes [I>=2σ (I)]	R1 = 0.0279, wR2 = 0.0706
Final R indexes [all data]	R1 = 0.0284, wR2 = 0.0712
Largest diff. peak/hole / e Å-3	0.16/-0.26
Flack parameter	0.00(4)
CCDC number	

Compound name	L-xylo-oxazolidinone	D-xylo-oxazolidinone
Identification code	xstr0852new1	xstr0792
Empirical formula	C6H9NO5	C6H9NO5
Formula weight	175.14	175.14
Temperature/K	150.00(10)	150.00(10)
Crystal system	orthorhombic	orthorhombic
Space group	P212121	P212121
a/Å	7.89996(11)	7.89890(10)
b/Å	9.14215(16)	9.14290(10)
c/Å	9.90528(12)	9.90440(10)
α/°	90	90
β/°	90	90
γ/°	90	90
Volume/Å3	715.385(19)	715.284(14)
Z	4	4
ρcalcg/cm3	1.626	1.626
μ/mm1	1.252	1.252
F(000)	368	368
Crystal size/mm3	0.24 × 0.068 × 0.043	0.286 × 0.227 × 0.128
Radiation	CuKα (λ = 1.54184)	CuKα (λ = 1.54184)
2Θ range for data collection/°	13.178 to 133.118	13.178 to 133.14

Index ranges	-9 ≤ h ≤ 9, -10 ≤ k ≤ 10, -11 ≤ l ≤ 11	-9 ≤ h ≤ 9, -10 ≤ k ≤ 10, -11 ≤ l ≤ 11
Reflections collected	23625	23635
Independent reflections	1264 [Rint = 0.0477, Rsigma = 0.0136]	1264 [Rint = 0.0256, Rsigma = 0.0066]
Data/restraints/parameters	1264/0/111	1264/0/111
Goodness-of-fit on F2	1.125	1.159
Final R indexes [I>=2σ (I)]	R1 = 0.0255, wR2 = 0.0640	R1 = 0.0253, wR2 = 0.0658
Final R indexes [all data]	R1 = 0.0266, wR2 = 0.0650	R1 = 0.0254, wR2 = 0.0658
Largest diff. peak/hole / e Å-3	0.13/-0.19	0.15/-0.28
Flack parameter	0.07(7)	-0.02(3)
CCDC number		

	L-ribo	D-ribo	rac-ribo
Compound name	oxazolidinone methyl thione	oxazolidinone methyl thione	oxazolidinone methyl thione
Identification code	xstr0825	xstr0808	xstr0868
Empirical formula	C7H11NO4S	C7H12N2O3S	C7H11NO4S
Formula weight	205.23	204.25	205.23
Temperature/K	150.03(10)	150.02(10)	152(5)
Crystal system	orthorhombic	orthorhombic	monoclinic
Space group	P212121	P212121	P21/c
a/Å	7.67430(10)	7.65600(10)	10.4331(3)
b/Å	8.78520(10)	8.76100(10)	10.7919(2)
c/Å	13.30560(10)	13.30630(10)	8.3347(2)
α/°	90	90	90
β/°	90	90	108.717(2)
γ/°	90	90	90
Volume/Å3	897.067(17)	892.510(17)	888.80(4)
Z	4	4	4
ρcalcg/cm3	1.52	1.52	1.534
μ/mm1	3.119	3.077	3.148
F(000)	432	432	432
Crystal size/mm3	? × ? × ?	? × ? × ?	? × ? × ?
Radiation	CuKα (λ = 1.54184)	CuKα (λ = 1.54184)	CuKα (λ = 1.54184)
2Θ range for data collection/°	12.072 to 133.11	12.096 to 133.158	8.95 to 147.498

Index ranges	-9 ≤ h ≤ 9, -10 ≤ k ≤ 10, -15 ≤ l ≤ 15	-9 ≤ h ≤ 8, -10 ≤ k ≤ 10, -15 ≤ l ≤ 15	-12 ≤ h ≤ 12, -13 ≤ k ≤ 13, -10 ≤ l ≤ 10
Reflections collected	29259	29118	30054
Independent reflections	1581 [Rint = 0.0459, Rsigma = 0.0130]	1570 [Rint = 0.0346, Rsigma = 0.0090]	1792 [Rint = 0.0289, Rsigma = 0.0088]
Data/restraints/parameters	1581/0/121	1570/0/121	1792/0/121
Goodness-of-fit on F2	1.092	1.134	1.059
Final R indexes [I>=2σ (I)]	R1 = 0.0225, wR2 = 0.0576	R1 = 0.0247, wR2 = 0.0675	R1 = 0.0277, wR2 = 0.0732
Final R indexes [all data]	R1 = 0.0229, wR2 = 0.0581	R1 = 0.0247, wR2 = 0.0675	R1 = 0.0291, wR2 = 0.0746
Largest diff. peak/hole / e Å-3	0.15/-0.24	0.18/-0.33	0.33/-0.29
Flack parameter	-0.020(5)	0.011(5)	n/a
CCDC number			

Compound name	L-arabino oxazolidinone methyl thione
Identification code	xstr0801
Empirical formula	C7H11NO4S
Formula weight	205.23
Temperature/K	150.05(11)
Crystal system	monoclinic
Space group	C2
a/Å	13.1891(6)
b/Å	8.8629(4)
c/Å	7.7439(5)
α/°	90
β/°	94.119(5)
γ/°	90
Volume/Å3	902.87(8)
Z	4
ρcalcg/cm3	1.51
μ/mm1	3.099
F(000)	432
Crystal size/mm3	? × ? × ?
Radiation	CuKα (λ = 1.54184)
2Θ range for data collection/°	11.456 to 147.646

Index ranges	-16 ≤ h ≤ 16, -11 ≤ k ≤ 10, -9 ≤ l ≤ 9
Reflections collected	15950
Independent reflections	1798 [Rint = 0.0675, Rsigma = 0.0248]
Data/restraints/parameters	1798/1/121
Goodness-of-fit on F2	1.093
Final R indexes [I>=2σ (I)]	R1 = 0.0303, wR2 = 0.0693
Final R indexes [all data]	R1 = 0.0306, wR2 = 0.0696
Largest diff. peak/hole / e Å-3	0.25/-0.26
Flack parameter	0.001(10)
CCDC number	

6.16 Powder X-ray diffraction

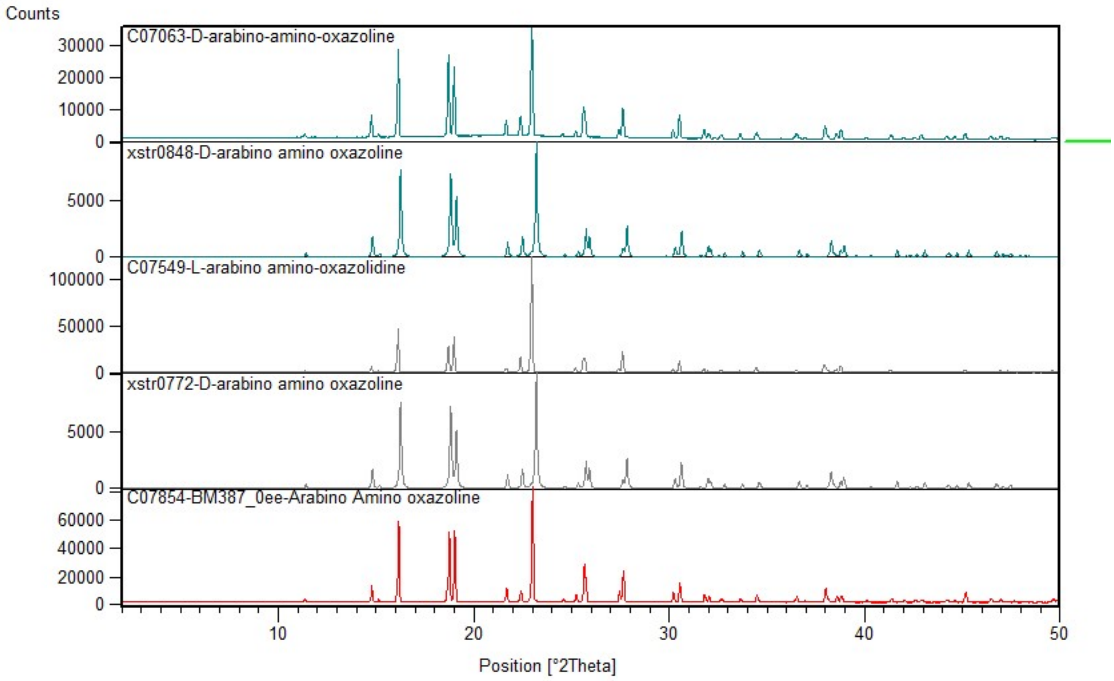

*Figure 148: PXRD arabino aminooxazoline (**AAO**)*

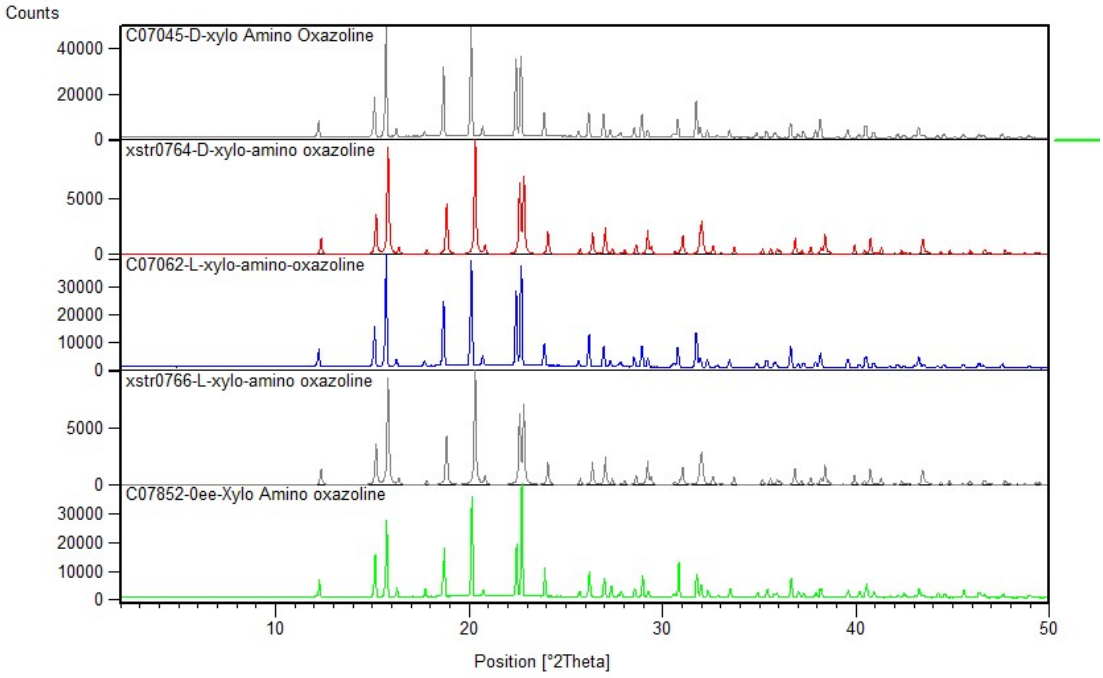

*Figure 149:PXRD xylo aminooxazoline (**XAO**)*

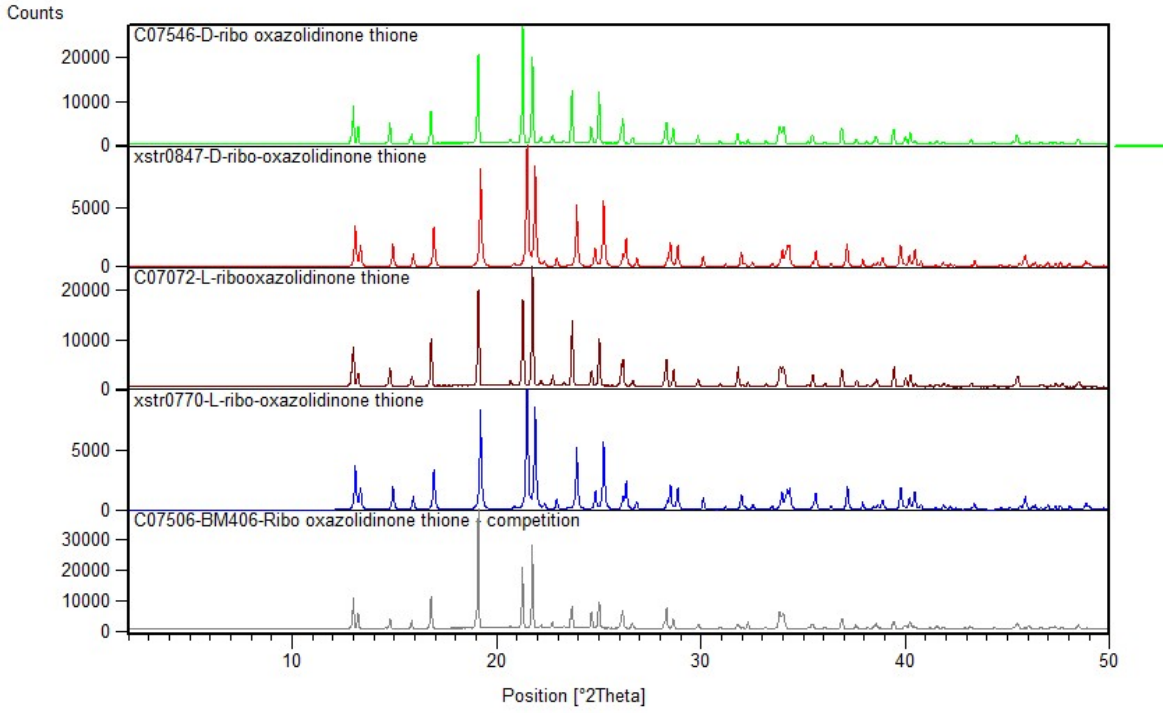

*Figure 150: PXRD **ROT***

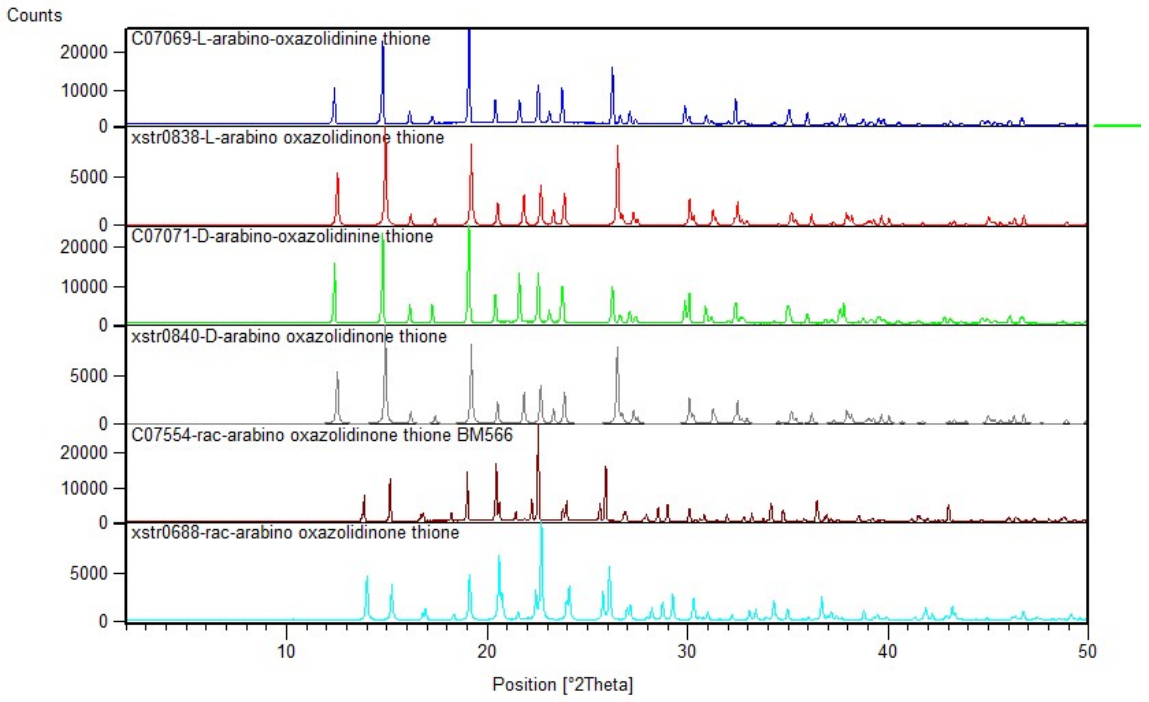

*Figure 151:PXRD **AOT***

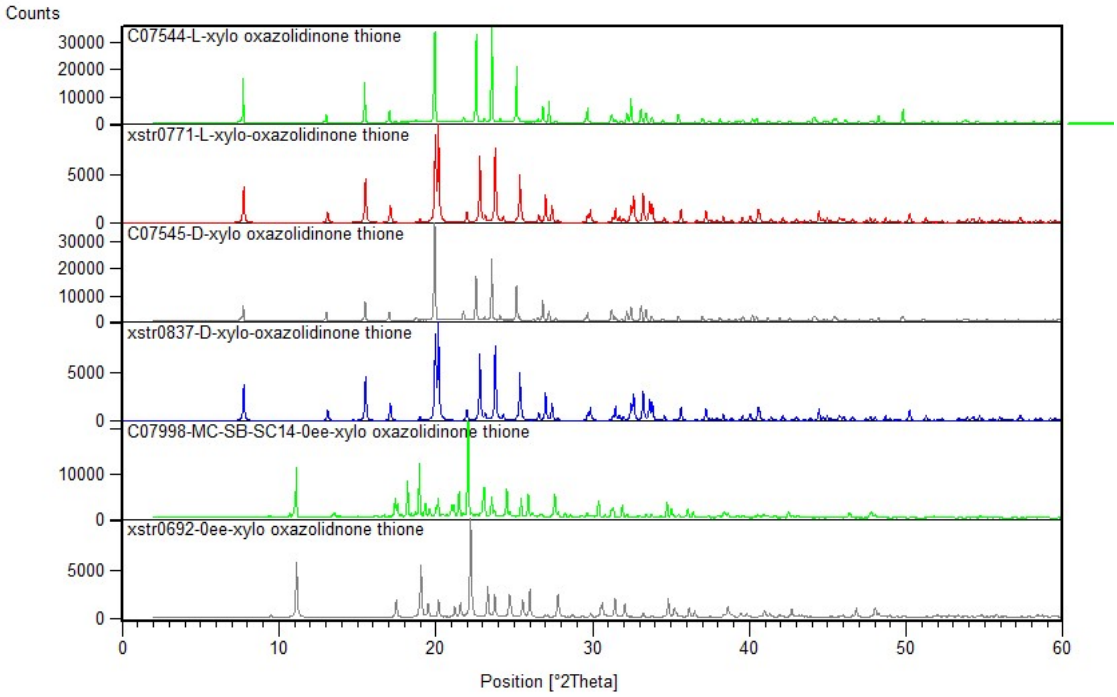

*Figure 152: PXRD **XOT***

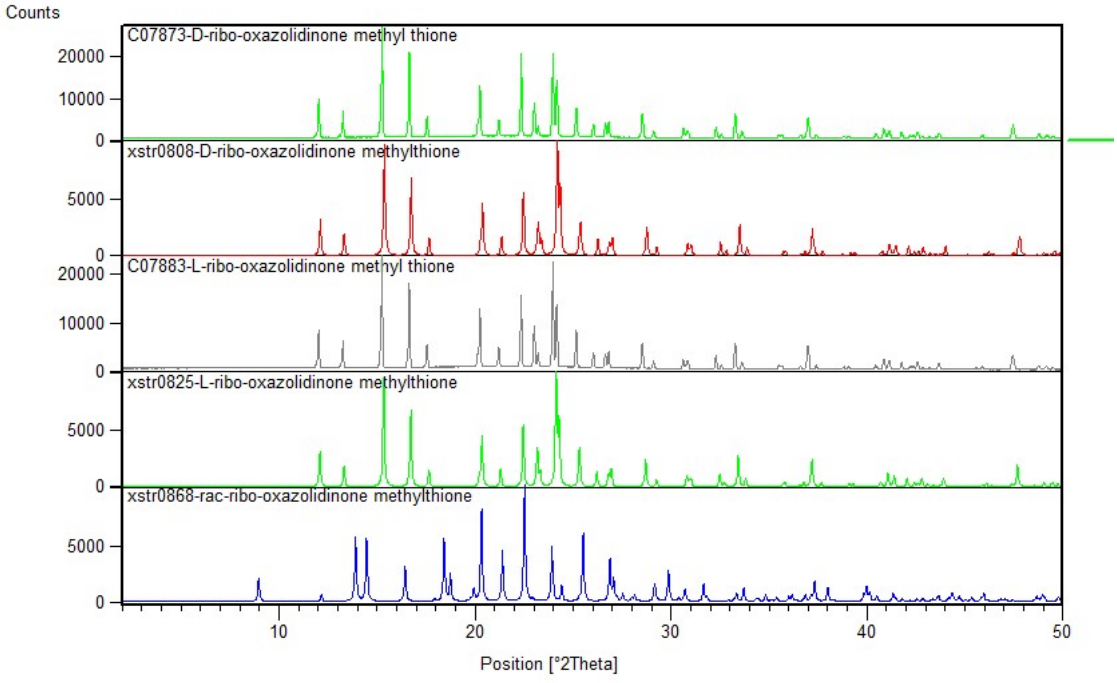

*Figure 153:PXRD of **RMOT***

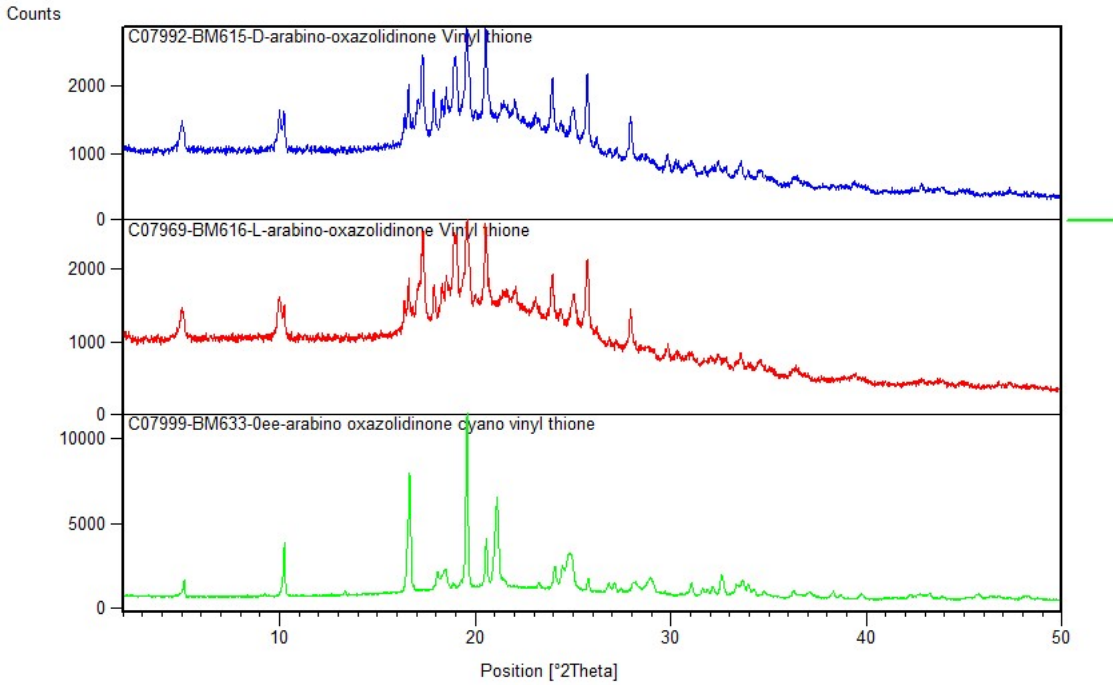

*Figure 154:PXRD of **ACVOT***

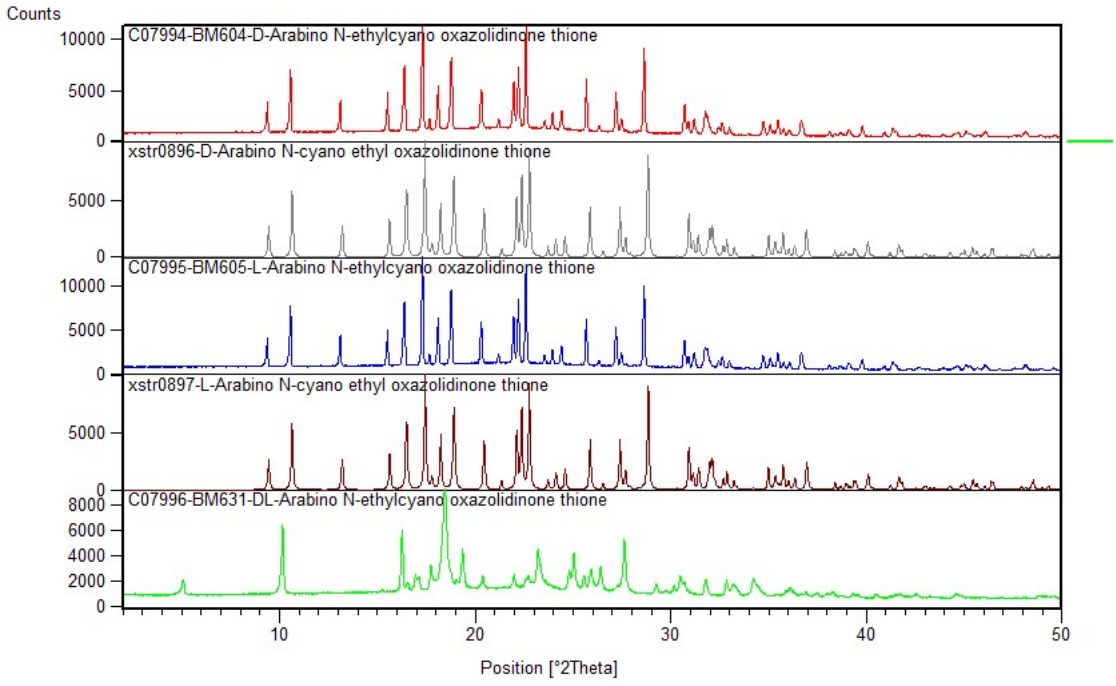

*Figure 155:PXRD of **ACEOT***

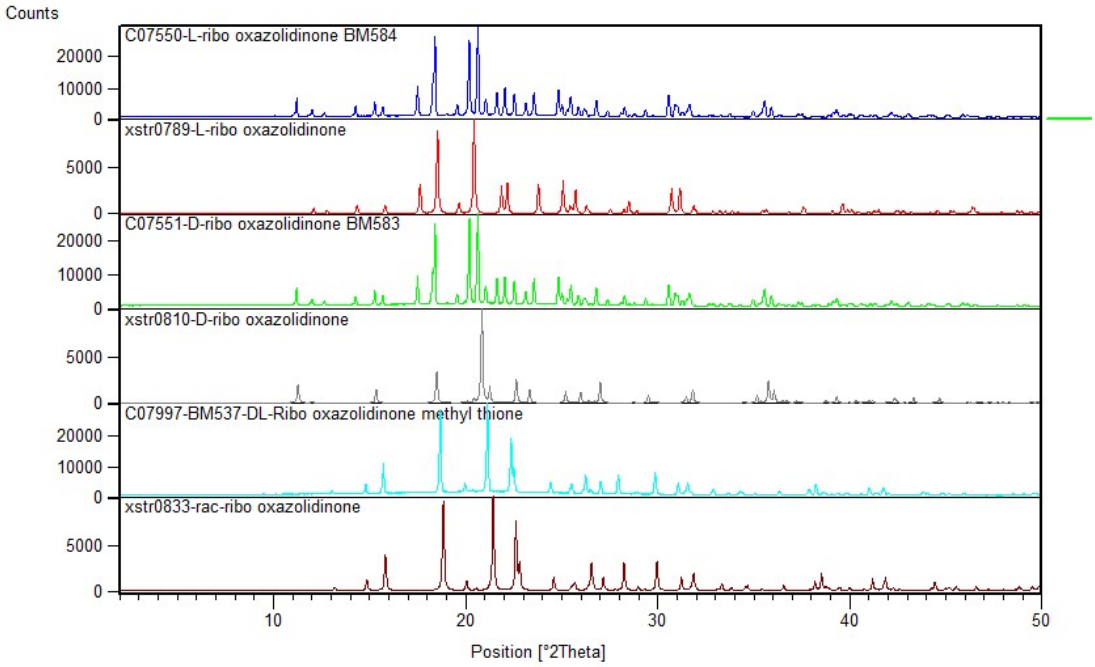

*Figure 156: PXRD of **ROX***

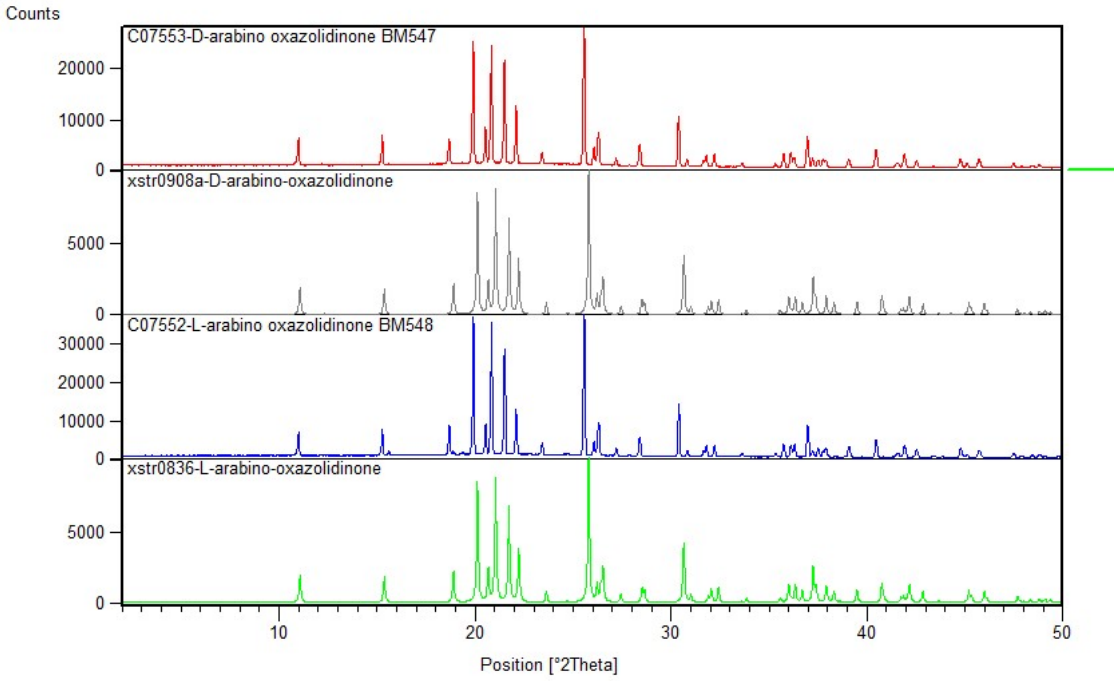

*Figure 157: PXRD of **AOX***

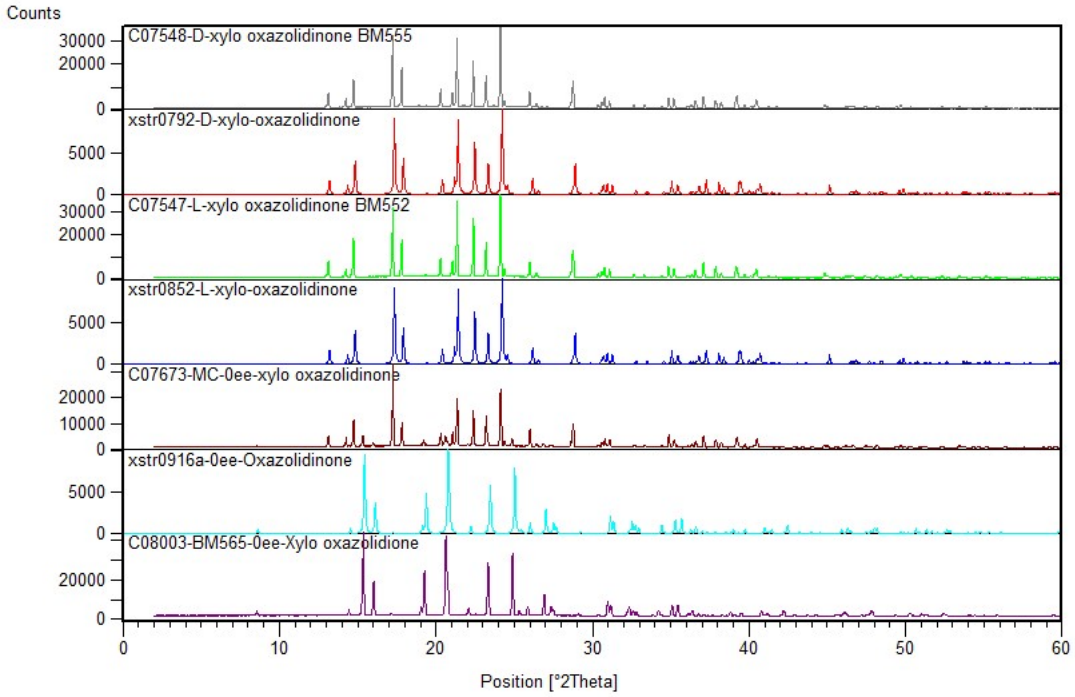

*Figure 158: PXRD of **XOX***

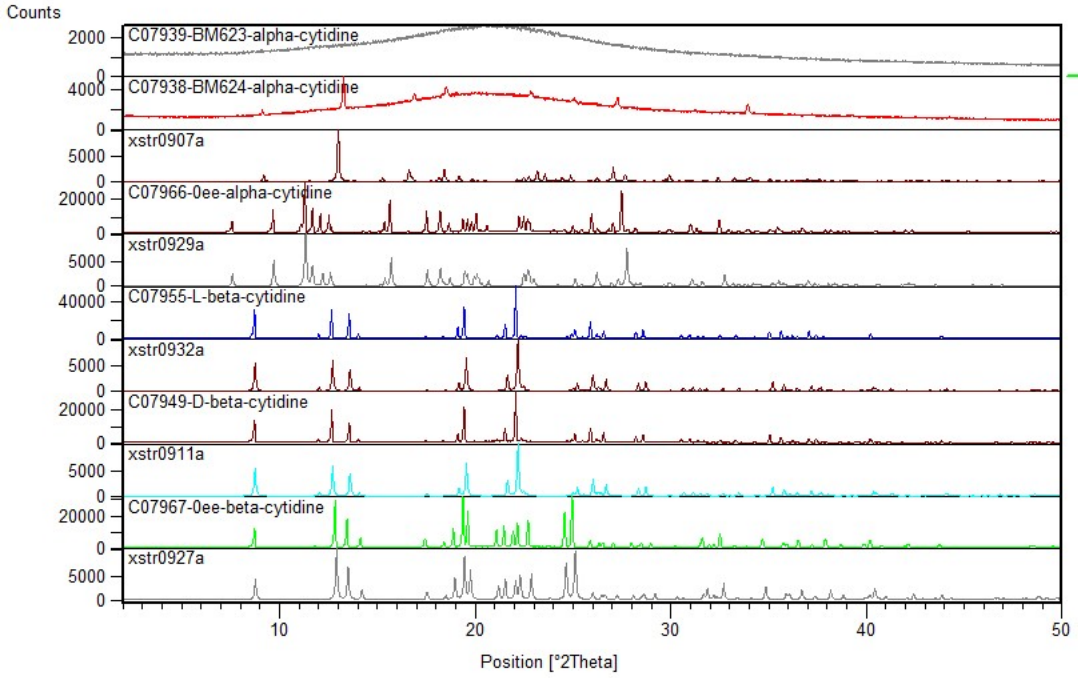

Figure 159: PXRD of cytidine

6.17 Graph Set Analysis

D RAO	**D AAO**	**D XAO**
CONGLOMERATE	CONGLOMERATE	CONGLOMERATE
C1,1(7) a	C1,1(7) a	C1,1(9) a
C1,1(5) b	C1,1(6) b	C1,1(6) b
C1,1(9) c	C1,1(7) c	C1,1(6) c
C1,1(7) d	C1,1(6) d	C1,1(7) d
C1,1(4) e	C2,2(8) >a>b	C2,2(7) >a<b
R2,2(10) >a<b	C2,2(13) >a<b	C2,2(15) >a>b
C2,2(11) >a>b	C4,4(21) >a>b<a<b	C4,4(22) >a>b<a<b
C2,2(6) >a>c	R4,4(21) >a>a>b>b	R4,4(22) >a>b<a>b
C2,2(16) >a<c	R6,6(33) >a>b>b<a<b<b	R6,6(34) >a>b>b<a>b>b
C4,4(22) >a>c<a<c	R6,6(35) >a>a>b<a<a<b	R6,6(40) >a>a>b<a<a<b
R4,4(22) >a>c<a>c	C2,2(10) >a>c	C2,2(10) >a>c
R6,6(36) >a>a>c<a<a<c	C2,2(15) >a<c	C2,2(14) >a<c
R6,6(40) >a>c>c<a>c>c	C4,4(25) >a>c<a<c	C4,4(24) >a>c<a<c
C2,2(10) >a>d	R4,4(25) >a>c<a>c	R6,6(36) >a>c>c<a>c>c
C2,2(15) >a<d	R6,6(39) >a>a>c<a<a<c	R6,6(42) >a>a>c>a>a<c
R4,4(24) >a>a>d>d	R6,6(39) >a>c>c<a>c>c	C2,2(6) >a>d
C4,4(25) >a>d<a<d	C2,2(9) >a>d	C2,2(16) >a<d
R6,6(39) >a>a>d<a<a<d	C2,2(13) >a<d	C4,4(22) >a>d<a<d
R6,6(39) >a>d>d<a<d<d	C4,4(22) >a>d<a<d	R6,6(36) >a>d>d<a>d>d
C2,2(11) >a>e	R4,4(22) >a>d<a>d	R6,6(40) >a>a>d>a>a<d
C2,2(13) >a<e	R6,6(34) >a>d>d<a>d>d	C2,2(9) >b>c

R4,4(22) >a>a>e>e	R6,6(36) >a>a>d<a<a<d	C2,2(11) >b<c
C4,4(24) >a>e<a<e	C2,2(11) >b>c	C4,4(20) >b>c<b<c
R6,6(32) >a>e>e<a<e<e	C2,2(13) >b<c	R4,4(20) >b>c>b<c
R6,6(38) >a>a>e<a<a<e	C4,4(24) >b>c<b<c	R6,6(32) >b>b>c>b>b<c
C2,2(12) >b<c	R4,4(24) >b>c<b>c	R6,6(32) >b>c>c<b<c<c
C2,2(12) >b>c	R6,6(36) >b>b>c<b<b<c	C2,2(9) >b>d
C4,4(24) >b>c<b<c	R6,6(38) >b>c>c<b>c>c	C2,2(13) >b<d
R4,4(24) >b>c<b>c	C2,2(12) >b<d	C4,4(22) >b>d<b<d
R6,6(34) >b>b>c<b<b<c	C2,2(14) >b>d	R4,4(22) >b>d>b<d
R6,6(42) >b>c>c<b>c>c	C4,4(26) >b>d<b<d	R6,6(34) >b>b>d>b>b<d
C2,2(8) >b>d	R4,4(26) >b>d<b>d	R6,6(36) >b>d>d<b<d<d
C2,2(12) >b<d	R6,6(38) >b>b>d<b<b<d	R1,2(8) >c<d
C4,4(20) >b>d<b<d	R6,6(38) >b>d>d<b>d>d	C2,2(13) >c>d
R4,4(20) >b>b>d>d	C2,2(7) >c<d	
R6,6(30) >b>b>d<b<b<d	C2,2(13) >c>d	
R6,6(34) >b>d>d<b<d<d	R4,4(20) >c>d<c<d	
C2,2(11) >b>e	R6,6(32) >c>d>d<c<d<d	
C2,2(12) >b<e	R6,6(34) >c>c>d<c<c<d	
R4,4(20) >b>b>e>e		
C4,4(23) >b>e<b<e		
R6,6(31) >b>e>e<b<e<e		
R6,6(33) >b>b>e<b<b<e		
C2,2(8) >c<d		
C2,2(16) >c>d		
C4,4(24) >c>d<c<d		

R4,4(24) >c>d>c<d		
R6,6(38) >c>d>d<c<d<d		
R6,6(42) >c>c>d>c>c<d		
C2,2(9) >c<e		
C2,2(13) >c>e		
C4,4(22) >c>e<c<e		
R4,4(22) >c>e>c<e		
R6,6(30) >c>e>e<c<e<e		
R6,6(40) >c>c>e>c>c<e		
R2,1(5) >d<e		
C2,2(11) >d>e		

D ROT	**D AOT**	**RAC AOT**	**D XOT**	**RAC XOT**
CONGLOMERATE	RACEMIC	RACEMIC	RACEMIC	RACEMIC
C1,1(9) a	C1,1(6) a	C1,1(4) a	C1,1(7) a	D1,1(2) a
C1,1(5) b	C1,1(6) b	C1,1(6) b	C1,1(7) b	D1,1(2) b
C1,1(7) c	C1,1(4) c	R2,2(18) >c>c	C1,1(6) c	D1,1(2) c
C2,2(12) >a<b	C2,2(4) >a>b	C2,2(14) >a>b	C2,2(10) >a>b	D1,1(2) d
C2,2(12) >a>b	C2,2(12) >a<b	C2,2(15) >a<b	C2,2(15) >a<b	D1,1(2) e
C4,4(24) >a>b<a<b	C4,4(16) >a>b<a<b	R4,4(29) >a>b<a<b	R4,4(25) >a>b<a<b	D1,1(2) f
R4,4(24) >a>b>a<b	R4,4(16) >a>a>b>b	R6,6(37) >a>a>b<a<a<b	R6,6(39) >a>a>b<a<a<b	C2,2(15) >a<b
R6,6(34) >a>b>b<a<b<b	R6,6(28) >a>a>b<a<a<b	R6,6(41) >a>b>b<a<b<b	R6,6(39) >a>b>b<a<b<b	C1,2(9) >a<c
R6,6(42) >a>a>b>a>a<b	R6,6(28) >a>b>b<a<b<b	R2,4(18) >a<c>a<c	C2,2(8) >a>c	R4,4(16) >a>d>a>d
C2,2(6) >a>c	C2,2(14) >a<c	C3,4(22) >a>c<a<c	C2,2(13) >a<c	C2,2(15) >a>e
C2,2(16) >a<c	C2,2(15) >a>c	R3,4(22) >a>c>a<c	R4,4(21) >a>c<a<c	C2,2(9) >a>f
C4,4(22) >a>c<a<c	C4,4(29) >a>c<a<c	R4,4(26) >a>c>a>c	R6,6(33) >a>c>c<a<c<c	C2,2(15) >b<c
R4,4(22) >a>c>a<c	R4,4(29) >a>c<a>c	R4,6(26) >a>a<c>a>a<c	R6,6(35) >a>a>c<a<a<c	C2,2(11) >b>d

R6,6(36) >a>c>c<a<c<c	R6,6(37) >a>c>c<a>c>c	R5,6(30) >a>a>c>a>a<c	C2,2(11) >b>c	C2,2(14) >b>e
R6,6(40) >a>a>c>a>a<c	R6,6(41) >a>a>c<a<a<c	R6,6(34) >a>a>c>a>a>c	C2,2(13) >b<c	C2,2(10) >b>f
R2,2(10) >b>c	C2,2(14) >b>c	C2,2(9) >b>c	R4,4(24) >b>c<b<c	R4,4(16) >c>d>c>d
C2,2(11) >b<c	C2,2(15) >b<c	C2,2(15) >b<c	R6,6(36) >b>c>c<b<c<c	C2,2(10) >c>e
	C4,4(29) >b>c<b<c	C4,4(24) >b>c<b<c	R6,6(38) >b>b>c<b<b<c	R2,2(14) >c>f
	R4,4(29) >b>c<b>c	R6,6(30) >b>b>c>b>b>c		C2,2(13) >d<e
	R6,6(37) >b>c>c<b>c>c	R6,6(36) >b>b>c>b>b<c		R4,4(26) >d<f>d<f
	R6,6(41) >b>b>c<b<b<c	R6,6(42) >b>b<c>b>b<c		C2,2(15) >e<f

D ROX	**RAC ROX**	**D AOX**	**D XOX**	**RAC XOX**
RACEMIC	RACEMIC	CONGLOMERATE	RACEMIC	RACEMIC
C1,1(7) a	C1,1(6) a	C1,1(7) a	R2,2(12) >a>a	C1,1(6) a
C1,1(7) b	C1,1(7) b	C1,1(7) b	C1,1(6) b	C1,1(9) b
C1,1(6) c	C1,1(7) c	C1,1(6) c	R2,2(8) >c>c	C2,2(9) >b>a
C2,2(10) >a>b	C2,2(11) >a>b	C2,2(10) >a>b	C2,2(4) >a>b	C2,2(15) >a<b
C2,2(15) >a<b	C2,2(13) >a<b	C2,2(15) >a<b	C2,2(12) >a<b	R3,3(15) >a>a>b
C4,4(25) >a>b<a<b	C4,4(24) >a>b<a<b	C4,4(25) >a>b<a<b	C4,4(16) >a>b<a<b	R4,4(24) >a>b<a<b
R6,6(39) >a>a>b>a>a<b	R4,4(24) >a>b<a>b	R6,6(39) >a>a>b>a>a<b	R6,6(20) >a>b>b>a>b>b	R5,5(33) >a>b>b>a<b
R6,6(39) >a>b>b<a>b>b	R6,6(36) >a>a>b<a<a<b	R6,6(39) >a>b>b<a>b>b	R6,6(28) >a>b>b<a>b>b	R6,6(42) >a>b>b<a<b<b
C2,2(8) >a>c	R6,6(38) >a>b>b<a>b>b	C2,2(8) >a>c	R6,6(36) >a<b<b>a<b<b	
C2,2(13) >a<c	C2,2(8) >a>c	C2,2(13) >a<c	C2,2(14) >a<c	
C4,4(21) >a>c<a<c	C2,2(13) >a<c	C4,4(21) >a>c<a<c	C2,2(15) >a>c	
R4,4(21) >a>a>c>c	C4,4(21) >a>c<a<c	R4,4(21) >a>a>c>c	C4,4(29) >a>c<a<c	
R6,6(33) >a>c>c<a<c<c	R4,4(21) >a>c<a>c	R6,6(33) >a>c>c<a<c<c	C2,2(14) >b>c	
R6,6(35) >a>a>c<a<a<c	R6,6(33) >a>a>c<a<a<c	R6,6(35) >a>a>c<a<a<c	C2,2(15) >b<c	

C2,2(11) >b>c	R6,6(35) >a>c>c<a>c>c	C2,2(11) >b>c	C4,4(29) >b>c<b<c	
C2,2(13) >b<c	R2,2(10) >b>c	C2,2(13) >b<c	R6,6(40) >b>b>c>b>b>c	
C4,4(24) >b>c<b<c	C2,2(15) >b<c	C4,4(24) >b>c<b<c	R6,6(41) >b>b>c>b>b<c	
R6,6(36) >b>c>c<b>c>c		R6,6(36) >b>c>c<b>c>c	R6,6(42) >b>b<c>b>b<c	
R6,6(38) >b>b>c>b>b<c		R6,6(38) >b>b>c>b>b<c		

D RMOT	**RAC RMOT**
RACEMIC	RACEMIC
C1,1(6) a	C1,1(7) a
C1,1(6) b	C1,1(5) b
C2,2(9) >a>b	R2,2(10) >a<b
C2,2(12) >a<b	C2,2(11) >a>b
C4,4(21) >a>b<a<b	
R6,6(33) >a>a>b>a>a<b	
R6,6(33) >a>b>b<a>b>b	

D RCVOT	**RAC RCVOT**	**D/ RAC ACVOT**
RACEMIC	RACEMIC	RACEMIC
C1,1(6) a	No crystal structure obtained	No crystal structure obtained
C1,1(6) b	Calculated by PXRD	Calculated by PXRD
C2,2(4) >b>a		
C2,2(12) >a<b		
R3,3(10) >a>a>b		
R4,4(16) >a>b<a<b		
R5,5(22) >a>b>b>a<b		
R6,6(28) >a>b>b<a<b<b		

D RCEOT	**RAC RCEOT**	**D ACEOT**	**RAC RCEOT**
RACEMIC	RACEMIC	RACEMIC	RACEMIC
C1,1(7) a	C1,1(6) a	C1,1(9) a	Calculated by PXRD
C1,1(6) b	C1,1(9) b	C1,1(6) b	
C2,2(11) >a>b	C2,2(9) >b>a	C2,2(9) >a>b	
C2,2(13) >a<b	C2,2(15) >a<b	C2,2(15) >a<b	
C4,4(24) >a>b<a<b	R3,3(15) >a>a>b	C4,4(24) >a>b<a<b	
R4,4(26) >a>a<b<b	R4,4(24) >a>b<a<b	R4,4(24) >a>b<a>b	
R6,6(36) >a>b>b<a<b<b	R5,5(33) >a>b>b>a<b	R6,6(36) >a>b>b<a>b>b	
R6,6(38) >a>a>b<a<a<b	R6,6(42) >a>b>b<a<b<b	R6,6(42) >a>a>b<a<a<b	

7 References:

1. Tassinari, F. *et al.* Enantioseparation by crystallization using magnetic substrates. *Chem. Sci.* **10**, 5246–5250 (2019).

2. Buick, R., Dunlop, J. S. R. & Groves, D. I. Stromatolite recognition in ancient rocks: an appraisal of irregularly laminated structures in an Early Archaean chert-barite unit from North Pole, Western Australia. *Alcheringa* **5**, 161–181 (1981).

3. Schopf, J. W. Earth's earliest biosphere: its origin and evolution. (1983).

4. Lal, A. K. Origin of Life. *Astrophys. Space Sci.* **317**, 267–278 (2008).

5. Kasting, J. F. & Brown, L. L. The early atmosphere as a source of biogenic compounds. *Mol. Orig. Life* 35–56 (1998).

6. Ehrenfreund, P. *et al.* Astrophysical and astrochemical insights into the origin of life. *Reports Prog. Phys.* **65**, 1427 (2002).

7. Cronin, J. R. Origin of organic compounds in carbonaceous chondrites. *Adv. Sp. Res.* **9**, 59–64 (1989).

8. Glavin, D., National, J. D.-P. of the & 2009, undefined. Enrichment of the amino acid L-isovaline by aqueous alteration on CI and CM meteorite parent bodies. *Natl. Acad Sci.*

9. Thaddeus, P. The prebiotic molecules observed in the interstellar gas. *Philos. Trans. R. Soc. London B Biol. Sci.* **361**, 1681–1687 (2006).

10. Raup, D. M. & Valentinet, J. W. *Multiple origins of life (extinction/bioclade/Precambrian/evolution/stochastic processes)*. *Proc. Natt Acad. Sci. USA* **80**, (1983).

11. Orgel, L. E. & Lohrmann, R. Prebiotic chemistry and nucleic acid replication. *Acc. Chem. Res.* **7**, 368–377 (1974).

12. Morasch, M. *et al.* Heated gas bubbles enrich, crystallize, dry, phosphorylate and encapsulate prebiotic molecules. *Nat. Chem.* **11**, 779–788 (2019).

13. Cockell, C. S. The origin and emergence of life under impact bombardment. in *Philosophical Transactions of the Royal Society B: Biological Sciences* **361**, 1845–1855 (Royal Society, 2006).

14. Miller, S. L. A production of amino acids under possible primitive earth conditions. *Science (80-.).* **117**, 528–529 (1953).

15. Miller, S. L. The mechanism of synthesis of amino acids by electric discharges. *Biochim. Biophys. Acta* **23**, 480–489 (1957).

16. Ueber die künstliche Bildung der Milchsäure und einen neuen, dem Glycocoll homologen Körper; - Strecker - 2006 - Justus Liebigs Annalen der Chemie - Wiley Online Library.

17. Parker, E. T. *et al.* A Plausible Simultaneous Synthesis of Amino Acids and Simple Peptides on the Primordial Earth. *Angew. Chemie* **126**, 8270–8274 (2014).

18. Cleaves, H. J., Chalmers, J. H., Lazcano, A., Miller, S. L. & Bada, J. L. A Reassessment of Prebiotic Organic Synthesis in Neutral Planetary Atmospheres. *Orig. Life Evol. Biosph.*

38, 105–115 (2008).

19. Brounce, M., Stolper, E. & Eiler, J. Redox variations in Mauna Kea lavas, the oxygen fugacity of the Hawaiian plume, and the role of volcanic gases in Earth's oxygenation. *Atmos. Planet. Sci.* **114**, (2017).

20. Petrology, S. F.-J. of & 2010, undefined. A reappraisal of redox melting in the Earth's mantle as a function of tectonic setting and time. *academic.oup.com*

21. Jiang, L. *et al.* Abiotic synthesis of amino acids and self-crystallization under prebiotic conditions. *Sci. Rep.* **4**, 6769 (2014).

22. Johnson, A. P. *et al.* The Miller volcanic spark discharge experiment. *Science (80-.).* **322**, 404–404 (2008).

23. Munñoz Caro, G. M. *et al.* Amino acids from ultraviolet irradiation of interstellar ice analogues. *Nature* **416**, 403–406 (2002).

24. DeMeo, F. E., Alexander, C. M. O. D., Walsh, K. J., Chapman, C. R. & Binzel, R. P. The compositional structure of the asteroid belt. in *Asteroids IV* 13–41 (University of Arizona Press, 2015). doi:10.1126/science.216.4553.1405

25. Kvenvolden, K. *et al.* Evidence for extraterrestrial amino-acids and hydrocarbons in the murchison meteorite. *Nature* **228**, 923–926 (1970).

26. E, O. L. Prebiotic Chemistry and the Origin of the RNA World. *Crit. Rev. Biochem. Mol. Biol.* **39**, 99–123 (2004).

27. Woese, C. The genetic code. (1967).

28. Crick, F. H. The origin of the genetic code. *J. Mol. Biol.* **38**, 367–379 (1968).

29. Joyce, G. F. The antiquity of RNA-based evolution. *Nature* **418**, 214–221 (2002).

30. Kruger, K. *et al.* Self-splicing RNA: autoexcision and autocyclization of the ribosomal RNA intervening sequence of Tetrahymena. *Cell* **31**, 147–157 (1982).

31. Robertson, M. P. & Joyce, G. F. The Origins of the RNA World. *Cold Spring Harb. Perspect. Biol.* a003608 (2010). doi:10.1101/cshperspect.a003608

32. Guerrier-Takada, C., Gardiner, K., Marsh, T., Pace, N. & Altman, S. The RNA moiety of ribonuclease P is the catalytic subunit of the enzyme. *Cell* **35**, 849–857 (1983).

33. Joyce, G. F. RNA evolution and the origins of life. *Nature* **338**, 217–224 (1989).

34. Neveu, M., Kim, H.-J. & Benner, S. A. The "Strong" RNA World Hypothesis: Fifty Years Old. *Astrobiology* **13**, 391–403 (2013).

35. Anastasi, C. *et al.* RNA: Prebiotic product, or biotic invention? *Chemistry and Biodiversity* **4**, 721–739 (2007).

36. Oró, J., biophysics, A. K.-A. of biochemistry and & 1962, undefined. Synthesis of purines under possible primitive earth conditions: II. Purine intermediates from hydrogen cyanide. *Elsevier*

37. Ferris, J., Sanchez, R., biology, L. O.-J. of molecular & 1968, undefined. Studies in prebiotic synthesis: III. Synthesis of pyrimidines from cyanoacetylene and cyanate. *Elsevier*

38. Sanchez, R., Ferris, J., biology, L. O.-J. of molecular & 1968, undefined. Studies in

prebiotic synthesis: IV. Conversion of 4-aminoimidazole-5-carbonitrile derivatives to purines. *Elsevier*

39. Shapiro, R. Prebiotic ribose synthesis: A critical analysis. *Orig. Life Evol. Biosph.* **18**, 71–85 (1988).

40. Pizzarello, S., Science, A. W.- & 2004, undefined. Prebiotic amino acids as asymmetric catalysts. *science.sciencemag.org*

41. Larralde, R., Robertson, M. P. & Miller, S. L. Rates of decomposition of ribose and other sugars: implications for chemical evolution. *Proc. Natl. Acad. Sci. U. S. A.* **92**, 8158–60 (1995).

42. Fuller, W. D., Sanchez, R. A. & Orgel, L. E. Studies in prebiotic synthesis: VI. Synthesis of purine nucleosides. *J. Mol. Biol.* **67**, 25–33 (1972).

43. Powner, M. W., Gerland, B. & Sutherland, J. D. Synthesis of activated pyrimidine ribonucleotides in prebiotically plausible conditions. *Nature* **459**, 239–242 (2009).

44. Choudhary, A., Kamer, K. J., Powner, M. W., Sutherland, J. D. & Raines, R. T. A Stereoelectronic Effect in Prebiotic Nucleotide Synthesis. *ACS Chem. Biol.* **5**, 655–657 (2010).

45. Sanchez, R. A. & Orgel, L. E. Studies in prebiotic synthesis: V. Synthesis and photoanomerization of pyrimidine nucleosides. *J. Mol. Biol.* **47**, 531–543 (1970).

46. Larralde, R., … M. R.-P. of the & 1995, undefined. Rates of decomposition of ribose and other sugars: implications for chemical evolution. *Natl. Acad Sci.*

47. Springsteen, G. & Joyce, G. F. Selective Derivatization and Sequestration of Ribose from a Prebiotic Mix. *J. Am. Chem. Soc.* **126**, 9578–9583 (2004).

48. Benner, S., Kim, H., Harbor, Z. Y.-C. S. & 2012, undefined. Setting the stage: the history, chemistry, and geobiology behind RNA. *cshperspectives.cshlp.org*

49. Schwartz, A. W. Evaluating the Plausibility of Prebiotic Multistage Syntheses. *Astrobiology* **13**, 784–789 (2013).

50. Hud, N., Cafferty, B., Krishnamurthy, R., biology, L. W.-C. & & 2013, undefined. The origin of RNA and “my grandfather’s axe”. *Elsevier*

51. Nagorski, R. W. & Richard, J. P. Mechanistic Imperatives for Aldose−Ketose Isomerization in Water: Specific, General Base- and Metal Ion-Catalyzed Isomerization of Glyceraldehyde with Proton and Hydride Transfer. *J. Am. Chem. Soc.* **123**, 794–802 (2001).

52. Islam, S. & Powner, M. W. Prebiotic Systems Chemistry: Complexity Overcoming Clutter. *Chem* **2**, 470–501 (2017).

53. Ritson, D. & Sutherland, J. D. Prebiotic synthesis of simple sugars by photoredox systems chemistry. *Nat. Chem.* **4**, 895–899 (2012).

54. Patel, B. H., Percivalle, C., Ritson, D. J., Duffy, C. D. & Sutherland, J. D. Common origins of RNA, protein and lipid precursors in a cyanosulfidic protometabolism. *Nat. Chem.* **7**, 301–307 (2015).

55. Ritson, D. J. & Sutherland, J. D. Synthesis of Aldehydic Ribonucleotide and Amino Acid Precursors by Photoredox Chemistry. *Angew. Chemie Int. Ed.* **52**, 5845–5847 (2013).

56. Becker, S. *et al.* Origin of life: A high-yielding, strictly regioselective prebiotic purine nucleoside formation pathway. *Science (80-.).* **352**, 833–836 (2016).

57. Burcar, B. *et al.* Darwin's Warm Little Pond: A One-Pot Reaction for Prebiotic Phosphorylation and the Mobilization of Phosphate from Minerals in a Urea-Based Solvent. *Angew. Chem. Int. Ed. Engl.* **55**, 13249–13253 (2016).

58. Kim, H.-J. *et al.* Evaporite Borate-Containing Mineral Ensembles Make Phosphate Available and Regiospecifically Phosphorylate Ribonucleosides: Borate as a Multifaceted Problem Solver in Prebiotic Chemistry. *Angew. Chem. Int. Ed. Engl.* **55**, 15816–15820 (2016).

59. Becker, S. *et al.* Unified prebiotically plausible synthesis of pyrimidine and purine RNA ribonucleotides. *Science (80-.).* **366**, 76–82 (2019).

60. Powner, M. W., Zheng, S.-L. & Szostak, J. W. Multicomponent assembly of proposed DNA precursors in water. *J. Am. Chem. Soc.* **134**, 13889–13895 (2012).

61. Keefe, A. D., Newton, G. L. & Miller, S. L. A possible prebiotic synthesis of pantetheine, a precursor to coenzyme A. *Nature* **373**, 683–685 (1995).

62. Saidul Islam, Dejan-Krešimir Bučar, Matthew W. Powner. Prebiotic selection and assembly of natural amino acids and ribonucleotides from complex mixtures. (2017).

63. Islam, S., Bučar, D.-K. & Powner, M. W. Prebiotic selection and assembly of proteinogenic amino acids and natural nucleotides from complex mixtures. *Nat. Chem.* **9**, 584–589 (2017).

64. Stairs, S. *et al.* Divergent prebiotic synthesis of pyrimidine and 8-oxo-purine ribonucleotides. *Nat. Commun.* **8**, 15270 (2017).

65. Chyba, C. & Sagan, C. Endogenous production, exogenous delivery and impact-shock synthesis of organic molecules: an inventory for the origins of life. *Nature* **355**, 125–132 (1992).

66. Lacasse, G. & Muchowski, J. M. Five-membered Heterocyclic Thiones. Part II. Oxazole-2-thione. *Can. J. Chem.* **50**, 3082–3083 (1972).

67. Acree, W. & Chickos, J. S. Phase Transition Enthalpy Measurements of Organic and Organometallic Compounds. Sublimation, Vaporization and Fusion Enthalpies From 1880 to 2010. *J. Phys. Chem. Ref. Data* **39**, 043101 (2010).

68. Roberts, S. J. *et al.* Selective prebiotic conversion of pyrimidine and purine anhydronucleosides into Watson-Crick base-pairing arabino-furanosyl nucleosides in water. *Nat. Commun.* **9**, (2018).

69. Martín-Pintado, N. *et al.* The solution structure of double helical arabino nucleic acids (ANA and 2'F-ANA): Effect of arabinoses in duplex-hairpin interconversion. *Nucleic Acids Res.* **40**, 9329–9339 (2012).

70. Jordan., P. & Kronig, R. D. L. Movements of the Lower Jaw of Cattle during Mastication. *Nature* **120**, 807–807 (1927).

71. Bonner, W. A. *The Origin and Amplification of Biomolecular Chirality*. **21**, (1991).

72. Quantitative, G. J.-C. S. H. S. on & 1987, undefined. Nonenzymatic template-directed synthesis of informational macromolecules. *symposium.cshlp.org*

73. Robertson, M. P. & Joyce, G. F. The origins of the RNA World. *Cold Spring Harb. Perspect. Biol.* **4**, 1 (2012).

74. Springsteen, G. & Joyce, G. F. Selective Derivatization and Sequestration of Ribose from a Prebiotic Mix. *J. Am. Chem. Soc.* **126**, 9578–9583 (2004).

75. Blackmond, D. G. The origin of biological homochirality. *Cold Spring Harb. Perspect. Biol.* **2**, a002147 (2010).

76. Gal, J. The discovery of biological enantioselectivity: Louis Pasteur and the fermentation of tartaric acid, 1857—A review and analysis 150 yr later. *Chirality* **20**, 5–19 (2008).

77. Pasteur, L. Memoire sur la relation qui peut exister entre la forme crystalline et la composition chimique, et sur la cause de la polarisation rotatoire. *Acad. Sci* **26**, 538 (1848).

78. Basic terminology of stereochemistry (IUPAC Recommendations 1996). *Pure Appl. Chem.* **68**, 2193–2222 (1996).

79. Nieuwenhuijzen, J. *Resolutions with families of resolving agents: principles and practice*. (2002).

80. Dupray, V. *Recrystallization of Enantiomers from Conglomerates*.

81. Jacques, J., Collet, A., Wilen, S. & Collet, A. *Enantiomers, racemates, and resolutions*. (1981).

82. Myrgorodska, I., Meinert, C., Martins, Z., Le Sergeant d'Hendecourt, L. & Meierhenrich, U. J. Molecular Chirality in Meteorites and Interstellar Ices, and the Chirality Experiment on Board the ESA Cometary Rosetta Mission. *Angew. Chemie Int. Ed.* **54**, 1402–1412 (2015).

83. Degens, E. T. & Bajor, M. Amino acids and sugars in the bruderheim and Murray meteorite. *Naturwissenschaften* **49**, 605–606 (1962).

84. Elsila, J. E. *et al.* Meteoritic Amino Acids: Diversity in Compositions Reflects Parent Body Histories. *ACS Cent. Sci.* **2**, 370–379 (2016).

85. Engel, M. H. & Nagy, B. Distribution and enantiomeric composition of amino acids in the Murchison meteorite. *Nature* **296**, 837–840 (1982).

86. Pizzarello, S., Schrader, D. L., Monroe, A. A. & Lauretta, D. S. Large enantiomeric excesses in primitive meteorites and the diverse effects of water in cosmochemical evolution. *Proc. Natl. Acad. Sci. U. S. A.* **109**, 11949–54 (2012).

87. Bissette, A. J. & Fletcher, S. P. Mechanisms of Autocatalysis. *Angew. Chemie Int. Ed.* **52**, 12800–12826 (2013).

88. Dadon, Z., Wagner, N. & Ashkenasy, G. The Road to Non-Enzymatic Molecular Networks. *Angew. Chemie Int. Ed.* **47**, 6128–6136 (2008).

89. Butlerow, A. No Title. *C. R. Hebd. Seances Acad. Sci.* (1861).

90. Luisi, P. L. *The emergence of life : from chemical origins to synthetic biology*.

91. Decker, P., Schweer, H., A, R. P.-J. of C. & 1982, undefined. Bioids: X. Identification of formose sugars, presumable prebiotic metabolites, using capillary gas chromatography/gas chromatography—mas spectrometry of n. *Elsevier*

92. Butlerow, A. Bildung einer zuckerartigen Substanz durch Synthese. *Justus Liebigs Ann. Chem.* **120**, 295–298 (1861).

93. Socha, R. F., Weiss, A. H. & Sakharov, M. M. Autocatalysis in the formose reaction. *React. Kinet. Catal. Lett.* **14**, 119–128 (1980).

94. Lambert, J. B., Gurusamy-Thangavelu, S. A. & Ma, K. The silicate-mediated formose reaction: bottom-up synthesis of sugar silicates. *Science* **327**, 984–6 (2010).

95. Gardner, P. M., Winzer, K. & Davis, B. G. Sugar synthesis in a protocellular model leads to a cell signalling response in bacteria. *Nat. Chem.* **1**, 377–383 (2009).

96. Breslow, R. On the mechanism of the formose reaction. *Tetrahedron Lett.* **1**, 22–26 (1959).

97. Schwartz, A. W. & de Graaf, R. M. The prebiotic synthesis of carbohydrates: A reassessment. *J. Mol. Evol.* **36**, 101–106 (1993).

98. Breslow, R. & Cheng, Z.-L. L-amino acids catalyze the formation of an excess of D-glyceraldehyde, and thus of other D sugars, under credible prebiotic conditions. *Proc. Natl. Acad. Sci. U. S. A.* **107**, 5723–5 (2010).

99. Blackmond, D. G., Moran, A., Hughes, M. & Armstrong, A. Unusual Reversal of Enantioselectivity in the Proline-Mediated α-Amination of Aldehydes Induced by Tertiary Amine Additives. *J. Am. Chem. Soc.* **132**, 7598–7599 (2010).

100. Hein, J. E. & Blackmond, D. G. On the Origin of Single Chirality of Amino Acids and Sugars in Biogenesis. *Acc. Chem. Res.* **45**, 2045–2054 (2012).

101. Frank, F. C. On spontaneous asymmetric synthesis. *Biochim. Biophys. Acta* **11**, 459–463 (1953).

102. Wynberg, H. Asymmetric Autocatalysis: Facts and Fancy. *J. Macromol. Sci. Part A - Chem.* **26**, 1033–1041 (1989).

103. Bolm, C., Bienewald, F. & Seger, A. *HIGHLIGHTS Asymmetric Autocatalysis with Amplification of Chirality***.

104. Soai, K., Niwa, S. & Hori, H. Asymmetric self-catalytic reaction. Self-production of chiral 1-(3-pyridyl)alkanols as chiral self-catalysts in the enantioselective addition of dialkylzinc reagents to pyridine-3-carbaldehyde. *J. Chem. Soc. Chem. Commun.* **0**, 982 (1990).

105. Blackmond, D. G., McMillan, C. R., Ramdeehul, S., Schorm, A. & Brown, J. M. Origins of asymmetric amplification in autocatalytic alkylzinc additions. *J. Am. Chem. Soc.* **123**, 10103–10104 (2001).

106. Soai, K., Hayase, T., Shimada, C. & Isobe, K. Catalytic asymmetric synthesis of chiral diol, bis[2-(1-hydroxyalkyl)-phenyl]ether, an asymmetric autocatalytic reaction. *Tetrahedron: Asymmetry* **5**, 789–792 (1994).

107. Lutz, F., Kawasaki, T., Asymmetry, K. S.-T. & 2006, undefined. Asymmetric autocatalysis of a ferrocene-containing chiral compound with amplification of chirality. *Elsevier*

108. Shibata, T. *et al.* Enantioselective synthesis of chiral 5-carbamoyl-3-pyridyl alcohols by asymmetric autocatalytic reaction. *Elsevier*

109. Sato, I., Urabe, H., Ishiguro, S., Shibata, T. & Soai, K. Amplification of Chirality from

Extremely Low to Greater than 99.5 % ee by Asymmetric Autocatalysis. *Angew. Chemie* **115**, 329–331 (2003).

110. Soai, K. *et al.* d- and l- Quartz Promoted Highly Enantioselective Synthesis of a Chiral Organic Compound. *J. Am. Chem. Soc* **121**, 11235–11236 (1999).

111. Shibata, T. *et al.* For spontaneous crystallizations as exceptions, see: Kondepudi, D. *Tetrahedron: Asymmetry* **374**, 3 (1997).

112. Kawasaki, T., Matsumura, Y., Tsutsumi, T., … K. S.- & 2009, undefined. Asymmetric autocatalysis triggered by carbon isotope (13C/12C) chirality. *science.sciencemag.org*

113. Kawasaki, T. *et al.* Asymmetric Autocatalysis: Triggered by Chiral Isotopomer Arising from Oxygen Isotope Substitution. *Angew. Chemie* **123**, 8281–8283 (2011).

114. Kawasaki, T., Ozawa, H., Ito, M. & Soai, K. Enantioselective Synthesis Induced by Compounds with Chirality Arising from Partially Deuterated Methyl Groups in Conjunction with Asymmetric Autocatalysis. *Chem. Lett.* **40**, 320–321 (2011).

115. Gehring, T., Quaranta, M., Odell, B., Blackmond, D. G. & Brown, J. M. Observation of a Transient Intermediate in Soai's Asymmetric Autocatalysis: Insights from 1H NMR Turnover in Real Time. *Angew. Chemie Int. Ed.* **51**, 9539–9542 (2012).

116. Quaranta, M., Gehring, T., Odell, B., Brown, J. M. & Blackmond, D. G. Unusual Inverse Temperature Dependence on Reaction Rate in the Asymmetric Autocatalytic Alkylation of Pyrimidyl Aldehydes. *J. Am. Chem. Soc.* **132**, 15104–15107 (2010).

117. Gridnev, I. D., Serafimov, J. M. & Brown, J. M. Solution Structure and Reagent Binding of the Zinc Alkoxide Catalyst in the Soai Asymmetric Autocatalytic Reaction. *Angew. Chemie Int. Ed.* **43**, 4884–4887 (2004).

118. and, F. G. B. & Blackmond*, D. G. Kinetic Evidence for a Tetrameric Transition State in the Asymmetric Autocatalytic Alkylation of Pyrimidyl Aldehydes†. (2003). doi:10.1021/JA034705N

119. Hein, J. E., Gherase, D. & Blackmond, D. G. Chemical and physical models for the emergence of biological homochirality. in *Biochirality* 83–108 (Springer, 2012).

120. Blackmond, D. G. Asymmetric autocatalysis and its implications for the origin of homochirality. *Proc. Natl. Acad. Sci. U. S. A.* **101**, 5732–6 (2004).

121. Blackmond, D. G. Description of the Condition for Asymmetric Amplification in Autocatalytic Reactions. *Adv. Synth. Catalyis* **344**, 156 (2002).

122. Matsumoto, A., Ide, T., Kaimori, Y., Fujiwara, S. & Soai, K. Asymmetric Autocatalysis Triggered by Chiral Crystal of Achiral Ethylenediamine Sulfate. *Chem. Lett.* **44**, 688–690 (2015).

123. Matsumoto, A. *et al.* Crystal Structure of the Isopropylzinc Alkoxide of Pyrimidyl Alkanol: Mechanistic Insights for Asymmetric Autocatalysis with Amplification of Enantiomeric Excess. *Angew. Chemie Int. Ed.* **54**, 15218–15221 (2015).

124. Kolb, V. M. *Handbook of Astrobiology*.

125. Matsumoto, A., Kawasaki, T. & Soai, K. Structural Study of Asymmetric Autocatalysis by X-Ray Crystallography. *Adv. Asymmetric Autocatalysis Relat. Top.* 183–202 (2017). doi:10.1016/B978-0-12-812824-4.00010-1

126. Singleton, D. A. & Vo, L. K. Enantioselective synthesis without discrete optically active additives. *J. Am. Chem. Soc.* **124**, 10010–10011 (2002).

127. Singleton, D. A. & Vo, L. K. A few molecules can control the enantiomeric outcome. Evidence supporting absolute asymmetric synthesis using the Soai asymmetric autocatalysis. *Org. Lett.* **5**, 4337–4339 (2003).

128. Feringa, B. L. & van Delden, R. A. Absolute Asymmetric Synthesis: The Origin, Control, and Amplification of Chirality. *Angew. Chemie Int. Ed.* **38**, 3418–3438 (1999).

129. Siegel, J. S. Homochiral imperative of molecular evolution. *Chirality* **10**, 24–27 (1998).

130. Gehring, T., Busch, M., Schlageter, M. & Weingand, D. A concise summary of experimental facts about the Soai reaction. *Chirality* **22**, E173–E182 (2010).

131. Tsogoeva, S. B. When chiral product and catalyst are the same: discovery of asymmetric organoautocatalysis. *Chem. Commun.* **46**, 7662 (2010).

132. Mauksch, M., Tsogoeva, S. B., Wei, S. & Martynova, I. M. Demonstration of spontaneous chiral symmetry breaking in asymmetric Mannich and Aldol reactions. *Chirality* **19**, 816–825 (2007).

133. Mauksch, M., Wei, S., Freund, M., Zamfir, A. & Tsogoeva, S. B. Spontaneous Mirror Symmetry Breaking in the Aldol Reaction and its Potential Relevance in Prebiotic Chemistry. *Orig. Life Evol. Biosph.* **40**, 79–91 (2010).

134. Blackmond, D. G. "If Pigs Could Fly" Chemistry: A Tutorial on the Principle of Microscopic Reversibility. *Angew. Chemie Int. Ed.* **48**, 2648–2654 (2009).

135. Blackmond, D. G. Challenging the concept of "recycling" as a mechanism for the evolution of homochirality in chemical reactions. *Chirality* **21**, 359–362 (2009).

136. Amedjkouh, M. & Brandberg, M. Asymmetric autocatalytic Mannich reaction in the presence of water and its implication in prebiotic chemistry. *Chem. Commun.* **0**, 3043 (2008).

137. Bailey, J. *et al.* Circular polarization in star- formation regions: implications for biomolecular homochirality. *Science* **281**, 672–4 (1998).

138. Bonner, W., Biosystems, E. R.- & 1987, undefined. Supernovae, neutron stars and biomolecular chirality. *Elsevier*

139. Suarez, M. & Schuster, G. B. Photoresolution of an Axially Chiral Bicyclo[3.3.0]octan-3-one: Phototriggers for a Liquid-Crystal-Based Optical Switch. *J. Am. Chem. Soc.* **117**, 6732–6738 (1995).

140. Kagan, H., Moradpour, A., Nicoud, J. F., Balavoine, G. & Tsoucaris, G. Photochemistry with circularly polarized light. Synthesis of optically active hexahelicene. *J. Am. Chem. Soc.* **93**, 2353–2354 (1971).

141. Inoue, Y. Asymmetric photochemical reactions in solution. *Chem. Rev.* **92**, 741–770 (1992).

142. Shibata, T. *et al.* Amplification of a Slight Enantiomeric Imbalance in Molecules Based on Asymmetric Autocatalysis: The First Correlation between High Enantiomeric Enrichment in a Chiral Molecule and Circularly Polarized Light. *J. Am. Chem. Soc.* **120**, 12157–12158 (1998).

143. Sato, I. *et al.* Determination of absolute configurations of amino acids by asymmetric autocatalysis of 2-alkynylpyrimidyl alkanol as a chiral sensor. *J. Organomet. Chem.* **692**, 1783–1787 (2007).

144. Engel, M., Nature, S. M.- & 1997, undefined. Isotopic evidence for extraterrestrial non-racemic amino acids in the Murchison meteorite. *nature.com*

145. Cronin, J. R. & Pizzarello, S. Science. *Science (80-.).* **154**, 377–380 (1997).

146. Pizzarello, S. & Cronin, J. . Non-racemic amino acids in the Murray and Murchison meteorites. *Geochim. Cosmochim. Acta* **64**, 329–338 (2000).

147. Sandford, S. A. *et al.* Organics captured from comet 81P/Wild 2 by the Stardust spacecraft. *Science* **314**, 1720–4 (2006).

148. Altwegg, K. *et al.* Prebiotic chemicals—amino acid and phosphorus—in the coma of comet 67P/Churyumov-Gerasimenko. *Sci. Adv.* **2**, e1600285 (2016).

149. Pizzarello, S. & Huang, Y. The deuterium enrichment of individual amino acids in carbonaceous meteorites: A case for the presolar distribution of biomolecule precursors. *Geochim. Cosmochim. Acta* **69**, 599–605 (2005).

150. Kawasaki, T. *et al.* Asymmetric autocatalysis triggered by carbon isotope (13C/12C) chirality. *Science* **324**, 492–5 (2009).

151. Matsumoto, A. *et al.* Asymmetric Induction by a Nitrogen ^{14} N/ ^{15} N Isotopomer in Conjunction with Asymmetric Autocatalysis. *Angew. Chemie* **128**, 15472–15475 (2016).

152. Matsumoto, A., Oji, S., Takano, S., … K. T.-O. & & 2013, undefined. Asymmetric autocatalysis triggered by oxygen isotopically chiral glycerin. *pubs.rsc.org*

153. Hawbaker, N. & Blackmond, D. Elucidating the Role of Isotopically Chiral Initiators in the Soai Asymmetric Autocatalytic Reaction. doi:10.26434/chemrxiv.5787984.v1

154. Hawbaker, N. A. & Blackmond, D. G. Rationalization of Asymmetric Amplification via Autocatalysis Triggered by Isotopically Chiral Molecules. *ACS Cent. Sci.* **4**, 776–780 (2018).

155. Robertson, M., Nature, S. M.- & 1995, undefined. An efficient prebiotic synthesis of cytosine and uracil. *nature.com*

156. Shapiro, R. Prebiotic cytosine synthesis: a critical analysis and implications for the origin of life. *Proc. Natl. Acad. Sci. U. S. A.* **96**, 4396–401 (1999).

157. Oró, J. Synthesis of adenine from ammonium cyanide. *Biochem. Biophys. Res. Commun.* **2**, 407–412 (1960).

158. Schwartz, A. W., Joosten, H. & Voet, A. B. Prebiotic adenine synthesis via HCN oligomerization in ice. *Biosystems* **15**, 191–193 (1982).

159. Callahan, M., Smith, K., … H. C.-P. of the & 2011, undefined. Carbonaceous meteorites contain a wide range of extraterrestrial nucleobases. *Natl. Acad Sci.*

160. Barker, D. L., Marsh, R. E. & IUCr. The crystal structure of cytosine. *Acta Crystallogr.* **17**, 1581–1587 (1964).

161. Kawasaki, T., Suzuki, K., Hakoda, Y. & Soai, K. Achiral Nucleobase Cytosine Acts as an Origin of Homochirality of Biomolecules in Conjunction with Asymmetric Autocatalysis. *Angew. Chemie* **120**, 506–509 (2008).

162. Kawasaki, T., Hakoda, Y., Mineki, H., Suzuki, K. & Soai, K. Generation of Absolute Controlled Crystal Chirality by the Removal of Crystal Water from Achiral Crystal of Nucleobase Cytosine. *J. Am. Chem. Soc.* **132**, 2874–2875 (2010).

163. Mineki, H., Kaimori, Y., Kawasaki, T., Matsumoto, A. & Soai, K. Enantiodivergent formation of a chiral cytosine crystal by removal of crystal water from an achiral monohydrate crystal under reduced pressure. *Tetrahedron: Asymmetry* **24**, 1365–1367 (2013).

164. Mineki, H., Hanasaki, T., Matsumoto, A., Kawasaki, T. & Soai, K. Asymmetric autocatalysis initiated by achiral nucleic acid base adenine: implications on the origin of homochirality of biomolecules. *Chem. Commun.* **48**, 10538 (2012).

165. Rikken, G., Nature, E. R.- & 2000, undefined. Enantioselective magnetochiral photochemistry. *nature.com*

166. Barron, L. D. Can a Magnetic Field Induce Absolute Asymmetric Synthesis? *Science (80-.).* **266**, 1491–1492 (1994).

167. Kelvin, W. Baltimore lectures on molecular dynamics and the wave theory of light. (1904).

168. Brochard, F. & de Gennes, P. G. Theory of magnetic suspensions in liquid crystals. *J. Phys.* **31**, 691–708 (1970).

169. et, P. C.-J. de physique théorique & 1894, undefined. Sur la symétrie dans les phénomènes physiques, symétrie d'un champ électrique et d'un champ magnétique. *jphystap.journaldephysique.org*

170. Rikken, G., Nature, E. R.- & 1997, undefined. Observation of magneto-chiral dichroism. *nature.com*

171. Kleindienst, P., letters, G. W.-C. physics & 1998, undefined. Interferometric detection of magnetochiral birefringence. *Elsevier*

172. Kumar, A., Capua, E., … M. K.-P. of the & 2017, undefined. Chirality-induced spin polarization places symmetry constraints on biomolecular interactions. *Natl. Acad Sci.*

173. Dor, O., Yochelis, S., Radko, A., … K. V.-N. & 2017, undefined. Magnetization switching in ferromagnets by adsorbed chiral molecules without current or external magnetic field. *nature.com*

174. Tassinari, F. *et al.* Enantioseparation by crystallization using magnetic substrates. *Chem. Sci.* (2019). doi:10.1039/C9SC00663J

175. Addadi, L. *et al.* Resolution of conglomerates by stereoselective habit modifications. *nature.com*

176. Smalley, I. & Marković, S. B. Controls on the nature of loess particles and the formation of loess deposits. *Quat. Int.* **502**, 160–164 (2019).

177. Blackmond, D. G. & Klussmann, M. Spoilt for choice: assessing phase behavior models for the evolution of homochirality. *Chem. Commun.* **0**, 3990 (2007).

178. Blackmond, D. G. "Chiral Amnesia" as a Driving Force for Solid-Phase Homochirality. *Chem. Eur. J.* **13**, 3290–3295 (2007).

179. Blackmond, D. G. & Klussmann, M. Investigating the evolution of biomolecular

homochirality. *AIChE J.* **53**, 2–8 (2007).

180. Meyerhoffer, W. Stereochemische Notizen. *Berichte der Dtsch. Chem. Gesellschaft* **37**, 2604–2610 (1904).

181. Klussmann, M. *et al.* Thermodynamic control of asymmetric amplification in amino acid catalysis. *Nature* **441**, 621–623 (2006).

182. Lombardo, T. G., Stillinger, F. H. & Debenedetti, P. G. Thermodynamic mechanism for solution phase chiral amplification via a lattice model. *Proc. Natl. Acad. Sci.* **106**, 15131–15135 (2009).

183. Morowitz, H. J. A mechanism for the amplification of fluctuations in racemic mixtures. *J. Theor. Biol.* **25**, 491–494 (1969).

184. Breslow, R. & Cheng, Z.-L. On the origin of terrestrial homochirality for nucleosides and amino acids. *Proc. Natl. Acad. Sci. U. S. A.* **106**, 9144–6 (2009).

185. Breslow, R. & Levine, M. S. Amplification of enantiomeric concentrations under credible prebiotic conditions. *Proc. Natl. Acad. Sci. U. S. A.* **103**, 12979–80 (2006).

186. Martin Klussmann, †,‡, Toshiko Izumi, §, Andrew J. P. White, †, Alan Armstrong, † and & Donna G. Blackmond*, †,§. Emergence of Solution-Phase Homochirality via Crystal Engineering of Amino Acids. (2007). doi:10.1021/JA0708870

187. Cherukuvada, S., Kaur, R. & Guru Row, T. N. Co-crystallization and small molecule crystal form diversity: From pharmaceutical to materials applications. *CrystEngComm* **18**, 8528–8555 (2016).

188. Hein, J. E., Gherase, D. & Blackmond, D. G. Chemical and Physical Models for the Emergence of Biological Homochirality. in 83–108 (Springer, Berlin, Heidelberg, 2012). doi:10.1007/128_2012_397

189. Kipping, F. S. & Pope, W. J. LXIII.—Enantiomorphism. *J. Chem. Soc. Trans.* **73**, 606–617 (1898).

190. McBride, J. M. & Carter, R. L. Spontaneous formation of enantiomorphic crystals with stirring. *Angew. Chem. Int. Ed. Engl* **30**, 293–295 (1991).

191. Kondepudi, D. K., Kaufman, R. J. & Singh, N. Chiral symmetry breaking in sodium chlorate crystallizaton. *Science (80-.).* **250**, 975–976 (1990).

192. Viedma, C. Chiral symmetry breaking during crystallization: complete chiral purity induced by nonlinear autocatalysis and recycling. *Phys. Rev. Lett.* **94**, 065504 (2005).

193. Blackmond, D. G. The origin of biological homochirality. *Philos. Trans. R. Soc. London B Biol. Sci.* **366**, 2878–2884 (2011).

194. An, G. *et al.* The racemate-to-homochiral approach to crystal engineering via chiral symmetry breaking. *CrystEngComm* **17**, 4421–4433 (2015).

195. Sögütoglu, L.-C., Steendam, R. R., Meekes, H., Vlieg, E. & Rutjes, F. P. Viedma ripening: a reliable crystallisation method to reach single chirality. *Chem. Soc. Rev.* **44**, 6723–6732 (2015).

196. Amabilino, D. B. & Kellogg, R. M. Spontaneous Deracemization. *Isr. J. Chem.* **51**, 1034–1040 (2011).

197. Gao, B., Zhang, Q., Yan, P., Hou, G. & Li, G. Cite this: CrystEngComm. **15**, 4167 (2013).

198. Sun, J. W. *et al.* Spontaneous resolution of racemic salen-type ligand in the construction of 3D homochiral lanthanide frameworks. *Cryst. Growth Des.* **14**, 5356–5360 (2014).

199. Steendam, R. R. E. *et al.* Enantiopure isoindolinones through Viedma ripening. *Chem. - A Eur. J.* **20**, 13527–13530 (2014).

200. Engwerda, A. H. J. *et al.* Deracemization of a Racemic Allylic Sulfoxide Using Viedma Ripening. *Cryst. Growth Des.* **17**, 4454–4457 (2017).

201. Voorhees ', P. W. The Theory of Ostwald Ripening. *Artic. J. Stat. Phys.* **38**, (1985).

202. Blackmond, D. "Chiral Amnesia" as a Driving Force for Solid-Phase Homochirality. **13**, 3290–3295

203. Havinga, E. Over de mogelijkheid van 'spontane asymmetrische synthese'. *Chem. Weekbl* **38**, 642–644 (1941).

204. Havinga, E. Spontaneous formation of optically active substances. *Biochim. Biophys. Acta* **13**, 171–174 (1954).

205. Noorduin, W. L. *et al.* Emergence of a single solid chiral state from a nearly racemic amino acid derivative. *J. Am. Chem. Soc.* **130**, 1158–1159 (2008).

206. Noorduin, W. L. *et al.* Scaling Up Attrition-Enhanced Deracemization by Use of an Industrial Bead Mill in a Route to Clopidogrel (Plavix). *Org. Process Res. Dev.* **14**, 908–911 (2010).

207. Noorduin, W. L. *et al.* Fast Attrition-Enhanced Deracemization of Naproxen by a Gradual In Situ Feed. *Angew. Chemie Int. Ed.* **48**, 4581–4583 (2009).

208. van der Meijden, M. W. *et al.* Attrition-Enhanced Deracemization in the Synthesis of Clopidogrel - A Practical Application of a New Discovery. *Org. Process Res. Dev.* **13**, 1195–1198 (2009).

209. Viedma, C., Ortiz, J. E., Torres, T. de, Izumi, T. & Blackmond, D. G. Evolution of Solid Phase Homochirality for a Proteinogenic Amino Acid. *J. Am. Chem. Soc.* **130**, 15274–15275 (2008).

210. Tsogoeva, S. B., Wei, S., Freund, M. & Mauksch, M. Generation of Highly Enantioenriched Crystalline Products in Reversible Asymmetric Reactions with Racemic or Achiral Catalysts. *Angew. Chemie Int. Ed.* **48**, 590–594 (2009).

211. Wilson, D. S. & Szostak, J. W. In Vitro Selection of Functional Nucleic Acids. *Annu. Rev. Biochem.* **68**, 611–647 (1999).

212. Steitz, T. A. & Moore, P. B. RNA, the first macromolecular catalyst: the ribosome is a ribozyme. *Trends Biochem. Sci.* **28**, 411–418 (2003).

213. Robertson, M. P. & Miller, S. L. An efficient prebiotic synthesis of cytosine and uracil. *Nature* **375**, 772–774 (1995).

214. Wakamatsu, H., Yamada, Y., Saito, T., Kumashiro, I. & Takenishi, T. Synthesis of Adenine by Oligomerization of Hydrogen Cyanide. *J. Org. Chem.* **31**, 2035–2036 (1966).

215. Joyce, G., Visser, G., Boeckel, C. Van, Nature, J. V. B.- & 1984, undefined. Chiral selection in poly (C)-directed synthesis of oligo (G). *nature.com*

216. Tamura, K. & Schimmel, P. Chiral-selective aminoacylation of an RNA minihelix. *Science*

(80-.). **305**, 1253 (2004).

217. Budin, I. & Szostak, J. W. Expanding Roles for Diverse Physical Phenomena During the Origin of Life. *Annu. Rev. Biophys.* **39**, 245–263 (2010).

218. Verlander, M. S., Lohrmann, R. & Orgel, L. E. Catalysts for the self-polymerization of adenosine cyclic 2',3'-phosphate. *J. Mol. Evol.* **2**, 303–316 (1973).

219. Inoue, T., Society, L. O.-J. of the A. C. & 1981, undefined. Substituent control of the poly (C)-directed oligomerization of guanosine 5'-phosphoroimidazolide. *ACS Publ.*

220. Ferris, J., Science, G. E.- & 1992, undefined. Oligomerization of ribonucleotides on montmorillonite: reaction of the 5'-phosphorimidazolide of adenosine. *science.sciencemag.org*

221. and, K. J. P. & Ferris*, J. P. Adenine Derivatives as Phosphate-Activating Groups for the Regioselective Formation of 3',5'-Linked Oligoadenylates on Montmorillonite: Possible Phosphate-Activating Groups for the Prebiotic Synthesis of RNA. (1997). doi:10.1021/JA9700764

222. Franklin, R. E. & Gosling, R. G. Molecular Configuration in Sodium Thymonucleate. *Nature* **171**, 740–741 (1953).

223. LYDON, J. E. The DNA double helix—the untold story. *Liq. Cryst. Today* **12**, 1–9 (2003).

224. Shadpour, S., Vanegas, J. P., Nemati, A. & Hegmann, T. Amplification of Chirality by Adenosine Monophosphate-Capped Luminescent Gold Nanoclusters in Nematic Lyotropic Chromonic Liquid Crystal Tactoids. *ACS Omega* **4**, 1662–1668 (2019).

225. Nakata, M., Zanchetta, G., Chapman, B., … C. J.- & 2007, undefined. End-to-end stacking and liquid crystal condensation of 6–to 20–base pair DNA duplexes. *science.sciencemag.org*

226. Collings, P. J., Hird, M. & Hird, M. Introduction to Liquid Crystals : Chemistry and Physics. (2017). doi:10.1201/9781315272801

227. Zanchetta, G., Nakata, M., … M. B.-P. of the & 2008, undefined. Phase separation and liquid crystallization of complementary sequences in mixtures of nanoDNA oligomers. *Natl. Acad Sci.*

228. Tuinier, R., Rieger, J. & de Kruif, C. . Depletion-induced phase separation in colloid–polymer mixtures. *Adv. Colloid Interface Sci.* **103**, 1–31 (2003).

229. *Chirality in Liquid Crystals*. (Springer-Verlag, 2001). doi:10.1007/b97374

230. Eelkema, R. & Feringa, B. L. Amplification of chirality in liquid crystals. *Org. Biomol. Chem.* **4**, 3729 (2006).

231. Nelson, K. E., Robertson, M. P., Levy, M. & Miller, S. L. Concentration by evaporation and the prebiotic synthesis of cytosine. *Orig. Life Evol. Biosph.* **31**, 221–9 (2001).

232. Pierre-Alain Monnard, *, Anastassia Kanavarioti, and & Deamer, D. W. Eutectic Phase Polymerization of Activated Ribonucleotide Mixtures Yields Quasi-Equimolar Incorporation of Purine and Pyrimidine Nucleobases. (2003). doi:10.1021/JA036465H

233. Stribling, R. & Miller, S. L. Template-directed synthesis of oligonucleotides under eutectic conditions. *J. Mol. Evol.* **32**, 289–295 (1991).

234. Baaske, P., Weinert, F., … S. D.-P. of the & 2007, undefined. Extreme accumulation of

nucleotides in simulated hydrothermal pore systems. *Natl. Acad Sci.*

235. Kelley, D., Karson, J., … G. F.-G.- & 2005, undefined. A serpentinite-hosted ecosystem: the Lost City hydrothermal field. *science.sciencemag.org*

236. Jones, A. L. & Milberger, E. C. Separation of Organic Liquid Mixtures by Thermal Diffusion. *Ind. Eng. Chem.* **45**, 2689–2696 (1953).

237. Budin, I., Bruckner, R. J. & Szostak, J. W. Formation of Protocell-like Vesicles in a Thermal Diffusion Column. *J. Am. Chem. Soc.* **131**, 9628–9629 (2009).

238. Anastasi, C., Crowe, M. A., Powner, M. W. & Sutherland, J. D. Direct Assembly of Nucleoside Precursors from Two- and Three-Carbon Units. *Angew. Chemie Int. Ed.* **45**, 6176–6179 (2006).

239. Blackmond, D. G. The Origin of Biological Homochirality. *Cold Spring Harb. Perspect. Biol.* **11**, a032540 (2019).

240. Saewan, N. *et al.* Exploratory Studies to Investigate a Linked Prebiotic Origin of RNA and Coded Peptides. 4th Communication. *Chem. Biodivers.* **2**, 66–83 (2005).

241. Sczepanski, J. T. & Joyce, G. F. A cross-chiral RNA polymerase ribozyme. *Nature* **515**, 440–442 (2014).

242. Maret, W. Zinc and Sulfur: A Critical Biological Partnership. *Biochemistry* **43**, 3301–3309 (2004).

243. Gorbalenya, A. E., Donchenko, A. P., Blinov, V. M. & Koonin, E. V. Cysteine proteases of positive strand RNA viruses and chymotrypsin-like serine proteases. A distinct protein superfamily with a common structural fold. *FEBS Lett.* **243**, 103–114 (1989).

244. He, W. *et al.* Citric acid cycle intermediates as ligands for orphan G-protein-coupled receptors. *Nature* **429**, 188–193 (2004).

245. Bernstein, J. *Polymorphism in molecular crystals*. (Oxford University Press).

246. Subramanian, S. & Zaworotko, M. J. Exploitation of the hydrogen bond: recent developments in the context of crystal engineering. *Coordination Chemistry Reviews* **137**, 357–401 (1994).

247. Review, R. P.-P. & 1955, undefined. Crystal engineering-new concept in crystallography. *Coll. PK, MD 20740-3844 USA*

248. Cohen, M., (Resumed, G. S.-J. of the C. S. & 1964, undefined. 383. Topochemistry. Part I. A Survey. *pubs.rsc.org*

249. Desiraju, G. R. Crystal engineering: From molecule to crystal. *Journal of the American Chemical Society* **135**, 9952–9967 (2013).

250. Yadav, P., Dutta, P. K. & Ballabh, A. Combinatorial library approach to realize 2-aminothiazole-based two-component hydrogelator: A structure - Property correlation. *Cryst. Growth Des.* **14**, 5966–5975 (2014).

251. Klussmann, M. *et al.* Thermodynamic control of asymmetric amplification in amino acid catalysis. *Nature* **441**, 621–623 (2006).

252. Gibson, S., Lanigan, R., … L. B.-O. & & 2015, undefined. A lactate-derived chiral aldehyde for determining the enantiopurity of enantioenriched primary amines. *pubs.rsc.org*

253. Donna G. Blackmond, *,†, Christopher R. McMillan, ‡, Shailesh Ramdeehul, ‡, Andrea Schorm, ‡ and & John M. Brown*, ‡. Origins of Asymmetric Amplification in Autocatalytic Alkylzinc Additions. (2001). doi:10.1021/JA0165133

254. Cronin, J. R. & Pizzarello, S. Enantiomeric Excesses in Meteoritic Amino Acids. *Science (80-.).* **275**, 951–955 (1997).

255. Hein, J., Tse, E., chemistry, D. B.-N. & 2011, undefined. A route to enantiopure RNA precursors from nearly racemic starting materials. *nature.com*

256. Kaboudin, B., Karami, L., Kato, J., … H. A.-T. & 2013, undefined. A catalyst-free, three-component decarboxylative coupling of amino acids with aldehydes and H-dialkylphosphites for the synthesis of α-aminophosphonates. *Elsevier*

257. Desiraju, G. R. Supramolecular Synthons in Crystal Engineering—A New Organic Synthesis. *Angewandte Chemie International Edition in English* **34**, 2311–2327 (1995).

[i] J. C. Jochims, A. Seeliger & G. Taigel, U¨ ber die reaktion der monosaccharide mit rhodanwasserstoffsa¨ure. Chem. Ber., **100**, 845–854 (1967).